Observations for Practical Fermi–Pasta–Ulam–Tsingou Systems



Heather Nelson

Mansfield College

University of Oxford

A thesis submitted for the degree of

Doctor of Philosophy

Hilary 2019

Acknowledgements

I would like to thank Professor Bhaskar Choubey and Professor Steve Collins for their encouragement and guidance as my supervisors, and Professor Chris Martin for his advice and assistance as my college advisor.

I thank my colleagues in the Microelectronics, Circuits and Analog Devices (MCAD) research group who have created a stimulating environment in which to conduct research on a day-to-day basis.

I am grateful to the Engineering and Physical Sciences Research Council (EPSRC) for funding my research through the Doctoral Training Award scheme, and also to the Department of Engineering Science and to Mansfield College who have supported me with facilities and funding to attend conferences.

I am fortunate to have some amazing friends, to whom I am indebted for their help and support through the highs and lows that are an inevitable part of research. Particular thanks go to Sue and Darren Maughan, Merel Lefferts, Victoria Grigson, Holly Norris, Rachael Wells, and Jennie Rolfe.

Finally I would like to thank my parents, Margaret and Nigel, and my sister, Catherine, for their unconditional love and support, no matter what crazy plans I dream up. Thank you!

Abstract

Nonlinear dynamics is a field that has been widely studied by mathematicians and scientists. However, engineers are yet to exploit the full potential of nonlinearity in coupled systems despite the majority of real physical systems being inherently nonlinear. Although a vast array of results has been generated from simulations, only a small number of physical systems have been investigated.

In a 1955 report, Fermi, Pasta, Ulam, and Tsingou reported recurrence of energy between modes in a simple mass-spring system containing a nonlinear coupling term. Extensive numerical simulations of the FPUT system have followed this discovery. However, minimal evidence of FPUT recurrence has been observed in physical systems.

This may be due to the effect of 'real-world' imperfections on the ideal systems used in the simulations. Variations between system components due to manufacturing tolerances and energy losses through damping are present in most physical systems. By understanding the effects of these imperfections, it may be possible to apply the results of the simulations to physical systems.

The effects of tolerance and damping on recurrence were studied using a series of simulations. The results demonstrate that such imperfections degrade the observation of recurrence, often leading to complete loss in moderately sized arrays. These simulations enabled the identification of a series of conditions under which a practical system might display recurrence. Tight tolerances, low damping, small array size and moderately weak coupling strengths are required.

An electronic amplifier circuit was designed to meet these constraints. Preliminary testing of this electronic system has provided early verification of the simulation results. FPUT recurrence was observed a system with four elements. These results suggest that without considering tolerances in real systems, the applicability of the results from simulations to physical systems may be limited.

Contents

List of Figures viii

List of Tables xv

List of Publications xvi

1 Introduction 1
- 1.1 Nonlinear systems . . . 2
- 1.2 The Fermi–Pasta–Ulam–Tsingou phenomenon . . . 2
  - 1.2.1 The FPUT-α model: quadratic nonlinearity . . . 4
  - 1.2.2 The FPUT-β model: cubic nonlinearity . . . 10
  - 1.2.3 Other nonlinearities . . . 11
  - 1.2.4 Different nonlinear coupling strength . . . 12
  - 1.2.5 Different initial conditions . . . 13
- 1.3 Superrecurrence . . . 13
- 1.4 Relevance of the FPUT phenomenon today . . . 16
- 1.5 Engineering motivation . . . 17
- 1.6 Physical realisation of the FPUT-α model . . . 18
- 1.7 Thesis overview . . . 19

2 Tolerance 21
- 2.1 Tolerance in physical systems . . . 23
- 2.2 Numerical experiment design . . . 25
  - 2.2.1 Reproduction of FPUT-α results . . . 26
  - 2.2.2 Chain length . . . 27
  - 2.2.3 Inclusion of tolerance . . . 27
  - 2.2.4 Choice of software . . . 29
  - 2.2.5 Use of Monte Carlo simulations . . . 30
- 2.3 Effect of tolerance on recurrence . . . 32
  - 2.3.1 Tolerance of $\pm 0.1\,\%$ . . . 33
  - 2.3.2 Tolerance of $\pm 1\,\%$ . . . 34
  - 2.3.3 Tolerance of $\pm 5\,\%$ . . . 35
  - 2.3.4 Tolerance of $\pm 10\,\%$ . . . 36

2.4 Arrays with different number of oscillators 37
2.4.1 Different number of oscillators with 0 % tolerance 37
2.4.2 Different number of oscillators with ±5 % tolerance 37
2.5 Tolerance on linear versus nonlinear terms 40
2.6 Different nonlinear coupling strengths 42
2.6.1 Varying coupling strength with 0 % tolerance 42
2.6.2 Varying coupling strength with ±5 % tolerance 44
2.6.3 Increased coupling strength at various tolerances 44
2.6.4 Tolerance on linear versus nonlinear terms 47
2.7 Order of tolerances 49
2.7.1 Outlier 49
2.7.2 Sorted tolerance values 51
2.8 Effect of tolerance on superrecurrence 54
2.9 Numerical stability test 58
2.10 Summary 59

3 Asymmetric tolerances **61**
3.1 Effect of asymmetric tolerance on recurrence 62
3.1.1 Tolerance of ±0.1 % 64
3.1.2 Tolerance of ±1 % 64
3.1.3 Tolerance of ±5 % 65
3.1.4 Tolerance of ±10 % 66
3.2 Arrays with different number of oscillators 68
3.3 Tolerance on linear versus nonlinear terms 70
3.4 Different nonlinear coupling strengths 72
3.4.1 Varying coupling strength with ±5 % tolerance 72
3.4.2 Increased coupling strength at various tolerances 74
3.4.3 Tolerance on linear versus nonlinear terms 75
3.5 Order of tolerances 77
3.6 Effect of tolerance on superrecurrence 81
3.7 Other tolerance structures 83
3.7.1 Alternative tolerance structure A 84
3.7.2 Alternative tolerance structure B 86
3.7.3 Alternative tolerance structure C 88
3.7.4 Section summary 90
3.8 Summary 91

4 Damped systems **92**
4.1 Damping overview 93
4.2 Effect of damping on recurrence 95
4.2.1 Equivalent quality factor of 10 000 99
4.2.2 Equivalent quality factor of 1000 102
4.3 Different nonlinear coupling strengths 104
4.3.1 Equivalent quality factor of 10 000 and coupling strength of 0.8 104
4.3.2 Equivalent quality factor of 1000 and coupling strength of 0.8 105
4.4 Effect of tolerance combined with damping 106
4.4.1 Symmetric system 107
4.4.2 Asymmetric system 113
4.5 Summary 119

5 Designing a physical FPUT system **121**
5.1 Electro-Mechanical analogies 122
5.1.1 An analogy of the FPUT system 123
5.2 Circuit design 124
5.2.1 Basic resonator circuit 125
5.2.2 Initial condition 129
5.2.3 Scaling factor 130
5.3 Component selection 131
5.3.1 Operational Amplifier 131
5.3.2 Multiplier 132
5.3.3 Analogue Switch 133
5.3.4 Passive components 133
5.4 Circuit layout 136
5.5 Testing 138
5.5.1 Test setup 138
5.5.2 Individual circuit response 139
5.5.3 Coupled response 139
5.6 Summary 145

6 Conclusions and future work **147**
6.1 Discussion 148
6.1.1 Variability due to manufacturing tolerance 148
6.1.2 Energy loss due to damping 149
6.1.3 Practical systems 150
6.2 Conclusions 151
6.3 Future Work 152
6.3.1 Further explorations of imperfections 152
6.3.2 Further explorations of practical systems 155

References **157**

Appendices

A Matlab Code **163**

B Python Code **165**

C Full Monte Carlo results for the symmetric system **168**
C.1 Tolerance of ±0.1 % 169
C.2 Tolerance of ±1 % 174
C.3 Tolerance of ±5 % 179
C.4 Tolerance of ±10 % 184

D Full Monte Carlo results for the asymmetric system **189**
D.1 Tolerance of ±0.1 % 190
D.2 Tolerance of ±1 % 195
D.3 Tolerance of ±5 % 200
D.4 Tolerance of ±10 % 205

List of Figures

1 Introduction

1.1 A 1D system of masses coupled via nonlinear springs in a similar manner to that used by Fermi, Pasta, Ulam, and Tsingou in their numerical experiments. 3
1.2 The first four modes of vibration for a string with two fixed ends. . 5
1.3 The FPUT recurrence phenomenon in a 32 mass system with a nonlinear coupling strength of $\alpha = 0.25$ and boundary condition $x_0 = x_N = 0$. 9
1.4 The FPUT recurrence phenomenon in a 64 mass system with a nonlinear coupling strength of $\beta = 8$ and boundary condition $x_0 = x_N = 0$. 11
1.5 The FPUT recurrence phenomenon in a 32 mass system with a nonlinear coupling strength of $\alpha = 1.0$ and boundary condition $x_0 = x_N = 0$. 12
1.6 Longer simulation of a 16 mass system with a nonlinear coupling strength of $\alpha = 0.25$ showing the superrecurrence period. 14
1.7 Longer simulation of a 17 mass system with a nonlinear coupling strength of $\alpha = 0.25$ showing the superrecurrence period. 15

2 Tolerance

2.1 Repeating the original FPUT-α simulations with 32 oscillators and a coupling strength of $\alpha = 0.25$, and a change of boundary condition to $x_0 = x_{N+1} = 0$. 26
2.2 Simulation of a 1D FPUT-α array with 64 oscillators and a coupling strength of $\alpha = 0.25$. 27
2.3 Gaussian distribution showing a 6σ spread. 28
2.4 Plots showing the first energy mode for 100 simulations of a 1D FPUT-α array with 64 oscillators and a coupling strength of $\alpha = 0.25$ at a tolerance of $\pm 5\,\%$. 31
2.5 Plot showing the mean, minimum and maximum values of the first energy mode for 100 simulations of a 1D FPUT-α array with 64 oscillators and a coupling strength of $\alpha = 0.25$ at a tolerance of $\pm 5\,\%$. 32

2.6 Simulations of a 1D FPUT-α array with 64 oscillators and a coupling strength of $\alpha = 0.25$ showing examples of different recurrence patterns at a tolerance of $\pm 0.1\,\%$. 33
2.7 Simulations of a 1D FPUT-α array with 64 oscillators and a coupling strength of $\alpha = 0.25$ showing examples of different recurrence patterns at a tolerance of $\pm 1\,\%$. 34
2.8 Simulations of a 1D FPUT-α array with 64 oscillators and a coupling strength of $\alpha = 0.25$ showing examples of different recurrence patterns at a tolerance of $\pm 5\,\%$. 35
2.9 Simulations of a 1D FPUT-α array with 64 oscillators and a coupling strength of $\alpha = 0.25$ showing examples of different recurrence patterns at a tolerance of $\pm 10\,\%$. 36
2.10 Simulations of 1D FPUT-α arrays with different numbers of oscillators, $0\,\%$ tolerance and a coupling strength of $\alpha = 0.25$. 38
2.11 Simulations of 1D FPUT-α arrays with different numbers of oscillators and a coupling strength of $\alpha = 0.25$ at a tolerance of $\pm 5\,\%$ 39
2.12 Simulations of a 1D FPUT-α array with 64 oscillators and a coupling strength of $\alpha = 0.25$ at various tolerances, showing the effect of tolerance on different parts of the array. 41
2.13 Simulations of 1D FPUT-α arrays with 64 oscillators, $0\,\%$ tolerance and different coupling strengths. 43
2.14 Simulations of 1D FPUT-α arrays with 64 oscillators, a tolerance of $\pm 5\,\%$ and different coupling strengths. 45
2.15 Simulations of 1D FPUT-α arrays with 64 oscillators and a coupling strength of $\alpha = 0.8$ at various tolerances. 46
2.16 Simulations of a 1D FPUT-α array with 64 oscillators and a coupling strength of $\alpha = 0.8$ at various tolerances, showing the effect of tolerance on different parts of the array. 48
2.17 Simulations of a 1D FPUT-α array with 64 oscillators and a coupling strength of $\alpha = 0.25$ showing the effect of applying tolerance to a single array element in different positions along the chain. 50
2.18 Simulations of a 1D FPUT-α array with 64 oscillators and a coupling strength of $\alpha = 0.25$ at a tolerance of $\pm 5\,\%$. The same set of tolerance values as used for Figure 2.8(i) is used in each simulation. However, a different method of sorting the values is used in each sub-figure. . 52
2.19 Simulations of a 1D FPUT-α array with 64 oscillators and a coupling strength of $\alpha = 0.25$ at a tolerance of $\pm 5\,\%$. Here, the ramp method of sorting is applied to remaining sets of tolerance values used in Figure 2.8. 53

2.20 Plot showing the mean, minimum and maximum values of the first energy mode for 100 simulations of a 1D FPUT-α array with 64 oscillators and a coupling strength of $\alpha = 0.25$ at a tolerance of $\pm 5\,\%$. These are shown for the tolerance values in a random order and sorted into a ramp format. 54
2.21 Longer simulations of a 1D FPUT-α array with 64 oscillators and $\alpha = 0.25$ showing the difference in superrecurrence between an array with $0\,\%$ tolerance and an array with a tolerance of $\pm 5\,\%$. 55
2.22 Simulations of a 1D FPUT-α array with 16 oscillators and a coupling strength of $\alpha = 0.25$ showing examples of recurrence at various tolerances. 56
2.23 Longer simulations of a 1D FPUT-α array with 16 oscillators and a coupling strength of $\alpha = 0.25$ showing the change in superrecurrence at various tolerances. 57
2.24 Comparison of the initial condition with the output from a time-reversed simulation for the system in Figure 2.7(i). 58
2.25 Absolute error between the initial condition and the result of time-reversed simulation for the system in Figure 2.7(i). 59

3 Asymmetric tolerances

3.1 Block diagram showing the elements used to form the FPUT equation and the associated tolerances for Equation (3.1). Here x_a, x_b and x_c represent any 3 elements in a longer chain. 63
3.2 Simulations of a 1D FPUT-α array with asymmetric tolerances, 64 oscillators, and a coupling strength of $\alpha = 0.25$ showing examples of different recurrence patterns at a tolerance of $\pm 0.1\,\%$. 64
3.3 Simulations of a 1D FPUT-α array with asymmetric tolerances, 64 oscillators, and a coupling strength of $\alpha = 0.25$ showing examples of different recurrence patterns at a tolerance of $\pm 1\,\%$. 65
3.4 Simulations of a 1D FPUT-α array with asymmetric tolerances, 64 oscillators, and a coupling strength of $\alpha = 0.25$ showing examples of different recurrence patterns at a tolerance of $\pm 5\,\%$. 66
3.5 Simulations of a 1D FPUT-α array with asymmetric tolerances, 64 oscillators, and a coupling strength of $\alpha = 0.25$ showing examples of different recurrence patterns at a tolerance of $\pm 10\,\%$. 67
3.6 Simulations of asymmetric 1D FPUT-α arrays with different numbers of oscillators and a coupling strength of $\alpha = 0.25$ at a tolerance of $\pm 5\,\%$. 69

3.7 Simulations of asymmetric 1D FPUT-α arrays with 64 oscillators and a coupling strength of $\alpha = 0.25$ at various tolerances, showing the effect of tolerance on different parts of the array. 71
3.8 Simulations of asymmetric 1D FPUT-α arrays with 64 oscillators, a tolerance of $\pm 5\,\%$ and different coupling strengths. 73
3.9 Simulations of asymmetric 1D FPUT-α arrays with 64 oscillators and a coupling strength of $\alpha = 0.8$ at various tolerances. 74
3.10 Simulations of asymmetric 1D FPUT-α arrays with 64 oscillators and a coupling strength of $\alpha = 0.8$ at various tolerances, showing the effect of tolerance on different parts of the array. 76
3.11 Simulations of an asymmetric 1D FPUT-α array with 64 oscillators and a coupling strength of $\alpha = 0.25$ at a tolerance of $\pm 5\,\%$. The same set of tolerance values as used for Figure 3.4(i) is used in each simulation. However, a different method of sorting the values is used in each sub-figure. 78
3.12 Simulations of an asymmetric 1D FPUT-α array with 64 oscillators and a coupling strength of $\alpha = 0.25$ at a tolerance of $\pm 5\,\%$. Here, the ramp method of sorting is applied to remaining sets of tolerance values used in Figure 3.4. 79
3.13 Plot showing the mean, minimum and maximum values of the first energy mode for 100 simulations of an asymmetric 1D FPUT-α array with 64 oscillators and a coupling strength of $\alpha = 0.25$ at a tolerance of $\pm 5\,\%$. These are shown for the tolerance values in a random order and sorted into a ramp format. 80
3.14 Simulations of an asymmetric 1D FPUT-α array with 16 oscillators and a coupling strength of $\alpha = 0.25$ showing examples of recurrence at various tolerances. 81
3.15 Longer simulations of an asymmetric 1D FPUT-α array with 16 oscillators and a coupling strength of $\alpha = 0.25$ showing the change in superrecurrence at various tolerances. 82
3.16 Block diagram showing the elements used to form the FPUT equation and the associated tolerances for Equation (3.2). Here x_a, x_b and x_c represent any 3 elements in a longer chain. 84
3.17 Simulations of an asymmetric 1D FPUT-α array with 64 oscillators and a coupling strength of $\alpha = 0.25$ at various tolerances, showing the effect of tolerance on different parts of the array for a system with a single tolerance on the forward linear coupling term and a single tolerance on the backward linear coupling term. 85

3.18 Block diagram showing the elements used to form the FPUT equation and the associated tolerances for Equation (3.3). Here x_a, x_b and x_c represent any 3 elements in a longer chain. 86
3.19 Simulations of an asymmetric 1D FPUT-α array with 64 oscillators and a coupling strength of $\alpha = 0.25$ at various tolerances, showing the effect of tolerance on different parts of the array for a system with separate tolerances on the forward linear coupling components and separate tolerances on the backward linear coupling components. 87
3.20 Block diagram showing the elements used to form the FPUT equation and the associated tolerances for Equation (3.4). Here x_a, x_b and x_c represent any 3 elements in a longer chain. 88
3.21 Simulations of an asymmetric 1D FPUT-α array with 64 oscillators and a coupling strength of $\alpha = 0.25$ at various tolerances, showing the effect of tolerance on different parts of the array for a system with separate tolerances on all the forward and backward linear and nonlinear coupling components. 89

4 Damped systems

4.1 The effect of different damping ratios on a second-order system. . . 94
4.2 Simulations of 1D FPUT-α arrays with 16 oscillators, no damping, a coupling strength of $\alpha = 0.25$ and various amplitudes for the displacement initial condition. 97
4.3 Simulations of 1D FPUT-α arrays with different numbers of oscillators, a quality factor of $Q = 10\,000$, and a coupling strength of $\alpha = 0.25$ showing the decay of energy over time. 100
4.4 Simulations of 1D FPUT-α arrays with different numbers of oscillators, a quality factor of $Q = 10\,000$, and a coupling strength of $\alpha = 0.25$. 102
4.5 Simulations of 1D FPUT-α arrays with different numbers of oscillators, a quality factor of $Q = 1000$, and a coupling strength of $\alpha = 0.25$ showing the decay of energy over time. 103
4.6 Simulations of 1D FPUT-α arrays with different numbers of oscillators, a quality factor of $Q = 10\,000$, and a coupling strength of $\alpha = 0.8$. 105
4.7 Simulations of 1D FPUT-α arrays with different numbers of oscillators, a quality factor of $Q = 1000$, and a coupling strength of $\alpha = 0.8$. 106
4.8 Simulations of 1D FPUT-α arrays with 16 oscillators, no damping, and a coupling strength $\alpha = 0.25$ at various tolerances. 108

4.9 Simulations of 1D FPUT-α arrays with 16 oscillators, a quality factor of $Q = 10\,000$, and a coupling strength of $\alpha = 0.25$ at various tolerances. 109
4.10 Simulations of 1D FPUT-α arrays with 16 oscillators, a quality factor of $Q = 1000$, and a coupling strength of $\alpha = 0.25$ at various tolerances. 110
4.11 Simulations of 1D FPUT-α arrays with 16 oscillators, no damping, and a coupling strength of $\alpha = 0.8$ at various tolerances. 111
4.12 Simulations of 1D FPUT-α arrays with 16 oscillators, a quality factor of $Q = 10\,000$, and a coupling strength of $\alpha = 0.8$ at various tolerances. 112
4.13 Simulations of 1D FPUT-α arrays with 16 oscillators, a quality factor of $Q = 1000$, and a coupling strength of $\alpha = 0.8$ at various tolerances. 113
4.14 Simulations of asymmetric 1D FPUT-α arrays with 16 oscillators, no damping, and a coupling strength of $\alpha = 0.25$ at various tolerances. 114
4.15 Simulations of asymmetric 1D FPUT-α arrays with 16 oscillators, a quality factor of $Q = 10\,000$, and a coupling strength of $\alpha = 0.25$ at various tolerances. 115
4.16 Simulations of asymmetric 1D FPUT-α arrays with 16 oscillators, a quality factor of $Q = 1000$, and a coupling strength of $\alpha = 0.25$ at various tolerances. 116
4.17 Simulations of asymmetric 1D FPUT-α arrays with 16 oscillators, no damping, and a coupling strength of $\alpha = 0.8$ at various tolerances. 117
4.18 Simulations of asymmetric 1D FPUT-α arrays with 16 oscillators, a quality factor of $Q = 10\,000$, and a coupling strength of $\alpha = 0.8$ at various tolerances. 118
4.19 Simulations of asymmetric 1D FPUT-α arrays with 16 oscillators, a quality factor of $Q = 1000$, and a coupling strength of $\alpha = 0.8$ at various tolerances. 119

5 Designing a physical FPUT system

5.1 Electrical analogies of the mechanical damped mass-spring system. . 124
5.2 Schematic diagram of a Tow–Thomas biquad filter circuit. 126
5.3 Schematic diagram for a single resonator module designed to form part of a coupled resonator circuit. 127
5.4 Schematic diagram for a single resonator module with provision to apply an initial condition. 129
5.5 A PCB for a single resonator circuit module. 137
5.6 Experimental results for four coupled resonator circuit modules with no damping. 140
5.7 Comparison of experimental circuit results and simulation results for four coupled resonators with no damping. 141

5.8 Experimental results for four coupled resonator circuit modules with a damping resistance of $R_3 = 16\,\mathrm{M\Omega}$. 142
5.9 Detailed view of the circuit response immediately after the system is released from rest with the energy in the initial condition of the first mode. The system comprises four coupled resonator circuits with a damping resistance of $R_3 = 16\,\mathrm{M\Omega}$. 142
5.10 Experimental results for four coupled resonator circuit modules with a damping resistance of $R_3 = 4\,\mathrm{M\Omega}$. 143
5.11 Detailed sections of the energy plot in Figure 5.10(ii) showing the circuit response at key points. The system comprises four coupled resonator circuits with a damping resistance of $R_3 = 4\,\mathrm{M\Omega}$. 144
5.12 Experimental results for four coupled resonator circuit modules with a damping resistance of $R_3 = 1\,\mathrm{M\Omega}$. 145
5.13 Comparison of experimental circuit results and simulation results for four coupled resonators with a damping resistance of $R_3 = 1\,\mathrm{M\Omega}$. . 145

C.1 Full set of 100 Monte Carlo simulations of 1D FPUT-α arrays with 64 oscillators and a coupling strength of $\alpha = 0.25$ at a tolerance of $\pm 0.1\,\%$. 170
C.2 Full set of 100 Monte Carlo simulations of 1D FPUT-α arrays with 64 oscillators and a coupling strength of $\alpha = 0.25$ at a tolerance of $\pm 1\,\%$. 175
C.3 Full set of 100 Monte Carlo simulations of 1D FPUT-α arrays with 64 oscillators and a coupling strength of $\alpha = 0.25$ at a tolerance of $\pm 5\,\%$. 180
C.4 Full set of 100 Monte Carlo simulations of 1D FPUT-α arrays with 64 oscillators and a coupling strength of $\alpha = 0.25$ at a tolerance of $\pm 10\,\%$. 185

D.1 Full set of 100 Monte Carlo simulations of asymmetric 1D FPUT-α arrays with 64 oscillators and a coupling strength of $\alpha = 0.25$ at a tolerance of $\pm 0.1\,\%$. 191
D.2 Full set of 100 Monte Carlo simulations of asymmetric 1D FPUT-α arrays with 64 oscillators and a coupling strength of $\alpha = 0.25$ at a tolerance of $\pm 1\,\%$. 196
D.3 Full set of 100 Monte Carlo simulations of asymmetric 1D FPUT-α arrays with 64 oscillators and a coupling strength of $\alpha = 0.25$ at a tolerance of $\pm 5\,\%$. 201
D.4 Full set of 100 Monte Carlo simulations of asymmetric 1D FPUT-α arrays with 64 oscillators and a coupling strength of $\alpha = 0.25$ at a tolerance of $\pm 10\,\%$. 206

List of Tables

2.1 Quality of recurrence for different tolerances applied to different parts of the array in a system with 64 oscillators and a coupling strength of $\alpha = 0.25$. 42

4.1 Time period of a single recurrence cycle for a given value of N . . . 99

5.1 Electro-Mechanical Analogies 123
5.2 Selected passive component values 134
5.3 Calculated passive component values 135
5.4 Desired vs design values 135
5.5 Measured natural frequencies of the oscillator circuits 139

List of Publications

Journal articles:

H. Nelson, M. A. Porter, and B. Choubey, "Variability in Fermi-Pasta-Ulam-Tsingou arrays can prevent recurrences", *Physical Review E*, vol. 98, no. 6, p. 062 210, Dec. 2018

Conferences:

H. Nelson and B. Choubey, "On the Effect of Variability and Chain Length on Fermi, Pasta and Ulam Matrices", in *2nd IMA Conference on Nonlinearity and Coherent Structures*, Norwich, Jun. 2017

H. Nelson, "Variability in Fermi, Pasta and Ulam Lattices", in *Dynamics Days Europe 2018*, Loughborough, Sep. 2018

1 Introduction

Contents

1.1 Nonlinear systems 2
1.2 The Fermi–Pasta–Ulam–Tsingou phenomenon 2
1.2.1 The FPUT-α model: quadratic nonlinearity 4
1.2.2 The FPUT-β model: cubic nonlinearity 10
1.2.3 Other nonlinearities 11
1.2.4 Different nonlinear coupling strength 12
1.2.5 Different initial conditions 13
1.3 Superrecurrence 13
1.4 Relevance of the FPUT phenomenon today 16
1.5 Engineering motivation 17
1.6 Physical realisation of the FPUT-α model 18
1.7 Thesis overview 19

Nonlinearity is a field which has intrigued mathematicians, scientists and engineers for decades, and there is a vast amount of literature available. The majority of real, physical systems are inherently nonlinear [4] and with the constant evolution of technology, and in particular continuing reductions in feature size of electronic devices [5], nonlinearity is becoming more prevalent.

Whilst there have been considerable numbers of studies regarding real, physical systems, a portion of the work on nonlinearity relates purely to ideal theoretical systems. This theoretical work can still offer significant insight for practical systems,

although additional work must be undertaken to understand the limitations a physical system will bring. For example, numerical experiments are often run on ideal systems which are homogeneous whereas real systems are heterogeneous due to manufacturing limitations. Additionally, numerical experiments on ideal systems do not consider factors such as damping and parasitic noise which are often inherent in physical systems. This thesis explores the effects of some of these imperfections in one such theoretical system.

1.1 Nonlinear systems

A system is said to be linear when it complies with the principles of superposition and scalability, i.e. if inputs u_1 and u_2 result in outputs of y_1 and y_2 respectively, then an input of $a_1u_1 + a_2u_2$ results in an output of $a_1y_1 + a_2y_2$ [4]. A nonlinear system is any system not governed by the principle of superposition.

One of the earliest nonlinear systems to be investigated with digital computer simulations was the simple nonlinear problem that led to the discovery of a surprising result — the Fermi–Pasta–Ulam–Tsingou phenomenon — which sparked a whole series of discoveries whilst attempting to explain the results. This simple problem provides a basis from which to investigate the effects of imperfections found in physical systems on ideal nonlinear equations.

1.2 The Fermi–Pasta–Ulam–Tsingou phenomenon

A simple nonlinear problem is that of a one-dimensional (1D) continuum with fixed ends and forces acting on the elements of this string. The forces acting on the elements contain higher-order terms in addition to a linear term. For simulation purposes a finite number of differential equations is required. Therefore, the continuum is discretised into a system of particles coupled to their nearest neighbours through a nonlinear interaction.

This problem formed the basis for one of the first sets of numerical experiments into nonlinear dynamics [6]. These computer simulations were carried out on the

MANIAC I computer at the Los Alamos Scientific Laboratory by Enrico Fermi, John Pasta, Stanislaw Ulam, and Mary Tsingou. The results of the numerical experiments were detailed in a technical report published in May 1955 [7]. Mary Tsingou was not listed on the original report as an author but was listed as having carried out some of the work. As such, the problem initially became known as the FPU phenomenon. In 2008, *Physics Today* featured an article in which Dauxois details Tsingou's role in coding the problem and producing some of the figures in the paper. In the article, he seeks to acknowledge her contribution going forward, hence what was originally known as the FPU phenomenon has become the FPUT phenomenon [8].

A representation of the dynamical system used for the FPUT experiments is shown in Figure 1.1. The particles are shown as masses which can only move in one dimension, the coupling forces are represented by springs which have both a linear and nonlinear element, and the chain is fixed at both ends.

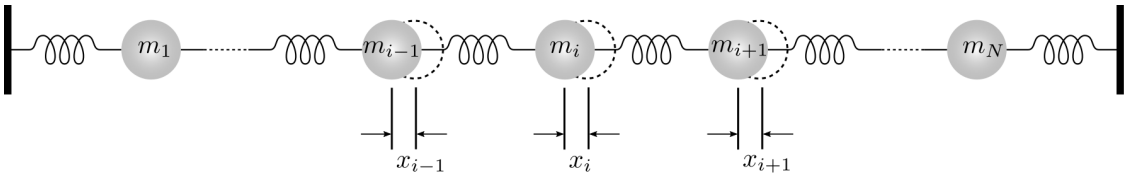


Figure 1.1: A 1D system of masses coupled via nonlinear springs in a similar manner to that used by Fermi, Pasta, Ulam, and Tsingou in their numerical experiments.

For a spring which operates under a purely linear law, the energy in a single 'normal' mode always remains in that mode. However, with a nonlinear spring, Fermi *et al.* expected that the nonlinear coupling would lead to equipartition of energy. That is, they expected that the energy introduced into the lowest frequency mode should have slowly distributed to the other modes until the energy was shared equally between the modes.

Their early simulations suggested that this was indeed the case, until one day, by accident, they left their simulation running for longer [7]. When they returned to the simulation, they noticed that the system had remained in the near equipartition state for a while before departing from it and almost all the energy was back in the initial mode. This phenomenon constitutes a 'recurrence' of energy between modes.

Fermi, Pasta, Ulam, and Tsingou studied three different types of nonlinearity, quadratic (the FPUT-α model), cubic (the FPUT-β model), and broken linear, demonstrating recurrence in all three cases [7]. Such 'FPUT recurrences' have been the subject of much research in the past half century, and the FPUT numerical experiments have led to a wealth of work on recurrences, nonlinear lattice systems, and other prominent topics [6], [8]–[15].

1.2.1 The FPUT-α model: quadratic nonlinearity

For a mass in the system shown in Figure 1.1, its motion is governed by the forces exerted on the springs to either side. For small displacements, this is purely linear and the forces acting on the mass can be described as:

$$F_{i+\frac{1}{2}} = k(x_{i+1} - x_i - d) \tag{1.1a}$$

$$F_{i-\frac{1}{2}} = k(x_i - x_{i-1} - d) \tag{1.1b}$$

where $F_{i+\frac{1}{2}}$ is the force between masses m_i and m_{i+1}, $F_{i-\frac{1}{2}}$ is the force between masses m_i and m_{i-1}, x_i is the movement of the i^{th} mass m_i (with $i \in \{1, \ldots, N-1\}$ and N is the number of masses in the chain), d the natural length of the spring and k the spring constant. It has also been assumed that the spring constant for all the springs is identical. This gives a net force acting on the mass of:

$$F = F_{i+\frac{1}{2}} - F_{i-\frac{1}{2}} \tag{1.2a}$$

$$= k(x_{i+1} - x_i - d) - k(x_i - x_{i-1} - d) \tag{1.2b}$$

$$= k(x_{i+1} + x_{i-1} - 2x_i) \tag{1.2c}$$

The equation of motion of the mass can be described using Newton's second law:

$$m_i \ddot{x}_i = k(x_{i+1} + x_{i-1} - 2x_i) \tag{1.3}$$

For larger displacements, behaviour of the spring may become nonlinear. The simplest form of this is a quadratic nonlinearity which can be added to the force term as follows:

$$F_{i+\frac{1}{2}} = k(x_{i+1} - x_i - d) + \alpha(x_{i+1} - x_i)^2 \tag{1.4a}$$

$$F_{i-\frac{1}{2}} = k(x_i - x_{i-1} - d) + \alpha(x_i - x_{i-1})^2 \tag{1.4b}$$

Using the nonlinear force and normalising for mass, the equation of motion then becomes:

$$\ddot{x}_i = \frac{k}{m_i}((x_{i+1} + x_{i-1} - 2x_i) + \alpha[(x_{i+1} - x_i)^2 - (x_i - x_{i-1})^2]) \tag{1.5}$$

or if the mass and spring constant are taken to be $m_i = k = 1$, then:

$$\ddot{x}_i = (x_{i+1} + x_{i-1} - 2x_i) + \alpha[(x_{i+1} - x_i)^2 - (x_i - x_{i-1})^2] \tag{1.6}$$

which is the first equation simulated by Fermi, Pasta, Ulam and Tsingou. This equation will be referred to as the FPUT-α system.

When conducting their numerical experiments, Fermi *et al.* fixed the ends of the chain so that $x_0 = x_N = 0$. They also used a simple initial condition whereby the string was started at rest with all of the energy in the first mode of the linear system, i.e. if one visualises the mass-spring system, the centre experiences the most deflection and this progressively decreases to the ends. The first four modes of vibration for a string with fixed ends are shown in Figure 1.2.

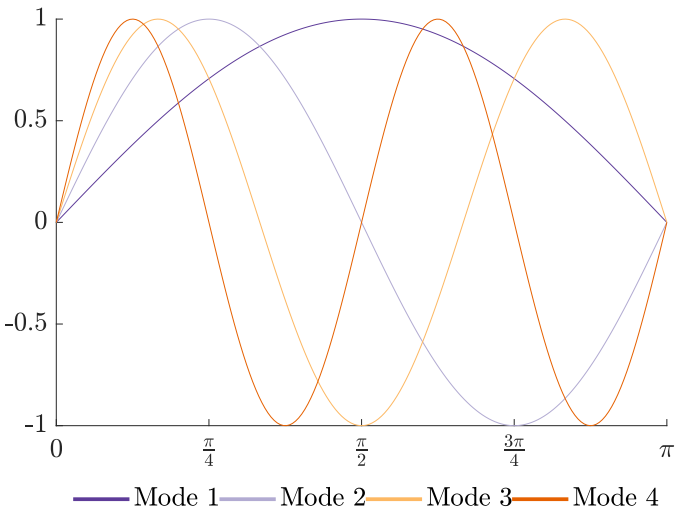


Figure 1.2: The first four modes of vibration for a string with two fixed ends.

Determining the modes of a linear system

The modes of a linear system can be determined by finding the eigenvectors and eigenvalues of the system. The set of equations described by Equation (1.3), can be rewritten in matrix form as

$$\mathbf{M}\ddot{\mathbf{x}} = \mathbf{K}\mathbf{x} \tag{1.7}$$

where $\mathbf{x}$ is a column vector for all values of x_i. The mass matrix $\mathbf{M}$ is given by

$$\mathbf{M} = \begin{bmatrix} m & 0 & 0 & 0 & \dots & 0 & 0 \\ 0 & m & 0 & 0 & \dots & 0 & 0 \\ 0 & 0 & m & 0 & \dots & 0 & 0 \\ \vdots & \vdots & \vdots & \vdots & \ddots & \vdots & \vdots \\ 0 & 0 & 0 & 0 & \dots & 0 & m \end{bmatrix} = m \begin{bmatrix} 1 & 0 & 0 & 0 & \dots & 0 & 0 \\ 0 & 1 & 0 & 0 & \dots & 0 & 0 \\ 0 & 0 & 1 & 0 & \dots & 0 & 0 \\ \vdots & \vdots & \vdots & \vdots & \ddots & \vdots & \vdots \\ 0 & 0 & 0 & 0 & \dots & 0 & 1 \end{bmatrix} = m\mathbf{I_n} \tag{1.8}$$

where $\mathbf{I_n}$ is the identity matrix. The tridiagonal stiffness matrix $\mathbf{K}$ is

$$\mathbf{K} = \begin{bmatrix} 2k & -k & 0 & 0 & \dots & 0 & 0 \\ -k & 2k & -k & 0 & \dots & 0 & 0 \\ 0 & -k & 2k & -k & \dots & 0 & 0 \\ \vdots & \vdots & \vdots & \vdots & \ddots & \vdots & \vdots \\ 0 & 0 & 0 & 0 & \dots & -k & 2k \end{bmatrix} \tag{1.9}$$

Since a linear system of this type will give oscillatory behaviour, solutions of the form $x_i(t) = A_i e^{j(\omega t+\phi)}$ can be substituted. The $e^{j(\omega t+\phi)}$ component cancels out and after rearranging the equation becomes

$$[\mathbf{K}m^{-1} - \omega^2\mathbf{I_n}]\mathbf{A} = \mathbf{0} \tag{1.10}$$

which is of the form $[\mathbf{S_n} - \lambda\mathbf{I_n}]\mathbf{A} = \mathbf{0}$ where $\mathbf{S_n}$ is the system matrix, $\mathbf{I_n}$ is the identity matrix, and $\mathbf{0}$ is the zero vector.

For Equation (1.10), a non-zero value for $\mathbf{A}$ can only be obtained if the determinant of the matrix $[\mathbf{S_n} - \lambda\mathbf{I_n}]$ is zero, i.e.

$$\left|\mathbf{K}m^{-1} - \omega^2\mathbf{I_n}\right| = 0 \tag{1.11}$$

For a mass spring system consisting of 3 masses with fixed ends, i.e. $N = 4$, using the mass and stiffness matrices defined by Equations 1.8 and 1.9 and taking $m = k = 1$

and $\lambda = \omega^2$, this produces a 3x3 matrix so that

$$\begin{aligned}\begin{vmatrix} 2-\lambda & -1 & 0 \\ -1 & 2-\lambda & -1 \\ 0 & -1 & 2-\lambda \end{vmatrix} &= (2-\lambda)((2-\lambda)^2 - 1) - (2-\lambda) \\ &= (2-\lambda)(\lambda^2 - 4\lambda + 2)\end{aligned} \tag{1.12}$$

giving eigenvalues of $\lambda = 2, 2 \pm \sqrt{2}$ and therefore resonant frequencies, or modes, of $\omega_1 = \sqrt{2-\sqrt{2}}$, $\omega_2 = \sqrt{2}$ and $\omega_3 = \sqrt{2+\sqrt{2}}$.

Determining the initial condition

Returning to the solution $x_i(t) = A_i e^{j(\omega t+\phi)}$ and assuming that the complex amplitude A_i is of the form $A_i = Ae^{j(i\theta)}$ then the solution becomes

$$x_i(t) = Ae^{j(\omega t+\phi)}e^{j(i\theta)} \tag{1.13}$$

where ϕ and θ are constants that can be obtained using the boundary conditions $x_0 = x_N = 0$. Using the first boundary condition, the following is obtained

$$0 = Ae^{j(\omega t+\phi)} \tag{1.14}$$

and taking the real part leads to $\phi = \frac{\pi}{2}$. The second boundary condition gives

$$0 = Ae^{j(\omega t+\frac{\pi}{2})}e^{j(N\theta)} \tag{1.15}$$

and taking the real part leads to the condition

$$0 = \sin(N\theta) \tag{1.16}$$

which is satisfied by

$$\theta = \frac{n\pi}{N} \tag{1.17}$$

where n denotes the mode.

Expanding Equation (1.13) using Euler's formula gives

$$x_i(t) = A(\cos(\omega t+\phi) + j\sin(\omega t+\phi))(\cos(\theta) + i\sin\theta) \tag{1.18}$$

and taking the real part becomes

$$x_i(t) = A(\cos(\omega t + \phi)\cos(\theta) + \sin(\omega t + \phi)\sin\theta) \tag{1.19a}$$

$$= A\cos(\omega t + \phi - \theta) \tag{1.19b}$$

$$= A\cos\left(\omega t + \frac{\pi i}{N} - \frac{\pi}{2}\right) \tag{1.19c}$$

$$= A\sin\left(\omega t + \frac{\pi i}{N}\right) \tag{1.19d}$$

Evaluating for an initial condition where all the energy is in the first mode with an amplitude $A = 1$ and the system starts from rest, this initial condition can be described by the following equations for displacement and velocity:

$$x_i = \sin\left(\frac{\pi i}{N}\right) \tag{1.20a}$$

$$\dot{x}_i = 0 \tag{1.20b}$$

where $i \in \{1, \ldots, N-1\}$.

FPUT recurrence

Simulating the FPUT-α equation with the initial condition of the first mode and analysing the results in the Fourier domain shows that, with time, the energy in the first mode starts to dissipate into the higher modes. However, after a further period of time, the energy returns to its initial condition with little loss (approximately 3 %). This effect is the FPUT 'recurrence' and the time taken for the energy to return to the first mode is referred to as the 'recurrence period'.

Figure 1.3 shows a MATLAB simulation depicting the recurrence phenomenon for a chain of 32 masses using the code published by Dauxois *et al.* [16]. Initially the energy is only in the first mode, shown in dark purple. With time, this dissipates into higher modes. Under equipartition, one would have expected complete dissipation amongst all modes. However, one can observe that by 151 time units the energy has returned to the first mode.

If the results in Figure 1.3 are compared to the original FPUT report, it can be observed that whilst the shape of the energy plot is the same, the scaling on the axes is in different units and Figure 1.3 shows fewer modes. Fermi *et al.* plotted

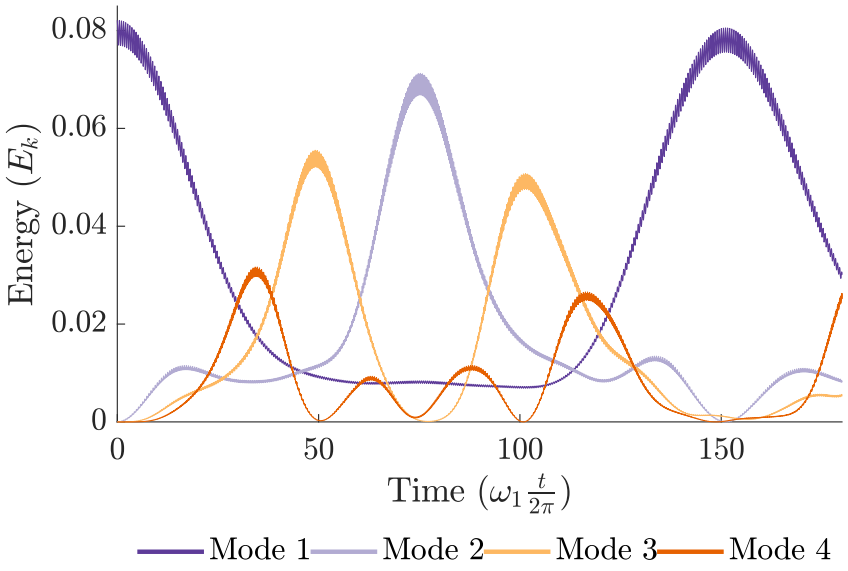


Figure 1.3: The FPUT recurrence phenomenon in a 32 mass system with a nonlinear coupling strength of $\alpha = 0.25$ and boundary condition $x_0 = x_N = 0$.

the energy in arbitrary units against the number of computational cycles. However, the code written by Dauxois *et al.* plots the total energy for each mode E_k against the number of periods of the first mode ($k = 1$), i.e. $\omega_1 \frac{t}{2\pi}$.

Here, the mode energy E_k is the sum of the kinetic and potential energies for each mode as represented by the linear forces only and given by

$$E_k = \frac{1}{2}(\dot{A}_k^2 + {\omega_k}^2 {A_k}^2) \tag{1.21}$$

where the normal mode co-ordinates A_k are

$$A_k = \sqrt{\frac{2}{N+1}} \sum_{i=1}^{N} x_i(t) sin \frac{ik\pi}{N+1} \tag{1.22}$$

and the normal mode frequencies ω_k are

$$\omega_k = 2sin\left(\frac{k\pi}{2(N+1)}\right) \tag{1.23}$$

The original paper plotted modes 1 to 5, with modes 6 to 32 gaining no more than 20 of their arbitrary energy units for the simulation, compared with 300 energy units for mode 1. This is equivalent to a maximum of 0.0122 of the energy units in Figure 1.3. This thesis continues with the units used by Dauxois *et al.* as they are independent of the time step used for the simulations, and restricts

plots to modes 1 to 4 for clarity of figures. This reduction in modes does not remove any data which would add a significant contribution to understanding the focus of the work in this thesis.

1.2.2 The FPUT-β model: cubic nonlinearity

A quadratic term is the simplest form of nonlinearity which can be added to the equation of motion for a mass-spring chain. However, higher order terms also produce nonlinearity. Fermi, Pasta, Ulam, and Tsingou considered a cubic nonlinearity which formed the FPUT-β equation:

$$\ddot{x}_i = (x_{i+1} + x_{i-1} - 2x_i) + \beta[(x_{i+1} - x_i)^3 - (x_i - x_{i-1})^3] \tag{1.24}$$

where β is the nonlinear coupling strength [7]. Springs with this type of nonlinearity are not readily available [17]. However, this type of nonlinearity could be generated in other types of system.

The result of simulating Equation (1.24) with 64 elements in the chain and a coupling strength β of 8 can be seen in Figure 1.4. This result is similar to the FPUT-α model, in that the energy initially transferred from the first mode to higher modes before returning to the first mode. However, in contrast to the quadratic force, the energy only transfers between the odd modes as the cubic force preserves the odd symmetry of the function and therefore maintains the symmetry of the mass-spring chain around its centre. The energy shift between the higher modes is not as pronounced as for the FPUT-α model, with the majority of the energy entering mode 3 and only a small amount reaching modes 5 and 7.

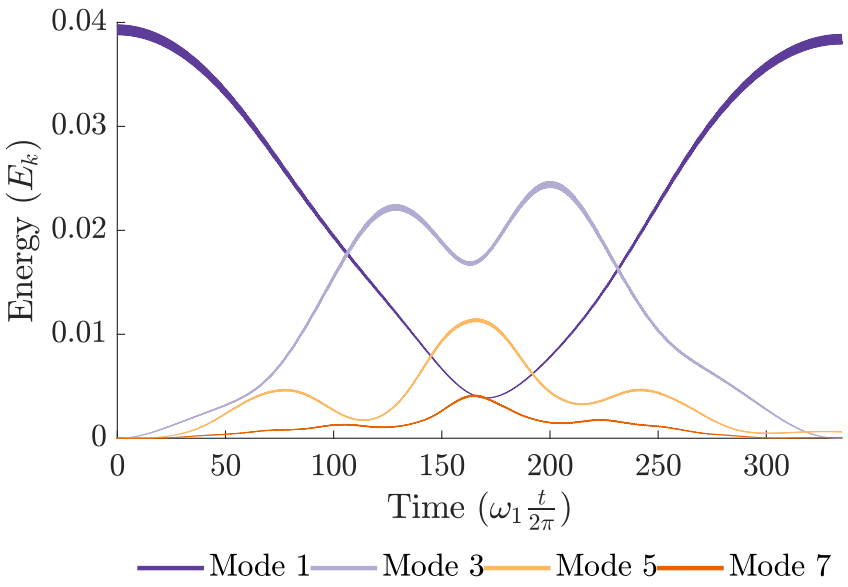


Figure 1.4: The FPUT recurrence phenomenon in a 64 mass system with a nonlinear coupling strength of $\beta = 8$ and boundary condition $x_0 = x_N = 0$.

1.2.3 Other nonlinearities

Although the FPUT-α and FPUT-β models are the two main types of system studied in the literature, other models for nonlinearity have shown recurrence of energy under the right conditions. In addition to the quadratic and cubic equations studied above, Fermi, Pasta, Ulam and Tsingou also considered a broken linear function. This took the form:

$$\ddot{x}_i = \delta_1(x_{i+1} - x_i) - \delta_2(x_i - x_{i-1}) + c \tag{1.25}$$

where δ_1, δ_2 and c are not constant [7]. To a limited extent, this broken linear function imitates the cubic nonlinearity and has been used to emulate the FPUT-β function [17].

Another system that has been studied is a combined α and β model described by the following equations of motion [12], [18], [19]:

$$\ddot{x}_i = (x_{i+1} + x_{i-1} - 2x_i) + \alpha[(x_{i+1} - x_i)^2 - (x_i - x_{i-1})^2] + \beta[(x_{i+1} - x_i)^3 - (x_i - x_{i-1})^3] \tag{1.26}$$

Multi dimensional FPUT lattices have also been of interest to some researchers who have shown that they exhibit similar exchanges of energy amongst a few select modes [20]–[22].

1.2.4 Different nonlinear coupling strength

The results presented for the FPUT-α model above use a weak value for the nonlinear coupling strength α of 0.25. Fermi, Pasta, Ulam and Tsingou also investigated the effect of a stronger quadratic term with a coupling strength of $\alpha = 1.0$, thereby increasing the level of nonlinearity in the system [7]. This results in a larger exchange of energy into modes 2 to 4 and a shorter recurrence period as shown in Figure 1.5.

This trend continues into the higher modes. For the stronger coupling strength of $\alpha = 1.0$, mode 9 receives a maximum energy of 0.0142 energy units. This is comparable to the 0.0122 received by mode 5 in the system with a coupling strength of $\alpha = 0.25$.

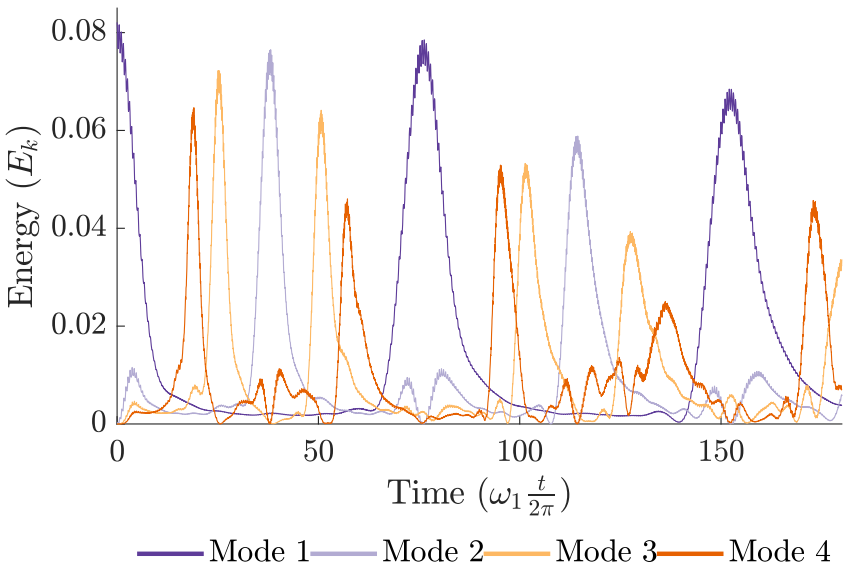


Figure 1.5: The FPUT recurrence phenomenon in a 32 mass system with a nonlinear coupling strength of $\alpha = 1.0$ and boundary condition $x_0 = x_N = 0$.

1.2.5 Different initial conditions

Alongside the initial condition of the first mode, Fermi, Pasta, Ulam and Tsingou also explored other types of initial condition: a saw-tooth triangular wave and combinations of low frequency modes, e.g. a split between modes 5 and 7. Over the intervening years, many other initial conditions have been studied [12], [20], [23]. One specific case has been termed the 'Anti-FPU problem' where energy is fed into the highest frequency modes as opposed to the lowest frequency modes chosen by Fermi, Pasta, Ulam and Tsingou [22], [24], [25].

Benettin, Livi, and Ponno have carried out further investigations into initial conditions and the impact of random versus coherent phase choices on achieving the metastable states required for FPUT recurrence. In their article, they also express concern over how relevant their results might be to physical systems as methods for producing the ideal initial conditions they explored are unclear [18].

The amplitude of the initial condition has also proven to be important. Initially suggested by Izrailev and Chirikov, the concept of a stochastic threshold above which motion is chaotic or disordered and below which the motion is ergodic has been found to exist [26]. Several years later, Fucito *et al.* first proposed what is now referred to as the 'metastability' state to describe the interactions occurring during FPUT recurrence [27]. This has led to the threshold also being referred to as the metastability threshold [28], [29]. Subsequent investigations have confirmed the existence of this threshold and expanded on the criterion that define it [12], [23], [30], although it is hard to extract a unified view from the different studies [19], [31], [32].

1.3 Superrecurrence

Over 60 years after the publication of the report by Fermi, Pasta, Ulam and Tsingou, the recurrence phenomenon they discovered is still not fully understood. Initially there was a great deal of scepticism about the results. The accuracy of the numerics was questioned [9] and there was doubt over whether the simulation time was long enough to observe equipartition [31], [33]. However, subsequent advances in

computer technology have allowed researchers to validate the results and it is now accepted that recurrence is not an artefact of the numerical experiments.

Whilst conducting further research into FPUT recurrence, several other discoveries have been made. One that is of particular interest was reported by James Tuck and Mary Menzel (née Tsingou) in 1972 [34]. Tuck and Menzel were motivated by speculation that the small energy reduction (approximately 3 %) in the return of energy to the first mode would just continue with subsequent peaks [33], eventually reducing the system to equipartition. As a result Tuck and Menzel performed simulations for much longer and to higher accuracies than those carried out in the early 1950s.

These numerical experiments not only demonstrated that the results of the original FPUT simulations were reproducible but that there was an additional 'superrecurrence' wherein the amount of energy which returned to the first mode initially decreased but then started to increase again, returning to within 1 % of the initial energy [34]. This effect can be observed in Figure 1.6 which shows the results for simulating a system with 16 masses and a coupling strength of 0.25. Here, the recurrence period is approximately 54 time units, and the superrecurrence period occurs over approximately 828 time units and 15 recurrence cycles.

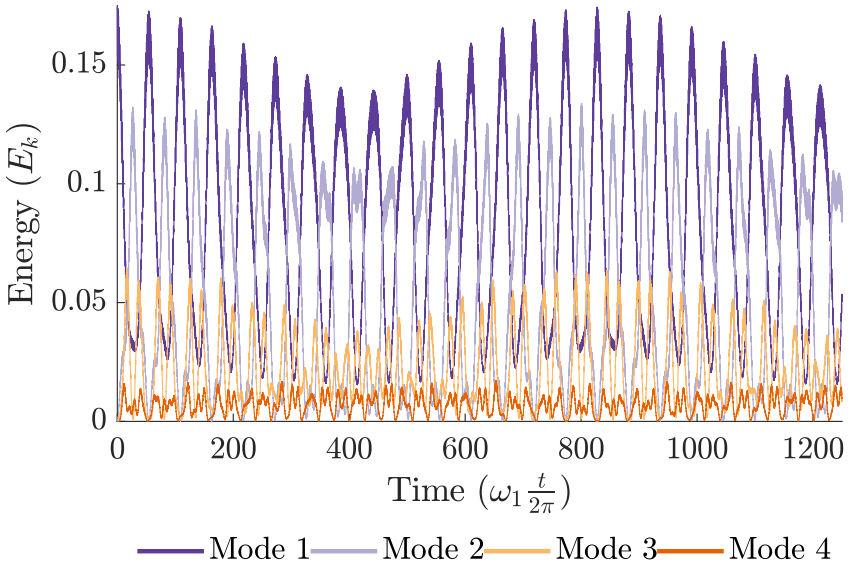


Figure 1.6: Longer simulation of a 16 mass system with a nonlinear coupling strength of $\alpha = 0.25$ showing the superrecurrence period.

Suspecting that this superrecurrence might be due to symmetry in the system, Tuck and Menzel also conducted a numerical experiment for a chain of 17 masses, making N prime [34]. These results are presented in Figure 1.7, where it can be seen that superrecurrence still occurs meaning it is not a result of symmetry. Observe that both the recurrence period and superrecurrence period have increased with the increased chain length. The recurrence period is now approximately 59 time units, and the superrecurrence period occurs over approximately 966 time units and 16 recurrence cycles.

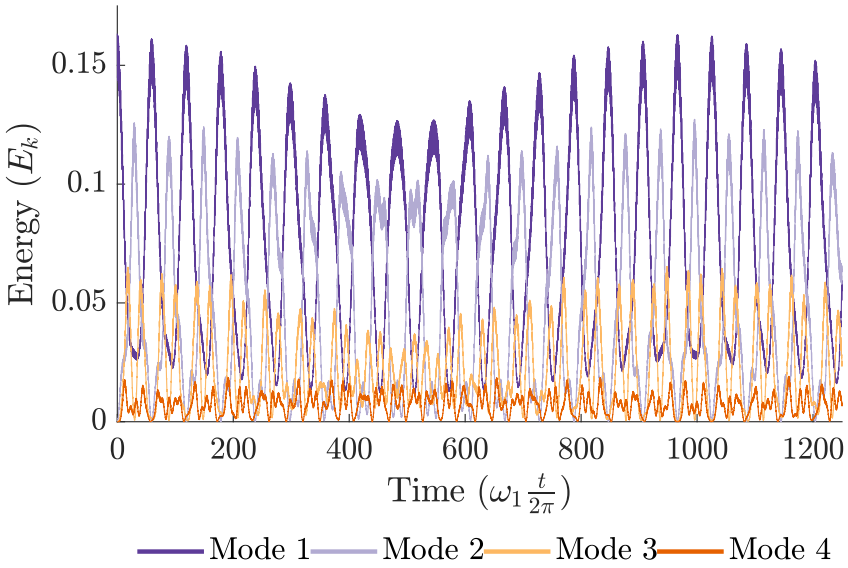


Figure 1.7: Longer simulation of a 17 mass system with a nonlinear coupling strength of $\alpha = 0.25$ showing the superrecurrence period.

These observations have subsequently been confirmed for the FPUT-α system by other researchers. These include Drago and Ridella, who also observed that the FPUT-β superrecurrences may be an artefact of numerical error [35]. Pace and Campbell have recently made similar observations, whilst also proving the existence of higher order superrecurrences or super-superrecurrences in the FPUT-α system [36].

1.4 Relevance of the FPUT phenomenon today

There is a growing need to study nonlinearity in physical systems due to the evolution of technology pushing more systems into the nonlinear realm. Despite the rich literature on theoretical results, relatively little has been reported experimentally, particularly with regard to the FPUT phenomenon. Some observations of recurrence have been made, predominately in optics [37]–[39], although evidence has also been shown under limited criteria in other media [17], [40], [41] and recently Midtvedt *et al.* proposed a NEMS graphene resonator system to explore Fermi–Pasta–Ulam physics [42].

It would be fair to say that, being the first numerical study to produce a previously unknown result, the FPUT phenomenon is the mother of computational nonlinear dynamics and has led to a large number of publications from the physics and applied mathematics community. Indeed, such is the importance of this problem to the community that the 50th Anniversary of the work saw a special issue of the journal *Chaos* [43] and at least three conferences dedicated to the problem [44]–[46]. Several reviews covering the history and progress of the problem have also been published [6], [9], [10], [14], [29], [31], [33], [47]. Additionally, researchers are still being challenged to find new approaches to the problem, for example Machado has recently suggested a fractional calculus approach [48], whilst Onorato *et al.* have used wave-wave interactions [11].

As such, an experimental setup validating the original paper would be highly beneficial to the nonlinear dynamics community. More importantly, however, it will enable the utilisation of rich behaviours observed in numerical simulations for sensing applications. For example, recurrence may lead to significant bandwidth reduction for large nonlinear sensor arrays as this has already been achieved with linear coupling [49]. Furthermore, MEMS systems, due to their increasing nonlinearity with shrinking size, stand to gain significantly from this rich literature leading to the design of enhanced sensitivity systems.

1.5 Engineering motivation

With the ever-increasing demand to make things smaller and lighter, miniaturised systems that combine mechanical and electronic structures are becoming commonplace. These Microelectromechanical systems (MEMS) are used in a wide variety of applications including automotive, medical, electronic, communication and defence. One field that is growing rapidly is the use of MEMS in sensing applications [50].

MEMS sensors have found applications in pressure sensing [51], mass sensing [49], material characterisation [52], acoustic imaging [53] and communications [54]. As with many other processes, improvements in fabrication technology means that MEMS are becoming smaller in size, making it possible to manufacture several transducers on a single substrate [53], [55]–[58]. Recent advances have pushed MEMS sensors to nanometre dimensions (NEMS) [59], [60]. This brings new challenges in accessing the transducers to be able to extract the data.

Traditionally, the transducers are accessed individually meaning that a large array will require a large number of connections. Greater numbers of transducers also lead to a significant increase in the amount of data being generated. Studies have been carried out into ways of limiting these requirements including compressed sensing [61] and reducing the number of transducers being used at a time by creating a synthetic aperture [62]–[64]. However, compressed sensing requires significant post-processing and most synthetic apertures produce less than optimal results. An alternative approach to reduce the data is to couple the transducers together, thereby requiring fewer access points. Coupling of transducers has been shown to lead to enhanced functionality and, more importantly, can result in fewer connections which is important in large arrays [65].

Studies into arrays of linear MEMS resonators with linear springs have already lead to very interesting results [65]. However, an inherent problem with the shrinkage in size of the MEMS devices is that it leads to nonlinearity, due to the driving force becoming very large relative to the surface area of the transducer [66]. Typically the coupling strength is smaller and weaker than the strength of the resonator. Hence, in coupled systems, the first thing to become nonlinear is the coupling spring [67].

1.6 Physical realisation of the FPUT-α model

Differential equations are often used to describe the behaviour of physical systems and, at first glance, designing a system to represent the FPUT-α equation is relatively straightforward. However, Equation (1.6) describes an ideal system wherein all the components are identical and there are no external influences present. Engineers know that physical realisations of such equations can never be ideal due to factors such as tolerance, damping and noise. As such, numerical experiments of ideal systems do not always show the results which can be expected from a real system. Therefore, in order to produce a physical realisation of an FPUT system, one must consider the imperfections introduced by constructing such a system.

As an inherent part of the manufacturing process, heterogeneities are introduced, for example, by component tolerances. Although component tolerances are well studied in many physical systems [49], [68], there have not been any investigations into their effects on FPUT lattices. Variations in mass in the form of alternating heavy and light particle chains have been studied [13], [69], as have variations in the coupling constant [70]. Neither of these scenarios is equivalent to the introduction of a tolerance on each element of the system. However, since Jackson demonstrated that changing the coupling constant for different particles stops recurrence if the variation is large enough [70], this raises concerns for systems where such imperfections occur in all elements of the system.

Impurities and defects in lattices have also attracted attention, including research on topics like Anderson phenomena and defect modes [15], [71]. Unfortunately, this is of little relevance to the problems posed here as these studies have an extremely different focus from the engineering-oriented work contained in this thesis. Additionally, it is not clear how to extrapolate the results of these studies to phenomena such as tolerance-based inhomogeneities in arrays.

In addition to the manufacturing variations described above, other imperfections are also present in physical realisations of systems. One example of this is energy loss through damping and, although this can be minimised by careful design, it can rarely be avoided completely. For example, any electronic circuit will have damping

due to resistance. There are some studies of driven-damped FPUT systems [22], [72]. However, the natural decay of a system through damping is also of interest, and it is this which forms a focus for consideration of damping in this thesis.

Another example of imperfection is parasitic noise, which can be spatial or temporal. Temporal noise in FPUT systems has received some attention [72], although it would appear that spatial noise has not. This thesis examines the effects of damping and component tolerances, the latter of which can also be considered as spatial noise. Temporal noise is inherent in all systems, for example as Johnson noise, Shot noise and Brownian noise in electronic circuits. This will have an impact on the system, however, by designing the system with a high enough signal-to-noise ratio (SNR) the effects can be minimised.

1.7 Thesis overview

The FPUT system (and most analytical and computational studies of it) assumes that the component parts are homogeneous [10], [12], [22], [69], [73], [74]. However, any physical system will have imperfections, such as variability in components due to manufacturing tolerances. Over the next five chapters, this thesis explores the impact of some real-world conditions on the theoretical experiments conducted by Fermi, Pasta, Ulam and Tsingou. It then presents an electronic experimental set-up which validates the results and shows the FPUT recurrence phenomenon in a physical system.

In Chapter 2, the influence of manufacturing tolerance, or variability, on the FPUT-α system is explored. The numerical method for the various simulations contained within the thesis is presented, and the impact of applying symmetric component tolerances to the FPUT-α system is explored. Chapter 3 continues the investigation into tolerances by evaluating various types of asymmetric tolerance structures. These variations in structure are brought about by different ways of constructing physical systems.

This is followed in Chapter 4 by the investigation of another imperfection found in physical systems, energy loss caused by damping. Numerical experiment results are presented for an FPUT-α system with the addition of various levels of damping. The combined effects of both tolerance and damping are then explored.

Taking into account the limitations proposed by the results in the previous chapters, Chapter 5 describes the design of a simple electronic system to experimentally test the FPUT phenomenon. The results of this physical implementation of the FPUT-α system with four damped oscillators and tolerance are presented. Finally, Chapter 6 contains concluding remarks and suggests some possible areas for future work.

2 Tolerance

Contents

2.1 Tolerance in physical systems 23
2.2 Numerical experiment design 25
2.2.1 Reproduction of FPUT-α results 26
2.2.2 Chain length 27
2.2.3 Inclusion of tolerance 27
2.2.4 Choice of software 29
2.2.5 Use of Monte Carlo simulations 30
2.3 Effect of tolerance on recurrence 32
2.3.1 Tolerance of $\pm 0.1\,\%$ 33
2.3.2 Tolerance of $\pm 1\,\%$ 34
2.3.3 Tolerance of $\pm 5\,\%$ 35
2.3.4 Tolerance of $\pm 10\,\%$ 36
2.4 Arrays with different number of oscillators 37
2.4.1 Different number of oscillators with $0\,\%$ tolerance 37
2.4.2 Different number of oscillators with $\pm 5\,\%$ tolerance . . . 37
2.5 Tolerance on linear versus nonlinear terms 40
2.6 Different nonlinear coupling strengths 42
2.6.1 Varying coupling strength with $0\,\%$ tolerance 42
2.6.2 Varying coupling strength with $\pm 5\,\%$ tolerance 44
2.6.3 Increased coupling strength at various tolerances 44
2.6.4 Tolerance on linear versus nonlinear terms 47
2.7 Order of tolerances 49
2.7.1 Outlier 49
2.7.2 Sorted tolerance values 51
2.8 Effect of tolerance on superrecurrence 54
2.9 Numerical stability test 58
2.10 Summary 59

A part of this chapter has been published as

H. Nelson, M. A. Porter, and B. Choubey, "Variability in Fermi-Pasta-Ulam-Tsingou arrays can prevent recurrences", *Physical Review E*, vol. 98, no. 6, p. 062 210, Dec. 2018

In the previous chapter, it was observed that despite extensive theoretical studies into the background of the FPUT recurrence phenomenon, physical realisations of such systems have been extremely limited. One reason for this could be that ideal equations are difficult, if not impossible, to implement as inherent manufacturing variations always introduce a tolerance between component parameters. This effect can be observed in any mechanical or electronic system [75]–[82]. Hence, the individual particles of any real array are not represented by ideal equations.

The FPUT equations describe an undamped system that continues to oscillate when released from rest. These differential equations can be realised in a number of different physical media (e.g. as an electronic circuit or a mechanical structure). To emphasise that the mathematics does not only refer to the mass-spring system described in Chapter 1, the particles of the array shall be referred to as 'oscillators' from this point forwards.

Most physical parameters associated with real devices also vary with environmental conditions such as temperature, pressure, and humidity [83]–[85]. Therefore, even if one could build an array of identical oscillators, it would be very likely that the individual oscillators would change during operation. Moreover, individual oscillators in a system would probably change in different ways, leading to further variability between the oscillators.

Such tolerances are well studied in most physical systems [49], [68]. However, FPUT and related arrays have received little attention with regard to tolerance. In order to experimentally observe the behaviour of practical systems, it is vital to understand the effects of tolerance on these systems in order to know the constraints under which a system could be built, if indeed it is possible. This can be achieved by studying the system under the influence of typical manufacturing tolerances observed in physical systems.

In this chapter, the system described by the FPUT-α equation is studied to investigate the impact of such variability on FPUT recurrences. Section 2.1 provides the background on tolerance from an engineering perspective. Section 2.2 details the methods used for the numerical experiments undertaken. The effects of different levels of tolerance on the FPUT-α array are then explored in Section 2.3. The next part of the chapter then considers the effect of changing other equation parameters at varying tolerances in Sections 2.4 to 2.7. The effects of tolerance on superrecurrence are investigated in Section 2.8. Finally, Section 2.9 describes numerical stability tests carried out to check the reliability of the calculations.

2.1 Tolerance in physical systems

In engineering, components are defined by a series of parameters, which may include physical parameters, such as dimensions, or electrical parameters, such as resistance or capacitance. Due to variations in the manufacturing process, it is difficult to build a batch of components where these parameters are identical and differences between parts are common. This is often referred to as tolerance, mismatch, or variability. As a result, systems are often designed such that these parameters can vary by some amount without having a significant impact on the ability of the system to function as it was designed. Thus, engineering tolerance is considered to be the limits by which the parameter of a component is permitted to vary from its nominal value due to these unintended variations [86]–[89].

Whilst it is desirable to have components that are as identical as possible, there is often a trade-off between cost and accuracy, since higher accuracy comes at an increased cost [80], [90], [91]. Manufacturing parts to a small (tight) tolerance is feasible. However it requires much more accurate tooling and often results in a higher rejection rate when parts do not meet the specification. Thus, a primary concern when considering the level of tolerance to specify for a component is to carefully assess how large the tolerance can be without affecting the desired performance. Additionally, when designing a system, it is important to consider that individual component tolerances accumulate, or 'stack', so the overall system tolerance may be higher than that of the individual parts.

Tolerance for a component parameter is specified using a range with upper and lower limits [87], [88], which are often symmetrical around the intended value although asymmetric limits are also possible. For example, in electronics, some types of capacitors are often specified with tolerance limits of $\pm 10\,\%$ meaning a 100 nF capacitor could vary in the range of 90 nF to 110 nF, whereas other types of capacitors are defined with limits of $-20\,\%$ to $+80\,\%$ and could vary in the range of 80 nF to 180 nF.

Tolerances in manufacturing are generally considered to follow a Gaussian distribution [87], [92], [93] and as such 99.73 % of components will sit within ± 3 standard deviations of the designed value. However, the tails of a normal distribution can extend well beyond this so a very small number of components will sit outside this range. Historically, this led to many parts being binned, with, for example, the 1 % resistors going into the 1 % bin, and ones outside that going into (e.g.) the 5 % bin. With modern methods, this is much less common as control over manufacturing tolerances is much improved so a set of components will often sit well within the specified range without any outliers.

2.2 Numerical experiment design

Investigating the effects of tolerance on an actual physical system would require the construction of numerous such systems which is both time consuming and expensive. Numerical experiments provide a faster and more cost effective method to investigate the effects of tolerance on an FPUT system.

In 2005, Dauxois, Peyrard, and Ruffo published simple MATLAB code which forms a good basis for performing a series of numerical experiments on the FPUT-α system as it is constructed in a format which means it is relatively straightforward to add tolerance to the parameters of the equation [16]. It uses a typical method for solving second order ordinary differential equations (ODEs), wherein the equation is reduced to a series of first order ODEs and the Runge–Kutta algorithm in the MATLAB ODE45 solver is used to approximate the solution [94]. The state-space representation of Equation (1.6) is

$$\dot{x}_i = y_i \tag{2.1a}$$

$$\dot{y}_i = (x_{i+1} + x_{i-1} - 2x_i) + \alpha[(x_{i+1} - x_i)^2 - (x_i - x_{i-1})^2] \tag{2.1b}$$

For ease of reference, their code is reproduced here in Appendix A.

In their paper, Dauxois *et al.* state that the two ends of the chain were assumed to be fixed, i.e. $x_0 = x_{N+1} = 0$ [16]. This is in contrast to the papers by Fermi *et al.* and Tuck *et al.* which use $x_0 = x_N = 0$ [7], [34]. There is a split across the literature between the two cases. It appears to be predominantly the older work which uses $N-1$ active particles (e.g. [26], [95]), whilst the more recent work appears to mainly focus on N active particles (e.g. [12], [96]). It is believed that this split is due to the confusion raised by the FPUT method having $N-1$ active particles meaning that N no longer refers to the number of degrees of freedom [36]. For this reason, the work contained within Chapters 2–5 of this thesis uses $x_0 = x_{N+1} = 0$ to denote the fixed end points, i.e. there are N active particles. This changes the equations

describing the displacement and velocity for the initial condition to:

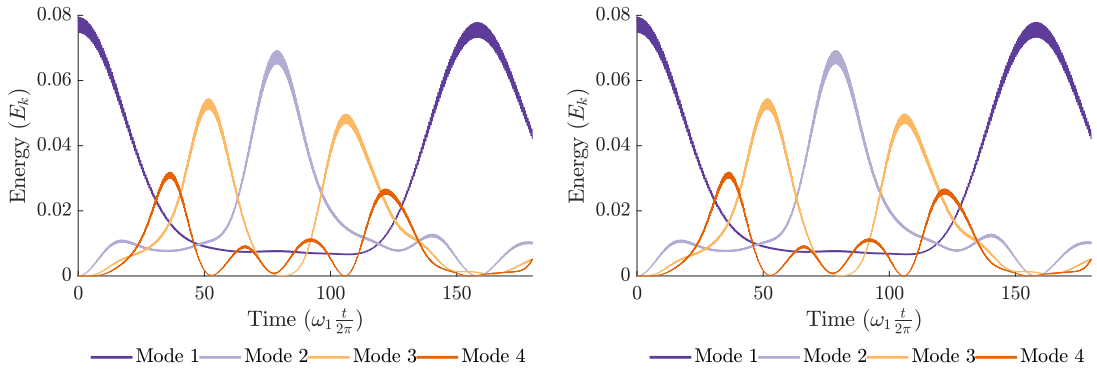
$$x_i = \sin\left(\frac{\pi i}{N+1}\right) \tag{2.2a}$$

$$\dot{x}_i = 0 \tag{2.2b}$$

where $i \in \{1, \ldots, N\}$ and the system is started from rest with the energy in the first mode.

2.2.1 Reproduction of FPUT-α results

Before introducing tolerance into the system, it was important to reproduce the results seen in the original report published by Fermi, Pasta, Ulam and Tsingou [7]. Starting with the most basic scenario described in the report, that of a 1D FPUT-α array with the initial condition of the first mode, the code written by Dauxois *et al.* was simulated. The results in Figure 2.1(i) show that the change of boundary condition has an effect on the recurrence period, increasing it to 158 time units from the 151 time units in the FPUT simulation (Figure 1.3). To ensure that the results are not the product of the chosen software, the computations were double-checked using Python with the ODEINT solver included in the SciPy package which implements a standard Lsoda algorithm [97]. The results of this simulation are shown in Figure 2.1(ii).



(i) MATLAB - Runge–Kutta ODE45 algorithm **(ii)** Python - SciPy Lsoda algorithm

Figure 2.1: Repeating the original FPUT-α simulations with 32 oscillators and a coupling strength of $\alpha = 0.25$, and a change of boundary condition to $x_0 = x_{N+1} = 0$.

2.2.2 Chain length

When the work in this thesis was originally conceptualised, the application in mind was for large arrays of oscillators. However, preliminary investigations showed that simulations with large numbers of oscillators were computationally expensive and took significant amounts of time to complete. Therefore, a chain of 64 oscillators was selected for the bulk of the simulations contained in this chapter as it provided a good balance between computational timescales and array size. The results for a 64 element array with a coupling strength α of 0.25 are shown in Figure 2.2. The time period of recurrence increases to 434 time periods for a 64 element array.

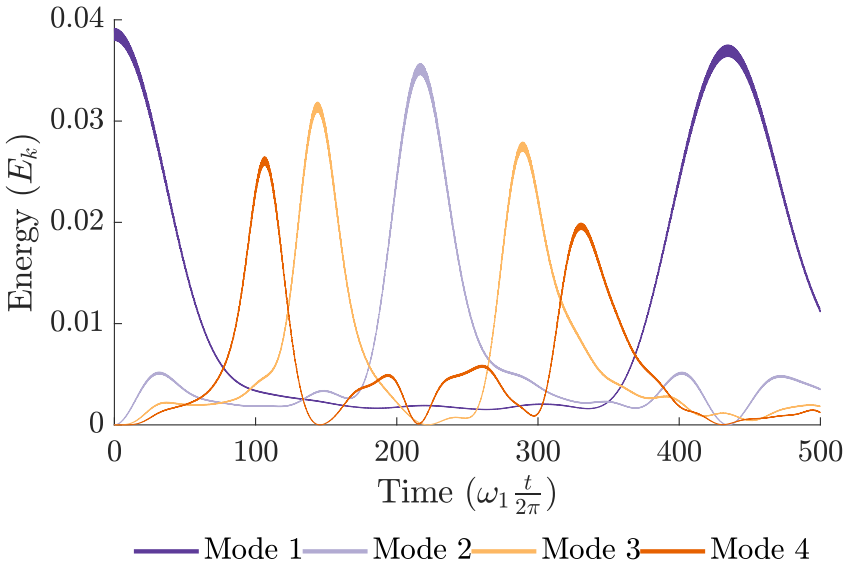


Figure 2.2: Simulation of a 1D FPUT-α array with 64 oscillators and a coupling strength of $\alpha = 0.25$.

2.2.3 Inclusion of tolerance

Once the original results had been replicated, the next step was to add tolerance to the system. In the FPUT equation (Equation (1.6)), each oscillator has its own linear stiffness strength and is coupled using a nonlinear parameter. A simple mass-spring system, such as the one shown in Figure 1.1, would have tolerances as applied in Equation (2.3) where t_i represents the combined tolerances seen

by each element of the system.

$$\ddot{x}_i = (t_{i+1}x_{i+1} + t_{i-1}x_{i-1} - 2t_ix_i) + \alpha[(t_{i+1}x_{i+1} - t_ix_i)^2 - (t_ix_i - t_{i-1}x_{i-1})^2] \quad (2.3)$$

Considering again the simple mass-spring system described by Equation (1.5), although the stiffness of the harmonic spring and the mass of the particles have been set to 1, variation can still occur between these elements and the corresponding values will not be exactly 1. The equation has been normalised for mass, which means that any variation in mass or spring stiffness of the connected springs is incorporated in the value of t_i.

The tolerance values for each simulation were generated using the RANDN function. This draws from a Gaussian distribution (Figure 2.3) of mean 0 and standard deviation 1. This distribution was chosen as it is commonly observed in manufacturing [87], [92], [93]. To obtain the tolerance values in the correct range, the output from the RANDN function was adjusted by shifting and scaling the distribution.

For a tolerance of τ %, this entails a value of t_i that is drawn from a Gaussian distribution with a mean of 1 and standard deviation of $\sigma = 1/3 \times 0.01\tau$. (For example, for 1 % tolerance, the standard deviation is 0.0033.) With a 6σ width (i.e. $\pm 3\sigma$), it can be noted that 99.73 % of the values of t_i fit within the interval [1 – 0.01τ, 1 + 0.01τ]. Any outlying values of t_i are placed on the corresponding edge of this interval.

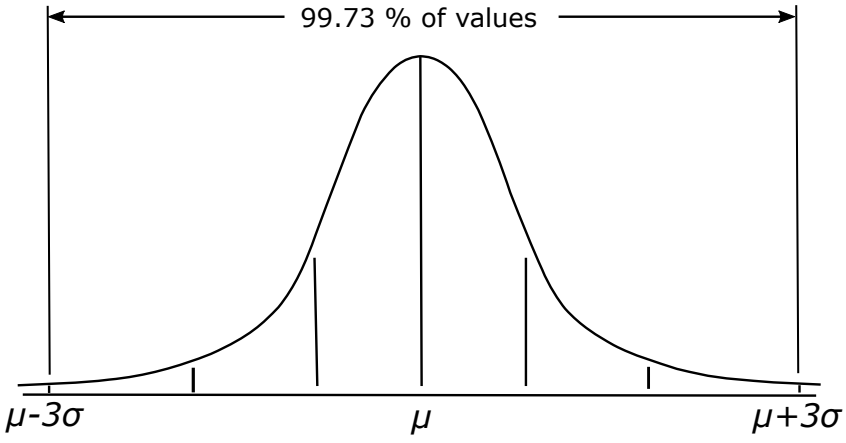


Figure 2.3: Gaussian distribution showing a 6σ spread.

2.2.4 Choice of software

Once tolerance had been included in the simulations, Python was found to perform marginally better than MATLAB and was therefore selected for use for the remainder of the thesis. For large numbers of oscillators and large tolerance values, the Python simulations were found to produce an error less frequently for the same timestep, relative tolerance and absolute tolerance values. The simulations also took less time to complete. This is perhaps due to the difference between the algorithms.

The FPUT problem in its standard form is solvable without very small time steps or tolerance values using the ODE45 algorithm in MATLAB. It can therefore be defined as a nonstiff problem. A stiff equation is one in which the solver, and in particular the time step, has to be constrained for stability rather than accuracy. Mathematical criteria for stiffness are not clearly defined [98]. Adding tolerance to the FPUT system appears to make it stiffer, particularly with large numbers of oscillators and large tolerance values, since reducing the time step and tolerance values of the function does not always result in an error free simulation.

The ODE45 function contained within the MATLAB ODE suite is designed for nonstiff systems. It uses a Runge–Kutta method based on the Dormand–Prince (4,5) pair and has a default order of 4. Although nominally a single-step solver, the steps can often be large meaning the resolution is not ideal for plotting. The ODE45 function therefore uses an additional interpolation, adding four evenly spaced points between each step to improve the resolution [99]. The ODE45 function was initially used with tolerance options of $Reltol = 1 \times 10^{-4}$, $Abstol = 1 \times 10^{-6}$ and the step size automatically determined by the solver. For the simulations that produced an error, alternative tolerances were tried, including matching those for the Python simulation although these did not resolve the error.

Meanwhile, the Python SCIPY library contains the ODEINT function which uses the LSODA algorithm from the FORTRAN library ODEPACK. It has the ability to switch automatically between nonstiff (Adams) and stiff (BDF) methods [100]. It uses the nonstiff method initially, and dynamically monitors the data in order to decide which method to use. The ODEINT function was used with the default

tolerance options of $rtol, atol = 1.490\,12 \times 10^{-8}$ and the step size automatically determined by the solver.

2.2.5 Use of Monte Carlo simulations

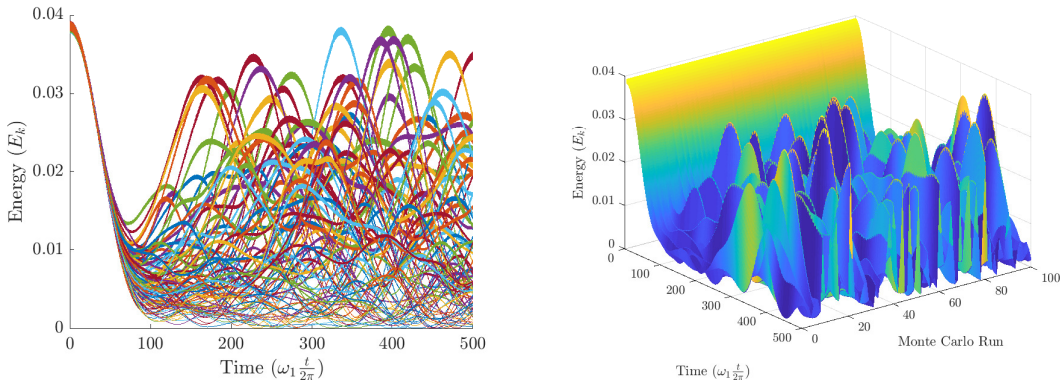
In light of manufacturing tolerances, the exact value of each parameter is difficult to determine. However, tolerance is statistical and Monte Carlo analysis is often applied to problems concerning tolerance to understand the resulting changes to system performance [77], [85], [90], [91]. Therefore, to help understand the effects of a random tolerance spread, Monte Carlo simulations were used to study a number of different sets of tolerance values applied to the FPUT system, while keeping fixed all other system parameters and the initial condition. Incidentally, the use of the Monte Carlo Method seems particularly appropriate here since both Enrico Fermi and Stanislav Ulam were involved in the early stages of developing it [101]–[103].

Multiple simulations that each use an independent draw of the tolerance values were undertaken, and then the dynamics of the oscillator arrays were examined. Typical simulations in this chapter were carried out with 64 elements and the nonlinear coupling strength, α, was taken to be 0.25. It was observed that 100 simulations provide a good statistical representation of the systems so this number was used as the basis to further explore the effects of tolerance. The precision (and hence reproducibility) in a manufactured system with a given tolerance spread is generally high, so the system in one realisation will always produce the same result (ignoring effects such as temporal noise). In this context, different runs of a Monte Carlo simulation represent individual manufactured systems.

Monte Carlo simulations produce outliers. In most of the figures contained within this thesis a single result that is representative of the majority of the Monte Carlo runs has been selected. These single results were selected by visually analysing the energy plots for all 100 Monte Carlo runs. For the initial tolerance results in Section 2.3, four results are presented for each tolerance level to give an overview of the range of responses produced by the system under various sets of tolerance values. In these figures, the first sub-figure is representative of the majority of the

results, the second and third sub-figures represent other frequently seen results, and the fourth sub-figure shows an outlier response.

To demonstrate the complexity of the range of responses, the first mode for each of the 100 Monte Carlo simulations of the symmetric system with 64 oscillators, a coupling strength α of 0.25, and a tolerance of $\pm 5\,\%$ are presented in Figure 2.4. All of the first mode energy responses are overlaid on the same set of axes in Figure 2.4(i), whilst Figure 2.4(ii) shows a 3D plot of the same. It can be seen that neither of these plots displays the data in a manner that is useful for interpretation.



(i) **(ii)**

Figure 2.4: Plots showing the first energy mode for 100 simulations of a 1D FPUT-α array with 64 oscillators and a coupling strength of $\alpha = 0.25$ at a tolerance of $\pm 5\,\%$.

In theory, it would be possible to present an average of all the results, for example by taking $Energy = (E_1 + E_2 + ... + E_{100})/100$, where E_i represents the energy of the mode considered for the ith Monte Carlo simulation at the given tolerance. However, an average of the results would not represent any real manufactured system in this context. Figure 2.5 shows the mean, minimum, and maximum values for the data presented in Figure 2.4. If one considers the mean line, this plot implies that recurrence does not occur in any of the simulations. However, the data in Figure 2.4 clearly shows that energy leaves and returns to the first mode in a large number of cases. Similarly, if one were to consider the minimum and maximum lines it is impossible to understand the movement of the energy out of and back into the first mode for each set of tolerance values.

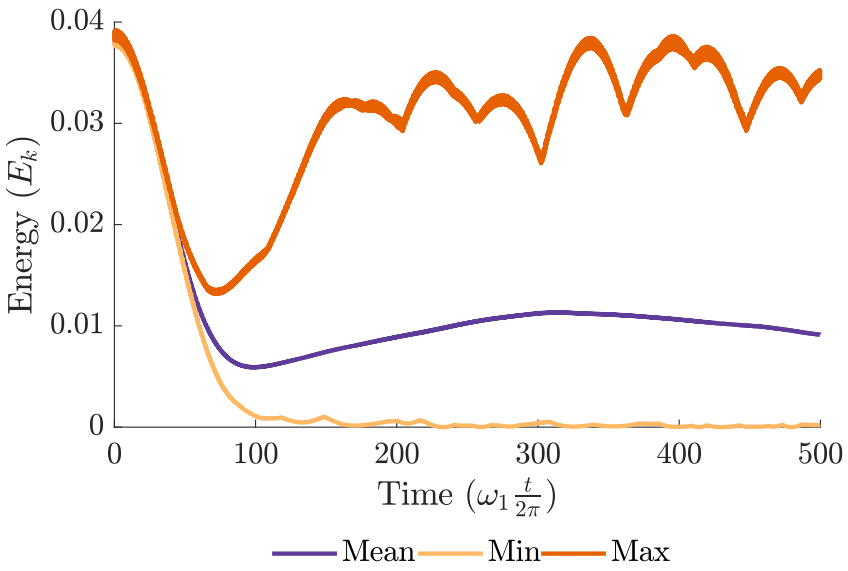


Figure 2.5: Plot showing the mean, minimum and maximum values of the first energy mode for 100 simulations of a 1D FPUT-α array with 64 oscillators and a coupling strength of $\alpha = 0.25$ at a tolerance of $\pm 5\,\%$.

2.3 Effect of tolerance on recurrence

Although mismatch between components can take on any percentage value, engineering tolerances are specified as a maximum constraint. Simulating the effect of every possible tolerance value would be prohibitive so a method of dividing these values is required. Widely available electronic components such as resistors and capacitors are grouped into tolerance categories, which can provide a good starting point for simulation. Therefore, the typical passive electronic component tolerances of $\pm 0.1\,\%$, $\pm 1\,\%$, $\pm 5\,\%$, and $\pm 10\,\%$ [83] are used for subsequent simulations in this thesis.

In this section, a small selection of the Monte Carlo runs will be shown to give an overview of the range of system responses to tolerance. The full results for these Monte Carlo runs are presented in Appendix C. Subsequent sections, however, will just present a typical result from a Monte Carlo simulation as described in Section 2.2.5.

2.3.1 Tolerance of ±0.1 %

Starting with a tolerance of ±0.1 %, it can be observed that the FPUT system in Equation (2.3) exhibits a very similar recurrence pattern to that of the ideal system with 0 % tolerance. A selection of four results from the 100 Monte Carlo runs are shown in Figure 2.6. These represent the range of responses produced by the different sets of values of t_i that are applied to the system.

There is minimal difference between the runs, but small variations are present. In particular, the shape of the peaks starts to vary. This is most prominent from a time of 300 periods of the first mode onwards, and in modes 3 and 4. For example, in Figure 2.6(i) the energy in the fourth mode falls off more sharply around 380 time periods than in Figure 2.6(ii).

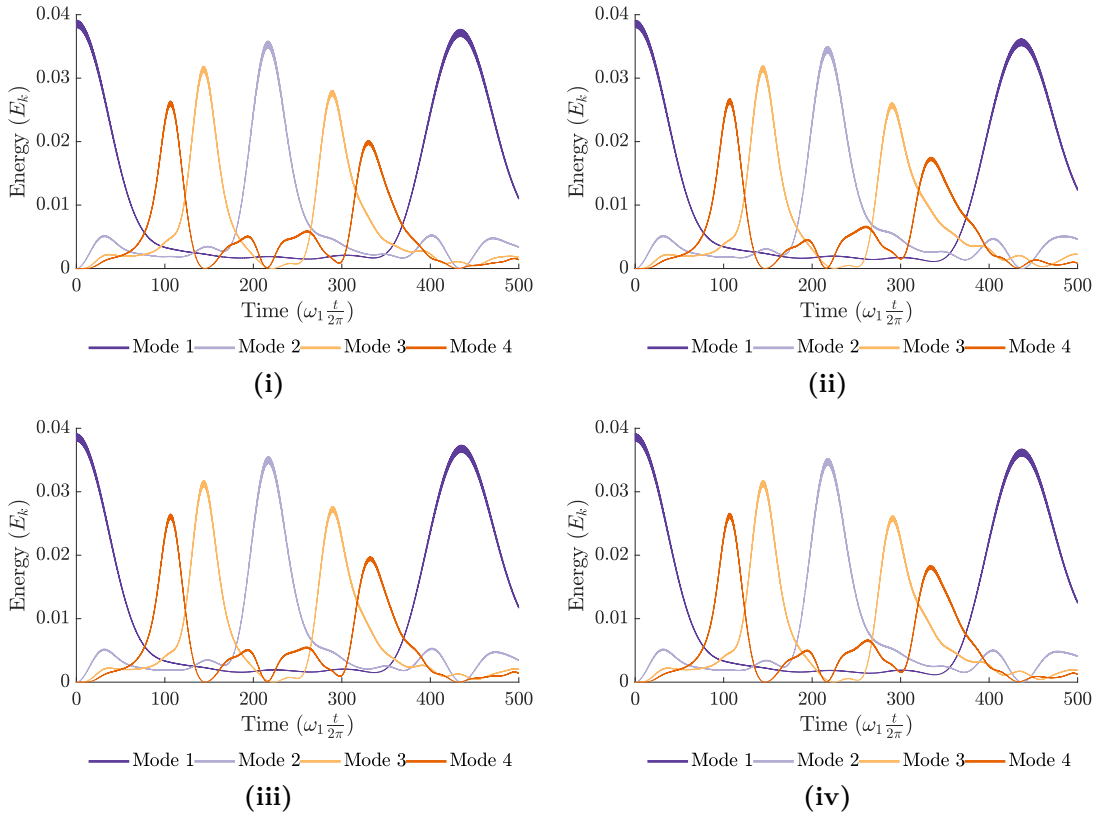


Figure 2.6: Simulations of a 1D FPUT-α array with 64 oscillators and a coupling strength of $\alpha = 0.25$ showing examples of different recurrence patterns at a tolerance of ±0.1 %.

2.3.2 Tolerance of ±1 %

On increasing the tolerance to ±1 %, the recurrence phenomenon starts to differ considerably from the ideal scenario of homogeneous system components. Figure 2.7 shows example results for a tolerance of ±1 %, where Figure 2.7(i) is representative of the response in more than 85 % of the cases. However, for some combinations of tolerance values, recurrence becomes weak (Figures 2.7(ii) and 2.7(iii)) or breaks down (Figure 2.7(iv)) when considering the amount of energy returning to the first mode. The timescale of the recurrence 'period' has also changed. In Figures 2.7(i) and 2.7(ii) the peak where the energy has returned to the first mode has moved to be much closer to a time of 400 periods of the first mode.

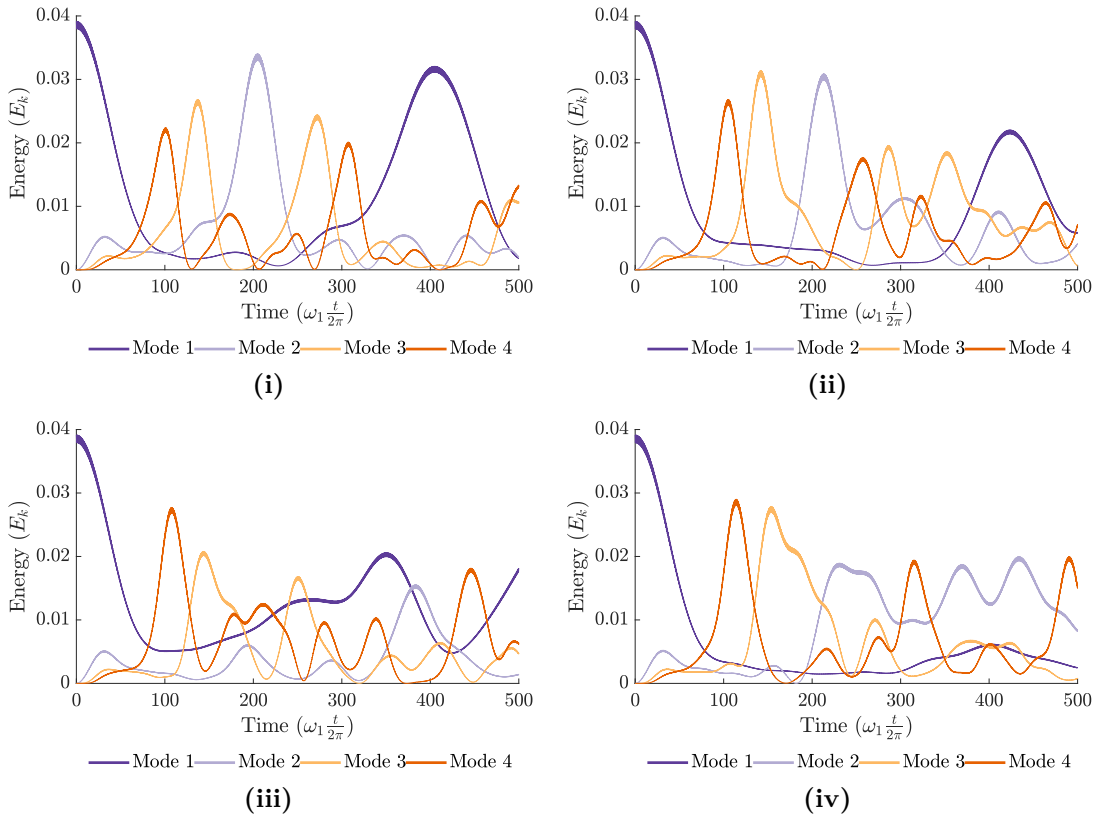


Figure 2.7: Simulations of a 1D FPUT-α array with 64 oscillators and a coupling strength of $\alpha = 0.25$ showing examples of different recurrence patterns at a tolerance of ±1 %.

2.3.3 Tolerance of ±5 %

Increasing the tolerance further to ±5 % (Figure 2.8), even less energy transfer to modes 2, 3, and 4 is seen in the majority of cases, and much less recurrence of energy appears to be taking place as shown in Figure 2.8(i). Figure 2.8(ii) shows another response whereby there is very little energy entering modes 2, 3, and 4 but is much more spread out across all 64 modes before returning to the first mode.

Another interesting system response is shown in Figure 2.8(iii) where the recurrence pattern has changed considerably between modes 2, 3, and 4 but a significant energy transfer is taking place. For one set of values of t_i from the 100 Monte Carlo runs undertaken, there was a recurrence output that closely resembled the recurrence seen in an ideal system. This suggests that there could be certain circumstances under which a tolerance of ±5 % may not prohibit recurrence taking place. This is explored later in this chapter.

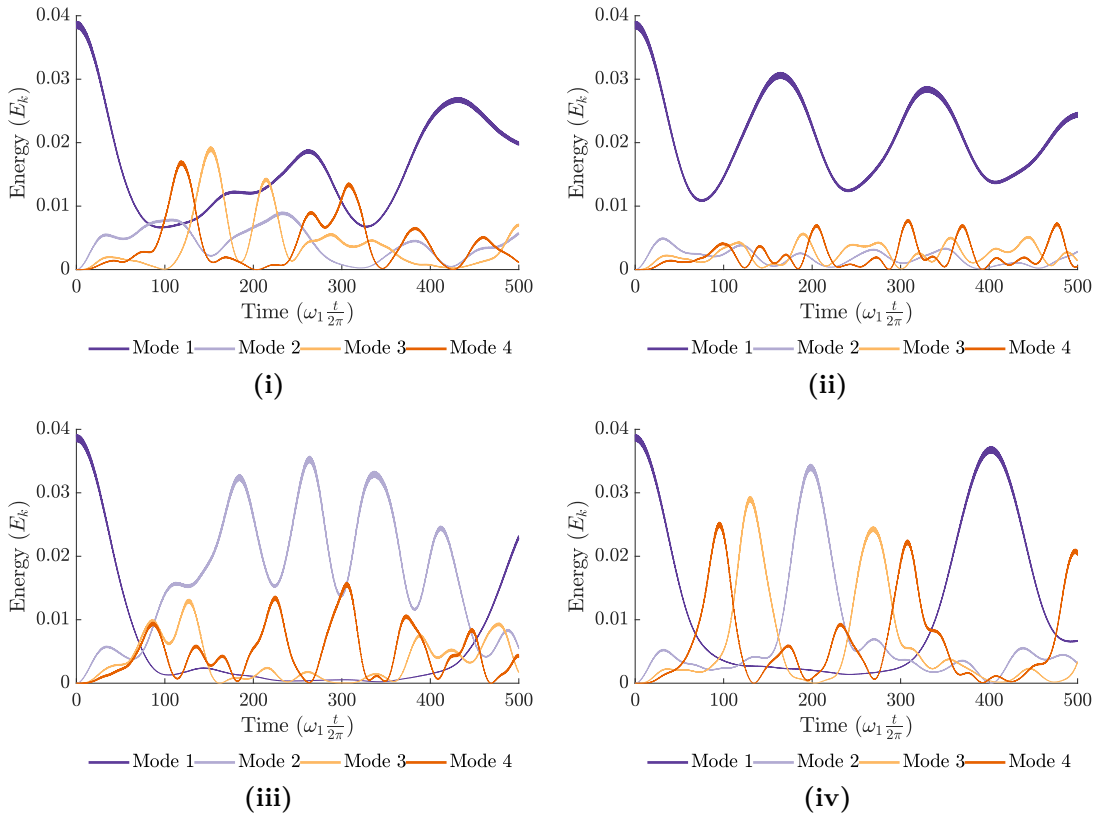


Figure 2.8: Simulations of a 1D FPUT-α array with 64 oscillators and a coupling strength of $\alpha = 0.25$ showing examples of different recurrence patterns at a tolerance of ±5 %.

2.3.4 Tolerance of ±10 %

At ±10 %, this steady decline in the quality of the recurrence with increasing tolerance is even more prominent. In most cases, a larger proportion of the energy stays in the first mode as shown in Figure 2.9(i). However, the amount of energy transferred into the higher modes does vary with different sets of values of t_i. In Figure 2.9(ii), very little energy is transferred into the higher modes.

A variety of different responses were also exhibited in a similar way to the variation shown at a tolerance of ±5 %. Figure 2.9 shows an interesting response whereby a different repeating recurrence pattern is occurring on a different time-scale to that of the homogeneous system. Finally, Figure 2.9(iv) shows a set of t_i values which lead to a large amount of energy being transferred between modes but very little returning to the first mode.

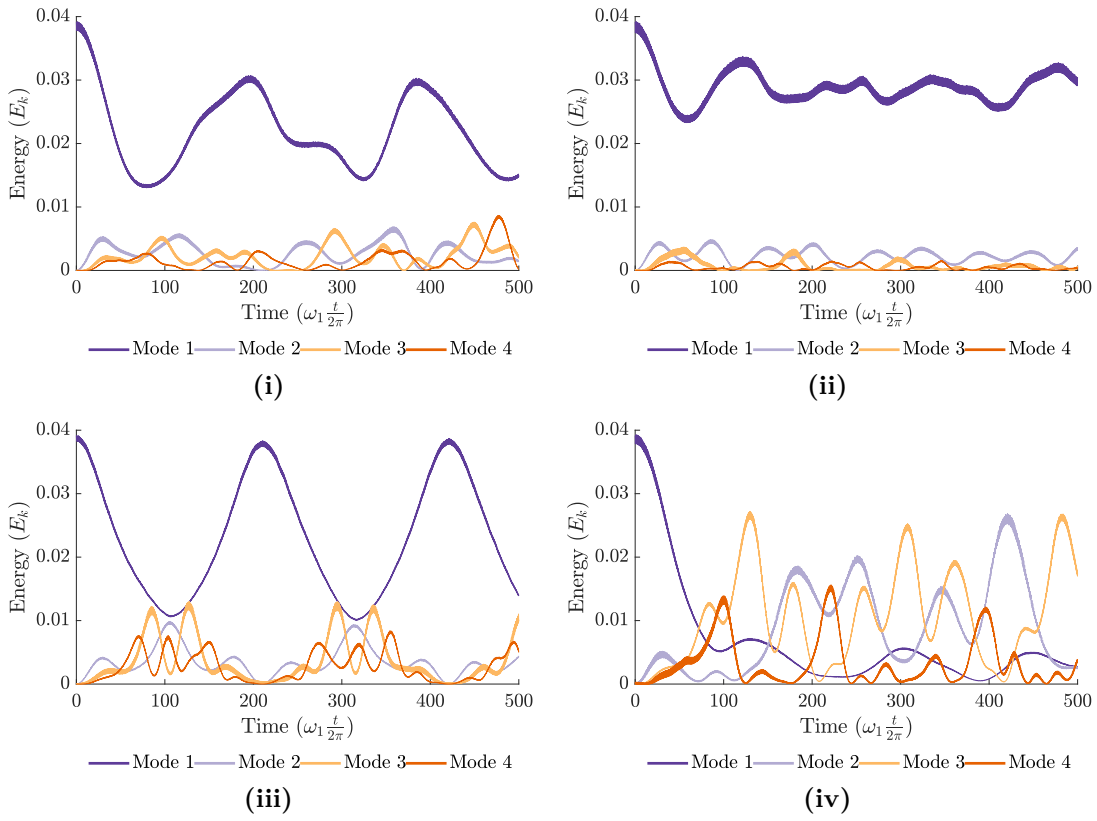


Figure 2.9: Simulations of a 1D FPUT-α array with 64 oscillators and a coupling strength of $\alpha = 0.25$ showing examples of different recurrence patterns at a tolerance of ±10 %.

2.4 Arrays with different number of oscillators

The first set of numerical experiments described in this chapter have used a fixed size array of 64 oscillators, wherein recurrence has been shown to break down as tolerance increases. However, the original FPUT report and numerous subsequent papers have observed that recurrence occurs in systems with different degrees of freedom. Since real systems will vary in size depending on application, the response of different array sizes to tolerance is important.

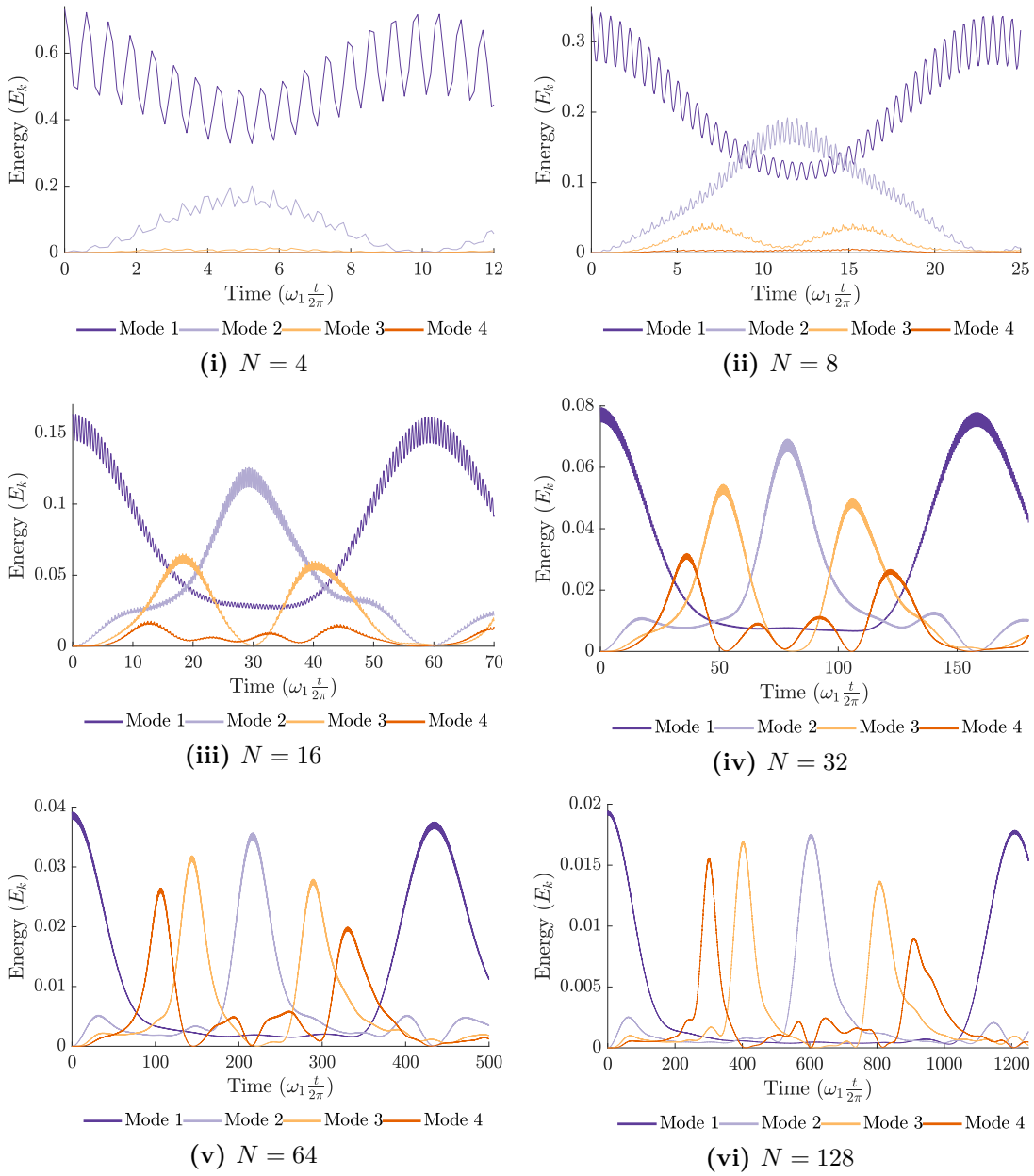
2.4.1 Different number of oscillators with 0 % tolerance

To explore this, 1D arrays of 4, 8, 16, 32, 64, and 128 oscillators with a coupling strength, α, of 0.25, and 0 % tolerance were simulated. These values were selected as many electronic systems are designed in sizes of 2^n. In Figure 2.10, it can be observed that when there are fewer oscillators in the system recurrence still occurs but there is less energy transferred into modes 3 and 4. With 8 oscillators, the energy being transferred into mode 2 is significantly reduced and with only 4 oscillators, recurrence is very weak.

2.4.2 Different number of oscillators with ±5 % tolerance

Figure 2.11 illustrates that 1D arrays with a larger number of oscillators experience a greater impact from incorporating tolerances. Introducing a tolerance of ±5 %, recurrence is of a similar level to that of 0 % tolerance for array sizes of up to 16 oscillators (Figures 2.11(i)–(iii)). However, the recurrence pattern is starting to change for an array of 32 oscillators (Figure 2.11(iv)). At 64 oscillators recurrence is becoming weak (Figure 2.11(v)), whereas recurrence has broken down completely when there are 128 oscillators (Figure 2.11(vi)).

Thus, by reducing the number of oscillators in a system, it may be possible to see recurrence at higher tolerances. However, recurrence is stronger in a system with a higher number of oscillators. These counter statements imply that there may be an optimal array size to observe good recurrence, and a very small range of array sizes in which to observe recurrence at all.

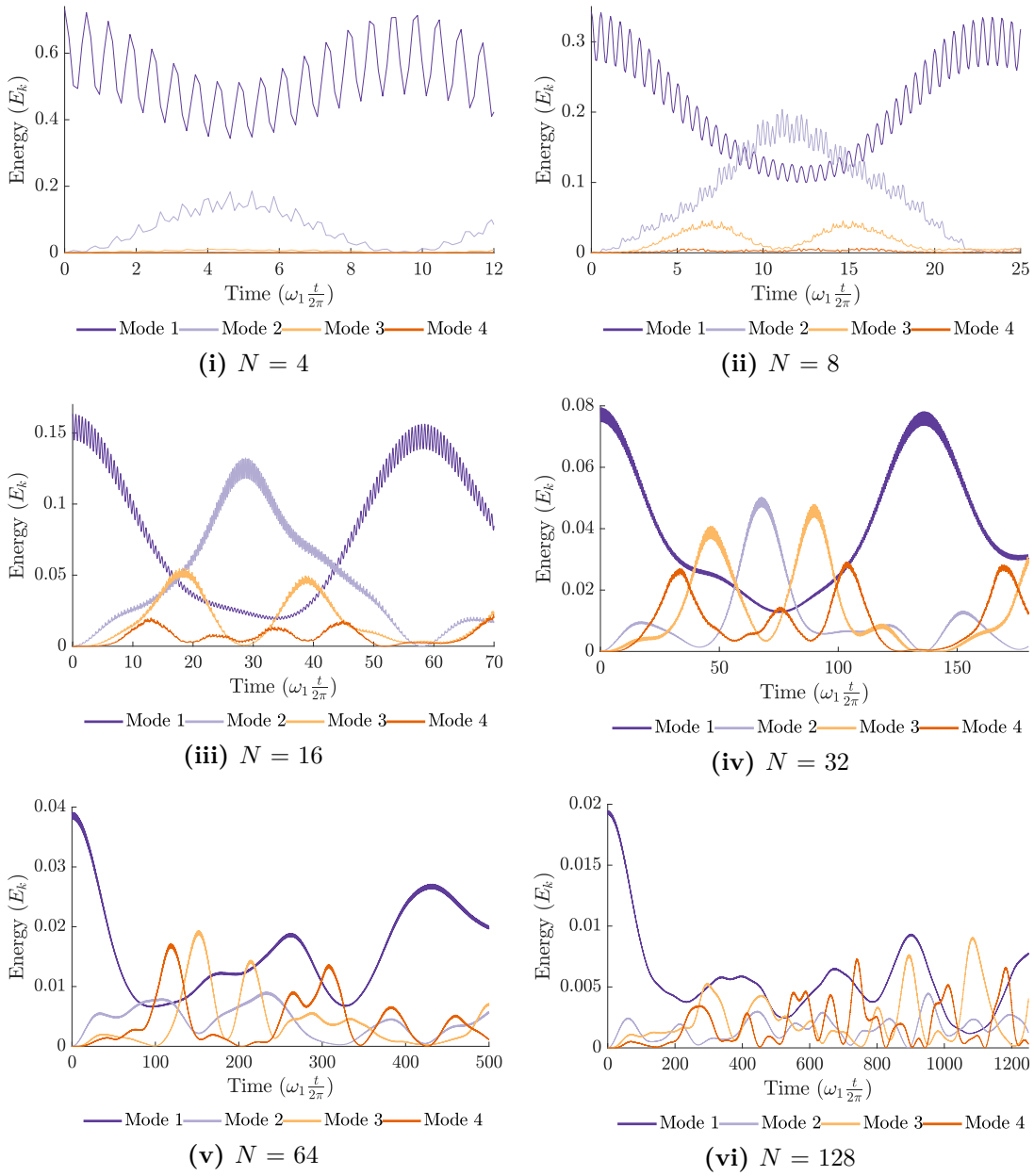


(i) $N = 4$ **(ii)** $N = 8$

(iii) $N = 16$ **(iv)** $N = 32$

(v) $N = 64$ **(vi)** $N = 128$

Figure 2.10: Simulations of 1D FPUT-α arrays with different numbers of oscillators, 0 % tolerance and a coupling strength of $\alpha = 0.25$.



(i) $N = 4$ **(ii)** $N = 8$

(iii) $N = 16$ **(iv)** $N = 32$

(v) $N = 64$ **(vi)** $N = 128$

Figure 2.11: Simulations of 1D FPUT-α arrays with different numbers of oscillators and a coupling strength of $\alpha = 0.25$ at a tolerance of $\pm 5\,\%$.

2.5 Tolerance on linear versus nonlinear terms

The classical FPUT system has equations with two parts: a discretised linear diffusion term and a nonlinear coupling term. To identify whether tolerances in the linear or nonlinear terms contribute more to the breakdown of recurrence, tolerances were independently applied to the linear terms and the nonlinear terms keeping all other parameters the same. As it is the nonlinear coupling that leads to recurrence, the initial expectation was that any tolerance in nonlinear coupling parameters should lead to a more severe breakdown of recurrence than incorporating tolerance in the linear parts. However, the results shown in Figure 2.12 suggest that this is not the case.

Figures 2.12(i)–(iii) are a repeat of Figures 2.7(i),2.8(i), and 2.9(i) and show the results of incorporating tolerance on both the linear and nonlinear terms. The simulations from these figures were repeated using the same tolerance values, except tolerances were only applied to the linear terms, as shown in Equation (2.4). The results are shown in Figures 2.12(iv)–(vi).

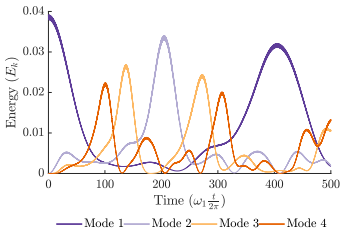
$$\ddot{x}_i = (t_{i+1}x_{i+1} + t_{i-1}x_{i-1} - 2t_ix_i) + \alpha[(x_{i+1} - x_i)^2 - (x_i - x_{i-1})^2] \tag{2.4}$$

Comparing Figures 2.12(i) and 2.12(iv), the energy profiles for a tolerance of $\pm 1\,\%$ on only the linear terms and on both the linear and nonlinear terms are very similar. Increasing the tolerance to $\pm 5\,\%$, there is a greater difference between the energy profiles, with a large amount of the energy disappearing from the first mode and taking longer to enter modes 2 to 4 when tolerance is only applied to the linear terms (Figures 2.12(ii) and 2.12(v)). At a tolerance of $\pm 10\,\%$, more energy stays in the first mode with a lot less being transferred into modes 2 to 4 when only the linear terms are subject to tolerance (Figures 2.12(iii) and 2.12(vi)).

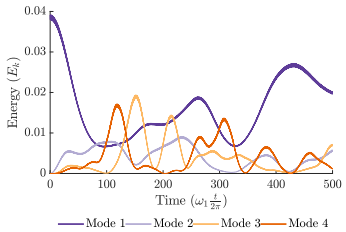
The simulations were then repeated using the same values of t_i but incorporating tolerance only in the nonlinear parts of the FPUT-α array, as shown in Equation (2.5). Figures 2.12(vii)–(ix) show the results of these simulations.

$$\ddot{x}_i = (x_{i+1} + x_{i-1} - 2x_i) + \alpha[(t_{i+1}x_{i+1} - t_ix_i)^2 - (t_ix_i - t_{i-1}x_{i-1})^2] \tag{2.5}$$

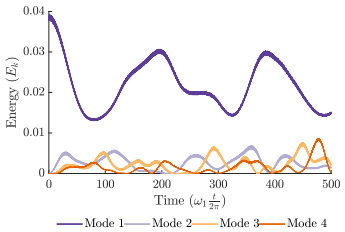
Tolerance in both the linear and nonlinear terms:



(i) ±1 %

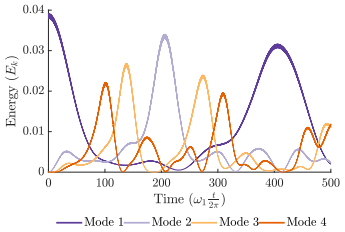


(ii) ±5 %

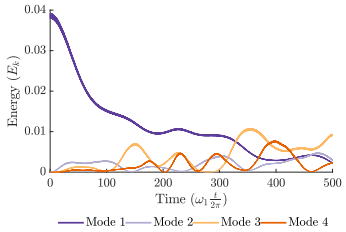


(iii) ±10 %

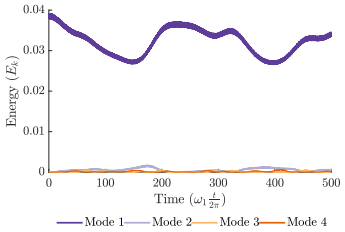
Tolerance in only the linear terms:



(iv) ±1 %

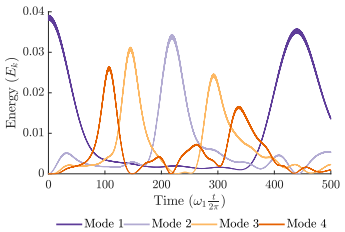


(v) ±5 %

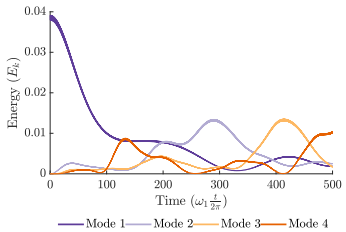


(vi) ±10 %

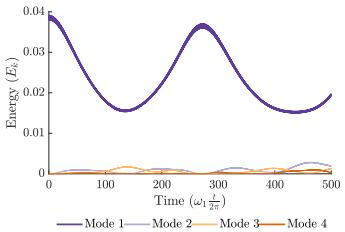
Tolerance in only the nonlinear terms:



(vii) ±1 %



(viii) ±5 %



(ix) ±10 %

Figure 2.12: Simulations of a 1D FPUT-α array with 64 oscillators and a coupling strength of $\alpha = 0.25$ at various tolerances, showing the effect of tolerance on different parts of the array.

Comparing Figures 2.12(i), 2.12(iv), and 2.12(vii), it can be observed that with ±1 % tolerance on only the nonlinear terms, recurrence is much closer to the case with 0 % tolerance (Figure 2.2). However at ±5 % (Figure 2.12(viii)) and ±10 % (Figure 2.12(ix)), tolerance on only the nonlinear terms has a similar effect to tolerance on only the linear terms. Table 2.1 summarises the quality of recurrence under each of these conditions.

Terms	±1 %	±5 %	±10 %
Both	Good	Reasonable	Poor
Linear	Good	Poor	Poor
Nonlinear	Excellent	Poor	Poor

Table 2.1: Quality of recurrence for different tolerances applied to different parts of the array in a system with 64 oscillators and a coupling strength of $\alpha = 0.25$.

2.6 Different nonlinear coupling strengths

Thus far, this chapter has focussed on a coupling strength α of 0.25. However, as Section 2.5 showed, with a weak coupling strength, tolerance on only the linear terms appears to have a marginally higher impact than tolerance on only the nonlinear terms. One explanation for this could be that there is less energy in the nonlinear terms. Therefore, exploring a range of coupling strengths will show the effect of changing the balance of energy between the linear and nonlinear terms.

In a large number of physical systems, the nonlinear coupling may be weak. However, as real systems will have different nonlinear coupling strengths exploring a range of values in the interval $0 < \alpha \leq 1$ at different tolerances will show if there are any correlations.

2.6.1 Varying coupling strength with 0 % tolerance

Before adding tolerance to the system, there is a need to understand the impact of changing the coupling strength on recurrence. Simulations with 0 % tolerance and different coupling strengths of 0.1, 0.25, 0.4, 0.6, 0.8, and 1.0 are shown in Figure 2.13. It can be observed that coupling strength affects both the period of recurrence and the amount of energy transferred into the lower modes.

The recurrence period reduces with increasing coupling strength. Hence, for an α value of 1.0 there are two recurrence cycles in approximately the same time frame as for a single recurrence cycle at an α value of 0.25. The energy in the first major peak for the second and third modes increases as the coupling strength increases, whilst the second major peak decreases. Interestingly, this change in energy pattern is similar to altering the number of oscillators in the chain, albeit with a different timescale.

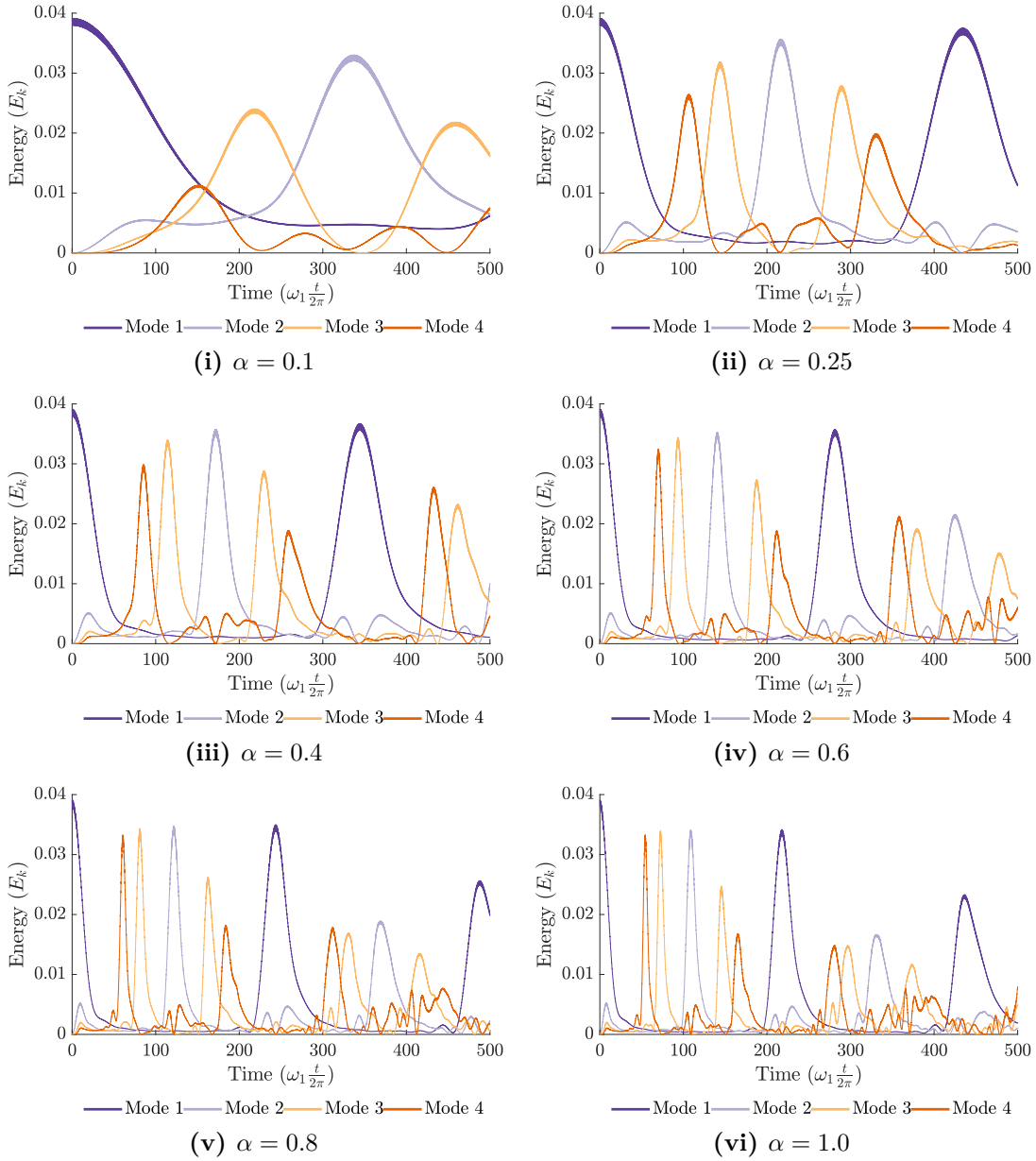


Figure 2.13: Simulations of 1D FPUT-α arrays with 64 oscillators, 0 % tolerance and different coupling strengths.

2.6.2 Varying coupling strength with ±5 % tolerance

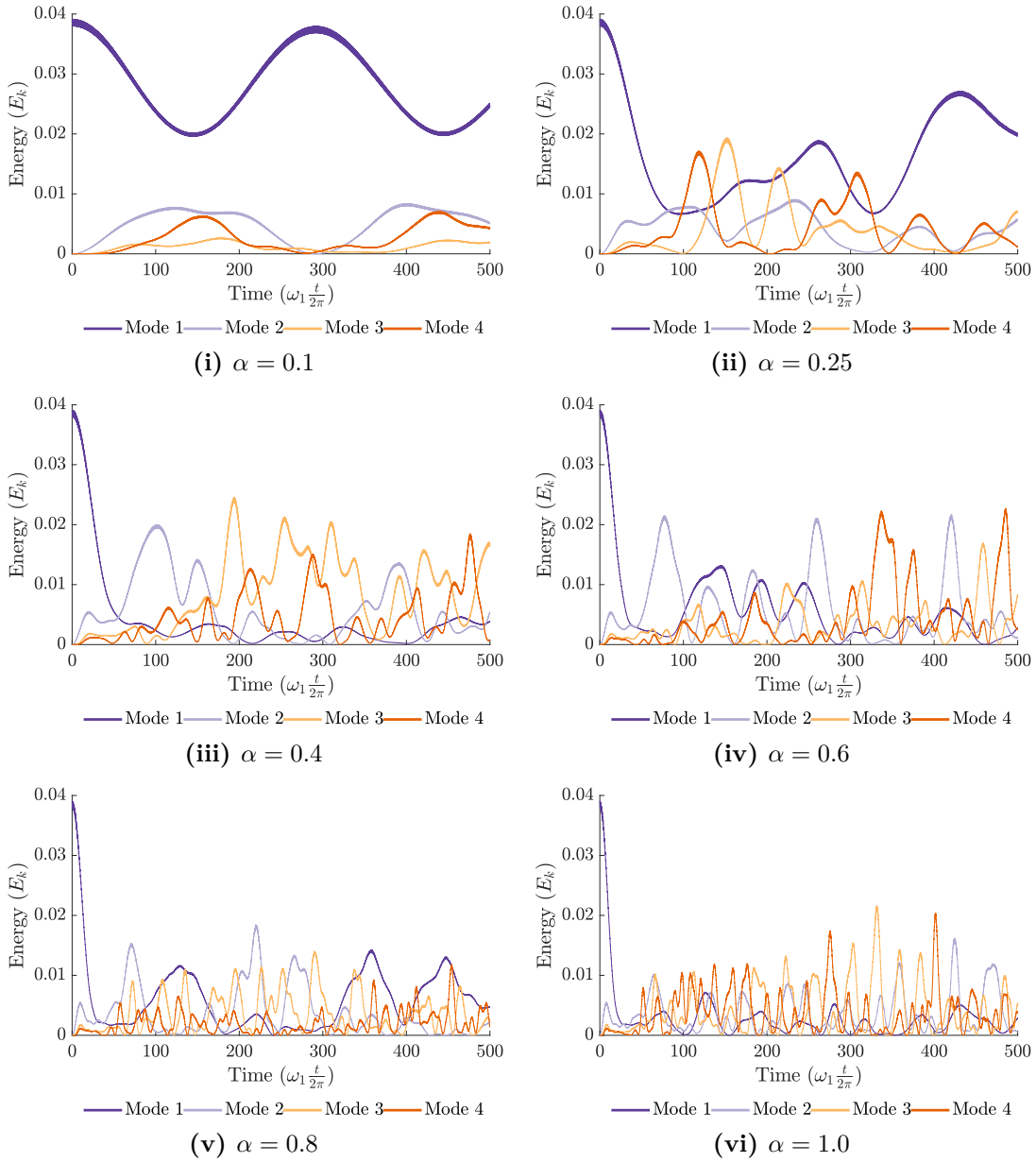
Given the results presented so far, one might therefore assume that the response to tolerance might be affected when the coupling strength is changed. It has been shown that the recurrence period decreases as coupling strength increases. Additionally, tolerance immunity is higher when there are fewer elements in the array. Fewer elements also results in a shorter recurrence period. Therefore, it would be a realistic assumption that immunity to tolerance would increase as coupling strength increases.

A tolerance of ±5 % has a significant impact on recurrence with $N = 64$ and $\alpha = 0.25$ but does not completely stop it, therefore these values are used to investigate the impact of changing the nonlinear coupling strength. Taking the same set of values for t_i used to produce Figure 2.8(i) and repeating the simulation with different coupling strengths will allow the results to be compared directly as the only changing variable is α.

Figure 2.14 shows the results of simulating the system with a tolerance of ±5 % and coupling strengths of 0.1, 0.4, 0.6, 0.8, and 1.0, in addition to the original simulation with $\alpha = 0.25$ repeated from Figure 2.8(i). These results show that, contrary to expectation, as the coupling strength increases, recurrence gets weaker with less energy returning to the first mode.

2.6.3 Increased coupling strength at various tolerances

To provide a wider comparison at different tolerance values, simulations were also run with a coupling strength of 0.8 at ±0.1 %, ±1 %, ±5 %, and ±10 %. These used the same values of t_i used in the simulations with a coupling strength of 0.25 and shown in Figures 2.6(i), 2.7(i), 2.8(i) and 2.9(i) respectively. The results shown in Figure 2.15, when compared with those for the simulations with a coupling strength of 0.25, show a similar pattern at the lower tolerances but at higher tolerances the exchange of energy between modes is significantly altered.



(i) $\alpha = 0.1$ **(ii)** $\alpha = 0.25$

(iii) $\alpha = 0.4$ **(iv)** $\alpha = 0.6$

(v) $\alpha = 0.8$ **(vi)** $\alpha = 1.0$

Figure 2.14: Simulations of 1D FPUT-α arrays with 64 oscillators, a tolerance of $\pm 5\,\%$ and different coupling strengths.

At ±0.1 % tolerance there is very little alteration to the recurrence. With a tolerance of ±1 % the shape of the peaks in the first recurrence cycle is starting change but more significant change occurs in the second recurrence cycle. When the tolerance is increased to ±5 % there is energy being transferred between the modes but the amount returning to the first mode is lower than with a coupling strength of 0.25. Finally, at a tolerance of ±10 % the energy is constantly shifting between the modes but no significant return to the first mode occurs. This is a change from a coupling strength of 0.25 where approximately half of the energy remained predominately in the first mode.

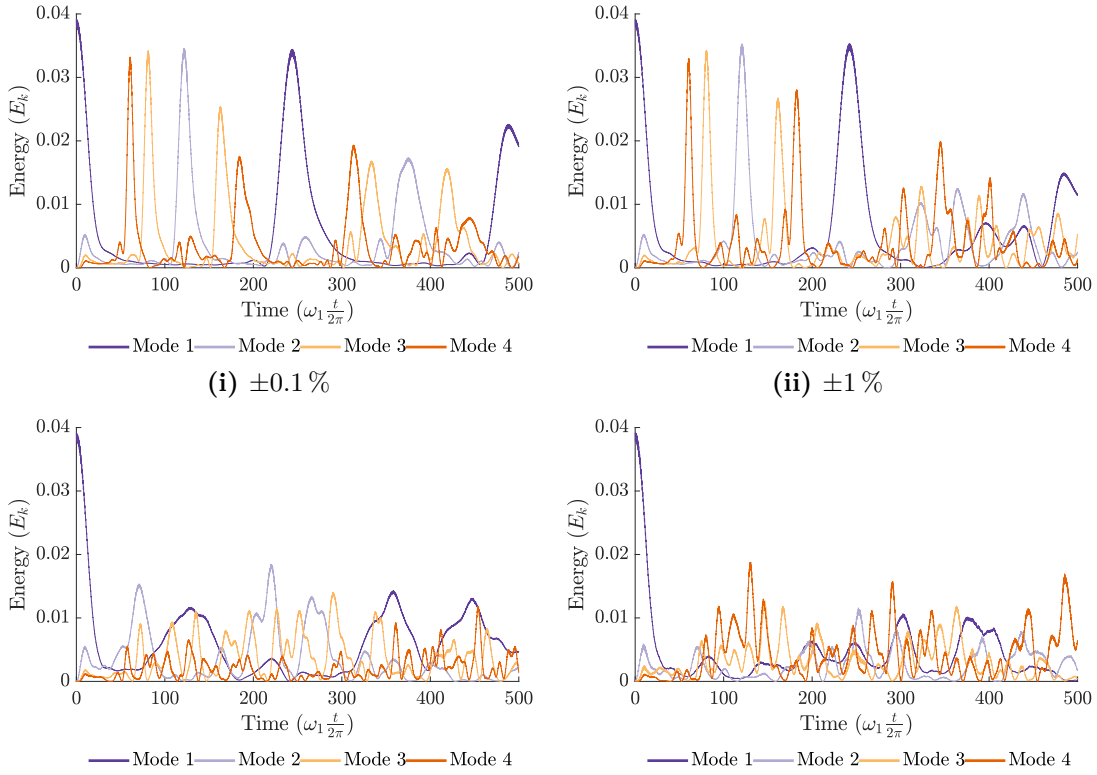


Figure 2.15: Simulations of 1D FPUT-α arrays with 64 oscillators and a coupling strength of $\alpha = 0.8$ at various tolerances.

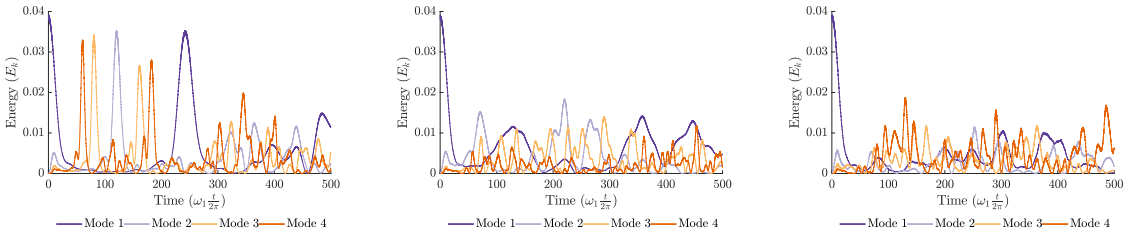
2.6.4 Tolerance on linear versus nonlinear terms

From the results presented so far in this section, it would appear that strongly coupled systems are more prone to mismatch due to tolerance. This suggests that the tolerance has a greater efect on the nonlinear term with a stronger coupling strength. To investigate this, the simulations for a coupling strength α of 0.8 were repeated with tolerances applied to just the linear terms or just the nonlinear terms. The results are presented in Figure 2.16 and since these simulations use the same values of t_i used in the simulations with a coupling strength of 0.25, the results are directly comparable to the results shown in Figure 2.12.

At a tolerance of $\pm 1\,\%$, tolerance on only the nonlinear terms for the stronger coupling strength of 0.8 results in a higher degradation of recurrence than tolerance on the linear terms (Figures 2.16(iv) and 2.16(vii)). This is the opposite effect to that for a coupling strength of 0.25 (Figures 2.12(iv) and 2.12(vii)). However, both cases show a lot less energy transfer between modes 1 to 4 than when the tolerances are on both the linear and nonlinear terms (Figure 2.16(i)).

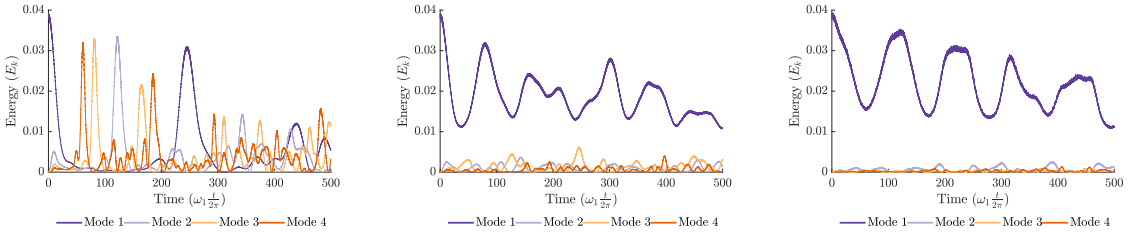
Increasing the tolerance to $\pm 5\,\%$, there is still more energy exchanged between modes when tolerance is applied to both the linear and nonlinear terms (Figure 2.16(ii)). However, the energy exchange between modes 1 to 4 is comparable for tolerances on only the linear terms and only the nonlinear terms (Figures 2.16(v) and 2.16(viii)). Interestingly, for the tolerance on only the nonlinear terms, there is a significantly stronger peak in the first mode at the point where the peak would occur for a full recurrence cycle. Further increase in the tolerance to $\pm 10\,\%$ shows a pattern in the energy transfer which is very similar to that for a tolerance of $\pm 5\,\%$ (Figures 2.16(iii), 2.16(vi), and 2.16(ix)).

Tolerance in both the linear and nonlinear terms:



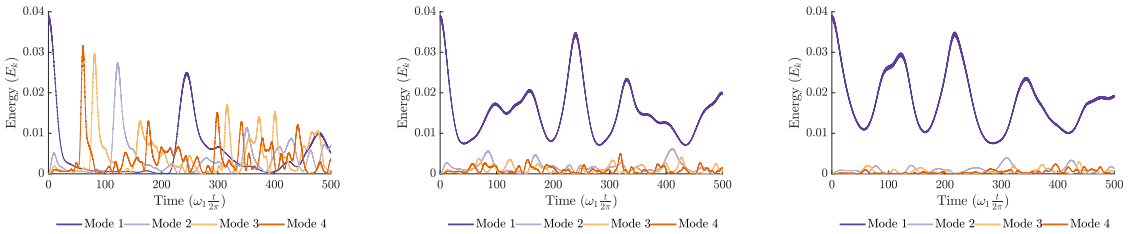
(i) ±1 % **(ii)** ±5 % **(iii)** ±10 %

Tolerance in only the linear terms:



(iv) ±1 % **(v)** ±5 % **(vi)** ±10 %

Tolerance in only the nonlinear terms:



(vii) ±1 % **(viii)** ±5 % **(ix)** ±10 %

Figure 2.16: Simulations of a 1D FPUT-α array with 64 oscillators and a coupling strength of $\alpha = 0.8$ at various tolerances, showing the effect of tolerance on different parts of the array.

Overall, it can be observed that the tolerance on the nonlinear terms has a greater effect on recurrence at a stronger coupling strength. This is not unexpected as it is the nonlinear term that leads to recurrence. Figures 2.16(iii), 2.16(vi), and 2.16(ix) show there is a different energy transfer happening between modes as tolerance increases, since little energy is present in modes 2 to 4. However, the energy return to the first mode for the recurrence peak is still present.

2.7 Order of tolerances

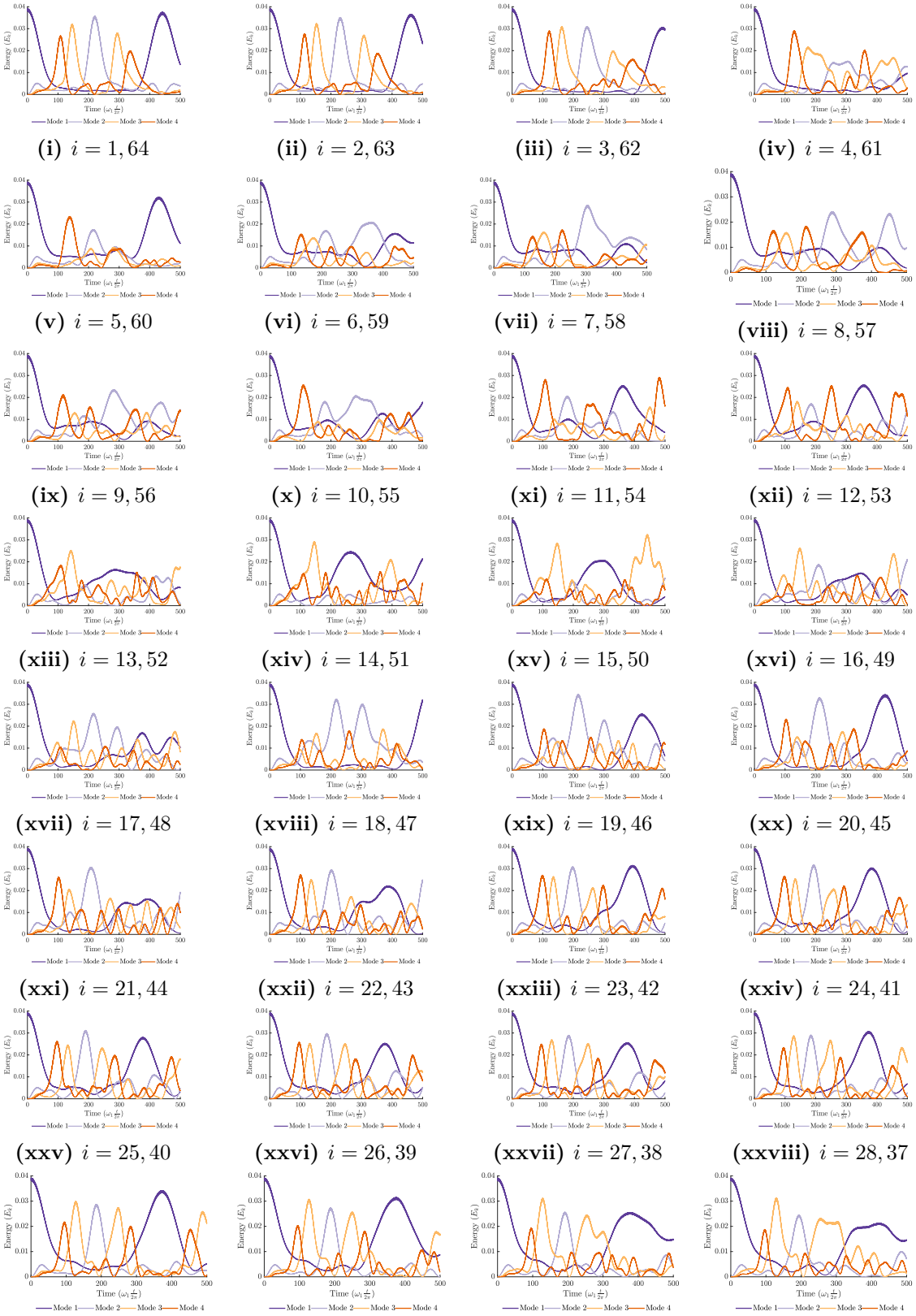
The effect of tolerance on a system is significant with large numbers of oscillators and higher tolerances. This is disappointing if the vast array of knowledge from literature is to be utilised in practical systems. However, it did raise the question as to whether the loss of recurrence was being caused by an individual tolerance outlier or whether it was down to the structure of the tolerances. As such, different techniques to try to mitigate for this reduction in recurrence were explored.

2.7.1 Outlier

The first step was to investigate whether a single outlier was causing a problem. The simplest way to do this was to put a maximum tolerance on a single element, whilst leaving all the others with 0 % tolerance. By applying a tolerance of +10 % to each element in the array in turn, the effect at each position could be identified. This was carried out for an array of 64 oscillators and coupling strength of 0.25.

The results of these simulations are shown in Figure 2.17, with Figure 2.17(i) showing tolerance applied to the first and last element of the array and Figure 2.17(xxxii) showing tolerance applied to elements 32 and 33 of the array. It can be observed that changing the element of the array to which tolerance is applied affects the impact of the outlier on recurrence. As one might expect with an initial condition of the first mode, the results are symmetrical. Hence, tolerance on the first element of the array has the same impact as tolerance on the last element of the array.

However, there are certain points in the array where the impact of the outlier is much greater than at other points. If the outlier is right at the edge of the array then there is little impact on recurrence. This increases as the outlier moves towards the centre but at the 20th element (Figure 2.17(xx)) the energy returning to modes 1, 2, and 4 is only minimally affected, whilst the return of energy in mode 3 is much lower. Continuing towards the centre of the array, the impact continues to change until the 29th element where recurrence is only minimally affected. The impact on recurrence then increases again towards the 32nd element.



(i) $i = 1, 64$ **(ii)** $i = 2, 63$ **(iii)** $i = 3, 62$ **(iv)** $i = 4, 61$

(v) $i = 5, 60$ **(vi)** $i = 6, 59$ **(vii)** $i = 7, 58$ **(viii)** $i = 8, 57$

(ix) $i = 9, 56$ **(x)** $i = 10, 55$ **(xi)** $i = 11, 54$ **(xii)** $i = 12, 53$

(xiii) $i = 13, 52$ **(xiv)** $i = 14, 51$ **(xv)** $i = 15, 50$ **(xvi)** $i = 16, 49$

(xvii) $i = 17, 48$ **(xviii)** $i = 18, 47$ **(xix)** $i = 19, 46$ **(xx)** $i = 20, 45$

(xxi) $i = 21, 44$ **(xxii)** $i = 22, 43$ **(xxiii)** $i = 23, 42$ **(xxiv)** $i = 24, 41$

(xxv) $i = 25, 40$ **(xxvi)** $i = 26, 39$ **(xxvii)** $i = 27, 38$ **(xxviii)** $i = 28, 37$

(xxix) $i = 29, 36$ **(xxx)** $i = 30, 35$ **(xxxi)** $i = 31, 34$ **(xxxii)** $i = 32, 33$

Figure 2.17: Simulations of a 1D FPUT-α array with 64 oscillators and a coupling strength of $\alpha = 0.25$ showing the effect of applying tolerance to a single array element in different positions along the chain.

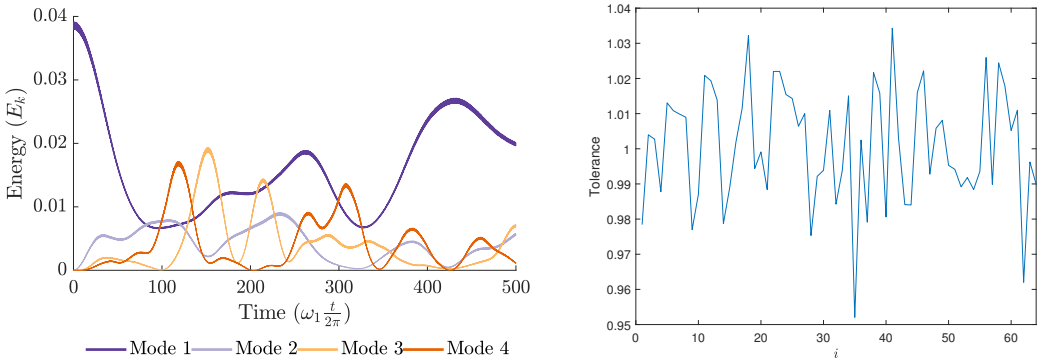
2.7.2 Sorted tolerance values

In the preceding sections, the tolerances have been applied to the system elements in a random manner. However, the outlier investigation suggested that the scale of the impact varies depending on which part of the array is affected by a large difference due to tolerance. Depending on system type and construction, it may be possible to characterise the individual elements before coupling them together. In systems where this is possible, this opens up the option to arrange the individual elements in a certain way if this aids performance.

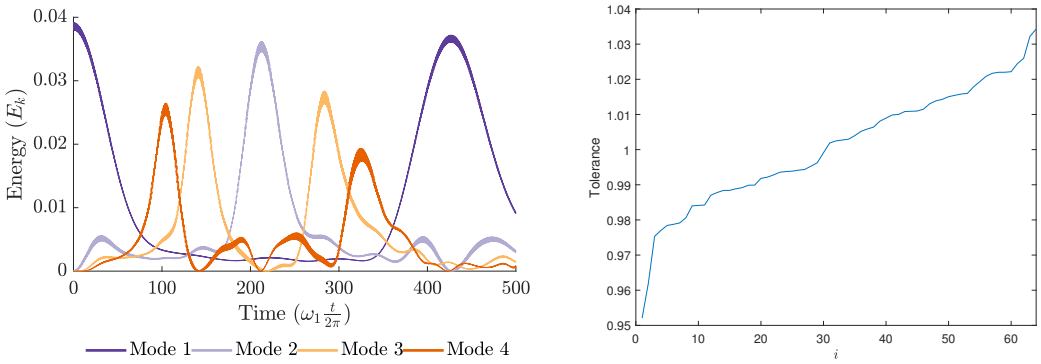
Continuing with the same dataset used in Section 2.6 (that of Figure 2.8(i)), and therefore values of $N = 64$, $\alpha = 0.25$, and tolerance of $\pm 5\,\%$, the tolerance values t_i were sorted before applying them to the system components. Figure 2.18(ii) shows the results if the tolerances are sorted into ascending order. Comparing this to Figure 2.18(i) where the tolerances are in a random order shows that recurrence is significantly improved and is much closer to the ideal. Figure 2.18(iii) shows the results if the tolerances are sorted into a 'peak', which results in a very different form of weak recurrence to the random order.

To understand whether this effect is specific to this set of tolerance values or whether it applies to all, additional sets of tolerance values were considered. The sets of values used for t_i in Figures 2.8(ii)–(iv) were also sorted into a ramp format and the simulations repeated. The results of these simulations are shown in Figure 2.19 and each sub-figure is directly comparable to the results in Figures 2.18(i) and 2.18(ii).

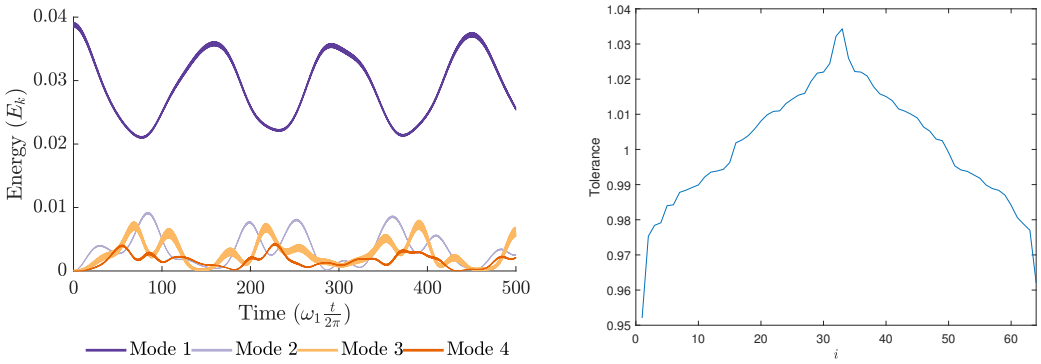
Two of the sets of values in Figure 2.19 show the same response as in Figure 2.18, that is recurrence is improved by sorting the tolerance values. For the set of values of t_i that were used for Figure 2.8(ii), once the values are sorted the output shows a full recurrence cycle (Figure 2.19(i)). Similarly, the system response for the same value set for Figure 2.8(iii) shows an improved recurrence once the values are sorted although the second half of the cycle has less energy returning to the modes (Figure 2.19(ii)).



(i) Random



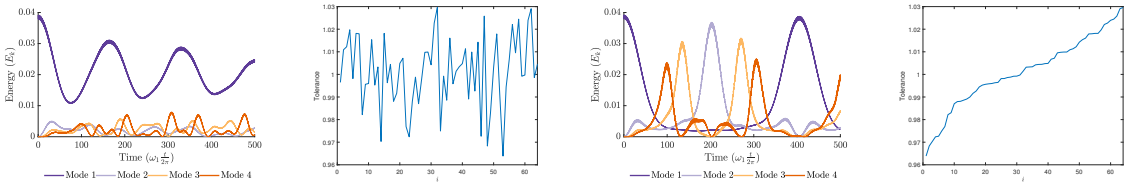
(ii) Ramp



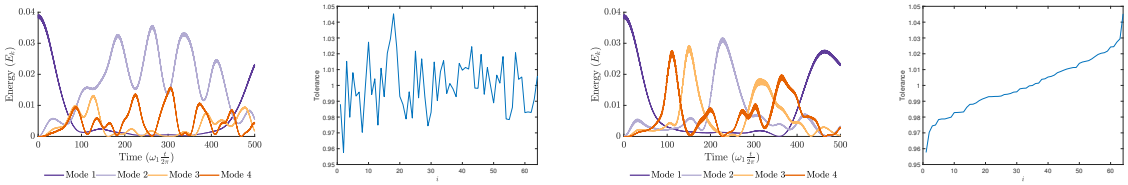
(iii) Peak

Figure 2.18: Simulations of a 1D FPUT-α array with 64 oscillators and a coupling strength of $\alpha = 0.25$ at a tolerance of $\pm 5\,\%$. The same set of tolerance values as used for Figure 2.8(i) is used in each simulation. However, a different method of sorting the values is used in each sub-figure.

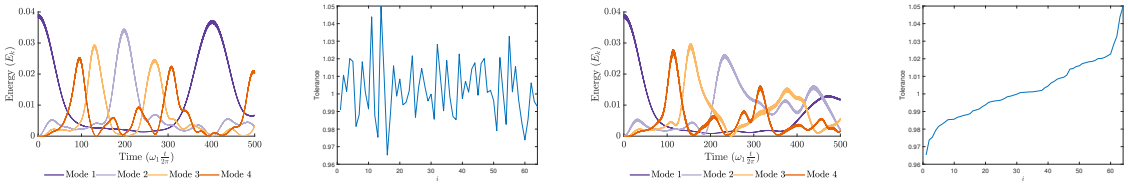
However, for the set of t_i values used for Figure 2.8(iv), the recurrence is severely affected in the second half of the cycle (Figure 2.19(iii)). Comparing this to when the values were in a random order, recurrence is actually not as good once the values have been sorted. Examining the plot showing the distribution of tolerance values, the random order is reasonably balanced along the chain, unlike the previous two cases. However, once the values are sorted there is a steep increase in tolerance towards one end.



(i) Same values of t_i as Figure 2.8(ii)



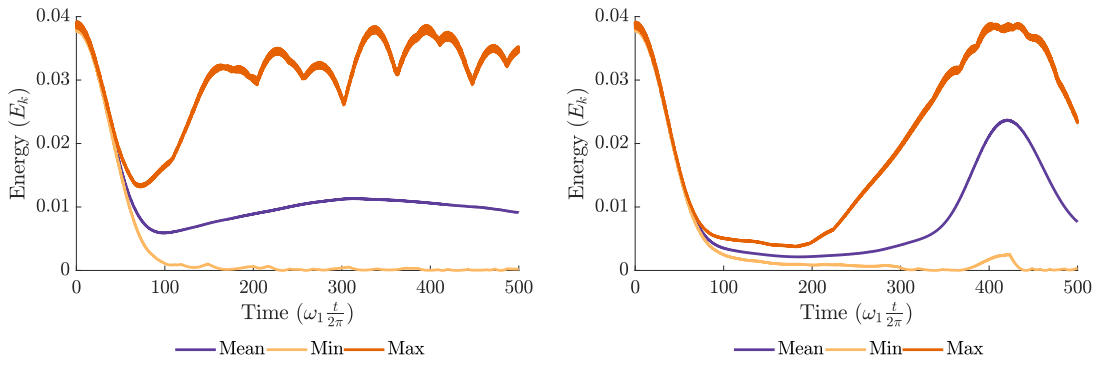
(ii) Same values of t_i as Figure 2.8(iii)



(iii) Same values of t_i as Figure 2.8(iv)

Figure 2.19: Simulations of a 1D FPUT-α array with 64 oscillators and a coupling strength of $\alpha = 0.25$ at a tolerance of $\pm 5\,\%$. Here, the ramp method of sorting is applied to remaining sets of tolerance values used in Figure 2.8.

In addition to this, the entire set of 100 Monte Carlo runs were sorted into ramp format and the mean, minimum and maximum plotted. This is presented in Figure 2.20 alongside the equivalent for the randomly ordered sets of tolerance values. These figures show that on average the quality of recurrence is improved. However, as shown in Figure 2.19(iii), this cannot be guaranteed for all sets of tolerance values.



(i) Random **(ii)** Ramp

Figure 2.20: Plot showing the mean, minimum and maximum values of the first energy mode for 100 simulations of a 1D FPUT-α array with 64 oscillators and a coupling strength of $\alpha = 0.25$ at a tolerance of $\pm 5\,\%$. These are shown for the tolerance values in a random order and sorted into a ramp format.

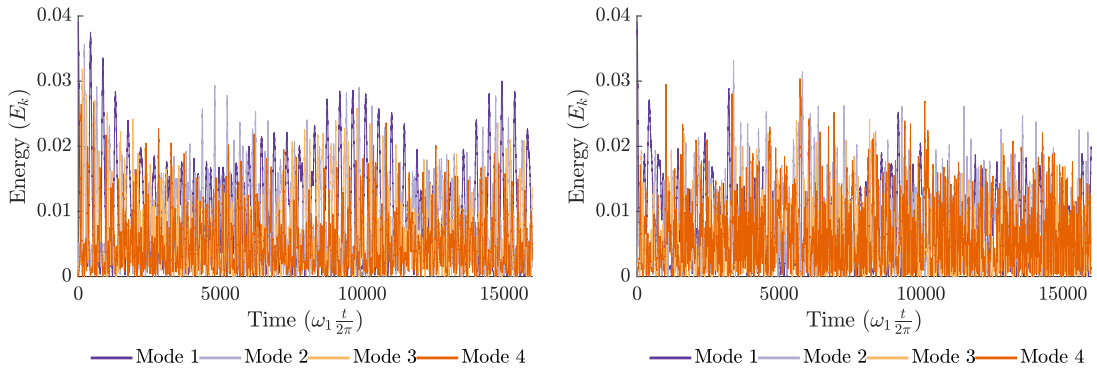
2.8 Effect of tolerance on superrecurrence

As described in Section 1.3, when an FPUT system is observed over a longer time period, a superperiod is apparent and this effect has been termed 'superrecurrence'. The numerical experiments in the early part of this chapter have shown that recurrence is affected by tolerance. However, this did raise the question of whether tolerance was completely killing recurrence, or if recurrence was just being delayed.

Continuing to use the example of a 64 element system with a coupling strength of 0.25 and a tolerance of $\pm 5\,\%$ using the same set of values for t_i as Figure 2.8(i) the simulation was run for a longer period of 16 000 cycles of the fundamental frequency. To allow for a comparison, the simulation was also run for the same time period with $0\,\%$ tolerance. The results of these simulations are shown in Figure 2.21.

The superrecurrence is less obviously periodic for a chain of 64 oscillators (Figure 2.21(i)) than it is for a chain of 16 oscillators (Figure 1.7), although there is a distinct undulation in the peaks of the first mode. At a tolerance of $\pm 5\,\%$, a single cycle of recurrence showed a weaker return of energy to the first mode (Figure 2.8(i)). However, running the simulation for longer shows that more energy does return to the first mode over time (Figure 2.21(ii)). The superrecurrence shown in the simulation with $0\,\%$ tolerance is virtually non-existent at $\pm 5\,\%$, although there is a

large variation between the amplitude of the first mode peaks. Energy exchange between the modes also appears much less consistent at the higher tolerance.



(i) 0 % **(ii)** ±5 %

Figure 2.21: Longer simulations of a 1D FPUT-α array with 64 oscillators and $\alpha = 0.25$ showing the difference in superrecurrence between an array with 0 % tolerance and an array with a tolerance of ±5 %.

Running a large number of simulations over a long period for a system of 64 oscillators requires a significant amount of computation time. To allow more flexibility, further investigations were carried out with a smaller array of oscillators. A chain length of 16 was chosen, in part because it is one of the sizes Tuck and Menzel used for their investigations [34]. The simulations were run for 2000 cycles of the fundamental frequency, which allows for two full cycles of the superperiod.

Section 2.4 showed that reducing the number of oscillators in the chain made the system more resilient to tolerance. Therefore, to gain an understanding of the effects of tolerance on the system, a single cycle of recurrence for tolerance values of ±0.1 %, ±1 %, ±5 %, and ±10 % is shown in Figure 2.22. Comparing these to Figure 2.11(iii) shows that there is very little impact on recurrence with a tolerance of ±0.1 % and ±1 %. However, at ±5 % tolerance recurrence is still present although less energy enters mode 3, whilst mode 2 is changing shape. By ±10 % tolerance the recurrence period has changed and the energy in modes 2 to 4 is significantly different.

The results of the longer simulations using the same sets of values of t_i are shown in Figure 2.23. At a tolerance of ±0.1 % (Figure 2.23(i)), the superrecurrence pattern is very similar to that with 0 % tolerance (Figure 1.7). A small increase in tolerance to ±1 % produces a significant impact on the superperiod (Figure 2.23(ii)).

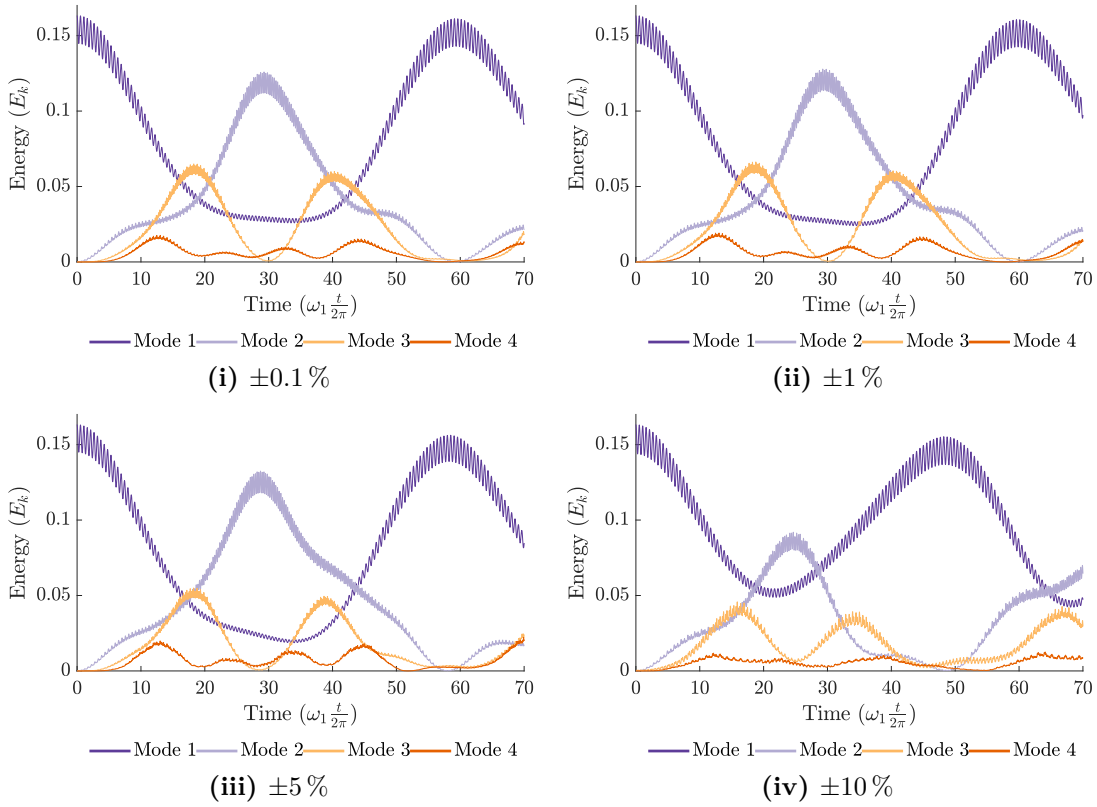


Figure 2.22: Simulations of a 1D FPUT-α array with 16 oscillators and a coupling strength of $\alpha = 0.25$ showing examples of recurrence at various tolerances.

This is in contrast to a single cycle of recurrence where very minimal difference is seen. There are the same number of recurrence peaks in the first mode seen in both Figures 2.23(i) and 2.23(ii). However, an additional peak in the second mode for a tolerance of ±1 % indicates that the standard recurrence period has reduced slightly. The superperiod shows a more marked difference. There are two cycles of the superperiod visible for 2000 cycles at a tolerance of ±0.1 % and almost three cycles at a tolerance of ±1 %. The amplitude of the superperiod also decreases with the increase in tolerance.

Increasing the tolerance further to ±5 % (Figure 2.23(iii)), the recurrence period has again reduced, with an additional two cycles of the first mode being present in the same time frame. The superperiod has remained approximately the same as for a tolerance of ±1 %, although the shape of the superrecurrence has changed slightly. Finally, at a tolerance of ±10 %, not only has a single recurrence cycle changed significantly, the superrecurrence has too. Figure 2.23(iv) shows an additional

10 cycles of recurrence compared to Figure 2.23(i). The superperiod has also reduced so that 11 cycles of the superrecurrence are observed. The amount of energy entering the higher modes continues to be lower throughout the full time period at $\pm 10\,\%$ tolerance.

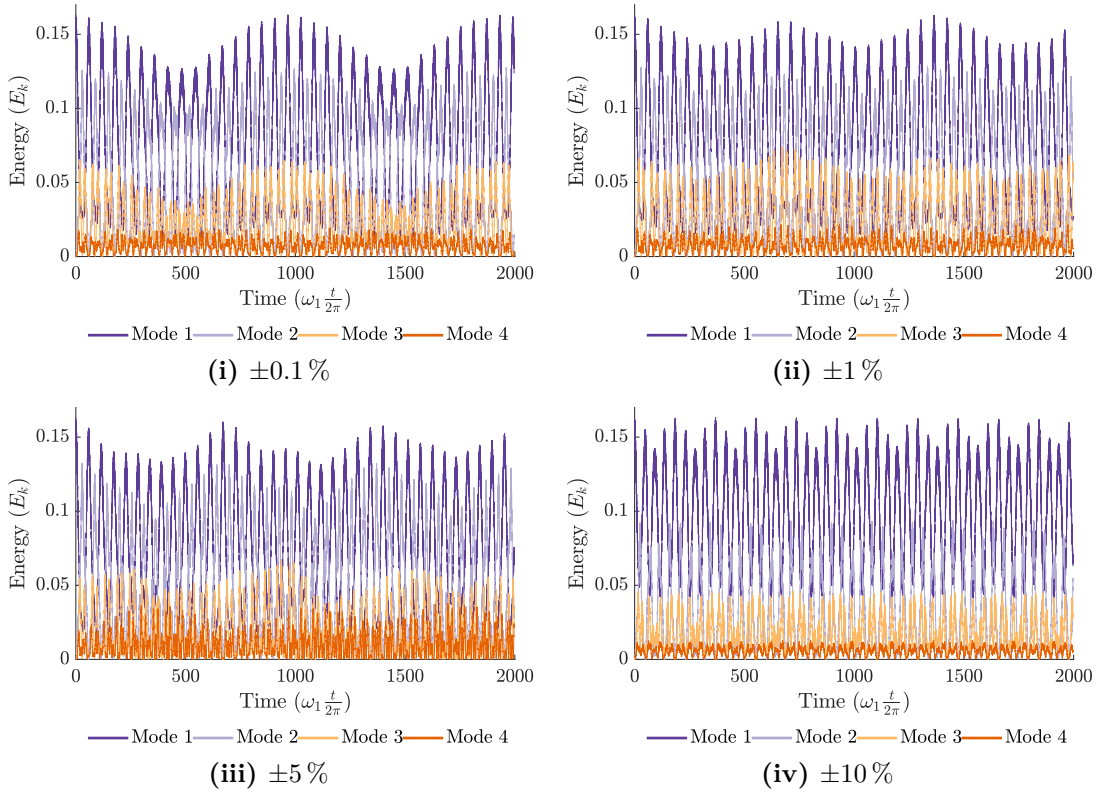


Figure 2.23: Longer simulations of a 1D FPUT-α array with 16 oscillators and a coupling strength of $\alpha = 0.25$ showing the change in superrecurrence at various tolerances.

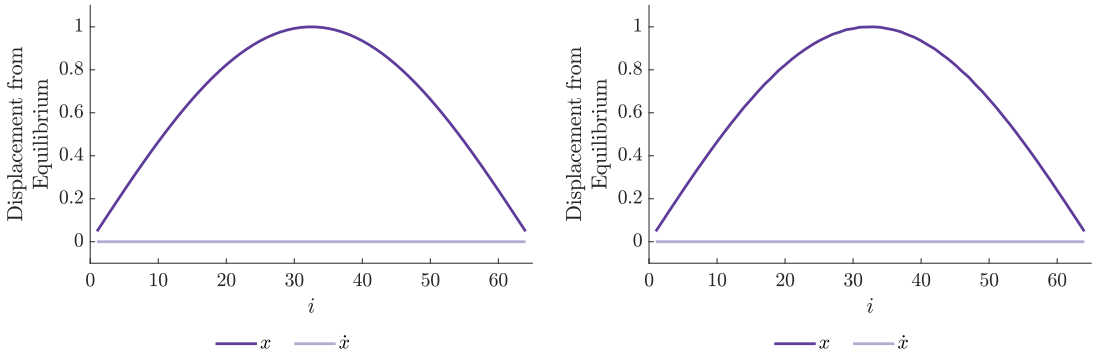
What stands out from these results is that although the energy exchange patterns for a single cycle of recurrence are significantly affected at a tolerance of $\pm 5\,\%$ in an array of 64 oscillators, energy exchange does continue to occur over a longer time period. Additionally, there is an increasing variation in superrecurrence with tolerance. Given the results presented in Section 2.3, it is likely that there will be a large range of responses to tolerance reflected in the superperiod as well as a single recurrence period. However, as the results presented in Figure 2.22 are representative of the majority response for those tolerances, it is expected that the superrecurrence will follow a similar pattern.

2.9 Numerical stability test

In order to check that the changes in recurrence due to the addition of tolerance were not due to a build up of numerical errors, a numerical stability test was performed in Python using ODEINT. This was performed by testing the simulation methodology used in this thesis to see if the results were time reversible. Using the same tolerances and values of N and α from the simulations presented in this chapter, the output was used as an initial condition and the equation of motion simulated backwards in time.

For each oscillator, the error between the initial condition for the forward simulation (i.e. the first mode described by Equation (2.2)) and the output of the reverse simulation was then calculated as a percentage. The maximum error among all oscillators for that simulation was then noted. These errors are below 0.5 % for $N \leq 64$ and below 4 % for $N = 128$.

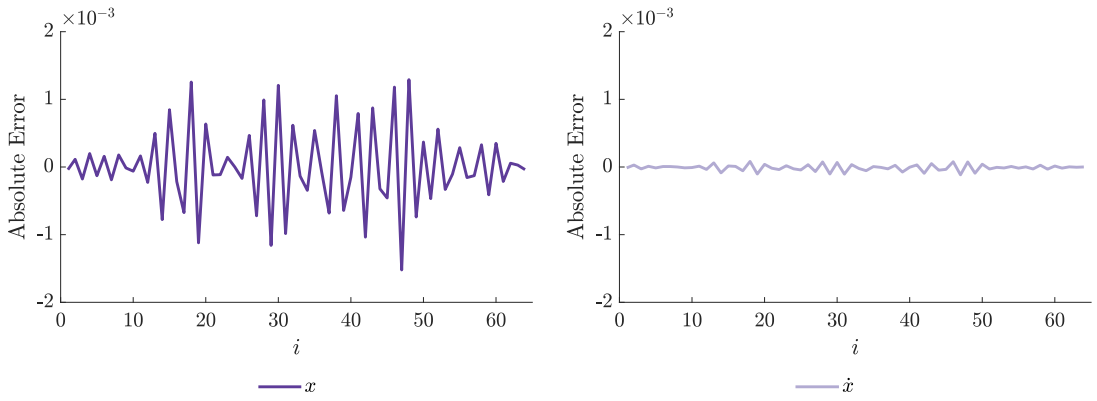
Figure 2.24(ii) shows a typical output after the time-reversed simulation; this is for a system with 64 elements, a coupling strength of 0.25, and a tolerance of ± 1 % with the same set of values of t_i as used for Figure 2.7(i). This illustrates that the result of the reverse simulation is close to the initial condition of an excitation in the first mode (Figure 2.24(i)).



(i) Initial condition of the first mode **(ii)** Result of reverse simulation

Figure 2.24: Comparison of the initial condition with the output from a time-reversed simulation for the system in Figure 2.7(i).

The absolute error between the initial condition and the output from the reverse simulation can be seen in Figure 2.25. This shows that the errors are numerically small, and for this particular example the maximum percentage error for x is 0.2 %.



(i) Absolute error for x **(ii)** Absolute error for $\dot{x}$

Figure 2.25: Absolute error between the initial condition and the result of time-reversed simulation for the system in Figure 2.7(i).

2.10 Summary

This chapter examined the effect of incorporating heterogeneity on a 1D FPUT-α array through numerical experiments. Such heterogeneity arises from the inherent tolerances of various manufacturing processes, so one must take it into consideration when building physical systems.

The results of the simulations illustrate that tolerance has a significant impact on recurrences in an FPUT system, both for a single recurrence period and the longer superperiod. In a 64-element system, for tolerance values that lie within the typical range for manufacturing tolerances, recurrence as demonstrated by Fermi *et al.* is destroyed. However, by reducing the number of oscillators in an FPUT system, one retains recurrence for some reasonable amount of tolerance before it breaks down.

By controlling manufacturing tolerance between nominally identical components, it may be possible to observe recurrence in an FPUT system with a small number of oscillators. However, tight tolerances are hard to achieve and are often very expensive. Therefore, producing such a system may not be practical. It is also worth noting that for seeing better recurrence, a larger number of oscillators is required. However, to handle tolerance, a smaller number of oscillators is better. These counter statements suggests that there may only be a very small window of array sizes to actually observe recurrence in a physical system.

In arrays where it is possible to characterise the individual elements before linking them together, it may be possible to improve the resilience of the system to tolerance by arranging the elements in a particular order, for example, by increasing overall tolerance. The nonlinear coupling strength is also an important factor to consider. A coupling strength that is very weak (in the order of 0.1) reduces the quality of recurrence. However, with increasing coupling strength the addition of tolerance has a greater impact, reducing recurrence.

3

Asymmetric tolerances

Contents

3.1 Effect of asymmetric tolerance on recurrence 62
3.1.1 Tolerance of ±0.1 % 64
3.1.2 Tolerance of ±1 % 64
3.1.3 Tolerance of ±5 % 65
3.1.4 Tolerance of ±10 % 66
3.2 Arrays with different number of oscillators 68
3.3 Tolerance on linear versus nonlinear terms 70
3.4 Different nonlinear coupling strengths 72
3.4.1 Varying coupling strength with ±5 % tolerance 72
3.4.2 Increased coupling strength at various tolerances 74
3.4.3 Tolerance on linear versus nonlinear terms 75
3.5 Order of tolerances 77
3.6 Effect of tolerance on superrecurrence 81
3.7 Other tolerance structures 83
3.7.1 Alternative tolerance structure A 84
3.7.2 Alternative tolerance structure B 86
3.7.3 Alternative tolerance structure C 88
3.7.4 Section summary 90
3.8 Summary 91

A part of this chapter has been published as

H. Nelson, M. A. Porter, and B. Choubey, "Variability in Fermi-Pasta-Ulam-Tsingou arrays can prevent recurrences", *Physical Review E*, vol. 98, no. 6, p. 062 210, Dec. 2018

The simulations detailed in Chapter 2 show results from symmetrically-coupled FPUT systems, whereby the force exerted on x_i by x_{i+1} (forward coupling) is subject to the same tolerances as the force exerted on x_{i+1} by x_i (backward coupling) as they are connected by a single component, e.g. a mechanical spring. However, in a variety of physical realisations of such a system, forward coupling and backward coupling are not always the same as they follow different paths through different components, e.g. in an electronic circuit. This asymmetry leads to another source of error. Different realisations of the system will also lead to tolerances being added into the equation in different forms and effectively altering the structure of the FPUT system.

This chapter starts by examining the effect of a change in structure for a typical electronic implementation of the FPUT equation on recurrence at various tolerances. It then explores the effects of other tolerance structures added to the FPUT equation.

3.1 Effect of asymmetric tolerance on recurrence

A typical electronic circuit constructed to emulate the FPUT equation may have a different group of passive components associated with each term of the equation. As each of these components may have a different tolerance, each term will inherently have an associated tolerance which varies between individual circuits. These tolerances can be incorporated into the FPUT-α array as follows:

$$\ddot{x}_i = (t_{i+1}x_{i+1} + t_{i-1}x_{i-1} - 2t_i x_i) + \alpha[f_i^{\text{nlin}}(x_{i+1} - x_i)^2 - b_i^{\text{nlin}}(x_i - x_{i-1})^2] \quad (3.1)$$

where the tolerances on the linear terms continue to be represented by t_i and the tolerances on the 'forward' and 'backward' nonlinear terms are represented by f_i^{nlin} and b_i^{nlin}, respectively. In the same manner as for variation in the masses in the symmetric implementation in Chapter 2, all component variations are combined into the single tolerance value attached to each of equation terms.

Figure 3.1 is a block diagram representation of the elements that form the FPUT equation with indication of how the tolerances are applied. A change in notation is used for the diagram where x_a, x_b and x_c represent any 3 elements in a longer chain. This is to avoid confusion with x_i, x_{i+1} and x_{i-1} changing depending on which element is being considered.

The central row provides the acceleration terms on the left hand side of the equation. The top and bottom rows represent the individual array elements, whilst the second and fourth rows represent the coupling. The tolerances on the linear terms are formed as the individual tolerances on the elements are dominant. For the nonlinear terms, the tolerance on the path from the nonlinear coupling block to the central row is dominant and these tolerances are different. One example of how this may occur is an additional buffer in the backwards path to create the inversion.

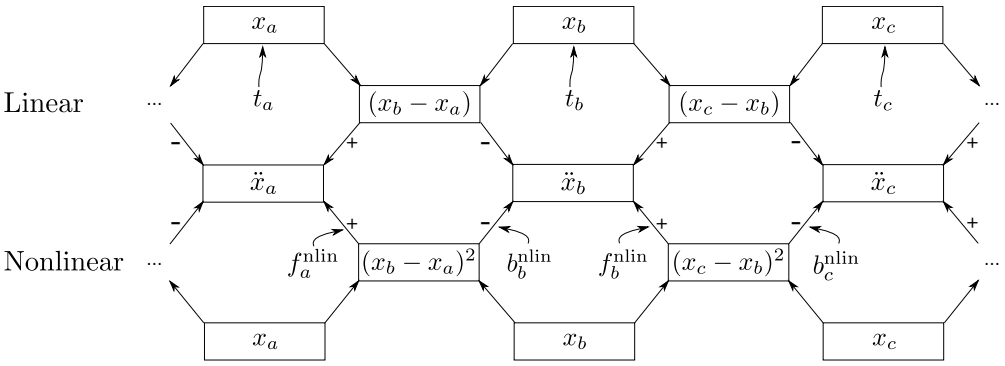


Figure 3.1: Block diagram showing the elements used to form the FPUT equation and the associated tolerances for Equation (3.1). Here x_a, x_b and x_c represent any 3 elements in a longer chain.

Using the same tolerance values as used in Chapter 2 (i.e. $\pm 0.1\,\%$, $\pm 1\,\%$, $\pm 5\,\%$, and $\pm 10\,\%$) and a coupling strength α of 0.25, the FPUT system in Equation (3.1) was simulated for 100 Monte Carlo runs at each tolerance. A representative set of results from these simulations are presented in this section and the corresponding sets of full results is presented in Appendix D. To identify any changes in recurrence due to the different tolerance structure, these results are compared to those for the symmetric system.

3.1.1 Tolerance of ±0.1 %

Starting with a tolerance of ±0.1 %, it can be seen that the results for the asymmetric system presented in Figure 3.2 are very similar to those for the symmetric system presented in Figure 2.6. Small variations in the shape of the energy in each mode do occur between runs and these are most prominent in modes 3 and 4.

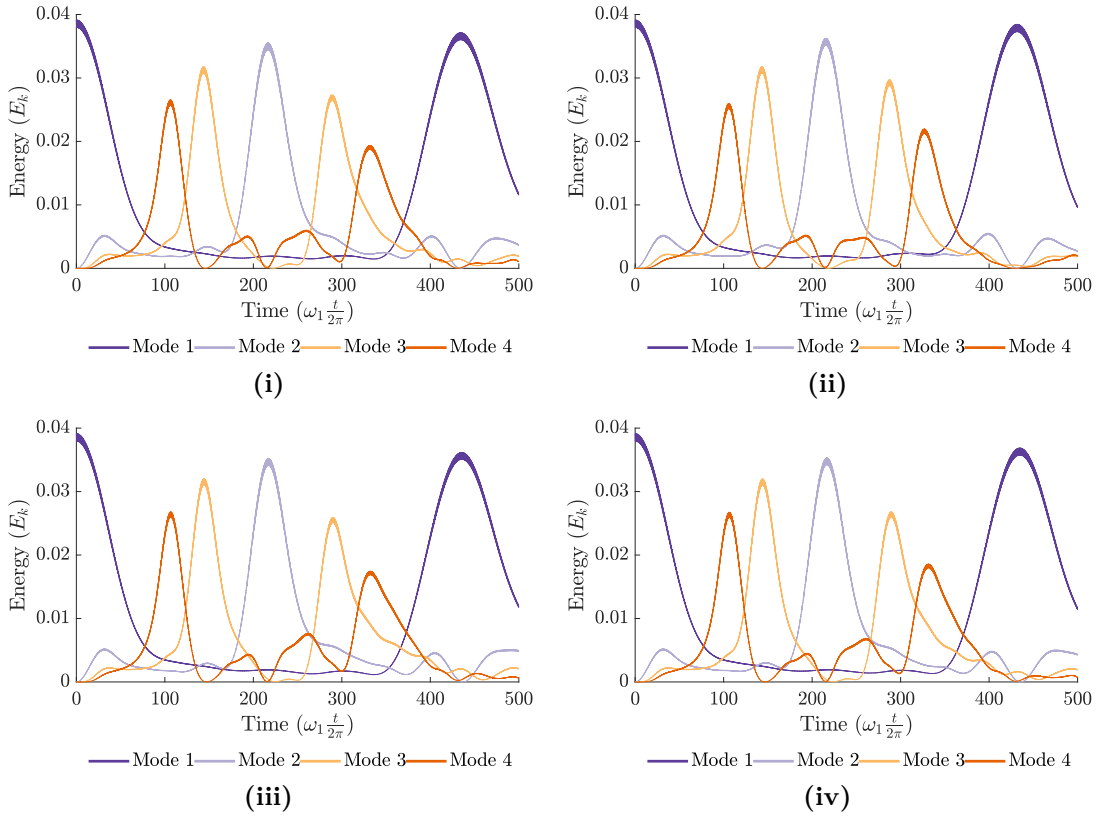


Figure 3.2: Simulations of a 1D FPUT-α array with asymmetric tolerances, 64 oscillators, and a coupling strength of $\alpha = 0.25$ showing examples of different recurrence patterns at a tolerance of ±0.1 %.

3.1.2 Tolerance of ±1 %

Increasing the tolerance to ±1 %, the differences between the symmetric and asymmetric system responses increase slightly. Comparing the results presented in Figure 3.3 to those presented in Figure 2.7, it can be seen that recurrence is still affected in a very similar manner. However, for the asymmetric system, 50 % of the responses are represented by Figures 3.3(i)–3.3(ii) where recurrence is still strong but the pattern of energy is affected, particularly in modes 3 and 4. As in the symmetric

system, the recurrence period has changed but has extended rather than contracted. The other 50 % of the responses are represented by Figures 3.3(iii)–3.3(iv) where recurrence of energy into the first mode becomes weak and the pattern of energy transfer between modes has altered significantly.

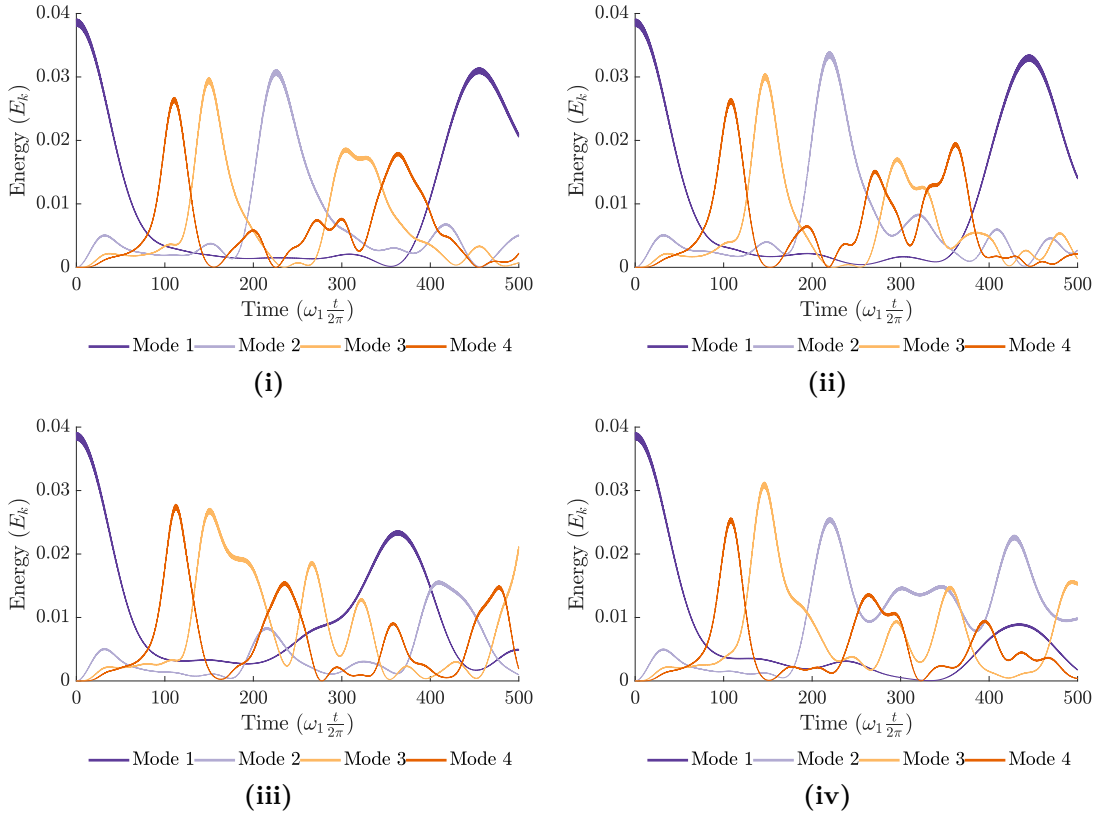


Figure 3.3: Simulations of a 1D FPUT-α array with asymmetric tolerances, 64 oscillators, and a coupling strength of $\alpha = 0.25$ showing examples of different recurrence patterns at a tolerance of $\pm 1\,\%$.

3.1.3 Tolerance of $\pm 5\,\%$

At $\pm 5\,\%$, the response of the system with asymmetric tolerances is again similar to that of the system with symmetric tolerances. The response of the asymmetric system varies widely with different sets of tolerance values. The predominant response shows some energy being transferred between the modes but without a significant return to the first mode. This is represented by Figures 3.4(i)–3.4(ii) and is comparable to the symmetric system response shown in Figure 2.8(i).

Figure 3.4(iii) shows a response where significant energy transfer is occurring into and out of the first mode on a different timescale to the recurrence period of the system with 0 % tolerance. However, there is reduced energy entering modes 2, 3, and 4. This is similar to the symmetric system response shown in Figure 2.8(ii). Finally, the response shown in Figure 3.4(iv) shows a recurrence pattern in the first mode where the two peaks are very distinctive but the energy in between those peaks doesn't drop as low. Less energy is also transferred into modes 2, 3, and 4, although the peaks for modes 2 and 4 occur in a similar position to a system with 0 % tolerance.

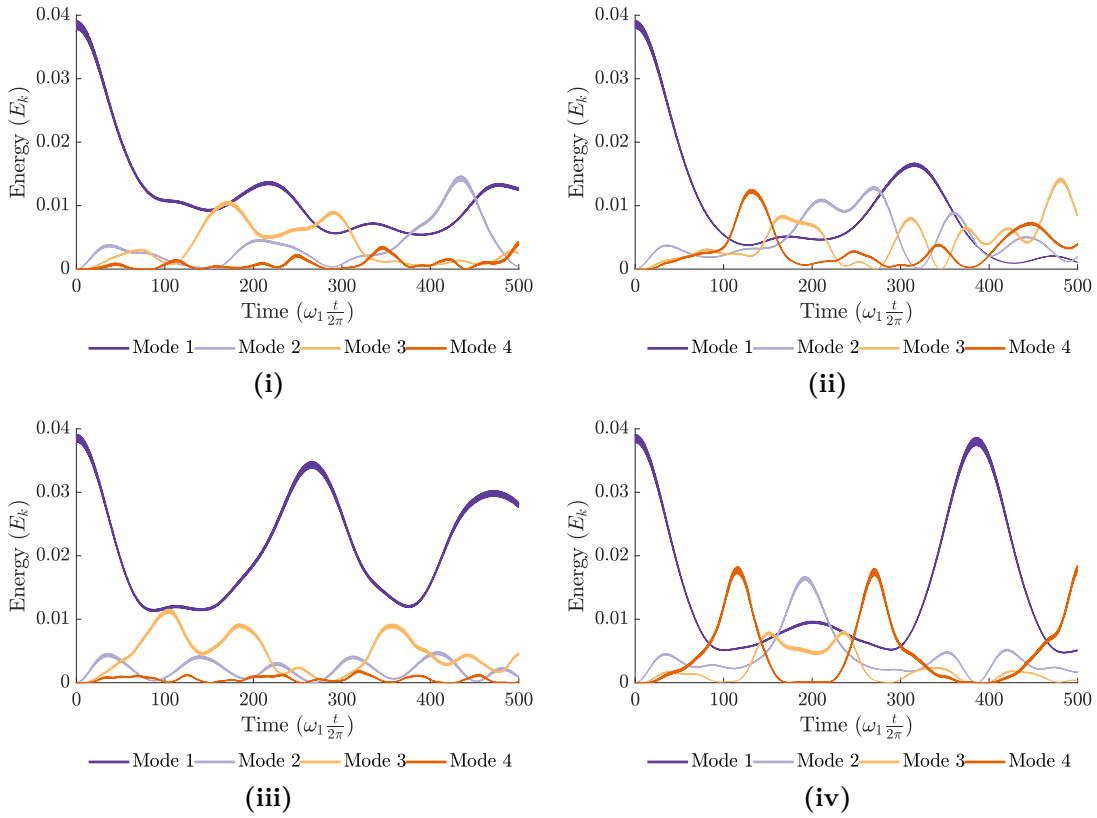


Figure 3.4: Simulations of a 1D FPUT-α array with asymmetric tolerances, 64 oscillators, and a coupling strength of $\alpha = 0.25$ showing examples of different recurrence patterns at a tolerance of ± 5 %.

3.1.4 Tolerance of ± 10 %

On increasing the tolerance to ± 10 %, recurrence is severely affected in the asymmetric system, as it is in the symmetric system. However, as observed at ± 1 % and ± 5 %, the impact is more significant for the asymmetric system. In the asymmetric

system, the majority of responses are represented by Figure 3.5(i), whereas only a small number of responses were represented by the comparable symmetric response shown in Figure 2.9(ii). Responses similar to those shown for the symmetric system in Figures 2.9(i) and 2.9(iii) do occur, however, energy transfer into modes 2, 3, and 4 is much lower in the asymmetric system as shown in Figures 3.5(ii) and 3.5(iii).

Additionally, in 22 % of cases the Python simulations failed as shown in Figure 3.5(iv). It is possible that under more stringent integrating options, a simulation with the sets of tolerance values involved might produce a solution. However, it was felt that the results obtained were sufficient to gain a basic understanding of the type of response that could be expected from an asymmetric system with a tolerance of ±10 %.

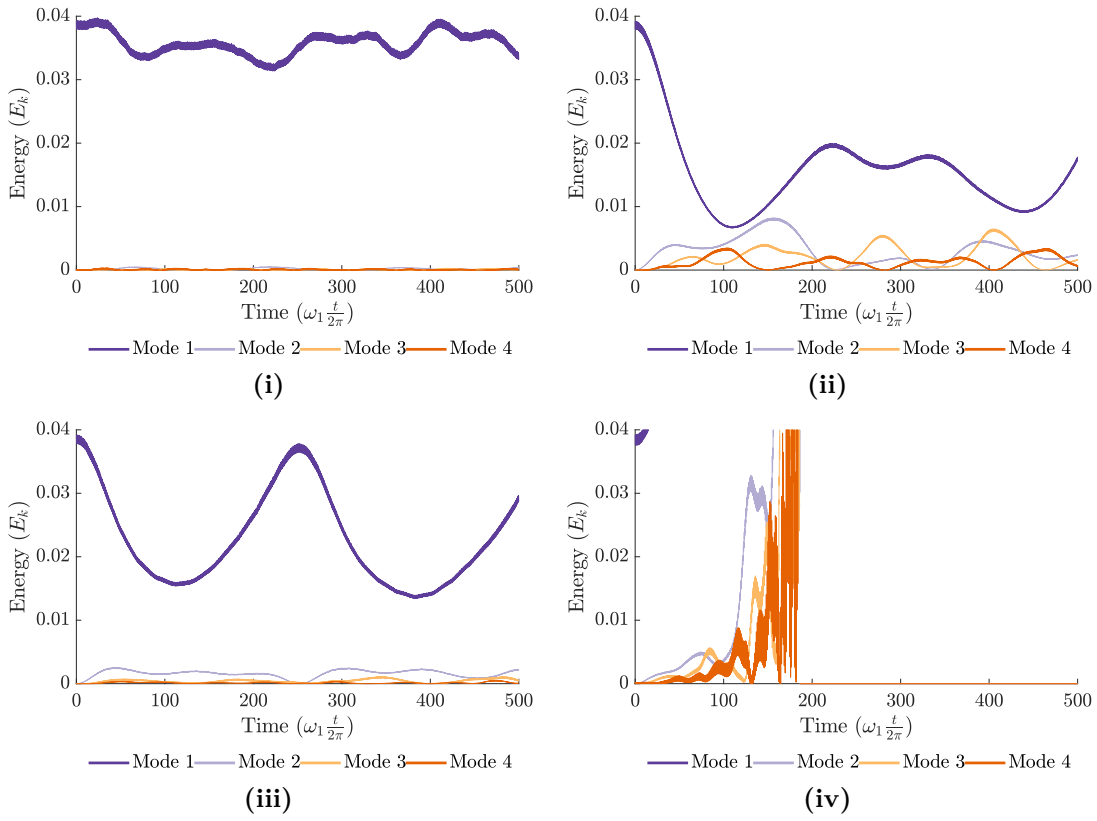


Figure 3.5: Simulations of a 1D FPUT-α array with asymmetric tolerances, 64 oscillators, and a coupling strength of $\alpha = 0.25$ showing examples of different recurrence patterns at a tolerance of ±10 %.

3.2 Arrays with different number of oscillators

In Section 2.4, it was shown that reducing the number of oscillators in a system improved the resilience of the system with regard to tolerance. Hence, as the previous section showed that the asymmetric system is less able to absorb tolerance, it might be expected that recurrence will be more affected even with a smaller number of oscillators. The simulation results for asymmetric systems of various sizes with a tolerance of $\pm 5\,\%$ presented in Figure 3.6 show this to be the case when compared to the results for the symmetric system in Figure 2.11.

For a chain length of 4 or 8 oscillators, the recurrence time period is altered slightly but the overall shape is similar to that for a system with $0\,\%$ tolerance (compare Figures 3.6(i)–3.6(ii) to Figures 2.10(i)–2.10(ii)). This is the same as for the symmetric system (Figures 2.11(i)–2.11(ii)). Increasing the chain length to 16 oscillators, in addition to the recurrence period changing, the shape of the energy in each mode is starting to change. This is more noticeable in the asymmetric system (Figure 3.6(iii)) than the symmetric system (Figure 2.11(iii)).

By a chain length of 32 oscillators, the asymmetric system (Figure 3.6(iv)) is diverging significantly further from the ideal system (Figure 2.10(iv)) than the symmetric system (Figure 2.11(iv)). This trend continues as the chain length increases further to 64 oscillators where recurrence has broken down for the asymmetric system (Figure 3.6(v)) but is still weak in the symmetric system (Figure 2.11(v)). At a chain length of 128 oscillators, recurrence has broken down in both systems; however, there is still more energy transfer happening between modes in the symmetric system (compare Figures 3.6(vi) and 2.11(vi)).

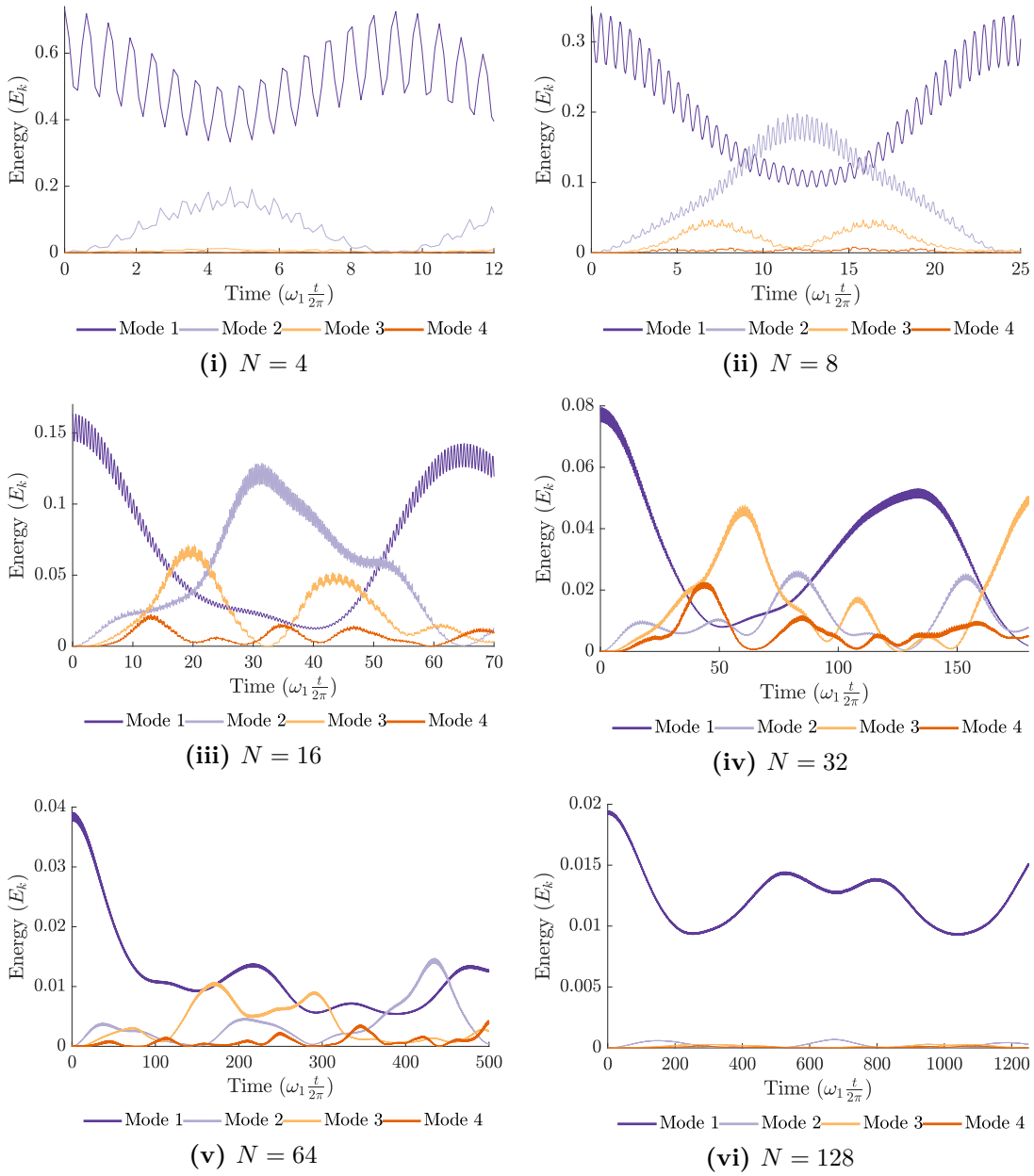


Figure 3.6: Simulations of asymmetric 1D FPUT-α arrays with different numbers of oscillators and a coupling strength of $\alpha = 0.25$ at a tolerance of $\pm 5\,\%$.

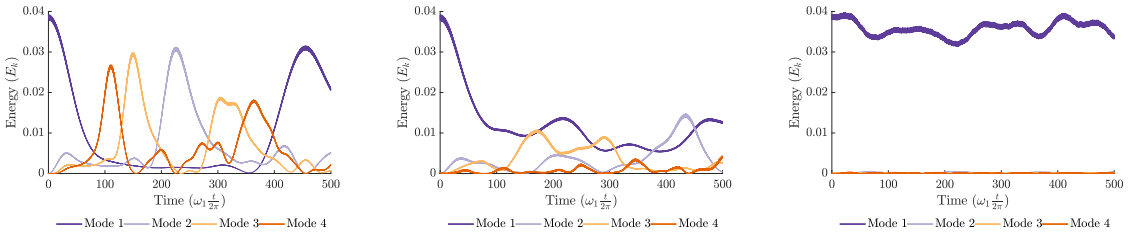
3.3 Tolerance on linear versus nonlinear terms

Sections 3.1 and 3.2 have shown that whilst the impact of tolerance is comparable in an asymmetric FPUT system to a symmetric FPUT system, recurrence in the asymmetric system breaks down for a smaller tolerance than it does in the symmetric system. As the different types of tolerance change the structure of the FPUT equation, it is worth considering the impact of tolerance on the linear and nonlinear terms for the asymmetric system as was done for the symmetric system (Section 2.5).

Comparing the results of this asymmetric system presented in Figure 3.7 to those of the symmetric system in Figure 2.12, it can be observed that the impact of tolerance is comparable in the two systems when tolerance is incorporated into both the linear and nonlinear terms. However, one interesting observation is that incorporating tolerance in only the nonlinear terms of the symmetric FPUT system has a comparable effect to that of adding it to only the linear terms (Figure 2.12), whereas incorporating tolerance in only the nonlinear terms in the asymmetric FPUT system seems to have significantly less impact than expected, as it can be observed that recurrence is close to that of an ideal system (Figures 3.7(vii)–3.7(ix)).

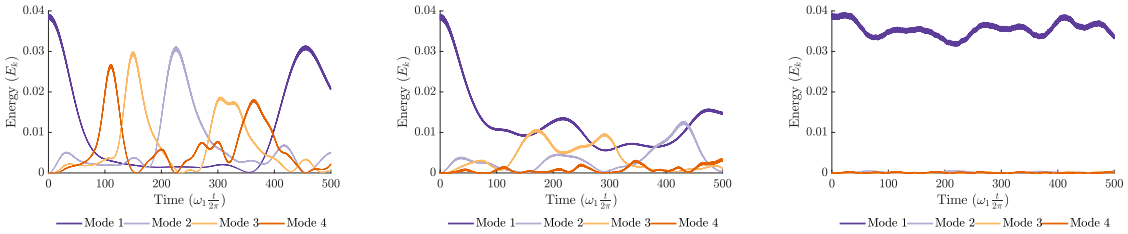
One possible explanation for this may be the difference in structure of the equation when tolerances are incorporated. The symmetric system includes tolerance on each of the individual elements inside the brackets of the quadratic terms. Consequently, the tolerances are squared, approximately doubling the amount of tolerance on some of the nonlinear terms. In contrast, the asymmetric system includes the tolerance outside of the brackets, maintaining the tolerance levels at the values stated. This is explored further in Section 3.7.

Tolerance in both linear and nonlinear terms:



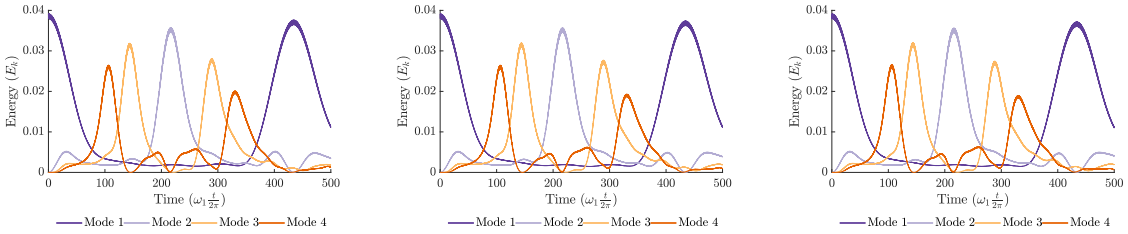
(i) ±1 % **(ii)** ±5 % **(iii)** ±10 %

Tolerance in the linear terms:



(iv) ±1 % **(v)** ±5 % **(vi)** ±10 %

Tolerance in the nonlinear terms:



(vii) ±1 % **(viii)** ±5 % **(ix)** ±10 %

Figure 3.7: Simulations of asymmetric 1D FPUT-α arrays with 64 oscillators and a coupling strength of $\alpha = 0.25$ at various tolerances, showing the effect of tolerance on different parts of the array.

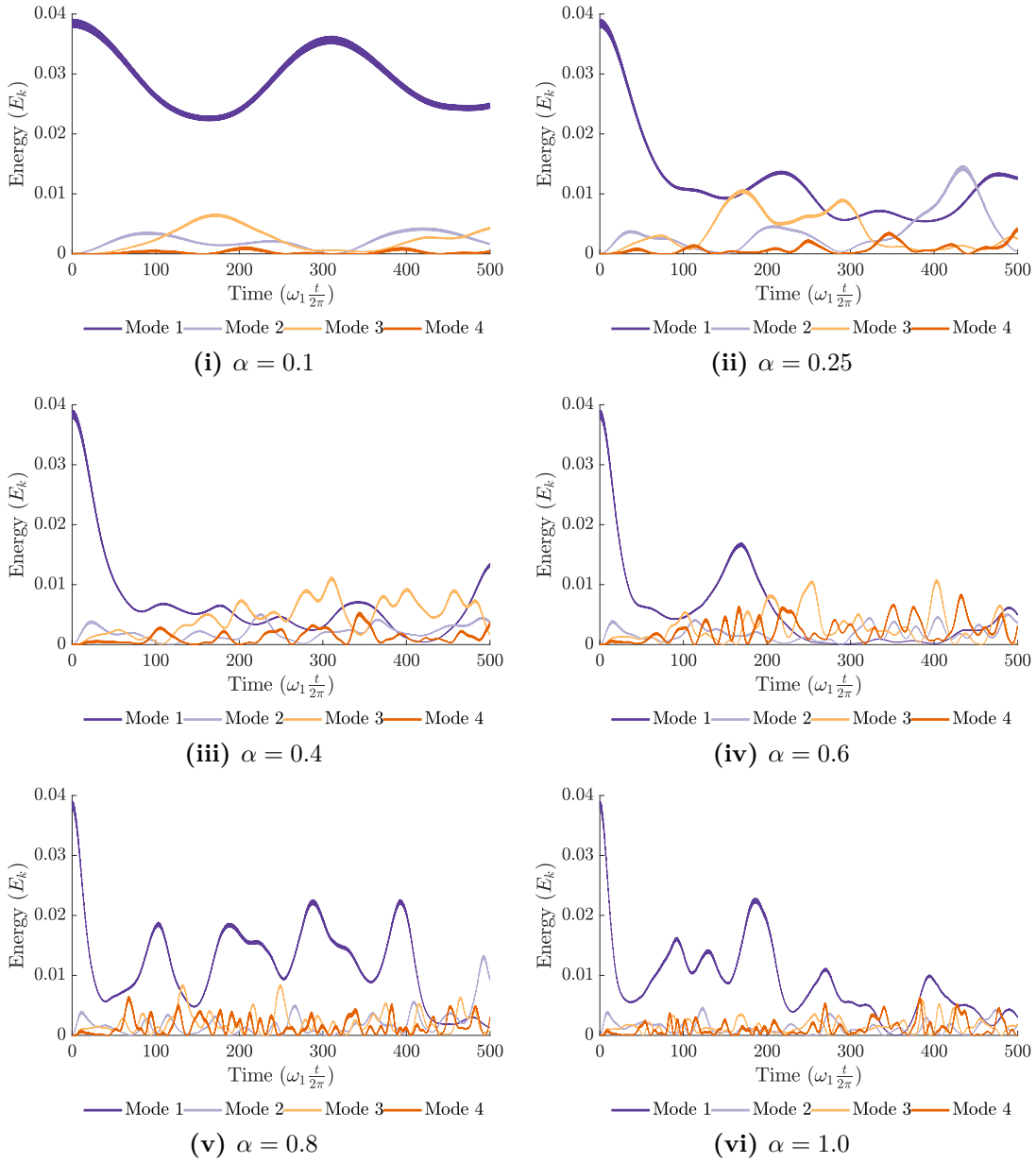
3.4 Different nonlinear coupling strengths

In Section 3.3, it was shown that tolerance on the nonlinear terms in the asymmetric system has a less significant impact on recurrence than in the symmetric one. However, when tolerance is included in both the linear and nonlinear terms, the asymmetric system is less immune to tolerance than the symmetric one. Section 2.6 showed that recurrence weakened with increasing coupling strength for the symmetric system at $\pm 5\,\%$ tolerance. It is therefore worth investigating whether the asymmetry improves the response at higher coupling strengths.

3.4.1 Varying coupling strength with $\pm 5\,\%$ tolerance

In Section 2.6, a tolerance of $\pm 5\,\%$, a chain length of 64 oscillators and a coupling strength of 0.25 were used to investigate the impact of changing the nonlinear coupling strength. Therefore, the same conditions will be used in this section. Taking the same set of values for tolerance used to produce Figure 3.4(i) and repeating the single simulation will allow the results to be compared directly as the only changing variable is α.

Figure 3.8 shows the results of the simulations with coupling strengths of 0.1, 0.4, 0.6, 0.8, and 1.0 in addition to the original simulation with a coupling strength of 0.25. These results show that, as the coupling strength increases, more energy is returning to the first mode. Additionally, although the peak energy in modes 2, 3, and 4 decreases, the transfer between these modes becomes more frequent. Comparing these results to Figure 2.14, it would appear that although the overall energy transfer in modes 2, 3, and 4 is lower, the energy returning to the first mode is greater.



(i) $\alpha = 0.1$ **(ii)** $\alpha = 0.25$

(iii) $\alpha = 0.4$ **(iv)** $\alpha = 0.6$

(v) $\alpha = 0.8$ **(vi)** $\alpha = 1.0$

Figure 3.8: Simulations of asymmetric 1D FPUT-α arrays with 64 oscillators, a tolerance of $\pm 5\,\%$ and different coupling strengths.

3.4.2 Increased coupling strength at various tolerances

In the same way as for the symmetric system, simulations were also undertaken with a coupling strength of 0.8 at tolerances of ±0.1 %, ±1 %, ±5 %, and ±10 %. These used the same values of tolerance as used in the simulations with a coupling strength of 0.25 and shown in Figures 3.2(i), 3.3(i), 3.4(i) and 3.5(i) respectively. The results shown in Figure 3.9 exhibit a similar pattern to those for the symmetric system in Figure 2.15, although the decline in recurrence occurs at a lower tolerance.

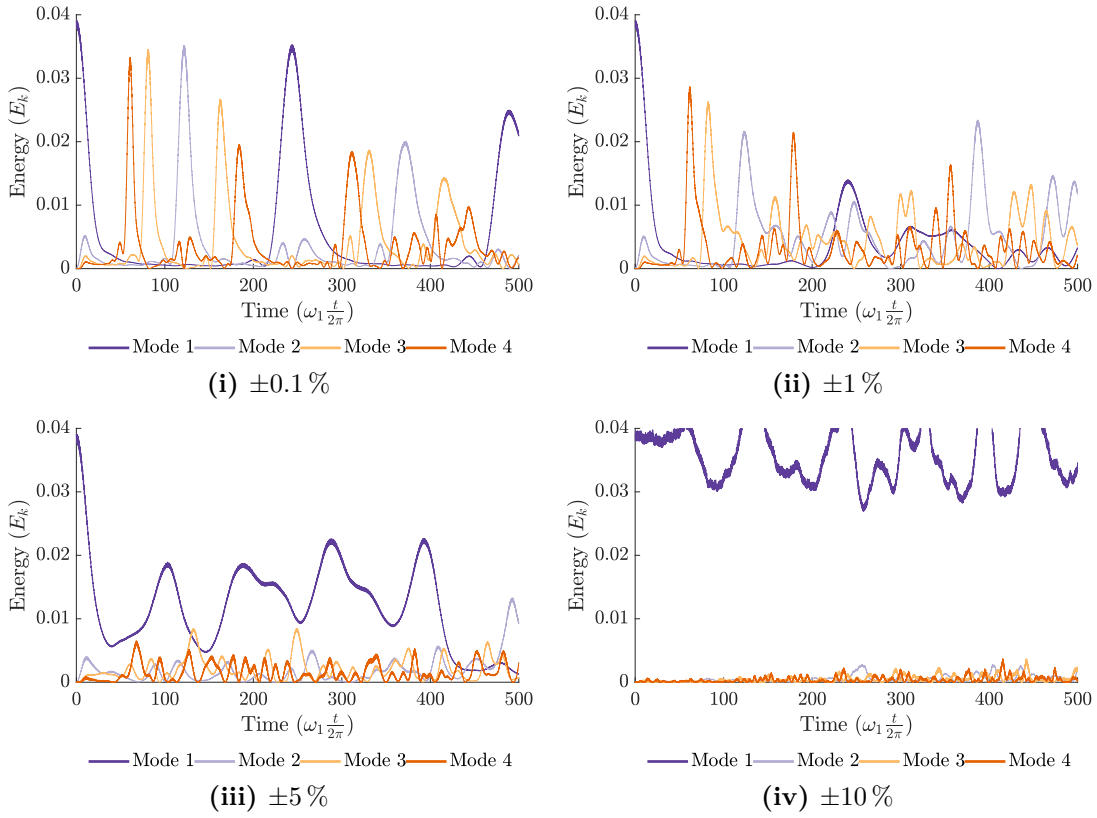


Figure 3.9: Simulations of asymmetric 1D FPUT-α arrays with 64 oscillators and a coupling strength of $\alpha = 0.8$ at various tolerances.

At ±0.1 % tolerance there is very little alteration to the recurrence. With a tolerance of ±1 % the shape of the peaks in the first recurrence cycle is starting to change. In particular, the energy returning to the first mode drops significantly. By the second cycle, recurrence has broken down although energy exchange between modes is still occurring. When the tolerance is increased to ±5 % there is energy being transferred between the modes but more energy remains in the first mode

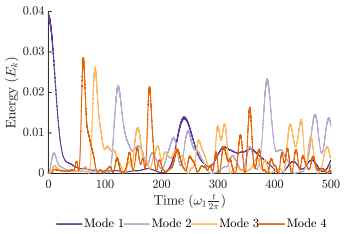
than with a coupling strength of 0.25. Finally, at a tolerance of ±10 % the majority of energy stays in the first mode and very little transfer to modes 2, 3, and 4 occurs. Interestingly, the energy in the system also appears to increase above the initial starting point. This may be due to numerical errors building up (similar to energy increase due to parasitic noise in an electronic system) but investigating the cause of this build up is beyond the scope of this thesis.

3.4.3 Tolerance on linear versus nonlinear terms

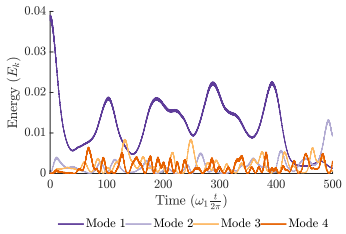
The simulations with tolerance on only the linear terms and only the nonlinear terms were repeated using an increased coupling strength of 0.8 and the same tolerance values as in Section 3.3. With the increase in coupling strength, the tolerance on the nonlinear terms has more impact as shown in Figure 3.10. Comparing the simulations with tolerance on only the nonlinear terms shown in Figures 3.10(vii), (viii), and (ix) to the simulation with 0 % tolerance shown in Figure 2.13(v), it can be observed that as the tolerance increases there is a change in the recurrence pattern. This is minimal at ±1 %, becoming more apparent in the 4th mode at ±5 % and more significant in all four modes at ±10 %.

This increased effect on the nonlinear terms is reflected in the difference between the results with tolerance on only the linear terms and tolerance on both the linear and nonlinear terms. At ±1 % the results are very similar, with some minor differences appearing in the second cycle (Figures 3.10(i) and (iv)). Increasing to ±5 % tolerance, the differences become more noticeable, particularly in the first mode after 200 time periods (Figures 3.10(ii) and (v)). At ±10 % tolerance, the differences are pronounced with a greater exchange of energy out of the first mode and into the higher modes (Figures 3.10(iii) and (vi)). This is not unexpected for this particular set of tolerance values, as when they are applied to only the nonlinear terms, there is more energy entering into the higher modes (Figure 3.10(ix)).

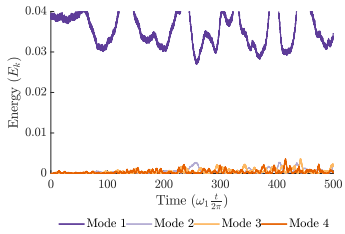
Tolerance in both the linear and nonlinear terms:



(i) ±1 %

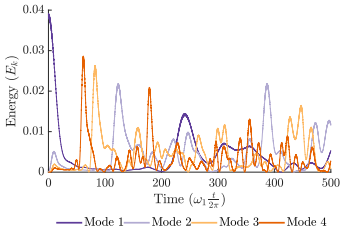


(ii) ±5 %

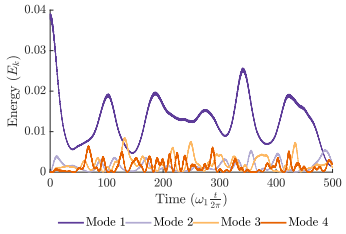


(iii) ±10 %

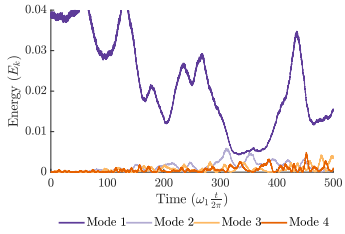
Tolerance in only the linear terms:



(iv) ±1 %

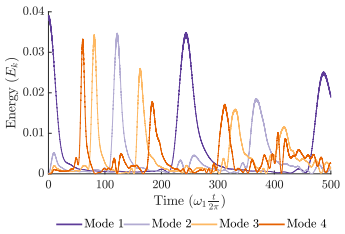


(v) ±5 %

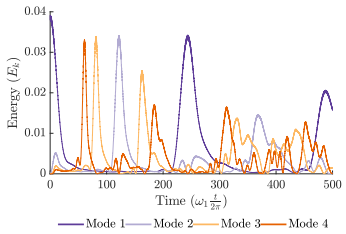


(vi) ±10 %

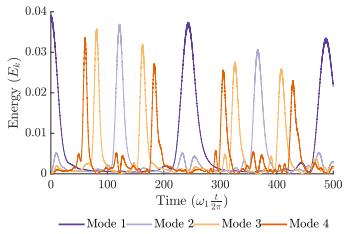
Tolerance in only the nonlinear terms:



(vii) ±1 %



(viii) ±5 %



(ix) ±10 %

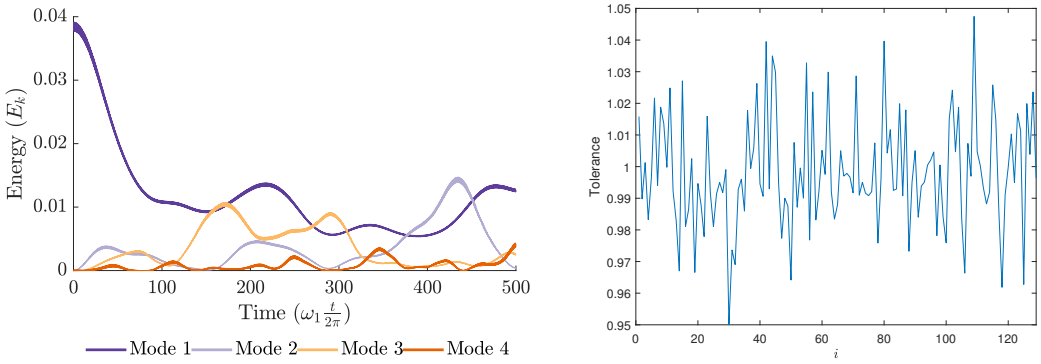
Figure 3.10: Simulations of asymmetric 1D FPUT-α arrays with 64 oscillators and a coupling strength of $\alpha = 0.8$ at various tolerances, showing the effect of tolerance on different parts of the array.

3.5 Order of tolerances

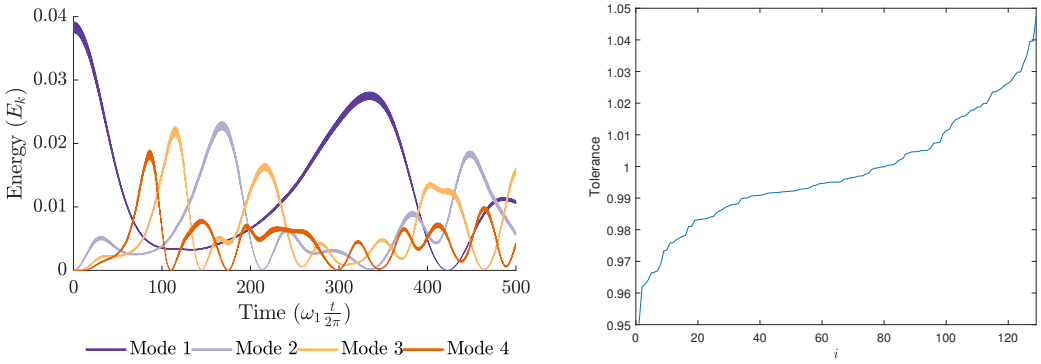
For the symmetric system in Chapter 2, sorting the tolerances into ascending order improved the resilience of the system to tolerance in the majority of cases. It is therefore worth investigating whether the same is true for the asymmetric system. Using the same set of tolerance values as used for Figure 3.4(i) and keeping all other parameters the same (i.e. $N = 64$, $\alpha = 0.25$, and tolerance=$\pm 5\,\%$), the simulations were repeated with the tolerance values sorted into different orders before applying them to the system components. The results of these simulations are shown in Figure 3.11, where the first 64 values represent the values of t_i and the remainder the values for f_i^{nlin} and b_i^{nlin}.

Figure 3.11(ii) shows the results if the tolerances are sorted into ascending order. Comparing this to Figure 3.11(i) where the tolerances are in a random order shows that recurrence is significantly improved, although the recurrence observed is not as close to that of the ideal system as the recurrence observed in the symmetric system. As only a single sample is considered here, this may be an artefact of the set of tolerance values rather than the overall response for multiple systems. However, the set of values chosen was representative of the majority of results for a tolerance of $\pm 5\,\%$, therefore one might assume that this is a generalised response.

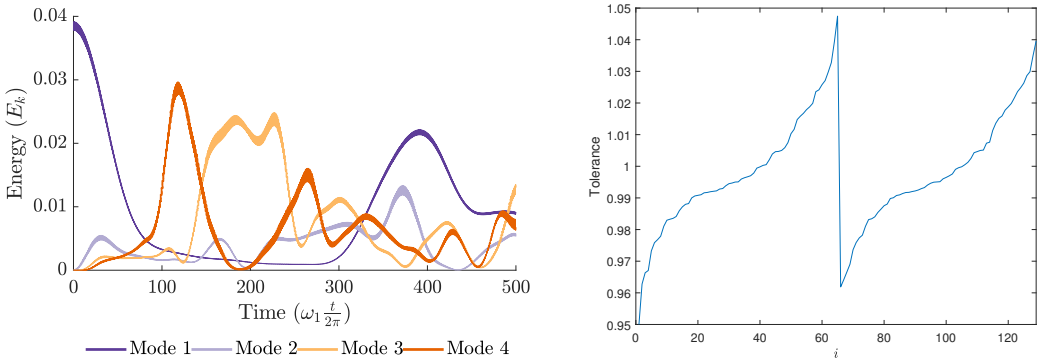
As this ramp data effectively sorts the tolerances on the linear terms into approximately values from a tolerance of $-5\,\%$ to $0\,\%$ and those for the nonlinear terms from $0\,\%$ to $+5\,\%$, the values were also sorted to be ascending across the full range for both terms, effectively creating a 'double ramp'. Figure 3.11(iii) shows the result of this simulation. Here it can be observed that recurrence has been improved but not to the same extent as for Figure 3.11(ii). This is not surprising since the single ramp effectively halves the amount of tolerance being applied to each term but introduces an offset which is similar to changing the coupling strength. However, the double ramp is likely to be closer to the physical implementation of the majority of systems and, therefore, sorting will be less effective in an asymmetric system than a symmetric one.



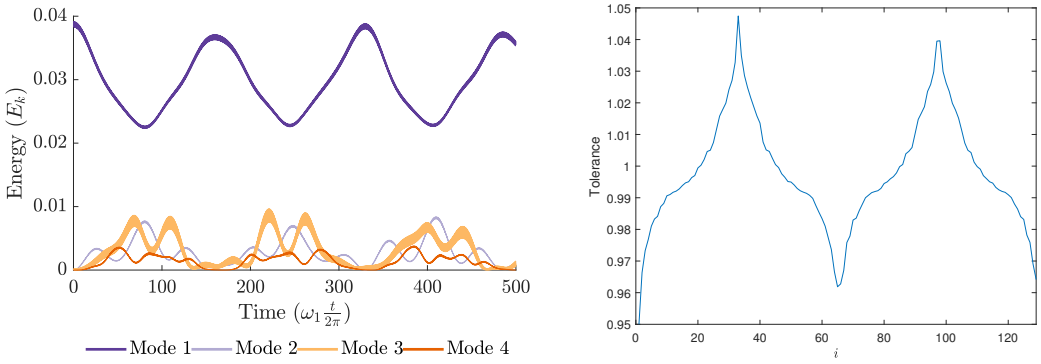
(i) Random



(ii) Ramp



(iii) Double Ramp

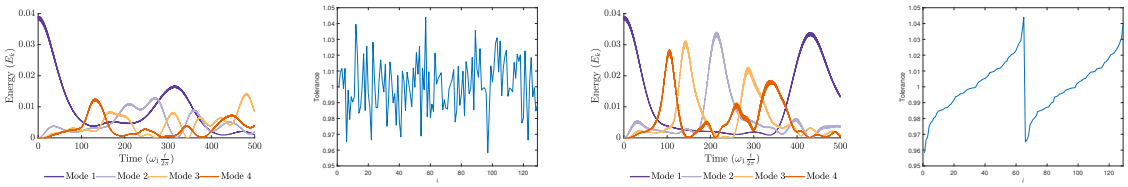


(iv) Double Peak

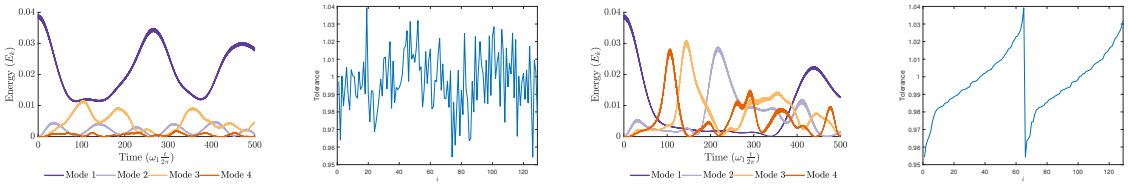
Figure 3.11: Simulations of an asymmetric 1D FPUT-α array with 64 oscillators and a coupling strength of $\alpha = 0.25$ at a tolerance of $\pm 5\,\%$. The same set of tolerance values as used for Figure 3.4(i) is used in each simulation. However, a different method of sorting the values is used in each sub-figure.

Continuing with the sorting split between the linear and nonlinear term tolerances, Figure 3.11(iv) shows the results if the tolerances are sorted into a 'double peak'. This shows a very similar response to the symmetric system, whereby the majority of the energy stays in the first mode but there is a small amount of energy transfer in modes 2 to 4. This suggests that this method of sorting will not be effective in any FPUT system.

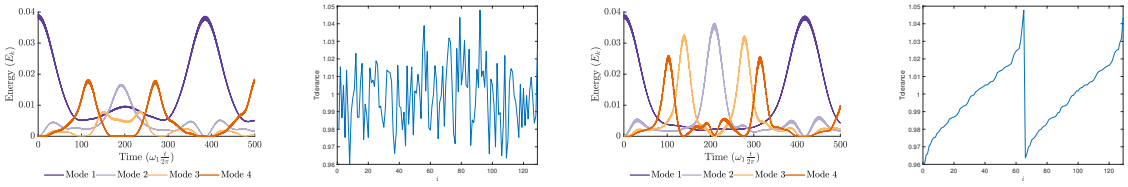
For the symmetric system, a selection of sets of tolerance values were explored to understand if the improvement due to sorting the tolerance values was limited to a particular set. The same principal was applied for the asymmetric system using the same sets of tolerance values used for Figure 3.4 but using the 'double ramp' method of sorting. The results of these simulations are shown in Figure 3.12 where it can be observed that, in all cases, sorting the tolerance values results in an improvement of recurrence.



(i) Same values of t_i as Figure 3.4(ii)



(ii) Same values of t_i as Figure 3.4(iii)

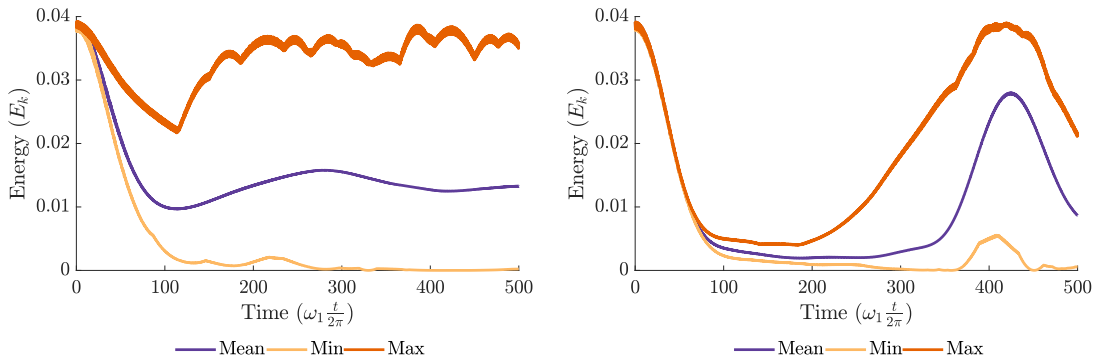


(iii) Same values of t_i as Figure 3.4(iv)

Figure 3.12: Simulations of an asymmetric 1D FPUT-α array with 64 oscillators and a coupling strength of $\alpha = 0.25$ at a tolerance of $\pm 5\,\%$. Here, the ramp method of sorting is applied to remaining sets of tolerance values used in Figure 3.4.

The values used to produce Figure 3.11(iii) result in the energy transfer pattern that is least close to ideal recurrence. This is followed by the values for Figure 3.12(ii), then Figure 3.12(i), and the best result is in Figure 3.12(iii). Examining the shape of the ramp graphs, this would appear to be related to the distribution of the tolerance values. Figure 3.11(iii) has the greatest range of the rate at which the tolerance values change, whereas the values for Figure 3.12(iii) change in a pattern that is closer to a straight line. As these values were randomly drawn from a Gaussian distribution, the set of values for Figure 3.12(iii) is likely to occur rarely, whereas the other sets of tolerance values are statistically more likely. Therefore, one might assume that recurrence can be improved by sorting the values, but it is unlikely to reach the same level as for an ideal system with 0 % tolerance.

Figure 3.13 shows the result of sorting the entire set of 100 Monte Carlo runs into ramp format and plotting the mean, minimum and maximum values for the first mode alongside the equivalent for the randomly ordered sets of tolerance values. In a similar manner to the symmetric system, these figures show that on average the quality of recurrence is improved. Comparison of the individual plots confirms this, although, as with the symmetric system, there is one set of values where recurrence degrades with sorting.



(i) Random **(ii)** Ramp

Figure 3.13: Plot showing the mean, minimum and maximum values of the first energy mode for 100 simulations of an asymmetric 1D FPUT-α array with 64 oscillators and a coupling strength of $\alpha = 0.25$ at a tolerance of $\pm 5\,\%$. These are shown for the tolerance values in a random order and sorted into a ramp format.

3.6 Effect of tolerance on superrecurrence

Section 2.8 demonstrated that tolerance also affects the superperiod for a symmetric FPUT-α system. The results presented so far in this chapter suggest that the asymmetric system generally reacts in a similar manner to the symmetric system although the level of response varies. It is therefore expected that tolerance will also affect superrecurrence in an asymmetric FPUT-α system. Maintaining the same system parameters as for the symmetric system, i.e. an array size of 16 oscillators and a coupling strength of 0.25, simulations were undertaken for a single recurrence cycle for the asymmetric system at tolerances of $\pm 0.1\,\%$, $\pm 1\,\%$, $\pm 5\,\%$, and $\pm 10\,\%$. These results are presented in Figure 3.14 where it can be observed that the recurrence period for a single cycle changes with tolerance.

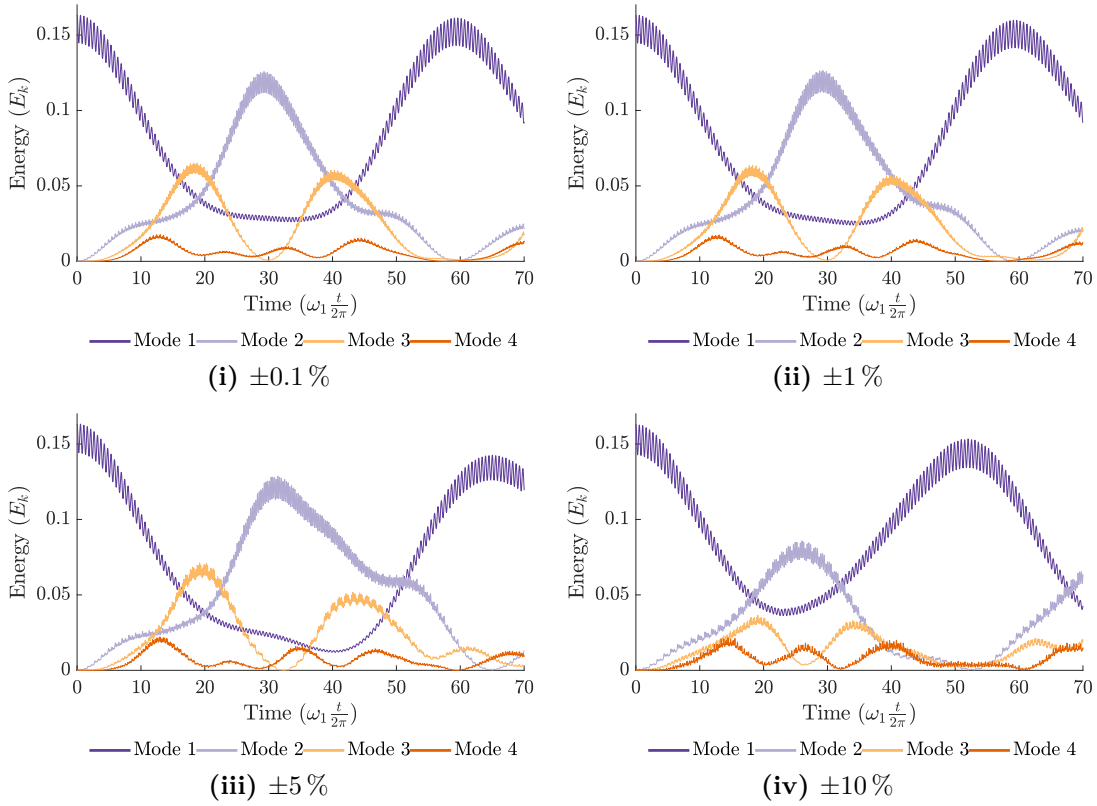


Figure 3.14: Simulations of an asymmetric 1D FPUT-α array with 16 oscillators and a coupling strength of $\alpha = 0.25$ showing examples of recurrence at various tolerances.

The system was then simulated for a longer time period. Figure 3.15 shows that the number of recurrence cycles occurring during the longer time period follows the same pattern. However, the superrecurrence period is affected differently. At a tolerance of ±0.1 %, Figure 3.15(i) shows that there is little change from a system with 0 % tolerance shown in Figure 1.7. Increasing the tolerance to ±1 %, there is still only a small change in recurrence for a single cycle (Figure 3.14(ii)). However, the change in superperiod becomes more apparent, and nearly three full cycles are visible (Figure 3.15(ii)).

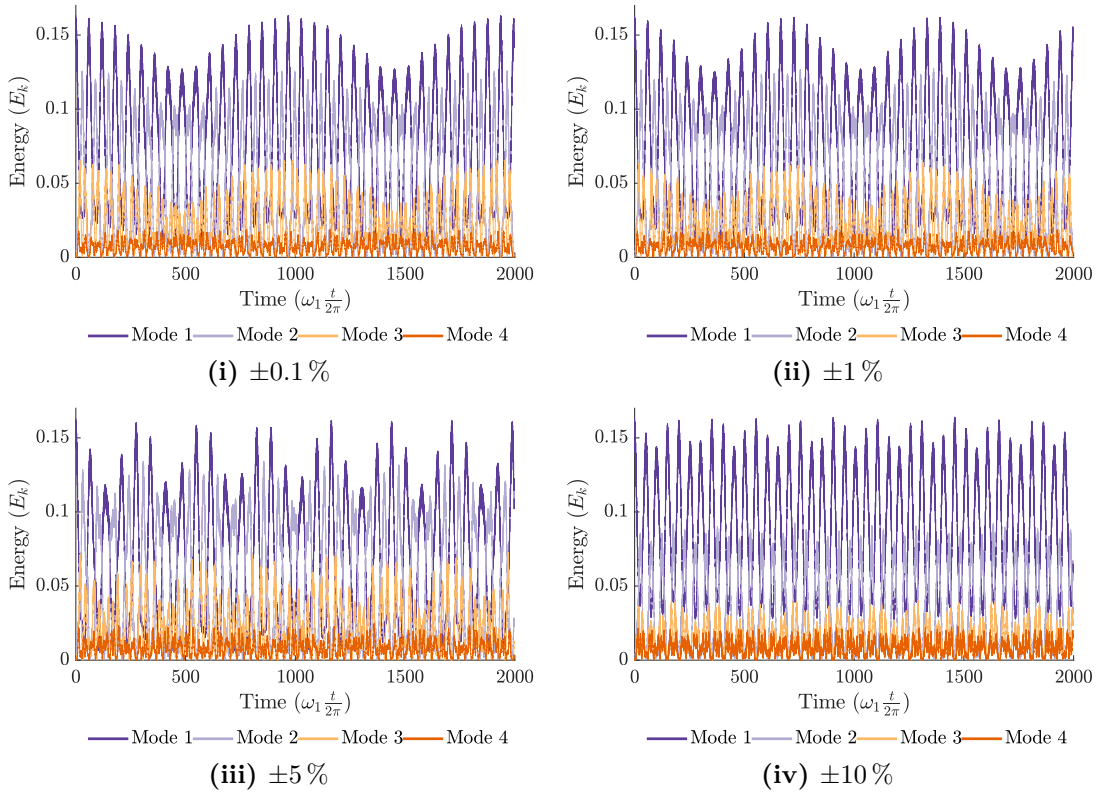


Figure 3.15: Longer simulations of an asymmetric 1D FPUT-α array with 16 oscillators and a coupling strength of $\alpha = 0.25$ showing the change in superrecurrence at various tolerances.

At ±5 % tolerance, both a single cycle of recurrence and the superperiod are more significantly affected. Figure 3.15(iii) shows that the superperiod still exists but has shortened again so that approximately seven cycles are seen within the time period shown. This is contrary to the recurrence period which has increased (Figure 3.14(iii)). Increasing the tolerance again to ±10 %, for a single cycle less

energy is entering the higher modes than at lower tolerances and the recurrence period has decreased (Figure 3.14(iv)). This trend is reflected in the superrecurrence. Additionally, the variation in the amount of energy returning to the first mode on each standard recurrence cycle is much lower than at the other tolerance levels (Figure 3.15(iv)).

Overall, these results are similar to those for the symmetric system. The main difference occurs in the period of the superrecurrence at a tolerance of $\pm 5\,\%$. However, as the single cycle of recurrence shows a greater variation at this tolerance, this is expected. Examining the response of a greater number of systems over a longer period is required for a more comprehensive identification of the different effects of tolerance on superrecurrence in the two systems.

3.7 Other tolerance structures

In section 3.3, it was observed that incorporating tolerances into the nonlinear terms had a much more significant effect in the symmetric FPUT lattices than in asymmetric ones. One possible explanation for this may be the different way in which the tolerances were applied to the systems and the resultant effect that this has on the structure of the original FPUT chain. To explore this further, different ways to incorporate the tolerances into the arrays were considered.

If the tolerances in Equation (2.3) are compared to those in Equation (3.1), one can see that the tolerances are applied differently to the nonlinear terms. In the symmetric equation the tolerances are applied to the individual x terms, whereas in the asymmetric equation they are applied to the nonlinear terms as a combined entity. This particular asymmetric format was chosen to reflect a common method of building electronic circuits to represent second order differential equations.

3.7.1 Alternative tolerance structure A

An alternative to this structure would be to apply different forward and backward tolerances to the linear components of an FPUT lattice, whilst keeping the tolerances on the nonlinear components the same as in Equation (3.1). There are two simple methods to achieve this. The first is to apply a single forward tolerance to the linear coupling term for the force exerted by x_i on x_{i+1} and a single backward tolerance to the linear coupling term for the force exerted on x_i by x_{i+1}. Using this method, the following equations of motion are obtained:

$$\ddot{x}_i = f_i^{\text{lin}}(x_{i+1} - x_i) + b_i^{\text{lin}}(x_{i-1} - x_i) + \alpha[f_i^{\text{nlin}}(x_{i+1} - x_i)^2 - b_i^{\text{nlin}}(x_i - x_{i-1})^2] \quad (3.2)$$

where the forward and backward tolerances on the linear terms are f_i^{lin} and b_i^{lin}, respectively. Figure 3.16 shows a block diagram representation of the system and these tolerances.

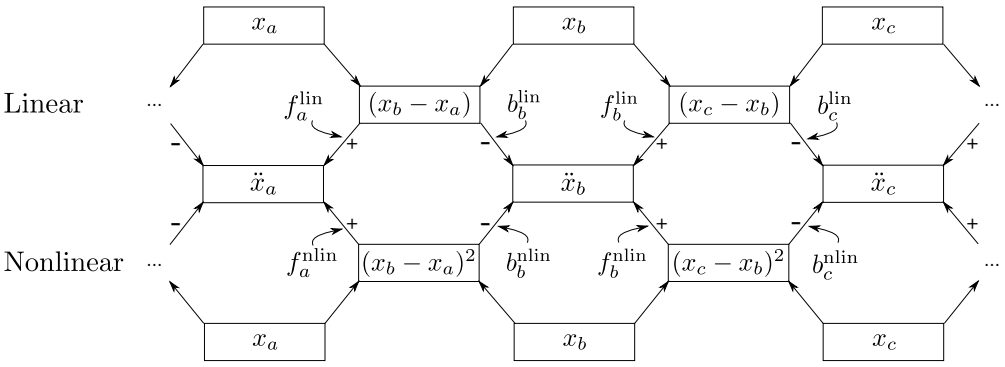
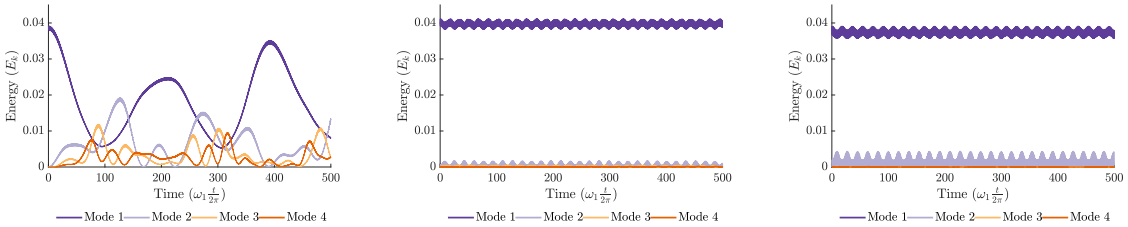


Figure 3.16: Block diagram showing the elements used to form the FPUT equation and the associated tolerances for Equation (3.2). Here x_a, x_b and x_c represent any 3 elements in a longer chain.

The results of simulating this equation with tolerances of $\pm 1\,\%$, $\pm 5\,\%$, and $\pm 10\,\%$ are shown in Figure 3.17. It can be observed that the tolerance on the linear terms is the significant factor, as for the previous asymmetric tolerance structure. However, comparing Figures 3.17 and 3.7, it can be seen that the energy profiles for the system with tolerance on both terms is much closer to the energy profile for the system with tolerance on only the linear terms for Equation (3.2). Here,

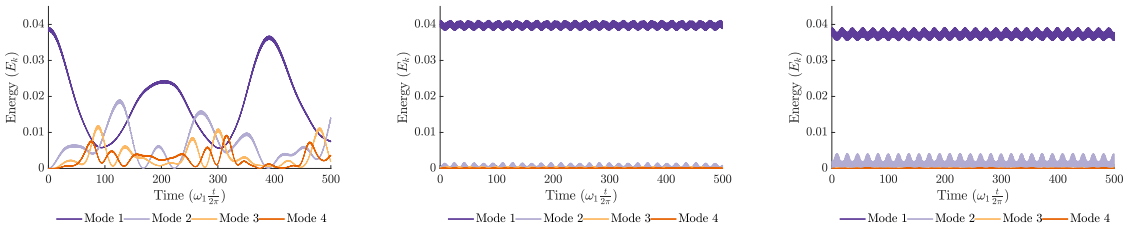
recurrence is altered by the tolerance on the nonlinear terms, although not to complete breakdown. Tolerance on the linear terms has a much more significant effect, with complete breakdown of recurrence occurring at ±5 %. This is more severe than the breakdown which occurred for either the symmetric or asymmetric structures (Figures 2.12 and 3.7).

Tolerance in both the linear and nonlinear terms:



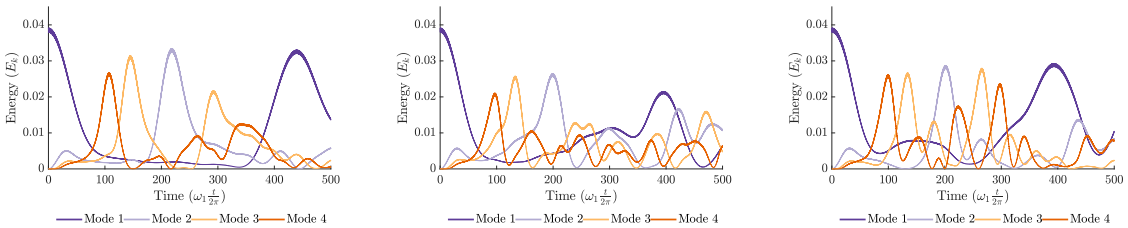
(i) ±1 % **(ii)** ±5 % **(iii)** ±10 %

Tolerance in only the linear terms:



(iv) ±1 % **(v)** ±5 % **(vi)** ±10 %

Tolerance in only the nonlinear terms:



(vii) ±1 % **(viii)** ±5 % **(ix)** ±10 %

Figure 3.17: Simulations of an asymmetric 1D FPUT-α array with 64 oscillators and a coupling strength of $\alpha = 0.25$ at various tolerances, showing the effect of tolerance on different parts of the array for a system with a single tolerance on the forward linear coupling term and a single tolerance on the backward linear coupling term.

3.7.2 Alternative tolerance structure B

A second method is to split the tolerances so separate forward tolerances are applied to x_i and x_{i+1}, and separate backward tolerances to x_i and x_{i-1}. This gives the following equations of motion:

$$\ddot{x}_i = (f_{i+1}x_{i+1} - f_i x_i) + (b_{i-1}x_{i-1} - b_i x_i) + \alpha[f_i^{\text{nlin}}(x_{i+1} - x_i)^2 - b_i^{\text{nlin}}(x_i - x_{i-1})^2] \quad (3.3)$$

where the forward and backward tolerances on element i are f_i and b_i, respectively. Figure 3.18 shows a block diagram representation of the system and these tolerances.

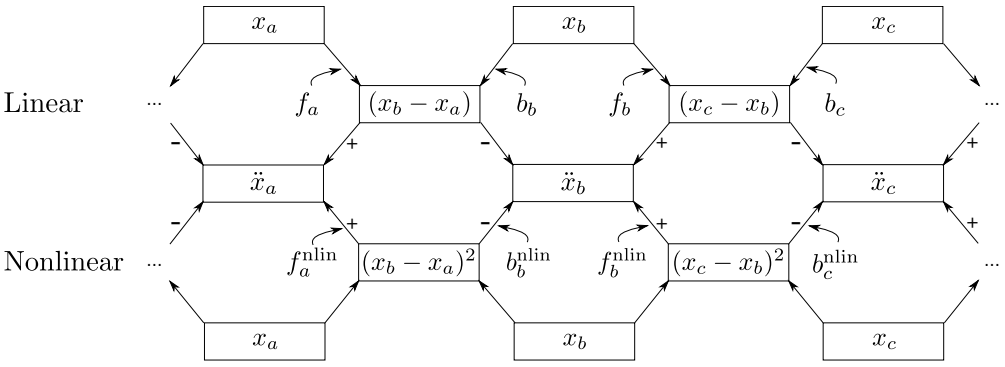
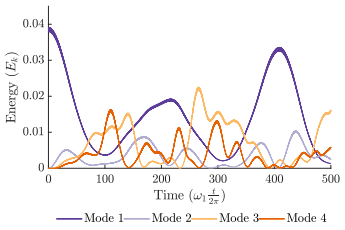


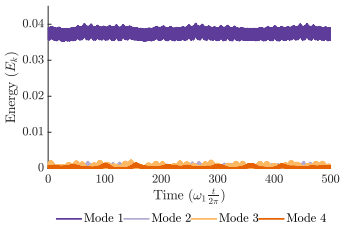
Figure 3.18: Block diagram showing the elements used to form the FPUT equation and the associated tolerances for Equation (3.3). Here x_a, x_b and x_c represent any 3 elements in a longer chain.

The results of simulating Equation (3.3) show that the trend seen for the asymmetric structures continues (Figure 3.19). The tolerance on the linear terms continues to dominate. Comparison of the response of this equation to tolerance on both the terms versus tolerance on only the linear terms is equivalent to that for Equation (3.2), i.e. it is almost identical. However, for Equation (3.3), it can be seen that there is a greater exchange of energy occurring at a tolerance of $\pm 10\,\%$.

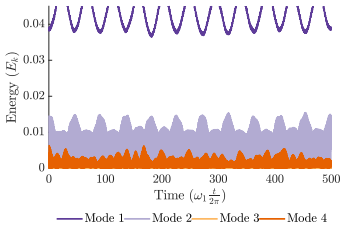
Tolerance in both the linear and nonlinear terms:



(i) ±1 %

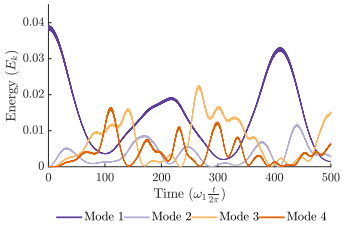


(ii) ±5 %

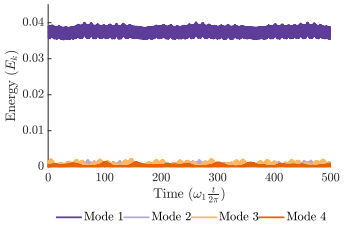


(iii) ±10 %

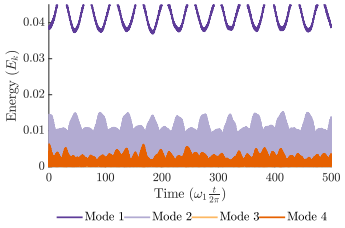
Tolerance in only the linear terms:



(iv) ±1 %

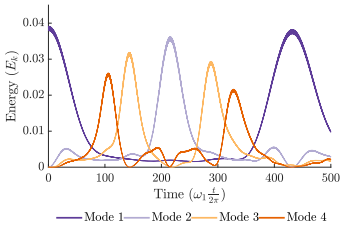


(v) ±5 %

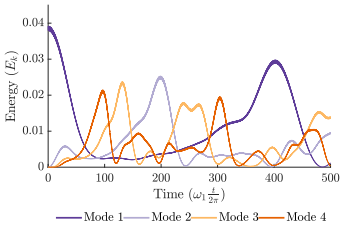


(vi) ±10 %

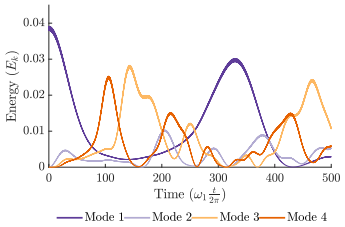
Tolerance in only the nonlinear terms:



(vii) ±1 %



(viii) ±5 %



(ix) ±10 %

Figure 3.19: Simulations of an asymmetric 1D FPUT-α array with 64 oscillators and a coupling strength of $\alpha = 0.25$ at various tolerances, showing the effect of tolerance on different parts of the array for a system with separate tolerances on the forward linear coupling components and separate tolerances on the backward linear coupling components.

3.7.3 Alternative tolerance structure C

It is still possible to split the tolerances further. If the tolerances are split in the nonlinear components so that the way tolerances are incorporated in asymmetric FPUT arrays more closely resembles that in symmetric FPUT arrays, the following equations of motion are obtained:

$$\ddot{x}_i = (f_{i+1}x_{i+1} - f_i x_i) + (b_{i-1}x_{i-1} - b_i x_i) + \alpha[(f_{i+1}x_{i+1} - f_i x_i)^2 - (b_i x_i - b_{i-1}x_{i-1})^2] \tag{3.4}$$

Figure 3.20 shows a block diagram representation of the system and these tolerances.

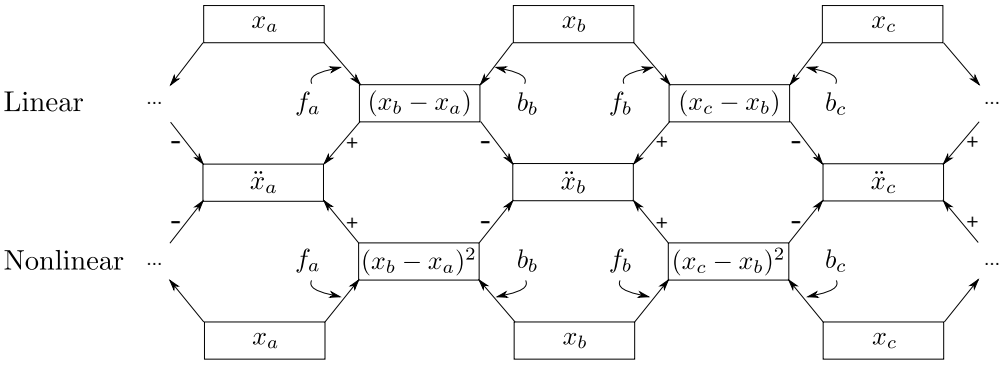
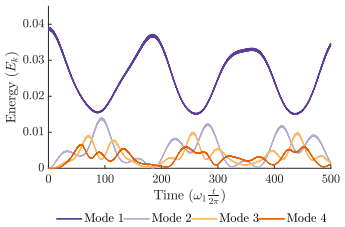


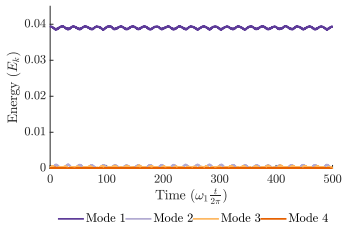
Figure 3.20: Block diagram showing the elements used to form the FPUT equation and the associated tolerances for Equation (3.4). Here x_a, x_b and x_c represent any 3 elements in a longer chain.

Figure 3.21 shows the results of simulating Equation (3.4). With this tolerance structure, the impact of tolerance on the nonlinear terms is at its most severe when compared to all the other structures contained within this thesis. However, tolerance on the linear term remains dominant at this coupling strength. Comparing the Figures 3.21(i)–3.21(iii) to Figures 3.21(iv)–3.21(vi), it can be observed that there is a greater difference between tolerance on both the linear and nonliner terms versus tolerance on only the linear terms than has been observed in the structures described by Equations (3.2) and (3.3).

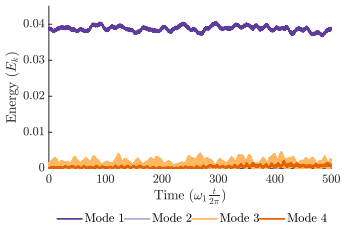
Tolerance in both the linear and nonlinear terms:



(i) ±1 %

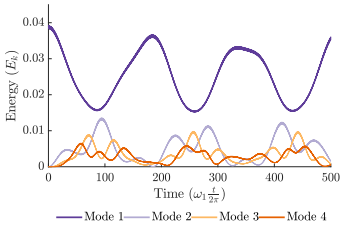


(ii) ±5 %

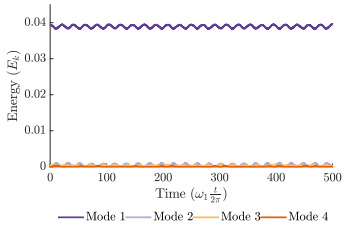


(iii) ±10 %

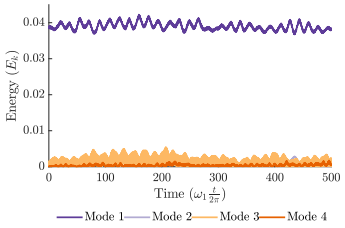
Tolerance in only the linear terms:



(iv) ±1 %

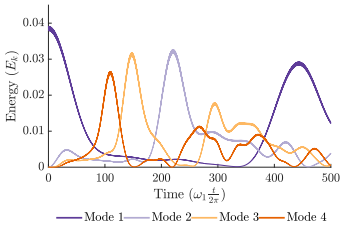


(v) ±5 %

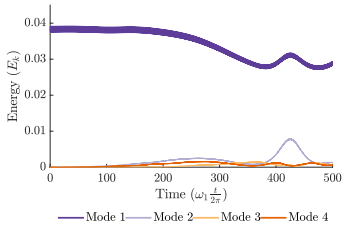


(vi) ±10 %

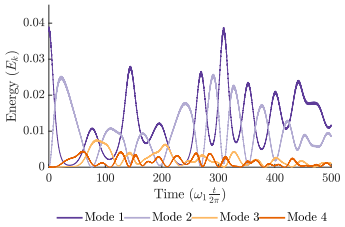
Tolerance in only the nonlinear terms:



(vii) ±1 %



(viii) ±5 %



(ix) ±10 %

Figure 3.21: Simulations of an asymmetric 1D FPUT-α array with 64 oscillators and a coupling strength of $\alpha = 0.25$ at various tolerances, showing the effect of tolerance on different parts of the array for a system with separate tolerances on all the forward and backward linear and nonlinear coupling components.

3.7.4 Section summary

The results of these simulations suggest that the different structure of the tolerances on the nonlinear terms has a more significant impact than the change in structure on the linear terms. The results for an increased coupling strength of 0.8 presented in Figures 2.16 and 3.10 show that the influence of the nonlinear terms increases with a stronger coupling strength. This is further supported by additional results at other coupling strengths which have not been presented in this thesis. Therefore, it is anticipated that this trend will continue for the alternative tolerance structures described by Equations (3.2)–(3.4).

Another interesting observation is the range of responses across the Monte Carlo simulations for each of these structures. At a tolerance of $\pm 10\,\%$, the structure described by Equation (3.4) shows the most variation and that described by Equation (3.2) the least. All the alternative structures show an increase of energy transfer into modes 2 to 4 compared to the asymmetric structure, however this is particularly prevalent in the structure described by Equation (3.4).

There is also an overall increase in energy in some of these systems, most noticeably at a tolerance of $\pm 10\,\%$, although it does occur occasionally at $\pm 5\,\%$. This suggests that the numerics might be questionable. For the asymmetric system described by Equation (3.1), the simulation failed to converge on several occasions at a tolerance of $\pm 10\,\%$. It is therefore worth treating these results with caution, since additional investigations into the reliability of the simulations at higher tolerance values have not yet been conducted. This is potentially symptomatic of the same problems seen by Pace and Campbell in their simulations where the increased chaotic behaviour meant the results were not time reversible [36].

3.8 Summary

The results presented in this chapter illustrate that the way in which one constructs an array of nonlinear oscillators, and more specifically the way in which one incorporates tolerances into such a system, has a major effect on the qualitative dynamics of such systems. Stepping away from a symmetric tolerance structure seen in a mass-spring system, towards an asymmetric structure seen in an electronic circuit, the inclusion of tolerance on the nonlinear terms appears to have a lower impact, resulting in a greater breakdown in recurrence in the asymmetric system since the linear component is much stronger.

Recurrence breaks down at a smaller tolerance in an FPUT-α system where the tolerances have been applied in an asymmetric manner than if they were incorporated in a symmetric form. Additionally, as the number of oscillators in a system is increased, it can be observed that recurrence breaks down for a smaller number of oscillators in the asymmetric FPUT system than in the symmetric system. Increasing the coupling strength results in more energy remaining in the first mode for the asymmetric structure than for the symmetric structure where more exchange happens between modes 2 to 4. Sorting the tolerances in both systems improves the recurrence when sorted into ascending order. The effect of tolerance on superrecurrence is also similar for both structures.

Tolerance structures are not just limited to those described here as symmetric and asymmetric. There are a large number of alternatives available. However, a brief consideration of three alternate structures has shown that whilst the linear term is consistently dominant, the impact of the tolerances on the nonlinear term can vary. For the nonlinear terms, applying tolerance to each quadratic term as a whole has a lower impact than applying different tolerance to each of the individual x terms. Thus the physical structure of any real system will have an effect of how resilient the system is to tolerance.

4

Damped systems

Contents

4.1 Damping overview 93
4.2 Effect of damping on recurrence 95
4.2.1 Equivalent quality factor of 10 000 99
4.2.2 Equivalent quality factor of 1000 102
4.3 Different nonlinear coupling strengths 104
4.3.1 Equivalent quality factor of 10 000 and coupling strength of 0.8 104
4.3.2 Equivalent quality factor of 1000 and coupling strength of 0.8 105
4.4 Effect of tolerance combined with damping 106
4.4.1 Symmetric system 107
4.4.2 Asymmetric system 113
4.5 Summary 119

The previous two chapters have explored the impact of component tolerances on an FPUT system. However, the assumption that all system components are identical is not the only assumption that is commonly made. The FPUT equation also describes an undamped system, or a system that oscillates with no losses. In reality, the majority of systems will have inherent damping due to energy loss through factors such as friction in a mechanical system or impedance in an electronic one.

In this chapter, the effects of damping on an FPUT system are explored. Section 4.1 gives an overview of damping. Section 4.2 explores the effect of damping on recurrence. Section 4.3 shows the effect of various nonlinear coupling strengths in a damped system. Finally, the combined effects of damping and tolerance are reported in Section 4.4.

4.1 Damping overview

Physical systems often suffer loss of energy due to external factors (e.g. from air resistance or friction) or internal factors (e.g. material properties). A system operating under such influences which dissipate energy from the system is said to be damped [104]. The damping force is related to the velocity of the object and acts to oppose the motion, i.e. in the same direction as the restoring force. Returning to the simple linear mass-spring system, the simplest approach to model dissipation is to incorporate a viscous dashpot into the equation. With the addition of this linear damping force, the equation of motion becomes

$$m\ddot{x} + c\dot{x} + kx = 0 \tag{4.1}$$

where m is the mass, c is the damping coefficient, and k is the spring constant. This can also be presented using the modal approach in matrix form as

$$\mathbf{M}\ddot{\mathbf{x}} + \mathbf{C}\dot{\mathbf{x}} + \mathbf{K}\mathbf{x} = 0 \tag{4.2}$$

where $\mathbf{M}$ is the mass matrix, $\mathbf{C}$ is the damping matrix, and $\mathbf{K}$ is the stiffness matrix.

The viscous dashpot is often modelled using proportional damping. Based on the modal analysis by Lord Rayleigh in 1877 [105] this states that the damping matrix has a proportional relationship to the mass and stiffness matrices given by

$$\mathbf{C} = \rho_1\mathbf{M} + \rho_2\mathbf{K} \tag{4.3}$$

where ρ_1 and ρ_2 are constants.

A dimensionless parameter called the damping ratio, denoted by ζ, is used to describe the behaviour of a damped harmonic oscillator. The damping coefficient c is related to the damping ratio ζ by

$$\zeta = \frac{\text{actual damping}}{\text{critical damping}} = \frac{c}{2\sqrt{km}} \tag{4.4}$$

Depending on the magnitude of the damping ratio, the behaviour of a damped harmonic oscillator can be described as one of four categories. These are shown in Figure 4.1 and are defined as:

- Undamped ($\zeta = 0$): In an ideal scenario, where the system is completely lossless and oscillates indefinitely.
- Underdamped ($\zeta < 1$): The system oscillates with the amplitude gradually decreasing to zero.
- Critically damped ($\zeta = 1$): The system returns to steady state as quickly as possible without oscillating.
- Overdamped ($\zeta > 1$): The system contains high losses and exponentially decays to steady state without oscillating.

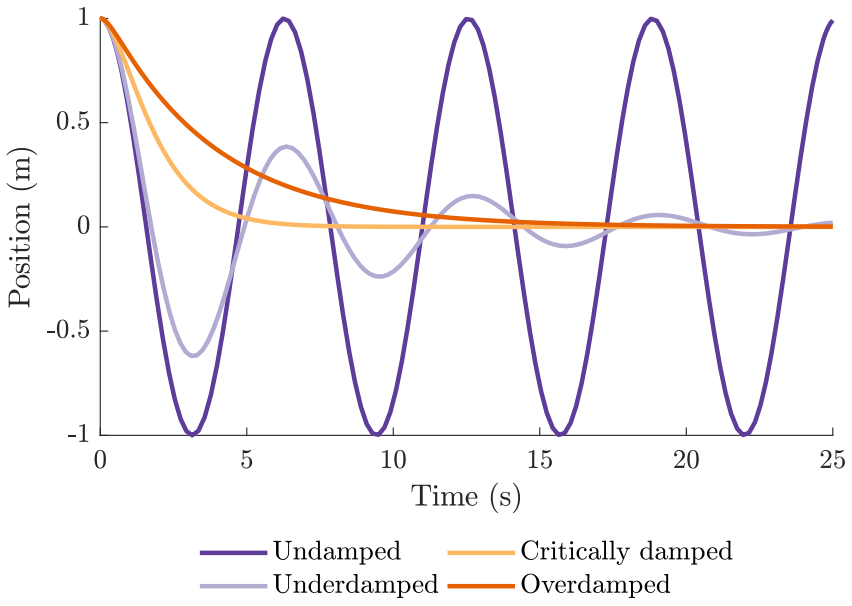


Figure 4.1: The effect of different damping ratios on a second-order system.

The damping in a linear system can also be described by its quality factor, denoted by Q. The quality factor is defined as

$$Q = 2\pi \times \frac{\text{energy stored}}{\text{energy loss per cycle}} \tag{4.5}$$

and is related to the damping ratio by

$$\zeta = \frac{1}{2Q}. \tag{4.6}$$

The natural frequency of the system defined in equation (4.1) is $\omega = \sqrt{k/m}$. Substituting using the equations for natural frequency, the critical damping coefficient and the damping ratio, equation (4.1) can be rewritten as

$$\ddot{x} + 2\zeta\omega\dot{x} + \omega^2 x = 0 \tag{4.7}$$

Furthermore, substituting for Q gives

$$\ddot{x} + \frac{\omega}{Q}\dot{x} + \omega^2 x = 0 \tag{4.8}$$

or with the addition of a driving force F

$$\ddot{x} + \frac{\omega}{Q}\dot{x} + \omega^2 x = F. \tag{4.9}$$

4.2 Effect of damping on recurrence

The traditional FPUT system is undamped. Therefore, in order to investigate the impact of damping on the system, a damping term must be added to the FPUT equation. Adding the simplest form of linear damping, and ignoring any damping in the coupling, the FPUT equation for quadratic type nonlinearity becomes

$$\ddot{x}_i + \nu\dot{x}_i = (x_{i+1} + x_{i-1} - 2x_i) + \alpha[(x_{i+1} - x_i)^2 - (x_i - x_{i-1})^2] \tag{4.10}$$

where ν is the mass normalised coefficient of damping. This equation is of a similar form to Equation (4.9). Therefore using a linear approximation for the nonlinear system the damping coefficient is

$$\nu = \frac{\omega}{Q} \tag{4.11}$$

where Q now becomes an equivalent quality factor since it is a linear term. As the quality factor is not very well defined for nonlinear systems, it is expected that an approximate result can be obtained by using this linear equivalent Q. It can be seen that by varying the equivalent quality factor whilst keeping the natural frequency constant, the effect of damping on the FPUT system can be explored.

A single recurrence cycle in an FPUT system requires several oscillations of the first mode frequency. Thus, in order to observe recurrence in a physical FPUT system, the system must be sufficiently underdamped to allow the system to resonate for enough periods of the first mode before significant energy is lost from the system. The exact number of oscillations required varies with chain length and coupling strength.

To achieve a sufficiently low level of damping, a high quality factor is required. However, this may be limited by the physical constraints of a system. For example, in an electronic circuit one must take into account sensible component values and current levels when designing for a specific Q value. As such, for a simple electronic circuit, it is estimated that the highest achievable quality factor is 10 000 which gives a very small damping ratio ζ of 5×10^{-5}.

An equivalent quality factor of 10 000 would allow 10 000 oscillations at the fundamental frequency to occur before energy is lost from the system. However, the energy decays exponentially so a significant proportion is lost in a much smaller number of oscillations. A common method of quantifying this in a linear system is to use a parameter known as the decay time. If the decay time τ_d is defined as the time to reach an energy of $\frac{A}{e}$ (where A is the starting amplitude) or approximately 37 %, then

$$\begin{aligned} Q &= \pi \times \text{no of cycles in decay time} \\ &= \pi f \tau_d \\ &= \omega \frac{\tau_d}{2} \end{aligned} \tag{4.12}$$

Therefore, using the linear approximation, for an equivalent quality factor of $Q = 10\,000$ and frequency of $\omega = 1$, the decay time τ_d is 20 000 s.

Considering the exponential decay, understanding the impact of reduced energy on FPUT recurrence is another key factor when applying damping to a system. Changing the amplitude of the displacement initial condition provides a simple method to vary the amount of energy available in the system. Figure 4.2 shows that when the amplitude of the displacement initial condition is reduced in a system with no damping, both the quality of the recurrence and the amount of energy being transferred into the higher modes decrease. It can also be observed that the period of the recurrence also increases with decreasing amplitude of the initial condition. Recurrence is weak when the amplitude of the initial condition is reduced from 1.0 to 0.5 and very little energy exchange happens when the amplitude is reduced to 0.25. Hence, the limit of 37 % of the original amplitude associated with the decay time provides a good basis for estimating the cut-off time after which the energy in a system will be too low for recurrence to be observed.

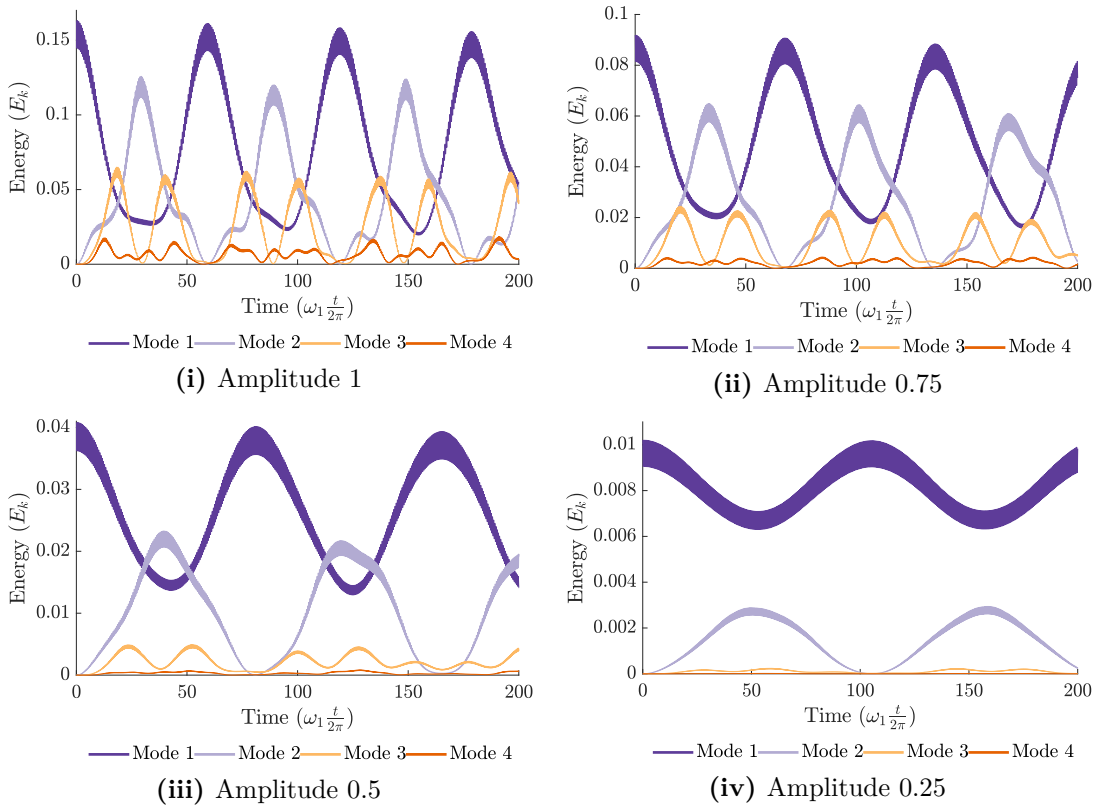


Figure 4.2: Simulations of 1D FPUT-α arrays with 16 oscillators, no damping, a coupling strength of $\alpha = 0.25$ and various amplitudes for the displacement initial condition.

To be able to compare the decay time to the length of a recurrence cycle, the duration of a recurrence cycle in seconds must be determined. The period of a system will vary with damping. However, since this is dependent on the amount of damping in the system and the proposed level of damping is low, using the period of the undamped system will provide a good enough approximation for the purposes of this comparison. Figure 2.11 shows the length of a recurrence cycle in number of cycles at the fundamental frequency. To convert this to seconds, a return to the linear mass-spring analogy shows that the time period for a cycle at the first mode frequency for a chain of N masses is

$$\tau_f = 2 \times \frac{\text{length}}{\text{velocity}} \tag{4.13}$$

where the length of the chain is $(N+1)d$. The velocity of a mechanical wave in the mass-spring system is given by

$$\text{velocity} = \sqrt{\frac{\text{elastic modulus}}{\text{mass density}}} = \sqrt{\frac{k}{m/d}} \tag{4.14}$$

so the time period becomes

$$\tau_f = 2(N+1)d\sqrt{\frac{m}{kd}} \tag{4.15}$$

or setting $m = k = d = 1$ as in the FPUT system, this simplifies to

$$\tau_f = 2(N+1) \tag{4.16}$$

Therefore, by multiplying the number of cycles at the fundamental frequency by $2(N+1)$ the duration of a recurrence cycle in seconds can be obtained. These results are presented in Table 4.1 and are rounded to the nearest integer.

N	Time ($\frac{\omega_1}{2\pi}$)	Time (s)
4	10	100
8	23	414
16	59	2006
32	158	10 428
64	434	56 420
128	1209	311 922

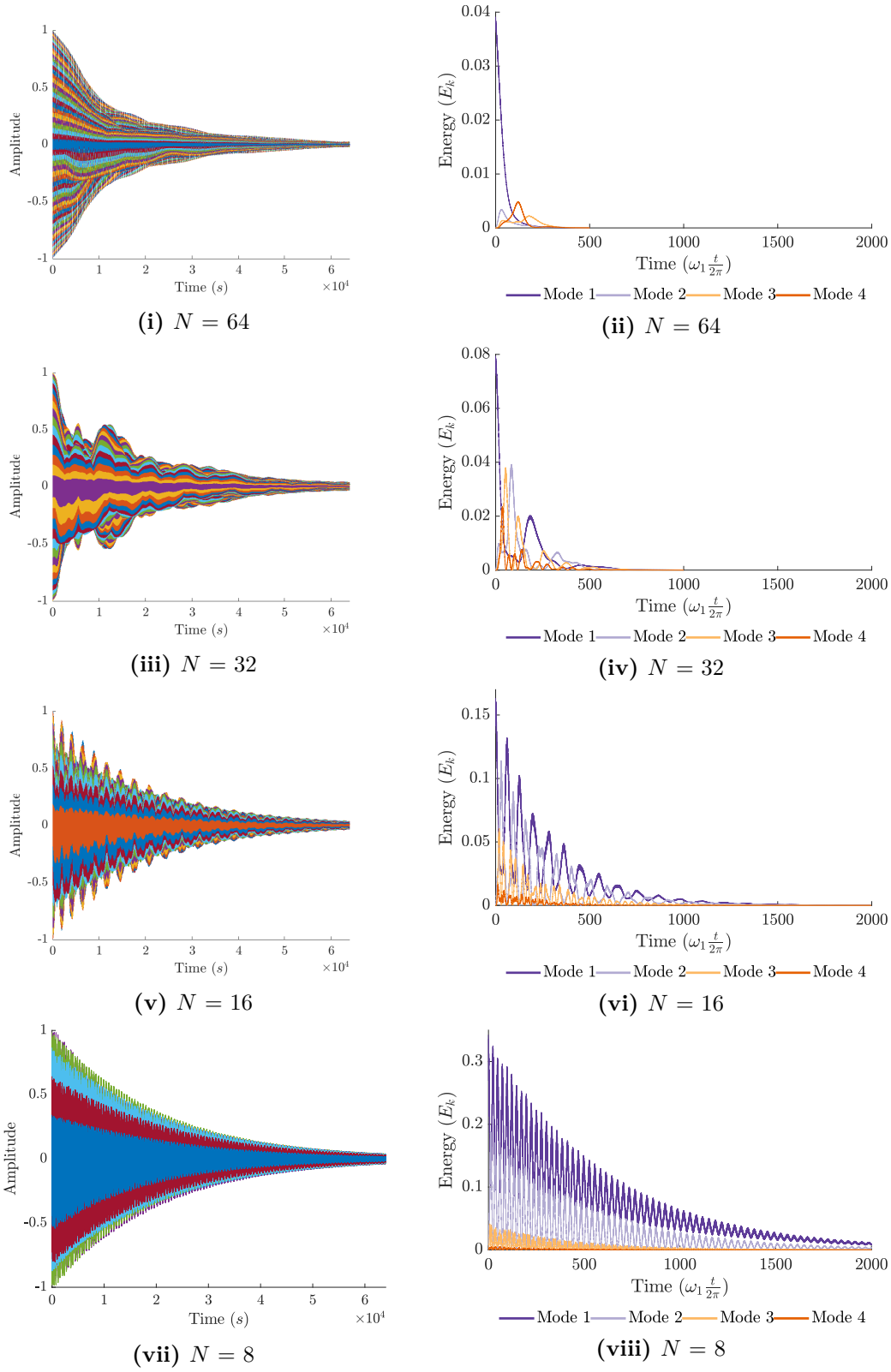
Table 4.1: Time period of a single recurrence cycle for a given value of N

Comparing the decay time to the values for the time taken for a single recurrence cycle shown in Table 4.1 allows an estimate of the maximum chain length that can be achieved at a certain equivalent quality factor. Starting with a decay time τ_d of 20 000 s for an equivalent quality factor of 10 000, it is anticipated that a chain length of 32 should allow at least one cycle of recurrence to be observed before the energy in the system drops too low. Similarly, if the equivalent quality factor was reduced by a factor of 10 to 1000, this would suggest that a chain length of 16 or fewer oscillators would be required to see recurrence.

4.2.1 Equivalent quality factor of 10 000

Figure 4.3 shows the results of simulating Equation (4.10) with an equivalent quality factor of 10 000 and a coupling strength α of 0.25. The system response is shown both in the time domain and the corresponding energy plot. Comparing Figures 4.3(i), 4.3(iii), 4.3(v), and 4.3(vii), one can observe that although the nonlinear coupling leads to differing amplitude patterns, the energy decays from the system at the same rate regardless of the chain length.

However, examining the energy plots in Figure 4.3 confirms the prediction made in the preceding section. A system with 64 oscillators loses energy too quickly to allow a full cycle of recurrence to occur as shown in Figure 4.3(ii). Reducing the chain length to 32 enables a single cycle of recurrence to be observed (Figure 4.3(iv)), whilst shortening the chain further to 16 and 8 oscillators reduces the recurrence period sufficiently for several cycles of recurrence to be shown (Figures 4.3(vi) and 4.3(viii)).



(i) $N = 64$ **(ii)** $N = 64$

(iii) $N = 32$ **(iv)** $N = 32$

(v) $N = 16$ **(vi)** $N = 16$

(vii) $N = 8$ **(viii)** $N = 8$

Figure 4.3: Simulations of 1D FPUT-α arrays with different numbers of oscillators, a quality factor of $Q = 10\,000$, and a coupling strength of $\alpha = 0.25$ showing the decay of energy over time.

To enable a better understanding of the energy transfer occuring between modes 1 to 4, Figure 4.4(i) shows the first 200 cycles at the fundamental frequency of the energy plot. For a system with 64 resonators, Figure 4.4(i) shows that there is very little energy being transferred between modes and recurrence does not occur.

At 32 resonators, the single cycle of recurrence is very weak with approximately 25 % of the energy returning to the first mode (Figure 4.4(ii)). The recurrence period has extended from 158 time units to 184 time units. If the level of energy returning to the first mode at 184 time units is compared to the level of energy in a linear system with equivalent damping at the same point, then only 82 % of the available energy has returned to the first mode in the nonlinear system, relative to the 98 % that returns to the first mode for an undamped system suggesting that damping has affected the modal interactions.

Shortening the chain length further to 16 resonators, recurrence is much stronger with the energy returning to the first mode decreasing to approximately 50 % after three cycles as shown in Figure 4.4(iii). The recurrence period has extended from 59 time units to 60 time units. The energy in the first mode returns to approximately 80 % of the initial energy after a single recurrence cycle. This is equivalent to 98 % of the energy in the equivalently damped linear system at the same time point, which puts the amount of recurrence at the same level as for the undamped system.

Reducing the chain further to 8 resonators, the shorter chain and hence shorter period for the first mode means that eight cycles of good quality recurrence can be observed in the first 200 periods of the first mode (Figure 4.4(iv)). The energy returning to the first mode has decreased to approximately 72 % after eight cycles. Approximately 95 % of the energy returns to the first mode after a single recurrence cycle, which is again equivalent to 98 % of that in the damped linear system. Thus, by keeping the number of oscillators low, the impact of damping can be minimised and several cycles of good quality recurrence can be observed.

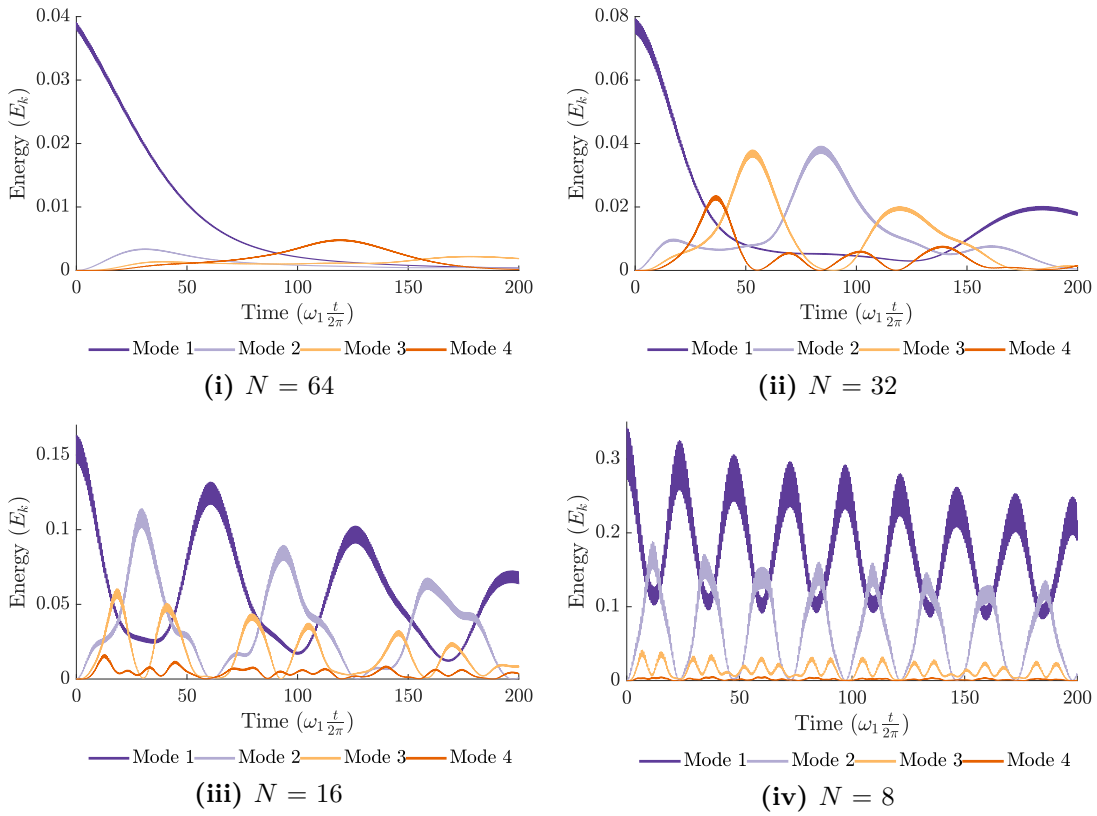
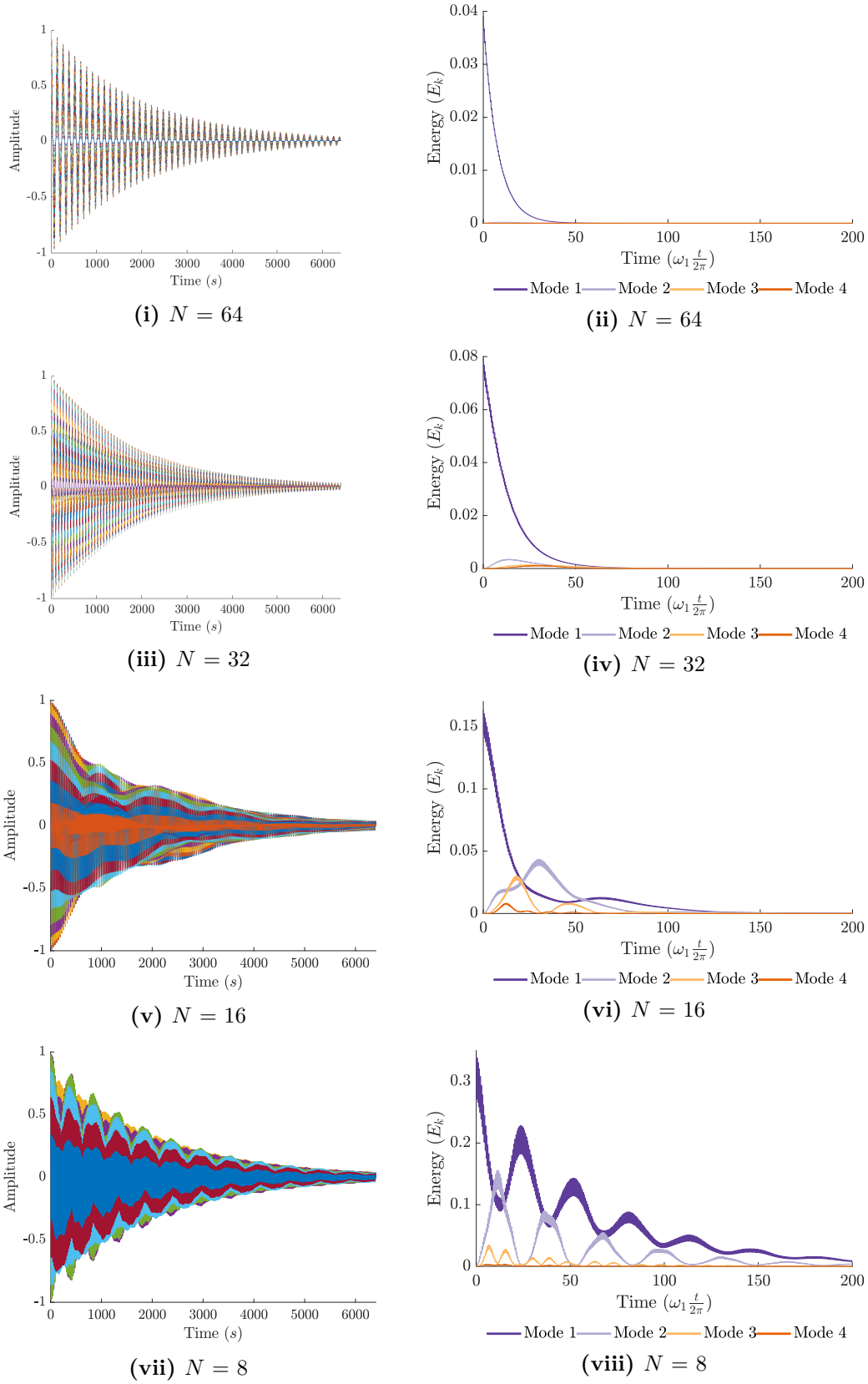


Figure 4.4: Simulations of 1D FPUT-α arrays with different numbers of oscillators, a quality factor of $Q = 10\,000$, and a coupling strength of $\alpha = 0.25$.

4.2.2 Equivalent quality factor of 1000

Since a quality factor of 10 000 is an estimate of the maximum possible Q value and this may be hard to achieve in a physical system, the impact of a lower quality factor on recurrence should be considered. Figure 4.5 shows that for a coupling strength α of 0.25 and with the number of oscillators as low as 8, the amount of damping in the system can be increased, by a factor of 10, whilst still being able to observe a few cycles of the phenomenon. This confirms the prediction that a short chain would be required to see recurrence, as the time period for a recurrence cycle decreases with decreasing chain length (Table 4.1). A single cycle of very weak recurrence occurs for a chain of 16 oscillators (Figure 4.5(vi)) and for a chain of 8 oscillators a few cycles of recurrence occur before too much energy is lost from the system (Figure 4.5(viii)).



(i) $N = 64$ **(ii)** $N = 64$

(iii) $N = 32$ **(iv)** $N = 32$

(v) $N = 16$ **(vi)** $N = 16$

(vii) $N = 8$ **(viii)** $N = 8$

Figure 4.5: Simulations of 1D FPUT-α arrays with different numbers of oscillators, a quality factor of $Q = 1000$, and a coupling strength of $\alpha = 0.25$ showing the decay of energy over time.

4.3 Different nonlinear coupling strengths

The results in the previous section suggest that with a coupling strength of 0.25 recurrence will only be observed in small systems with a quality factor of at least 1000. However Fermi, Pasta, Ulam and Tsingou showed that the time needed to observe recurrence reduces when the coupling strength increases as shown in Figures 1.3 and 1.5. Thus it might be expected that increasing the coupling strength in a damped FPUT system would allow more cycles of recurrence to be observed before too much energy is lost from the system.

4.3.1 Equivalent quality factor of 10 000 and coupling strength of 0.8

The results of simulating the damped FPUT system with a coupling strength α of 0.8 and an equivalent quality factor Q of 10 000 are shown in Figure 4.6. Comparing these results to those for an α value of 0.25 in Figure 4.4 shows that increasing the strength of the nonlinear coupling coefficient does indeed increase the presence of recurrence in the transient response.

For a chain length of 64 oscillators, Figure 4.6(i) shows that the system does not exhibit a full cycle of recurrence but in comparison to the response at $\alpha = 0.25$ as shown in Figure 4.4(i) there is more energy entering modes 3 and 4. Comparing Figure 4.6(ii) with Figure 4.4(ii) shows that a system with a quality factor of 10 000 and a chain length of 32 exhibits a stronger return of energy to the first mode with the increased coupling strength of 0.8. The recurrence period is also significantly reduced, though not enough to enable any additional full cycles of recurrence. Decreasing the number of oscillators to $N = 16$ and comparing Figure 4.6(iii) with Figure 4.4(iii), it may be observed that, in addition to the increase in recurrence strength, an additional cycle of recurrence occurs before the energy reduces by half. Similarly, with $N = 8$ (Figures 4.6(iv) and 4.4(iv)), there are more cycles of recurrence for the same drop in energy.

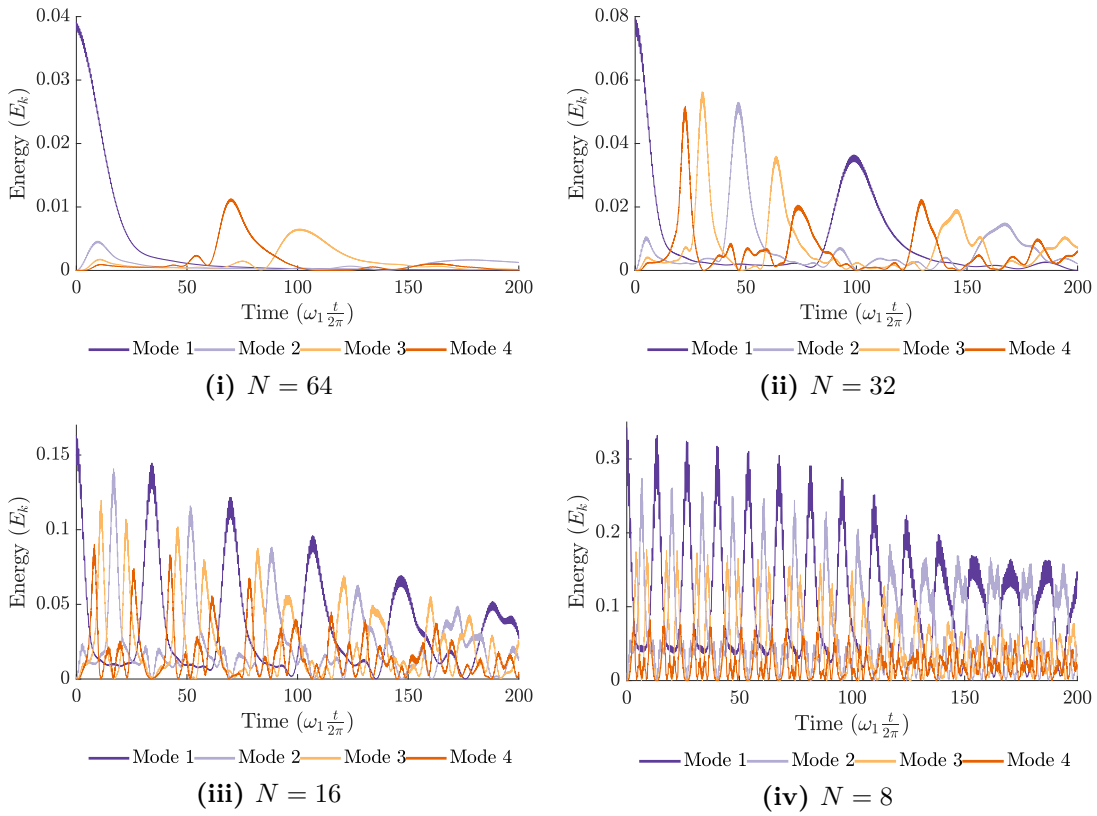


Figure 4.6: Simulations of 1D FPUT-α arrays with different numbers of oscillators, a quality factor of $Q = 10\,000$, and a coupling strength of $\alpha = 0.8$.

4.3.2 Equivalent quality factor of 1000 and coupling strength of 0.8

Reducing the quality factor to 1000, Figure 4.7 shows that, as expected, the energy decays in the system faster than for a quality factor of 10 000. For a chain length of 64, this means that the energy is lost from the system before any energy exchange between modes takes place (Figure 4.7(i)). Reducing the chain length to 32, no cycles of recurrence are present although a small amount of energy exchange does take place (Figure 4.7(ii)). Decreasing the number of oscillators to 16, there is a greater return of energy to the first mode and a clearer single recurrence cycle. At a chain length of 8 (Figures 4.7(iv)) a few additional cycles of recurrence can be observed before the energy is lost from the system.

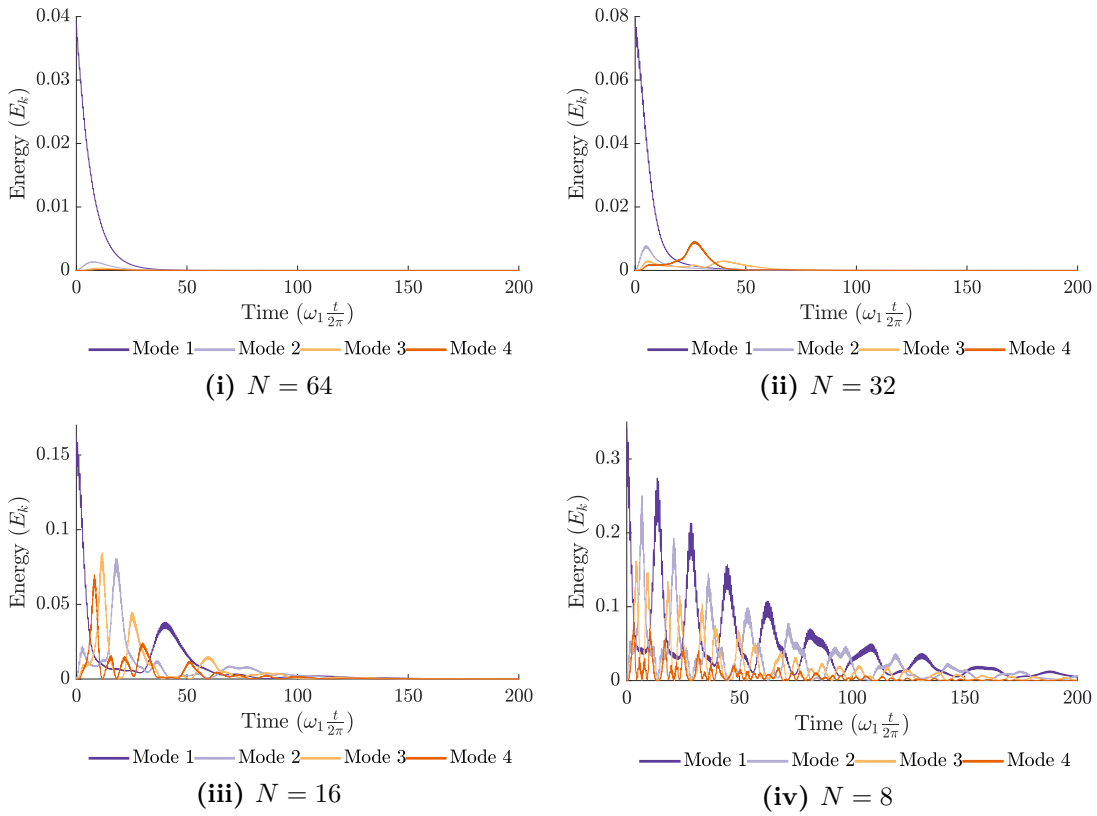


Figure 4.7: Simulations of 1D FPUT-α arrays with different numbers of oscillators, a quality factor of $Q = 1000$, and a coupling strength of $\alpha = 0.8$.

4.4 Effect of tolerance combined with damping

Any real system is inherently likely to have both tolerance and damping present. Therefore, the combined effects of these imperfections need to be explored. To facilitate direct comparison to the results with either tolerance or damping included, this section continues to consider the proportional damping introduced at the start of this chapter. No tolerance is incorporated into the damping term, and the tolerance application remains the same as in Chapters 2 and 3. In reality, the damping is unlikely to be purely viscous and will be subjected to variations. However, consideration of the simpler form presented in this thesis will still provide insight into the combined effects of tolerance and damping.

In Chapter 2, it was shown that adding tolerance to the components of an FPUT system affects the amount of recurrence seen in the system, with higher tolerance values leading to less, or even lost, recurrence. In the first part of this chapter, it was shown that as damping reduces the amount of energy in the system over time, recurrence is not always present in a damped FPUT system. Damping needs to be low enough to allow for sufficient oscillations at the first mode frequency to occur before energy is lost from the system for recurrence to occur. These results suggest that observing recurrence in a damped, heterogeneous system would only be possible under tightly controlled conditions.

The results presented in this thesis so far have shown that there is a correlation between the number of oscillators in the system and the amount of tolerance or damping that a system can incur before recurrence is no longer present. The earlier parts of this chapter have shown that a low number of oscillators provides the best chance of seeing a few cycles of recurrence, particularly with stronger damping (i.e. a lower Q value). The results presented in Chapter 2 demonstrated that recurrence is less affected by higher tolerances when there were fewer oscillators in the system. Considering these results, it would be reasonable to infer that a system with both damping and tolerance would have stronger recurrence when the number of oscillators is low.

4.4.1 Symmetric system

In the previous section, results for a system of 16 oscillators with 0 % tolerance and various combinations of damping and coupling strength were presented. To provide a full overview of the effects of both parameters separately, Figure 4.8 presents the results for a system with 16 oscillators, no damping, and either 0 % tolerance or tolerances of ±1 %, ±5 %, or ±10 %.

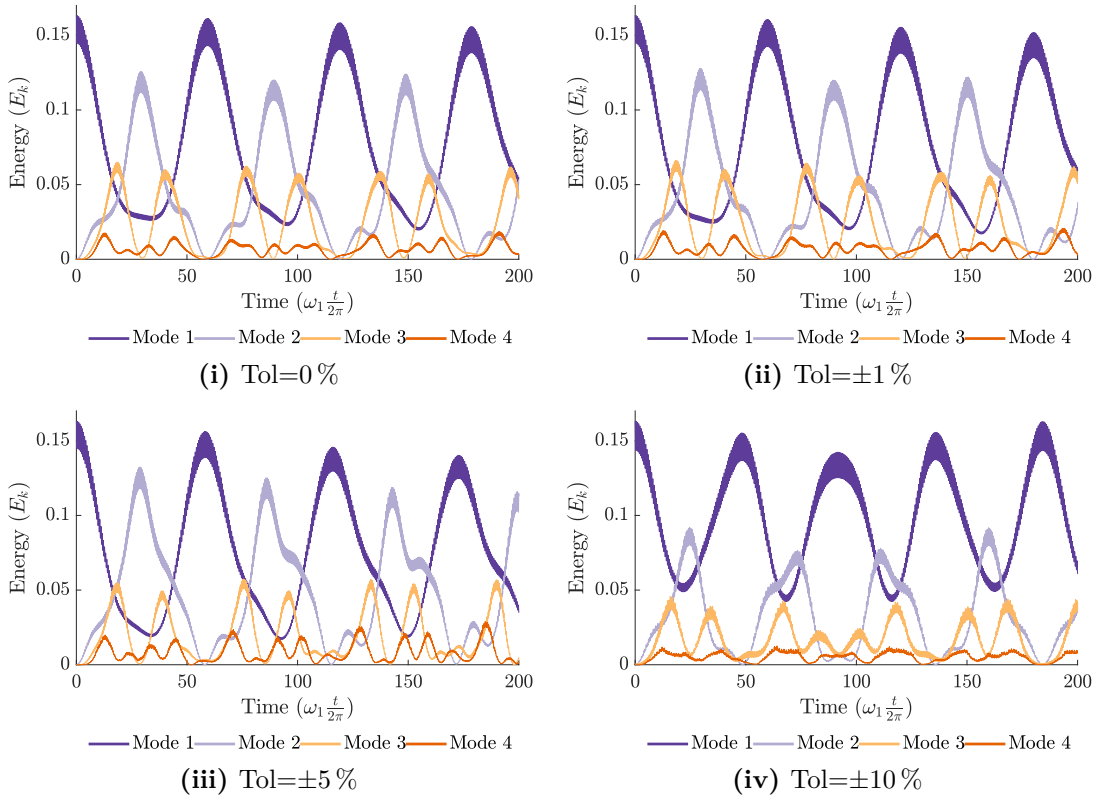


Figure 4.8: Simulations of 1D FPUT-α arrays with 16 oscillators, no damping, and a coupling strength $\alpha = 0.25$ at various tolerances.

Quality factor of 10 000 and coupling strength of 0.25

Adding an equivalent quality factor of 10 000 to the simulations in Figure 4.8 and keeping the tolerance values the same, the simulations were repeated. The results are presented in Figure 4.9 and show that the quality of the recurrence is further degraded by the addition of damping to the system. It is possible to observe several cycles of recurrence up to a tolerance of ±10 %.

Interestingly, by comparing Figures 4.9 and 4.8, it can be seen that despite the decrease in amplitude, the pattern of energy transfer between modes is almost identical for the first 100 time periods. However, after this point, the shape of the energy in the modes starts to change with damping. In particular, the time period of the recurrence increases. This is consistent with the results presented in Figure 4.2, where the recurrence period and pattern changes with decreasing energy in the initial condition.

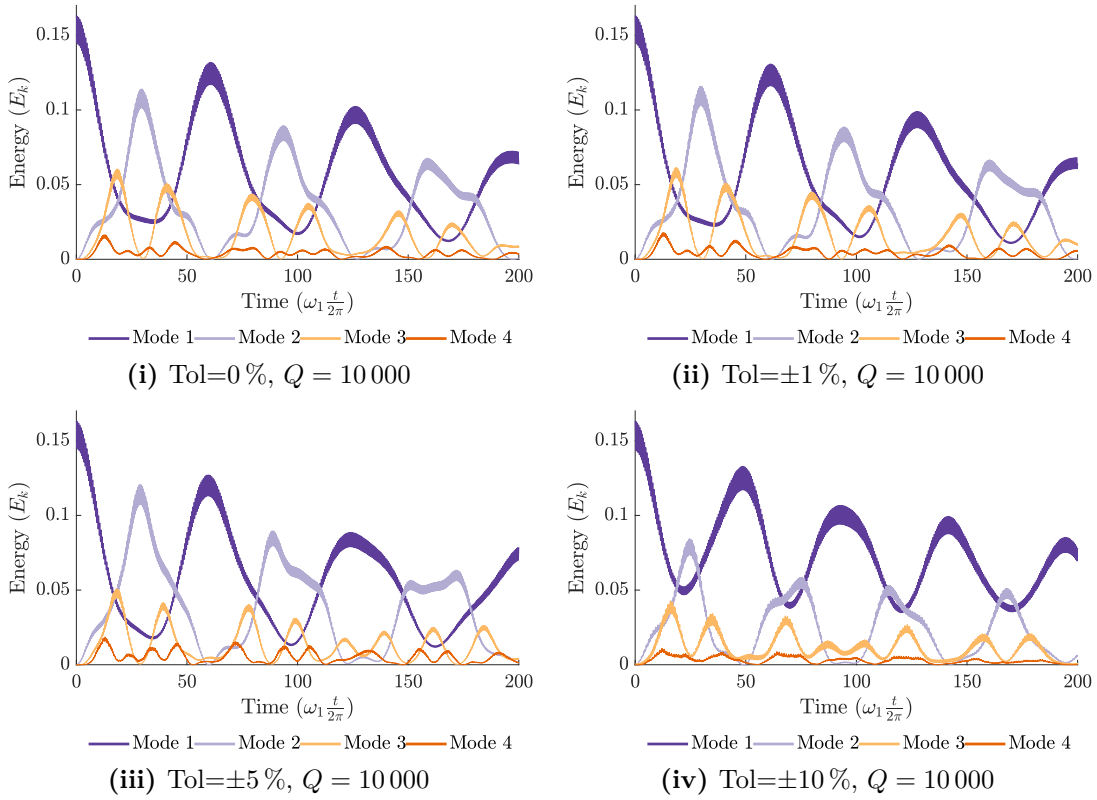


Figure 4.9: Simulations of 1D FPUT-α arrays with 16 oscillators, a quality factor of $Q = 10\,000$, and a coupling strength of $\alpha = 0.25$ at various tolerances.

Quality factor of 1000 and coupling strength of 0.25

Keeping the tolerance matrix the same and decreasing the quality factor to 1000, recurrence is very weak even with 0 % tolerance (Figure 4.10(i)). The energy has almost disappeared from the system after 100 cycles at the fundamental frequency. Additionally, very little energy has returned to the first mode at approximately 60 cycles where the first peak would occur with no damping.

Comparing the results at different tolerances in Figure 4.8, it can be seen that the energy transfer with 0 % tolerance and at tolerances of ±1 % and ±5 % is very similar for the first 100 cycles at the fundamental frequency. However, at a tolerance of ±10 % the recurrence period has shortened. The damped response reflects this with Figures 4.10(i)–(iii) appearing almost identical and Figure 4.10(iv) retaining more energy in the first mode for a longer period.

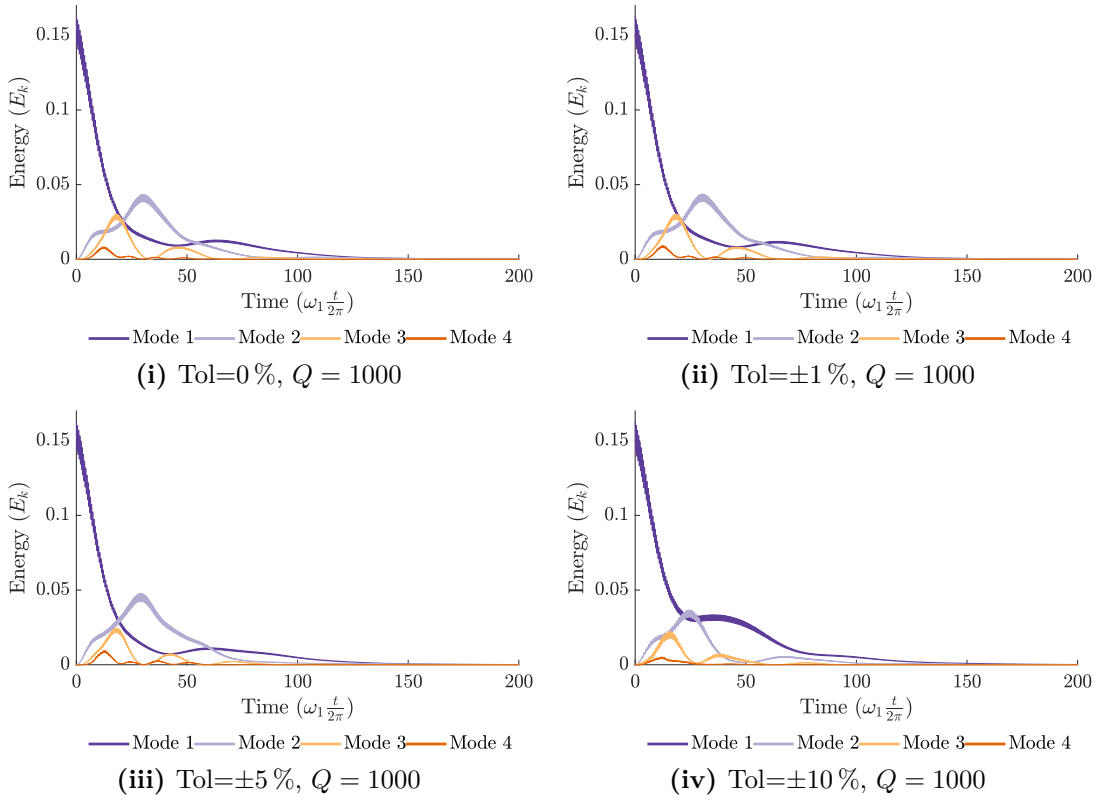
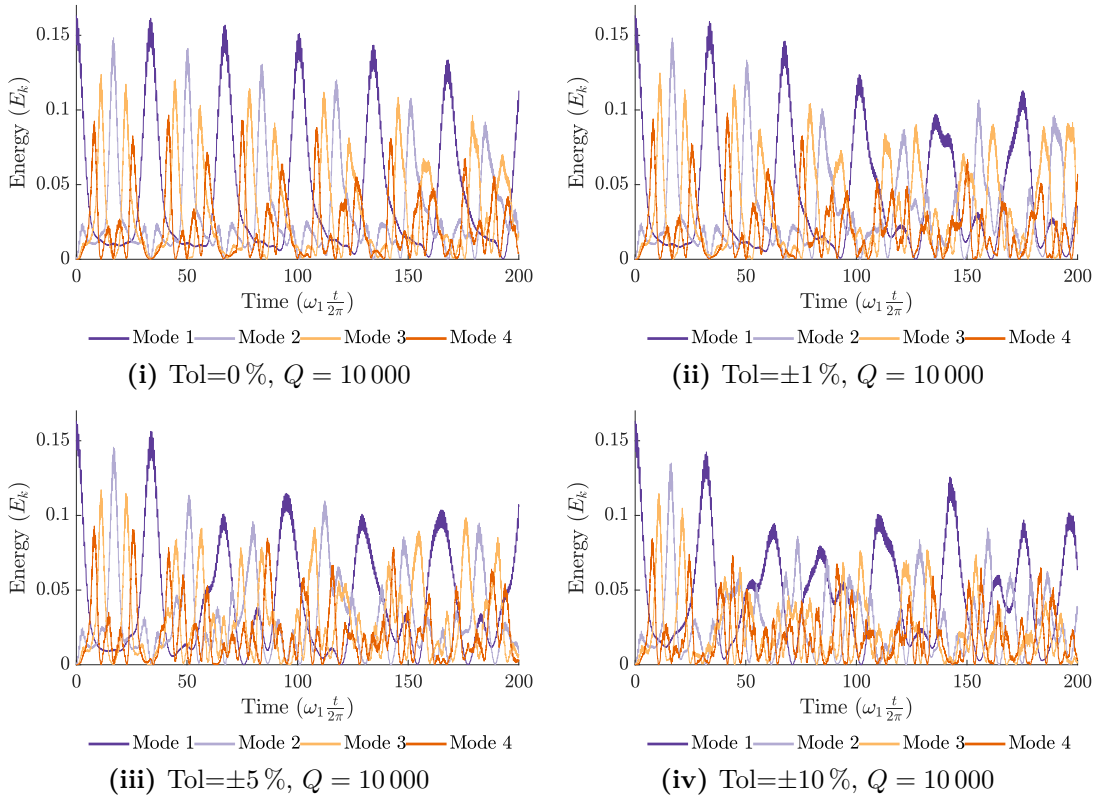


Figure 4.10: Simulations of 1D FPUT-α arrays with 16 oscillators, a quality factor of $Q = 1000$, and a coupling strength of $\alpha = 0.25$ at various tolerances.

Increased nonlinear coupling strength of 0.8

Section 2.6 showed that increasing coupling strength whilst keeping the tolerance constant decreased the presence of recurrence in the system. However, Section 4.3 showed that increasing coupling strength in a damped system increases the number of cycles of recurrence that can be observed before the energy is lost from the system. Thus, exploring the combined effects of tolerance and damping with a stronger coupling strength is important.

Figure 4.11 presents the results for simulating a 16 element system with a coupling strength of 0.8, no damping, and either 0 % tolerance or tolerances of ±1 %, ±5 %, or ±10 %. These results, combined with those for the system with damping and 0 % tolerance presented in Figures 4.6 and 4.7, can be used as a basis for comparison for the simulations with damping and tolerance.



(i) Tol=0 %, $Q = 10\,000$ **(ii)** Tol=±1 %, $Q = 10\,000$

(iii) Tol=±5 %, $Q = 10\,000$ **(iv)** Tol=±10 %, $Q = 10\,000$

Figure 4.11: Simulations of 1D FPUT-α arrays with 16 oscillators, no damping, and a coupling strength of $\alpha = 0.8$ at various tolerances.

Quality factor of 10 000 and coupling strength of 0.8

The results of simulating the same combinations of damping and tolerance in Figure 4.9 with an increased coupling strength of $\alpha = 0.8$ are shown in Figure 4.12. As would be expected, more cycles of recurrence take place during the same time period than for a coupling strength of $\alpha = 0.25$, so more cycles take place before the energy is lost from the system than are seen in Figure 4.9.

However, as with a coupling strength of 0.25, for the first 100 cycles of the fundamental frequency the shape of the exchange of energy between modes is similar to that without damping (Figure 4.12), although the amplitude of the peaks changes. After 100 cycles the time period of the recurrence starts to extend and the energy shapes are altered. As the tolerance increases, this change in shape appears to become more significant.

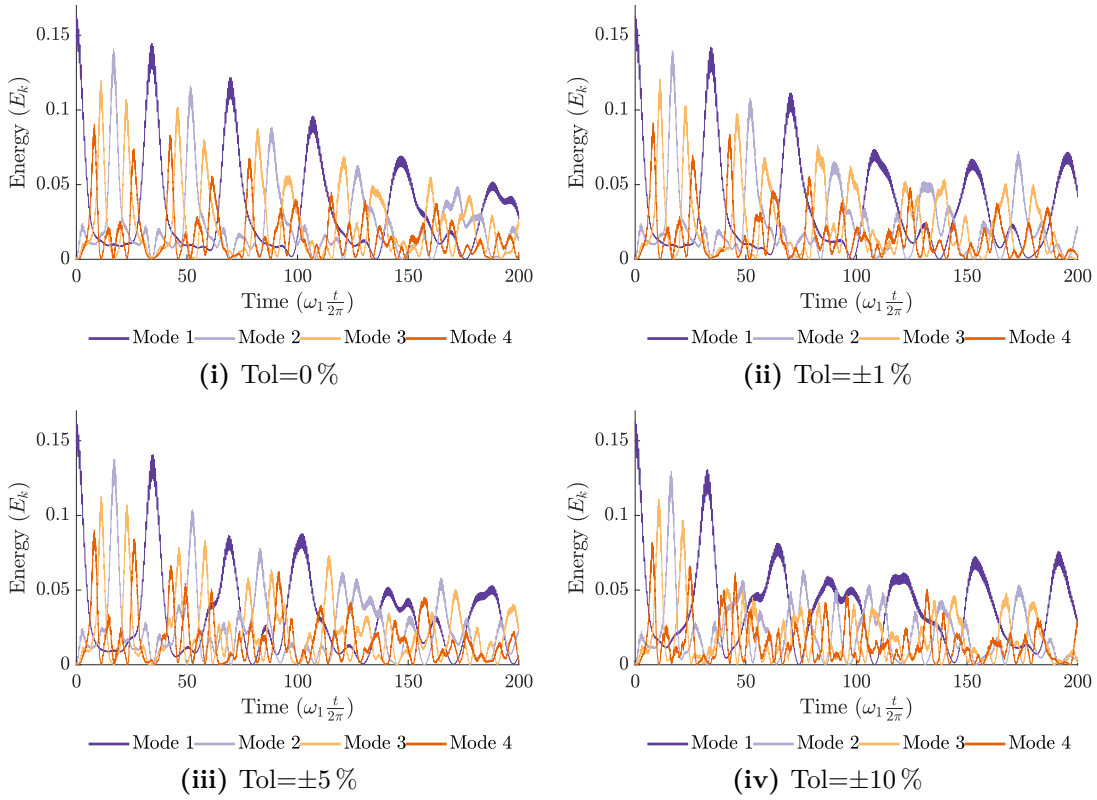
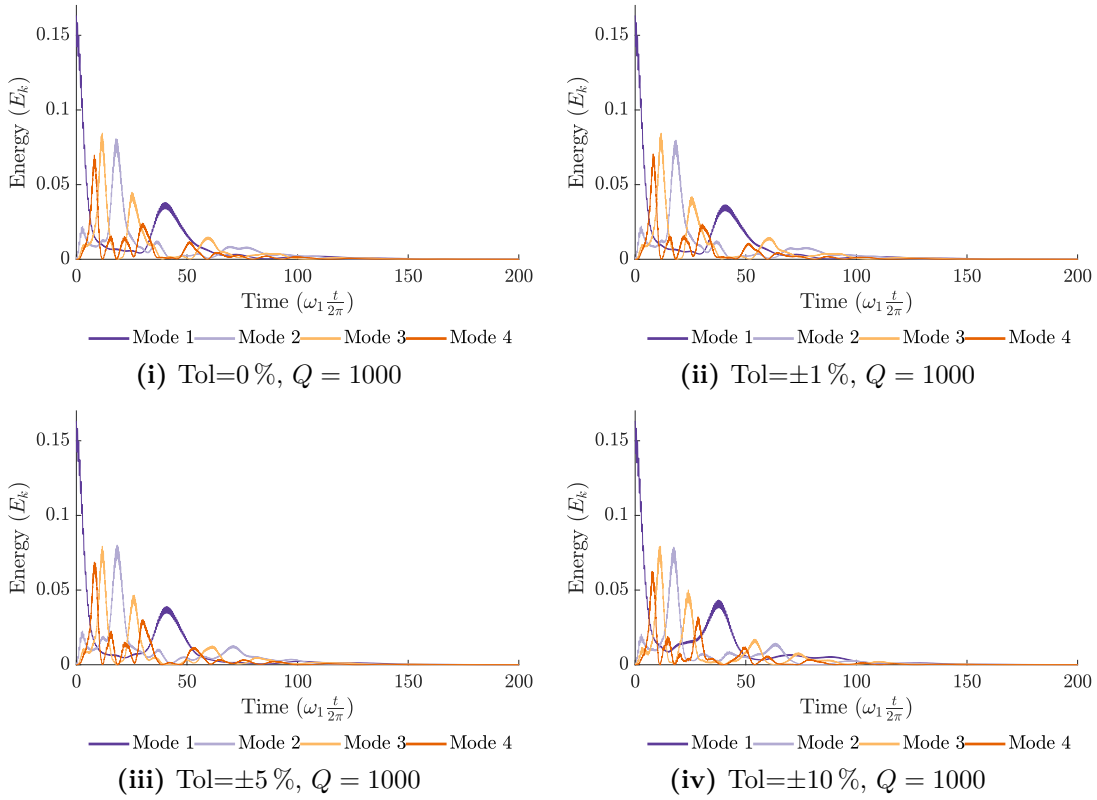


Figure 4.12: Simulations of 1D FPUT-α arrays with 16 oscillators, a quality factor of $Q = 10\,000$, and a coupling strength of $\alpha = 0.8$ at various tolerances.

Quality factor of 1000 and coupling strength of 0.8

Decreasing the quality factor to 1000, the overall response of the system at different tolerances is as expected. As was seen for a quality factor of 10 000, more recurrence is seen for a coupling strength of 0.8 (Figure 4.13) than for a coupling strength of 0.25 (Figure 4.10). However, only a single full cycle is seen.

Interestingly, the amount of energy returning to the first mode is higher for a tolerance of ±10 % (Figure 4.13(iv)) despite the amount returning to the first mode being lower with no damping (Figure 4.11(iv)). Similarly the amount transferred to the second mode following the first mode peak is higher at both ±5 % and ±10 % (Figures 4.13(iii) and 4.13(iv)). This may be due less to energy dropping out of these modes prior to the peaks (Figures 4.11(iii) and 4.11(iv)).



(i) Tol=0 %, $Q = 1000$ **(ii)** Tol=±1 %, $Q = 1000$

(iii) Tol=±5 %, $Q = 1000$ **(iv)** Tol=±10 %, $Q = 1000$

Figure 4.13: Simulations of 1D FPUT-α arrays with 16 oscillators, a quality factor of $Q = 1000$, and a coupling strength of $\alpha = 0.8$ at various tolerances.

4.4.2 Asymmetric system

In the previous section, results for a symmetric system of 16 oscillators with various combinations of tolerance, damping, and coupling strength were presented. Chapter 2 showed that an asymmetric system was less resilient to tolerance. It is therefore worth investigating whether combining damping and tolerance has a greater effect on the asymmetric system in Equation (3.1). Adding a damping term to the system, the equation of motion becomes

$$\ddot{x}_i + \nu\dot{x}_i = (t_{i+1}x_{i+1} + t_{i-1}x_{i-1} - 2t_i x_i) + \alpha[f_i^{\text{nlin}}(x_{i+1} - x_i)^2 - b_i^{\text{nlin}}(x_i - x_{i-1})^2] \quad (4.17)$$

As for the symmetric system, to provide a full overview of the effects of both parameters separately, Figure 4.14 presents the results for a system with 16 oscillators, no damping, and either 0 % tolerance or tolerances of ±1 %, ±5 %, or ±10 %.

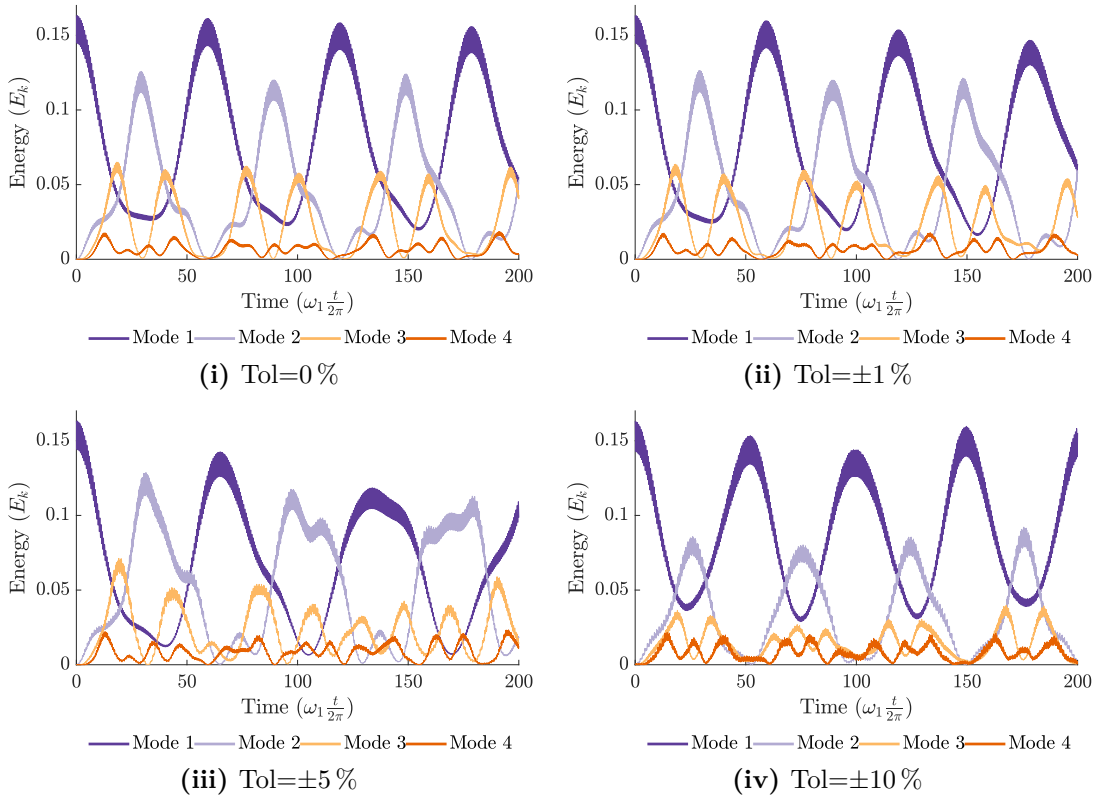


Figure 4.14: Simulations of asymmetric 1D FPUT-α arrays with 16 oscillators, no damping, and a coupling strength of $\alpha = 0.25$ at various tolerances.

Quality factor of 10 000 and coupling strength of 0.25

The results of simulating Equation (4.17) with a quality factor of 10 000 and a coupling strength of 0.25 are shown in Figure 4.15. Comparing these results to Figure 4.14, it can be seen that the asymmetric system responds to combined damping and tolerance in a similar manner to the symmetric system. That is, the amplitude of the peaks decreases, but the shape of the energy in each mode remains the same until approximately 100 cycles, after which the recurrence period extends and the shape changes.

The scale of the time shift is consistent between the symmetric and asymmetric systems. This suggests that the shift is due to the decrease in energy in the system, as opposed to the change in structure of the FPUT equation resulting from the addition of the tolerance terms.

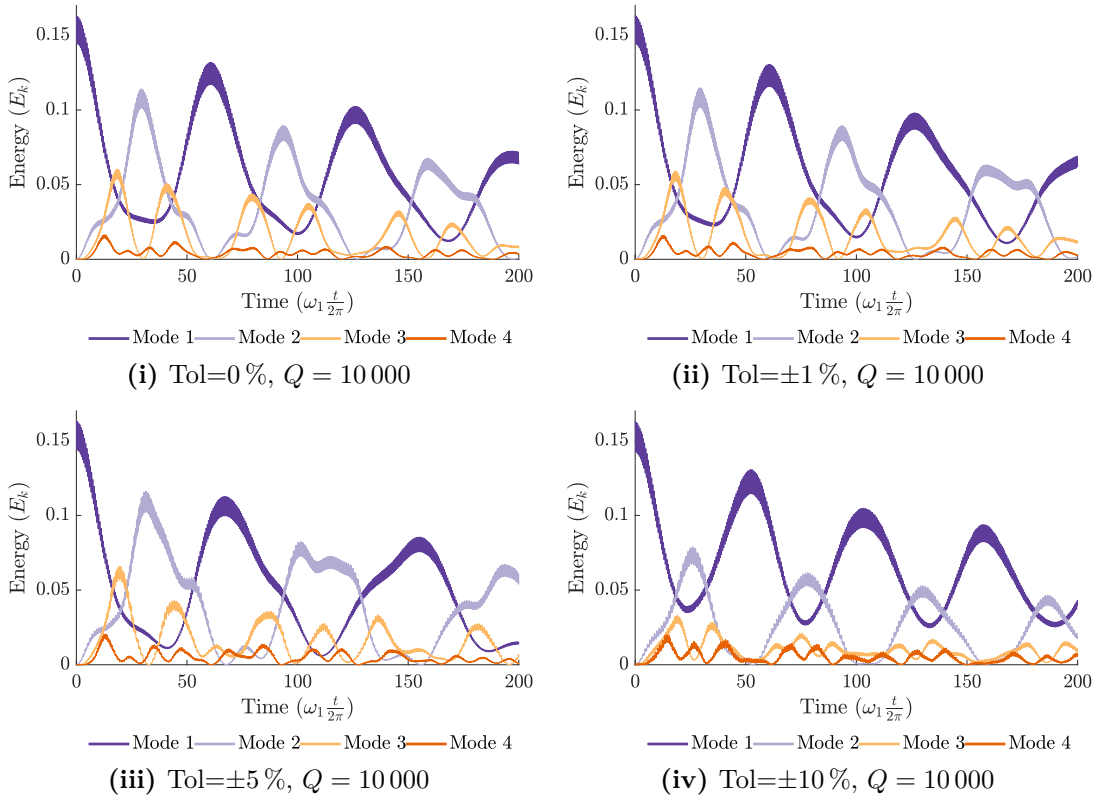


Figure 4.15: Simulations of asymmetric 1D FPUT-α arrays with 16 oscillators, a quality factor of $Q = 10\,000$, and a coupling strength of $\alpha = 0.25$ at various tolerances.

Quality factor of 1000 and coupling strength of 0.25

Reducing the quality factor to 1000, and simulating the system with the same tolerance values used for the higher quality factor, the results can be seen in Figure 4.16. As expected, only a single cycle of very weak recurrence occurs. Comparing Figures 4.16(i) and 4.16(ii) shows that the energy patterns are very similar for 0 % tolerance and ±1 % tolerance. This is consistent with the first cycle of recurrence with no damping shown in Figures 4.14(i) and 4.14(ii).

At a tolerance of ±5 %, the recurrence pattern starts to change with no damping (Figure 4.14(iii)) and this is reflected in the damped system (Figure 4.16(iii)). When the tolerance is increased further to ±10 %, less energy is transferred out from the first mode with no damping (Figure 4.14(iv)) and this is also true in the damped system (Figure 4.16(iv)).

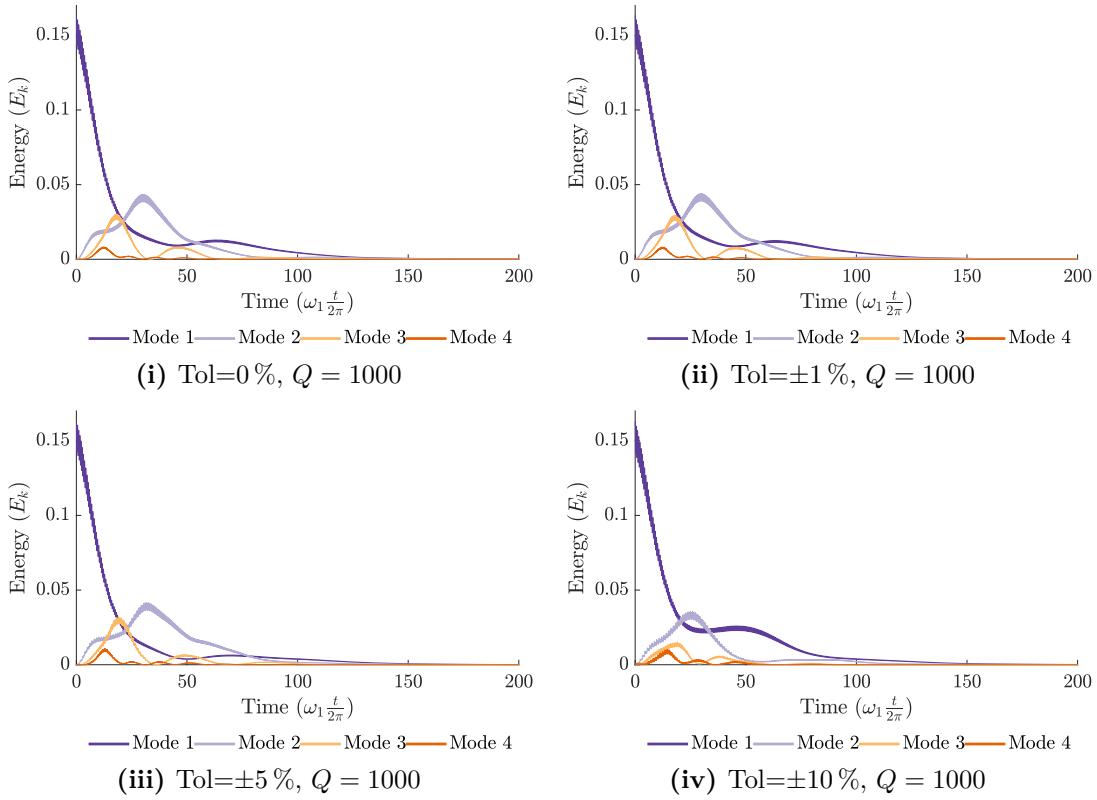


Figure 4.16: Simulations of asymmetric 1D FPUT-α arrays with 16 oscillators, a quality factor of $Q = 1000$, and a coupling strength of $\alpha = 0.25$ at various tolerances.

Increased nonlinear coupling strength

Section 3.4 showed that the asymmetric system responded in a similar manner to the symmetric system for an increased coupling strength, although recurrence was more severely affected at lower tolerances. Section 4.4.1 showed that an increase in coupling strength had no significant effect on how the system responded to the combined effect of damping and tolerance. This section explores the effect of increasing the nonlinear coupling strength for the asymmetric system.

Figure 4.17 presents the results for simulating a 16 element system with a coupling strength of 0.8, no damping, and either 0 % tolerance or tolerances of ±1 %, ±5 %, or ±10 %. These results, combined with those for the system with damping but 0 % tolerance presented earlier in presented in Figures 4.6 and 4.7, can be used as a basis for comparison for the simulations with damping and tolerance.

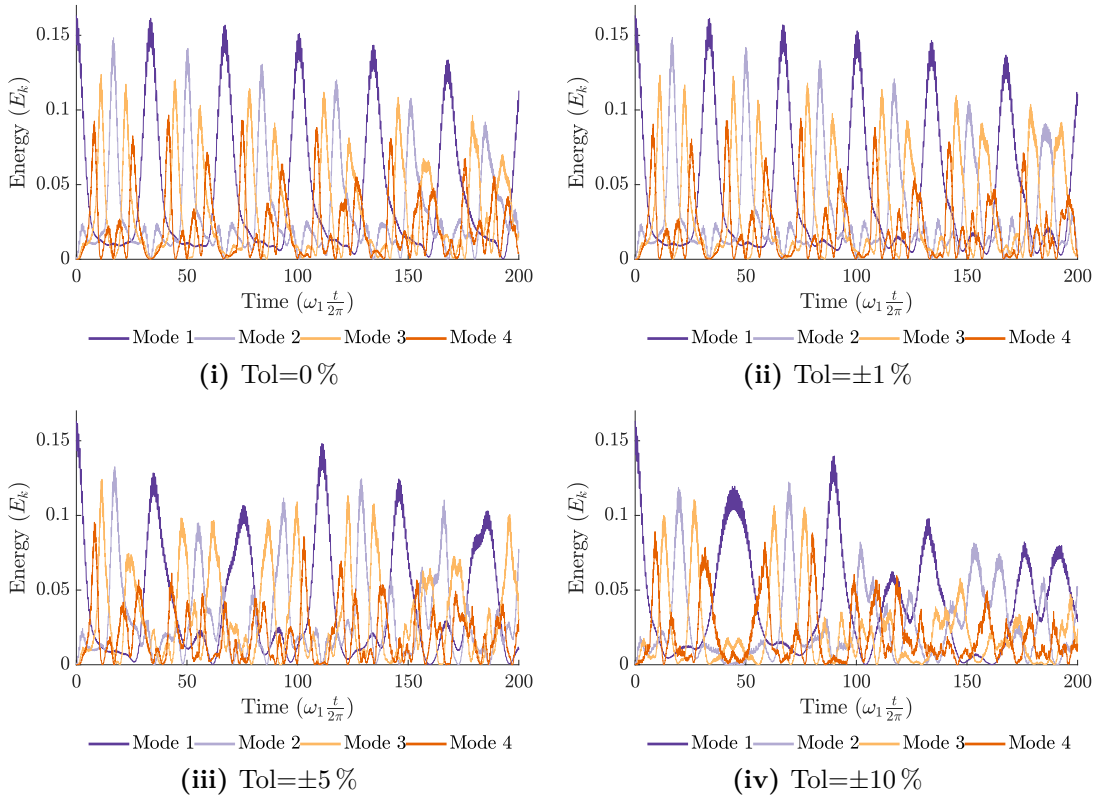
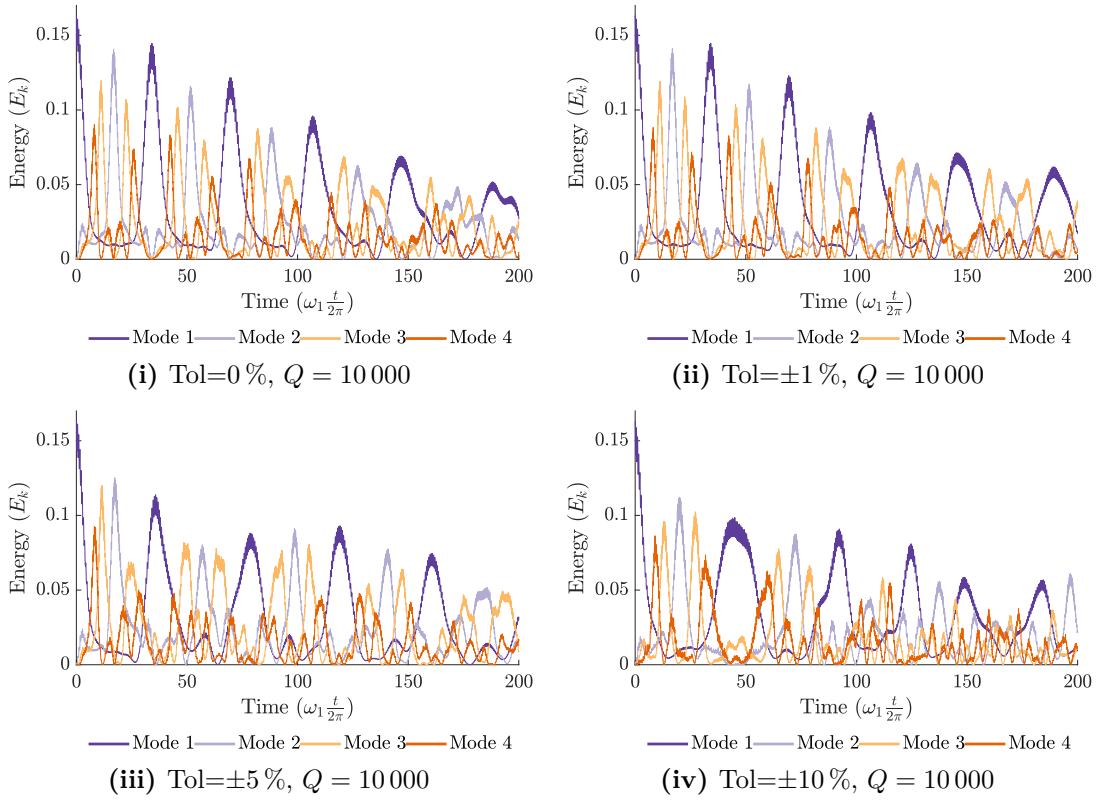


Figure 4.17: Simulations of asymmetric 1D FPUT-α arrays with 16 oscillators, no damping, and a coupling strength of $\alpha = 0.8$ at various tolerances.

Quality factor of 10 000 and coupling strength of 0.8

The results of simulating Equation (4.17) with a quality factor of 10 000, keeping the tolerance matrix the same whilst increasing the coupling strength to 0.8 are shown in Figure 4.18. As for the symmetric system, the change in recurrence period and shape starts to occur much earlier, at around 50 cycles. Similarly, there are more cycles of recurrence taking place at the higher coupling strength than at a coupling strength of 0.25 (Figures 4.15 and 4.18).

The change in shape is visible in all four modes and at all tolerance levels. However, it is much more prominent early on in the first mode at a tolerance of ±10 % (Figure 4.18(iv)). This is a contrast to the symmetric system where the change in the first mode occurs at a similar time for a tolerance of ±10 % as at the other tolerance values (Figure 4.12).



(i) Tol=0 %, $Q = 10\,000$ **(ii)** Tol=±1 %, $Q = 10\,000$

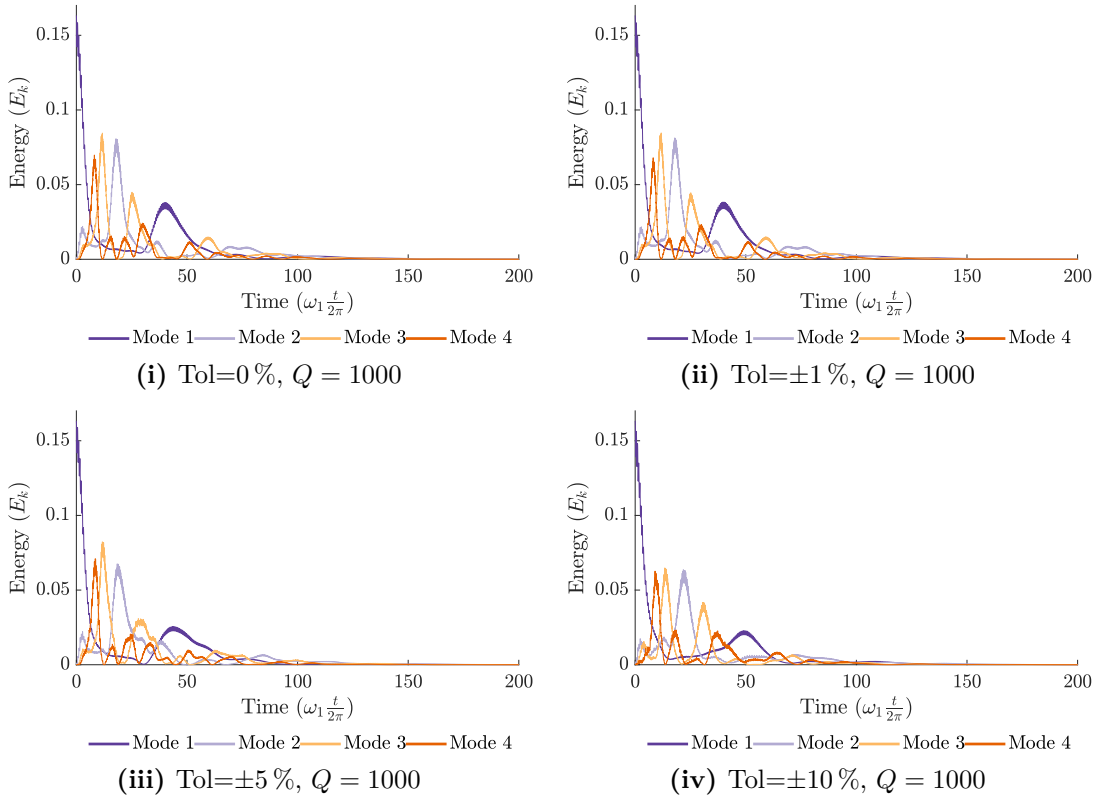
(iii) Tol=±5 %, $Q = 10\,000$ **(iv)** Tol=±10 %, $Q = 10\,000$

Figure 4.18: Simulations of asymmetric 1D FPUT-α arrays with 16 oscillators, a quality factor of $Q = 10\,000$, and a coupling strength of $\alpha = 0.8$ at various tolerances.

Quality factor of 1000 and coupling strength of 0.8

Reducing the quality factor to 1000, the number of cycles of recurrence present is reduced to a single cycle at all values of tolerance (Figure 4.19). However, recurrence is stronger than for a coupling strength of 0.25 (Figure 4.16), and the amount of energy returning to the first mode is much more significant. A comparison of Figures 4.19 and 4.17 highlights that the recurrence period has extended slightly with the addition of damping.

Unlike the results for the symmetric system presented in Figure 4.13, the amount of energy returning to the first mode in the asymmetric system is consistent with the relative peak sizes with no damping. As the energy in the first mode drops to a similar amplitude for all levels of tolerance in Figure 4.19, this may confirm the supposition that the larger peak in Figure 4.13(iv) is due to the larger amount of energy that stays in the first mode in that particular configuration.



(i) Tol=0 %, $Q = 1000$ **(ii)** Tol=±1 %, $Q = 1000$

(iii) Tol=±5 %, $Q = 1000$ **(iv)** Tol=±10 %, $Q = 1000$

Figure 4.19: Simulations of asymmetric 1D FPUT-α arrays with 16 oscillators, a quality factor of $Q = 1000$, and a coupling strength of $\alpha = 0.8$ at various tolerances.

4.5 Summary

This chapter began by exploring the impact of damping on an FPUT system. The simulation results presented show that it should be possible to experimentally observe a few cycles of the recurrence phenomenon in a damped FPUT system comprising of 8 resonators and having a quality factor of $Q \geq 1000$. However, systems with a higher number of resonators will not show a full recurrence cycle with an equivalent quality factor of 1000. Increasing the quality factor to 10 000 will allow several cycles of recurrence to be observed in a system with 16 resonators and a single cycle for a system with 32 resonators, although systems with 64 or more resonators will not show any recurrence.

The chapter then went on to investigate the effects of combining tolerance and damping in an FPUT system. The results presented in Chapter 2 demonstrated that a low number of oscillators would reduce the impact of tolerance on a system,

whilst the results in the early part of this chapter show that a low number of oscillators reduces the impact of damping on the system due to the reduced number of natural oscillation periods in a single recurrence cycle. If the effects of these two imperfections are combined, it is tolerance that has the most significant effect on the shape of the energy in each mode, whilst the level of damping is the predominant factor affecting the number of cycles that can be observed before too much energy is lost from the system.

Another important parameter to consider is the coupling strength. In Section 2.6 it was shown that increasing coupling strength whilst keeping the tolerance constant decreased the presence of recurrence in the system. In contrast, Section 4.3 shows that increasing coupling strength in a damped system increases the number of cycles of recurrence that can be observed before the energy is lost from the system as the recurrence period is shorter. Thus, it can be argued that there is an optimal value for α at which the combined effects of damping and tolerance have the minimum effect on recurrence. It is also likely that this value will vary for different combinations of tolerance and damping.

It can therefore be surmised that if the damping and tolerance in a system are low enough, the recurrence phenomenon could be observed in the transient response of the system. However, the number of oscillators must be small and the coupling strength needs to be carefully selected. Although this information provides a useful insight into systems with natural decay, in the applications such as sensing the system would need to be driven. Investigation of driven damped FPUT systems with tolerance is beyond the scope of this thesis yet should be considered for practical applications.

5

Designing a physical FPUT system

Contents

5.1 Electro-Mechanical analogies 122
5.1.1 An analogy of the FPUT system 123
5.2 Circuit design 124
5.2.1 Basic resonator circuit 125
5.2.2 Initial condition 129
5.2.3 Scaling factor 130
5.3 Component selection 131
5.3.1 Operational Amplifier 131
5.3.2 Multiplier 132
5.3.3 Analogue Switch 133
5.3.4 Passive components 133
5.4 Circuit layout 136
5.5 Testing 138
5.5.1 Test setup 138
5.5.2 Individual circuit response 139
5.5.3 Coupled response 139
5.6 Summary 145

A physical representation of the FPUT-α system used in the numerical experiments could be realised in a number of media. However, the predominant driving force behind the work in this thesis is the applicability of the results of nonlinear numerical experiments to MEMS sensing applications. Due to the processes involved, MEMS devices take a significant amount of time and money to design and manufacture. A simpler, faster alternative was therefore required to carry out initial feasibility studies. Since board level electronic circuits are generally quick and cheap to produce, this provided an ideal starting point to investigate the effects of nonlinear coupling. The results from these studies could then form the basis of a set of design requirements for a MEMS sensor.

Resonators are widely used in MEMS for various applications. These include mass [66], ultrasound [106] and surface acoustic wave (SAW) [107] transducers. As resonators become smaller due to advancements in manufacturing, inherent nonlinearity within these devices increases [5], [108]. Hence, resonators are a good way to study nonlinear coupling experimentally and investigate its effects on coupled transducer arrays.

This chapter introduces an electronic implementation of the FPUT-α equation (Equation (1.6)). Section 5.2 describes the design of the circuit, whilst Section 5.3 expands on the component choices and Section 5.4 gives an overview of the layout of the circuit. The results obtained from testing the circuit are presented in Section 5.5.

5.1 Electro-Mechanical analogies

In the previous chapters, the predominant focus has been in relation to lumped mechanical systems containing masses, springs and viscous dashpots. However, building such a system will be easier and more adaptable as an electronic circuit. Thus, a method of converting the mechanical system into an electrical one is required.

Electro-mechanical analogies were initially developed in the 19th Century by James Clerk Maxwell to aid the understanding of electrical properties in more familiar mechanical terms. However, as understanding of electrical systems evolved, it was found that electrical systems could aid the understanding of more complex mechanical systems. Ironically, it is these types of analogies that form the basis for analog computing which was used to solve differential equations prior to the advent of digital computing, and it was on one of these early digital computers that Fermi *et al.* conducted their numerical experiments.

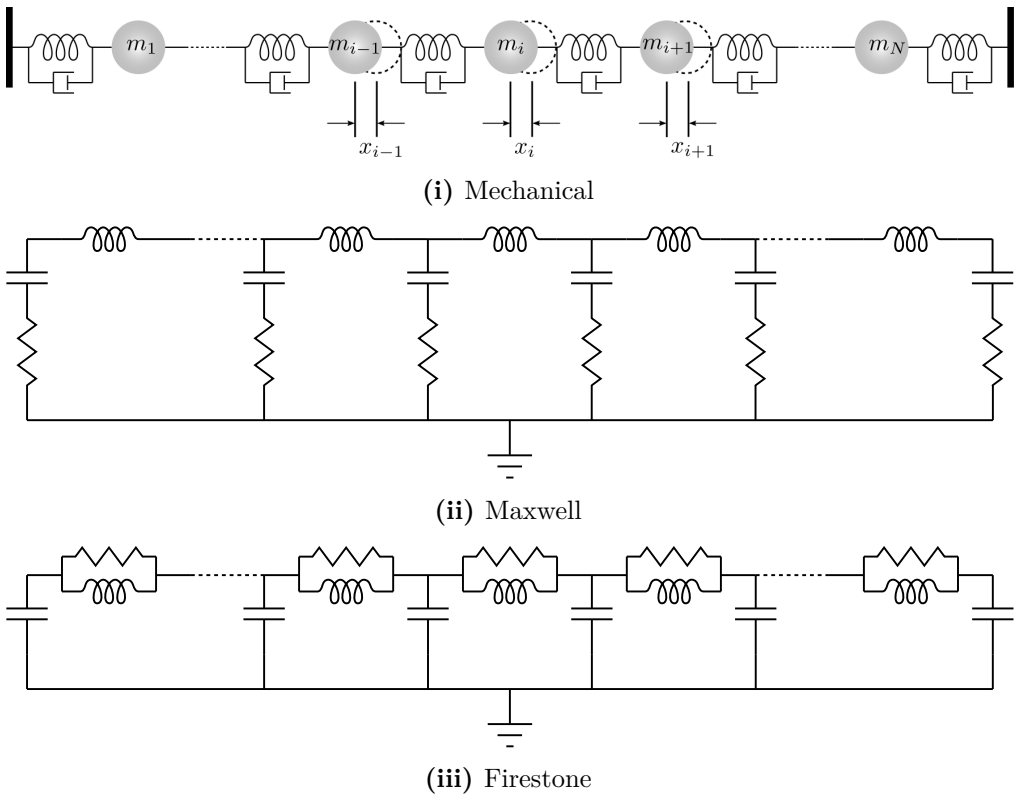
5.1.1 An analogy of the FPUT system

To move from the mass-spring system introduced in Chapters 1–3 to an electronic implementation, an electrical analogy is required for the force, mass, spring and viscous dashpot elements of the mechanical system. There are two main analogies in use, that developed by Maxwell [109] which relates force to voltage and another developed later by Firestone [110] which relates force to current. A summary of these analogies is presented in Table 5.1.

Mechanical		Maxwell		Firestone	
Force	F	Voltage	V	Current	I
Velocity	v	Current	I	Voltage	V
Mass	m	Inductor	$L \equiv m$	Capacitor	$C \equiv m$
Spring	k	Capacitor	$C \equiv 1/k$	Inductor	$L \equiv 1/k$
Damper	c	Resistor	$R \equiv c$	Resistor	$R \equiv 1/c$

Table 5.1: Electro-Mechanical Analogies

Figure 5.1 shows a physical comparison of the electrical Maxwell and Firestone circuits to the mechanical damped mass-spring system. As these circuits include damping, they do not directly model the FPUT-α system. Damping has been included as it is inherent in any real physical system (in a circuit the resistance of the wires will provide damping) and should not be neglected here.



(i) Mechanical

(ii) Maxwell

(iii) Firestone

Figure 5.1: Electrical analogies of the mechanical damped mass-spring system.

5.2 Circuit design

The previous section showed that it is possible to realise the second order differential equation describing the damped FPUT-α system with a combination of resistors, capacitors and inductors. Commonly known as RLC circuits, these circuits are comprised of purely passive components. However, they are limited in their accuracy due to non-ideal behaviours including attenuation of the signal. Additionally, integrating circuits should ideally have a phase shift of $-90°$ between input and output, whereas an RLC circuit has a $0°$ phase shift at resonance. The system has therefore been built using an active component, an operational amplifier (hereafter simply referred to as an op-amp); these provide a much better phase shift response and also have the advantage of being able to provide a gain component to control the signal amplitude.

An op-amp is a versatile device that takes a differential input and produces a single-ended output signal. Depending on the configuration of the circuit in

which it is used, an op-amp can be used to perform various precise mathematical operations on the input signals, including voltage summation, subtraction and integration. This makes them an ideal choice for implementing the FPUT equation whilst minimising the number of additional components.

One key consideration when designing the circuit is whether to create a single large circuit with multiple nodes or whether to create a modular system whereby each node would be represented by an individual circuit. A modular system was selected for this design as this would provide maximum flexibility for testing the system. For example, different numbers of circuits could be connected together, or the circuits could be connected together in different orders to test whether the sorting of tolerances does improve recurrence as was suggested in Section 2.7.

5.2.1 Basic resonator circuit

Differential equations of the form shown in Equation (1.6) can be studied electronically using analogue oscillators based on biquadratic (biquad) filters constructed from op-amps [111]. However, electronic oscillators have unstable initial states and therefore do not respond well to initial conditions. Introducing weak damping into the system converts the oscillators to resonators. This will reduce the response of the system with time, although if the damping is sufficiently low it will still be possible to observe a few cycles of the recurrence phenomenon as shown in Chapter 4. Importantly, the introduction of weak damping mimics the behaviour of MEMS systems as the majority of them are inherently damped. By using electronic resonators, this study is therefore of direct relevance to such systems.

To form an FPUT-α system using op-amps, two integrators are required to form the second order differential equation, along with summing capability to link the individual elements of the chain. There are several standard op-amp circuits that provide this functionality. One such circuit, known as the Tow–Thomas Biquad Filter [112], is shown in Figure 5.2. The power supply lines, decoupling capacitors and off-board connectors are omitted from this and subsequent circuit diagrams.

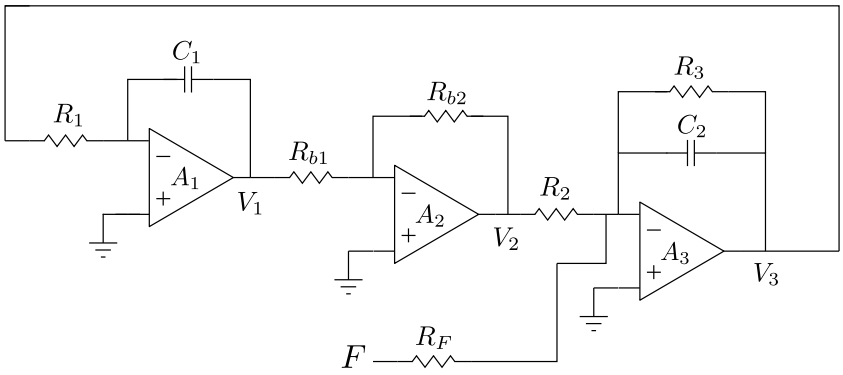


Figure 5.2: Schematic diagram of a Tow–Thomas biquad filter circuit.

There are three main constituent parts to this circuit: an inverting integrator(A_1), an inverting amplifier (A_2), and a summing inverting integrator (A_3). Examining each of these in turn enables one to understand how the FPUT equation can be formed from these components. The response of the ideal inverting integrator A_1 with input of V_3 and output V_1 can be expressed as:

$$\begin{aligned} V_1 &= -\frac{1}{R_1 C_1}\int_0^t V_3 \,\mathrm{d}t \\ \dot{V}_1 &= -\frac{V_3}{R_1 C_1} \end{aligned} \tag{5.1}$$

Similarly, the response for the inverting amplifier A_2 with input of V_1 and output V_2 can be expressed as:

$$V_2 = -\frac{R_{b2}}{R_{b1}} V_1 \tag{5.2}$$

Adding the feedback resistor R_3 to the summing integrator A_3 provides a DC gain control and therefore introduces a damping term. The response for the summing integrator A_3, with inputs of V_2 and F, and output V_3 is therefore:

$$\begin{aligned} V_3 &= -\int_0^t \frac{1}{R_3 C_2} V_3 + \frac{1}{R_2 C_2} V_3 + \frac{1}{R_F C_2} F \,\mathrm{d}t \\ \dot{V}_3 &= -\frac{V_3}{R_3 C_2} - \frac{V_2}{R_2 C_2} - \frac{F}{R_F C_2} \end{aligned} \tag{5.3}$$

Combining Equations (5.1), (5.2) and (5.3) gives the second-order transfer function for the circuit shown in Figure 5.2 as:

$$-R_1 C_1 \ddot{V}_1 = \frac{R_1 C_1}{R_3 C_2}\dot{V}_1 + \frac{R_{b2}}{R_{b1} R_2 C_2} V_1 - \frac{1}{R_F C_2} F \tag{5.4}$$

Considering V_1 as x_i and rearranging the equation leads to:

$$\ddot{x}_i + \frac{1}{R_3 C_2}\dot{x}_i = -\frac{R_{b2}}{R_{b1}R_1C_1R_2C_2}x_i + \frac{1}{R_1C_1R_FC_2}F \tag{5.5}$$

which is of a similar form to the FPUT equation if F is formed of the coupling terms.

The expanded schematic in Figure 5.3 shows the addition of these coupling terms to form the FPUT system. The linear coupling can simply be provided by tapping the output from A_1. The x_i term can be fed to the adjacent circuits in the chain providing the x_{i+1} and x_{i-1} terms.

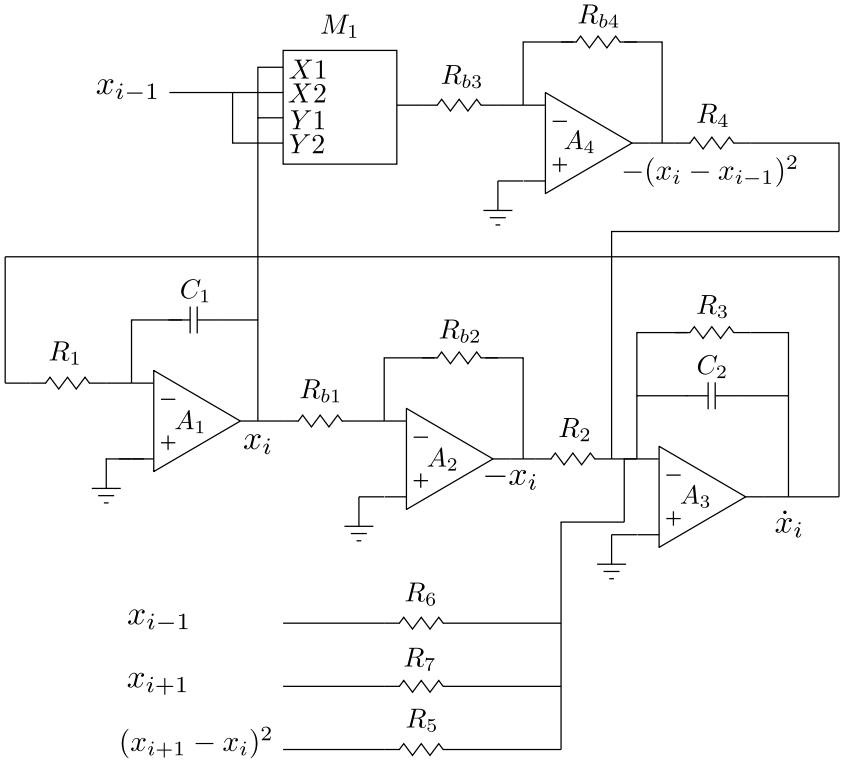


Figure 5.3: Schematic diagram for a single resonator module designed to form part of a coupled resonator circuit.

The nonlinear coupling signals are more complex due to their quadratic nature and additional circuitry must be included to produce these terms. The simplest way to do this is by using a four quadrant analogue multiplier, shown on the schematic in Figure 5.3 as M_1. These are readily available in integrated circuits (ICs) and are often based on the Gilbert Cell, a circuit traditionally constructed of transistors and diodes [113]. This is used once on each circuit, generating the $(x_i - x_{(i-1)})^2$

term which is then inverted by the inverting amplifier A_4. The output from the multiplier is also fed to the previous circuit to create the $(x_{(i+1)} - x_i)^2$ term for that circuit. Including the amplifier A_4 inverts the output from the multiplier as required for the FPUT equation and also provides the opportunity to scale the output from the multiplier if required by adjusting the gain.

Replacing the F term, the equation of the circuit then becomes

$$\ddot{x}_i + \frac{1}{R_3C_2}\dot{x}_i = \frac{1}{R_1C_1}\left\{\frac{1}{R_7C_2}x_{i+1} + \frac{1}{R_6C_2}x_{i-1} - \frac{R_{b2}}{R_{b1}R_2C_2}x_i + \frac{1}{R_5C_2}(x_{i+1} - x_i)^2 - \frac{R_{b4}}{R_{b3}R_4C_2}(x_i - x_{i-1})^2\right\} \quad (5.6)$$

which is of the same form as the damped FPUT equation (Equation (4.10)).

The FPUT-α equation requires a 1:1:2 ratio for the x_{i+1}, x_{i-1}, and x_i terms, and a ratio of 1:1 for the $(x_{i+1} - x_i)^2$ and $(x_i - x_{i-1})^2$ terms. Therefore, by setting $R_4 = R_5$, $R_6 = R_7 = \frac{R_{b1}R_2}{2R_{b2}}$, and $R_{b3} = R_{b4}$, and substituting into Equation (5.6), the equation simplifies to:

$$\ddot{x}_i + \frac{1}{R_3C_2}\dot{x}_i = \frac{R_{b2}}{R_{b1}R_1C_1R_2C_2}\{x_{i+1} + x_{i-1} - 2x_i\} + \frac{1}{R_1C_1R_4C_2}\left\{(x_{i+1} - x_i)^2 - (x_i - x_{i-1})^2\right\} \quad (5.7)$$

Comparing this to Equation (4.8), the equations are of the same form. The effective quality factor Q, equivalent linear frequency ω, and coupling strength α are therefore governed by Equations (5.8)–(5.10).

$$\nu = \frac{\omega}{Q} = \frac{1}{R_3C_2} \quad (5.8)$$

$$\omega = \sqrt{\frac{R_{b2}}{R_{b1}R_1C_1R_2C_2}} \quad (5.9)$$

$$\alpha = \frac{1}{R_1C_1R_4C_2} \quad (5.10)$$

These show that the resonant frequency, quality factor and coupling strength of the circuit can be altered independently of each other by changing the appropriate resistor values. However, care must be taken to maintain the ratio between the equation elements as described by the FPUT-α equation.

5.2.2 Initial condition

To allow an initial condition to be applied to the resonators, a quad analogue switch was included as shown in Figure 5.4. When the output enable for the switches is active, the initial condition is applied. The circuit is allowed to settle in this state so that x_i is held at a steady voltage of an amplitude corresponding to the circuit location in the chain, and $\dot{x}_i$ is held at 0 V. When the output enable is set to inactive, the circuit is put into the normal operating state, the x_i and $\dot{x}_i$ terms are free to change, and the system is released from rest.

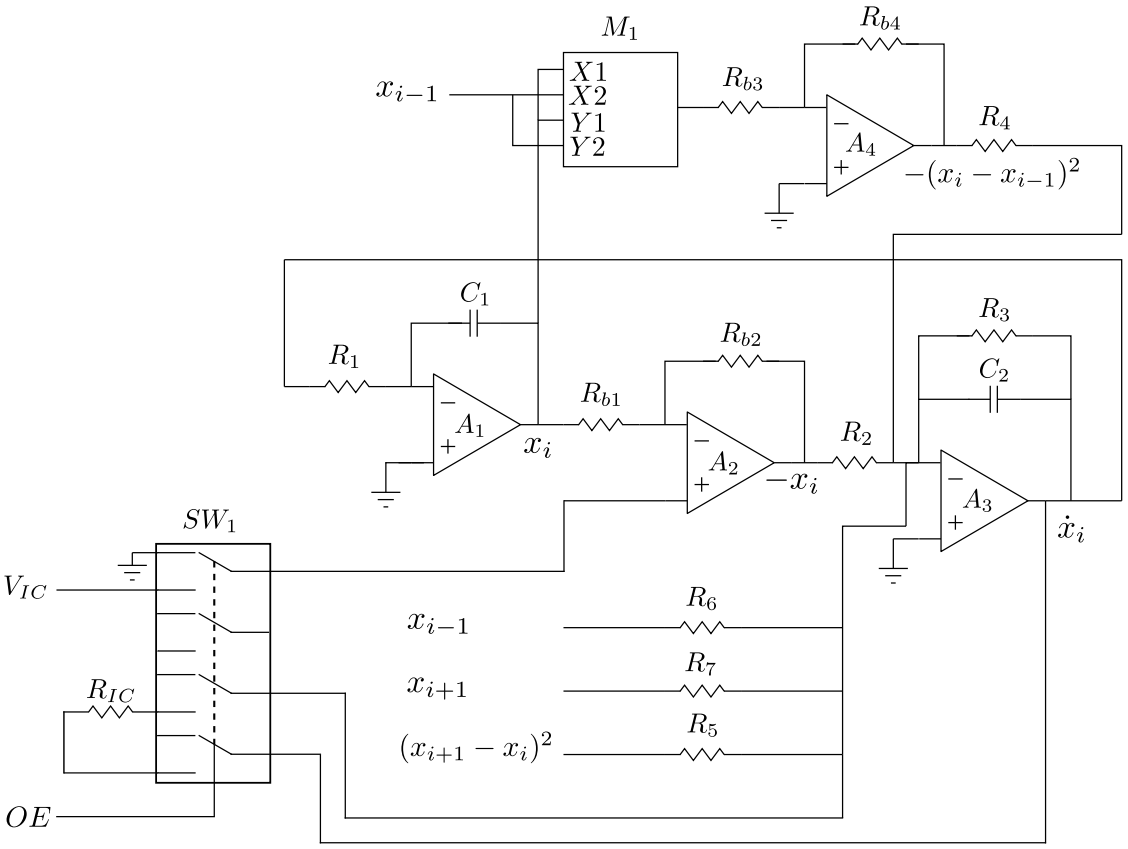


Figure 5.4: Schematic diagram for a single resonator module with provision to apply an initial condition.

One switch connects the positive terminal of A_2 to an external voltage for the initial condition or 0 V for normal operation. By applying this voltage to the positive terminal of A_2, the golden rules of op-amps [83] mean that the negative terminal matches the voltage and this then ensures the same voltage is at the output from A_1, i.e. for x_i.

Another two switches connect a resistor across the terminals of C_2 for the initial condition. This provides a DC bypass path shorting out the capacitor and ensuring $\dot{x}_i$ is at 0 V. Although R_3 is present in the circuit, this option was included to allow the circuit to be used as an oscillator rather than a resonator if required (i.e. if R_3 is not fitted). Additionally a much smaller value of resistance was used to ensure that the initial condition was effective.

5.2.3 Scaling factor

The original FPUT numerical experiments, and the simulations included in this thesis, were run with an angular frequency ω of $\sqrt{2}\,\mathrm{rad\,s^{-1}}$. However, setting the same resonant frequency for the circuit is impractical as the resistor and capacitor values required would be either much too large or much too small. As such, a time scaling factor was used to obtain more practical values. To keep measurements in the time domain simple, the frequency, f, will be increased to 10 kHz. Since $\omega = 2\pi f$, this requires a scaling factor of $\sqrt{2}\pi \times 10^4$ and adjusts Equations (5.8), (5.9) and (5.10) to:

$$\nu = \frac{\omega}{Q} = \frac{1}{\sqrt{2}\pi \times 10^4 R_3 C_2} \tag{5.11}$$

$$\omega = \frac{1}{\sqrt{2}\pi \times 10^4}\sqrt{\frac{R_{b2}}{R_{b1}R_1C_1R_2C_2}} \tag{5.12}$$

$$\alpha = \frac{1}{(\sqrt{2}\pi \times 10^4)^2 R_1C_1R_4C_2} = \frac{1}{2\pi^2 \times 10^8 R_1C_1R_4C_2} \tag{5.13}$$

5.3 Component selection

Selection of the correct components for building a circuit is critical to ensuring that a design functions as intended. A single component with the wrong parameters could easily stop the circuit from working correctly. There are a variety of factors to consider, and it is often a trade-off to decide which component matches the most requirements.

When selecting the components for this prototype build, ease of construction and testing of the circuits was important. Identifying devices in packages that were capable of being soldered by hand was important to reduce build costs and allow flexibility, as was easy access to component pins for testing and debug. However, keeping the design as compact as possible to minimise track lengths and therefore improving noise immunity was also important so small surface-mount devices were utilised where possible.

5.3.1 Operational Amplifier

Ideal op-amps have infinite differential gain, zero common mode gain, zero offset voltage and zero bias current. Practically, this translates to devices with a large voltage gain, a high input impedance, and a low bias current [83], [114]. In order to be able to see the recurrence phenomenon in an op-amp based electronic resonator circuit, an op-amp with high bandwidth is required to maintain filter precision [115]. A low input bias current is also required because to achieve a high quality factor, R_3 must have a high resistance value resulting in a low feedback current. For this to have an impact at the negative terminal of the op-amp the input bias current must also be low.

New advances in circuit technology mean that op-amps with a wide gain bandwidth product and low bias current are becoming a reality. With several of these now on the market with slightly differing characteristics, the first challenge was to select a suitable part for the application. In addition to the characteristics mentioned above, the operating voltage of the op-amp is of interest, as, if the operating range is too small, the signals of interest will be lost in the noise floor of the circuit.

The device selected was the Texas Instruments OPA4354, a high-speed, voltage-feedback CMOS op-amp in a quad package. Designed for high-speed applications, it has a unity gain bandwidth of 250 MHz and is also stable for unity gain applications. Operating from power supply rails of ±2.5 V, with an output swing to within 100 mV of the rails, a low bias current of 3 pA, and a spectral noise density of 12 nV/$\sqrt{\text{Hz}}$ at 10 kHz, this device provides the necessary characteristics for building the FPUT circuit.

5.3.2 Multiplier

Analog multipliers are available in three main types:

- single quadrant: both inputs and the output are unipolar
- two quadrant: one of the inputs is unipolar, the other input and the output are bipolar
- four quadrant: both inputs and the output are bipolar

To generate the nonlinear coupling terms a four quadrant multiplier with differential inputs is required. The Analog Devices AD633 multiplier is a low cost device that provides this functionality with a typical accuracy of ±1 % and a guaranteed total accuracy of ±2 % of full scale. With a 1 MHz bandwidth, a 20 V µs^{-1} slew rate, spectral noise density of 0.9 µV/$\sqrt{\text{Hz}}$ at 10 kHz, and power supply voltage range from ±8 V to ±18 V this device provides the functionality required at a reasonable cost. More accurate parts are available, e.g. the Analog Devices AD534 at ±0.25 %, but at nearly five times the cost this was deemed to be unnecessary for the initial design.

The AD633 also has the added advantage that it divides the output by 10 (a built in feature) which ensures that the squared output doesn't become too large and overdrive the op-amps. The full transfer function for the AD633 is therefore:

$$W = \frac{(X1 - X2)(Y1 - Y2)}{10} + Z \tag{5.14}$$

where W is the output, $X1$, $X2$, $Y1$ and $Y2$ are differential inputs, and Z is a summing input. For this circuit, Z is set to 0 V.

The output scaling factor of the AD633 needs to be taken into account when calculating component values. Including this scaling factor into the equation, the coupling strength becomes:

$$\alpha = \frac{1}{2\pi^2 \times 10^9 R_1 C_1 R_4 C_2} \tag{5.15}$$

5.3.3 Analogue Switch

The analogue switch selected was the Analog Devices ADG734. This is a quad single-pole double-throw (SPDT) switch package with a low on resistance (2.5 Ω typical) and a fast switching time (19 ns). The power supply rails are also compatible with the op-amps at ±2.5 V.

5.3.4 Passive components

Physical size

To reduce the amount of noise in the circuitry, it was decided to keep all components as small as possible whilst still being able to easily solder them by hand. As such, the passive components (resistors and capacitors) were selected to be in an 0402 package size where possible. The only exceptions to this were the bulk decoupling capacitors, as the voltage rating needed to be higher than that available in the 0402 package size, and the feedback capacitors C_1 and C_2, where a larger 0805 package size gave more flexibility for changing capacitance values should this be required.

Tolerance

All resistor values were selected with a tolerance of ±0.1 %, as these are readily available in the 0402 package size and are not prohibitively expensive. Keeping the tolerances of these components low will help to reduce stacked tolerances across the board which will not only include the other components, but variations in the PCB itself such as track lengths, dielectric thickness and solder joints.

The feedback capacitors were selected to have a ±1 % tolerance with COG dielectric, the bulk decoupling capacitors a ±5 % tolerance with X7R dielectric and the high-frequency decoupling capacitors a ±10 % tolerance with X7R dielectric.

These part choices were partly governed by availability at the time of ordering, the 100 nF high-frequency decoupling capacitors in particular were in short supply at the required voltage rating.

Value

The common method of selecting passive values is to set a few 'obvious' components at common values and then calculate the remainder. This is obviously a subjective process. However, there is generally a narrower range of capacitor values to choose from so this provides a good starting point. These were set as $C_1 = C_2 = 10\,\text{nF}$. Another easily selectable set of values is the resistors for the two inverting amplifiers, A_2 and A_4. To set a gain of 1, and to limit the current involved, the resistor values were selected as $R_{b1} = R_{b2} = 10\,\text{k}\Omega$, and $R_{b3} = R_{b4} = 10\,\text{k}\Omega$. To set the frequency at the desired value of 10 kHz, this leaves R_1 and R_2. However, from the observations earlier, setting R_2 at a value which will allow R_6 and R_7 to be easily calculated makes sense if $R_{b1} = R_{b2}$. Therefore R_2 was set as $1\,\text{k}\Omega$. These values are summarised in Table 5.2.

Designator	Selected Value
R_2	$1\,\text{k}\Omega$
R_{b1}	$10\,\text{k}\Omega$
R_{b2}	$10\,\text{k}\Omega$
R_{b3}	$10\,\text{k}\Omega$
R_{b4}	$10\,\text{k}\Omega$
C_1	10 nF
C_2	10 nF

Table 5.2: Selected passive component values

Substituting the selected values into Equation (5.12) then gives R_1 as $2.53\,\text{k}\Omega$ which is not a standard value. Referring to the resistor standards, 2.49 and 2.55 are standard values in the E96 series which has a nominal tolerance of 1 %, and 2.52 is available in the E192 series which has a nominal tolerance of $\leq$0.5 %. The obvious choice would be $2.52\,\text{k}\Omega$, however, this was not readily available from the distributors being used so a value of $2.55\,\text{k}\Omega$ was selected for R_1.

With the value of R_2 selected as 1 kΩ, R_6 and R_7 are easily calculated as 2 kΩ, which is a standard value in the E192 series. Similarly, with the value of C_2 set, and the desired values for frequency (10 kHz) and quality factor (10 000), R_3 can be calculated from Equation (5.11) as 15.92 MΩ. Again, this is not a standard value and the closest available resistor from the distributors being used had a value of 16 MΩ and a tolerance of ±5 % (E24 series). The coupling strength is now set by remaining two resistors, R_4 and R_5. For a value of $\alpha = 0.25$, using Equation (5.15) gives $R_4 = R_5 = 800\,\Omega$. The closest value available in the E192 series is 806 Ω. The calculated values and the corresponding selected value are summarised in Table 5.3.

Designator	Calculated Value	Selected Value
R_1	2.53 kΩ	2.55 kΩ
R_3	15.92 MΩ	16 MΩ
R_4	800 Ω	806 Ω
R_5	800 Ω	806 Ω
R_6	2 kΩ	2 kΩ
R_7	2 kΩ	2 kΩ

Table 5.3: Calculated passive component values

As some of the values selected for the passives are not the ideal calculated values, the impact of this on the circuit design needs to be understood. Substituting the selected values back into Equations (5.12), (5.11) and (5.15) allows one to calculate the actual circuit values. The results of these calculations are shown in Table 5.4 alongside the originally desired values and show that none of the differences exceed 0.4 %.

Parameter	Desired Value	Design Value
Q	10 000.000	10 019.589
f (kHz)	10.000	9.967
α	0.250	0.246

Table 5.4: Desired vs design values

5.4 Circuit layout

Circuit designers often simulate circuits in specialist software using SPICE models prior to commencing the layout. Providing the quality of the models being used is good enough, circuit performance and reliability can be optimised. It can be particularly useful for understanding the impact of noise levels in the circuit. Unfortunately, thorough simulation of the FPUT circuit being implemented was not possible. Despite trying multiple different combinations of simulation parameters, it was not possible to quickly find a solution to the errors that occurred. Since the circuit was relatively simple to construct, it was decided that building a prototype would be more expedient than resolving the errors in the SPICE simulation.

A very early 'proof of concept' circuit was constructed on stripboard to minimise the initial design time required and provide maximum flexibility during the prototyping phase. Limited testing was conducted but the early results using two operational amplifier based resonators with nonlinear coupling were promising. The quality factor of the circuit was shown to be high enough that coupling together four resonators should enable at least a few cycles of the recurrence phenomenon to be seen. However, the circuit was very susceptible to parasitic noise. Whilst there was scope for some circuit improvements to attempt to reduce the noise to acceptable levels, it was felt that the options were too limited for the scale of reduction required.

To improve noise immunity, a double-sided printed circuit board (PCB) with appropriate power and ground planes, shorter trace lengths, and surface mount components was designed, as shown in Figure 5.5. Right-angled board edge connectors were used so that the modular PCB units can easily be plugged together with minimal need for external wiring looms. These male and female connectors can be seen on opposite edges of the board. Once the desired number of modules have been connected together, the connectors at either end of the chain can then be used to apply power to the array and create the boundary conditions.

The PCBs were fabricated by Newbury Electronics using their PCB Train express service. The boards are 2 layer and plated through hole (PTH). The substrate used was FR4 (Ventec VT-481), with a 1 oz copper thickness, immersion silver (I.S.) finish and green solder resist. The overall physical size is 40 mm × 50 mm. The overall thickness is 1.6 mm, with a tolerance specified by the fabricator of ±10 %.

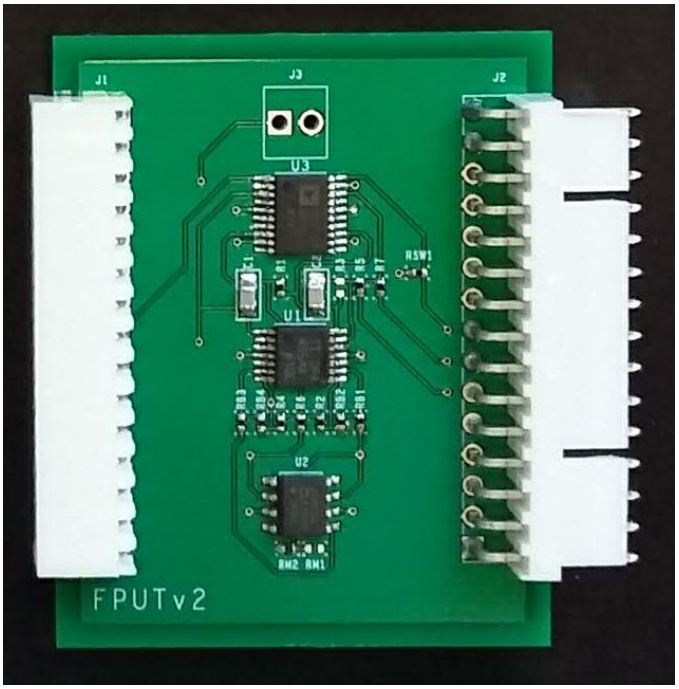


Figure 5.5: A PCB for a single resonator circuit module.

5.5 Testing

5.5.1 Test setup

A National Instruments PCI-6133 data acquisition (DAQ) board was used for data collection. It is a simultaneous-sampling, multifunction DAQ device offering 8 analogue inputs (14-Bit, 2.5 MS/s/ch) and digital triggering. This was connected to a National Instruments BNC-2110 shielded connector block to allow easy interface to the circuit.

The initial condition was created using the analogue outputs of a Data Translation DT9834 USB data acquisition module. This was required in addition to the National Instruments PCI-633 since the connector block (BNC-2110) does not provide any analogue outputs and the sampling rate of the DT9834 is too low to be used for this application (500 kHz overall).

The enable signal for the analogue switch controlling the application of the initial condition was generated using a TT*i* TGA12104 arbitrary waveform generator. This signal was also provided to the National Instruments PCI-6133 as a trigger signal to start the data collection.

Control of the DAQs was performed using a MATLAB script with sampling taking place at the maximum frequency, i.e. 2.5 MS/s/ch. The time domain data was saved to a MATLAB data file and then an additional script was used to run the data through the energy transform section of the code written by Dauxois *et al.* [16]. The circuit output could then be compared to the results obtained from the numerical experiments.

The ± 2.5 V and ± 15 V power rails for the circuits were provided by Agilent E3631A DC power supplies. An Agilent MSO9104A oscilloscope was used for measuring the individual circuit frequencies and monitoring signals on the PCB.

5.5.2 Individual circuit response

Initially, R_3 was left unconnected, leading to the circuit acting as an oscillator. The natural frequency of the system was measured for each circuit individually. These values are recorded in Table 5.5 alongside the percentage variation from the design frequency. This percentage variation gives the overall tolerance value for each circuit.

The difference in frequency is caused by the variability, or tolerance, of the individual system components. It should be understood that these tolerances are not just limited to the passive components for which a low tolerance can be selected. There is also variability between the op-amps, multipliers, solder joints, and PCBs (including variations in track widths and lengths, substrate thickness, etc.).

Circuit	Natural Frequency (kHz)	Tolerance (%)
A	9.942	−0.25
B	9.947	−0.20
C	9.969	+0.02
D	9.962	−0.05

Table 5.5: Measured natural frequencies of the oscillator circuits

An approximation of the noise level in the circuit was also made using an oscilloscope. This was estimated to be $10.5\,\mathrm{mV_{rms}}$. For a nominal signal amplitude of 1 V this gives a signal-to-noise ratio (SNR) of approximately 4534 or taking the noise as a percentage of the signal, a noise level of 0.2 %. This is a crude approximation as oscilloscopes do introduce noise into a circuit and no mitigation was made for this. Therefore, one might expect that the actual noise value is lower than this.

5.5.3 Coupled response

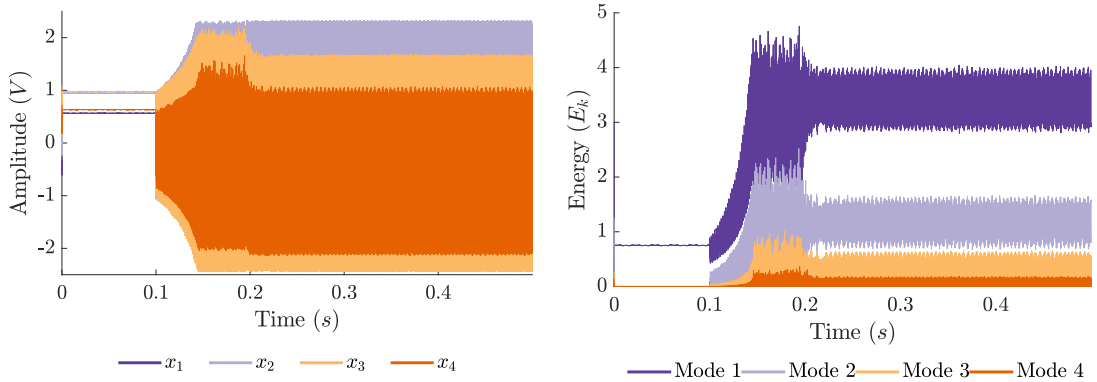
To test the coupled response of the system, the four circuits were coupled together with the tolerances in ascending order (i.e. A-B-D-C). Alongside the low number of oscillators and the tight tolerances achieved in building the circuits (Table 5.5), the results in Section 3.5 suggest that this should provide the best chance of seeing recurrence.

The initial condition voltages for x_i were calculated using Equation (2.2), giving 0.59 V for x_1 and x_4, and 0.95 V for x_2 and x_3. The boundary conditions were set by connecting the x_{i-1} input to circuit A to ground (0 V). Similarly, the x_{i+1} input to circuit C was connected to ground. As the $(x_i - x_{i-1})^2$ term is created on circuit A, the boundary condition for the nonlinear coupling is available. However, at the other end of the chain, the $(x_{i+1} - x_i)^2$ term needs to be generated. To achieve this, an extra PCB with only the multiplier fitted was connected to this end of the chain.

Undamped

Initially, R_3 was not fitted to any circuits to enable the response of the system with no damping to be observed. Figure 5.6(i) shows the the undamped response of four coupled oscillators in the time domain. During the first 0.1 s the initial condition is applied. The initial condition is then released and the system response can be observed.

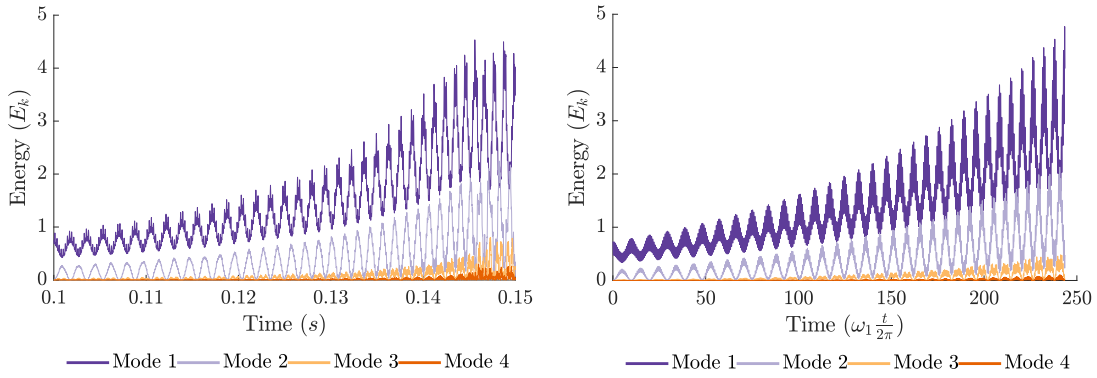
The corresponding energy plot for modes 1 to 4 is shown in Figure 5.6(ii). The energy in the system increases over time from the level given by the initial condition until a steady state is reached. This indicates that there is negative damping in this system. A small amount of positive feedback is created in the system as the phase shifts introduced by the op-amps are not perfect. This positive feedback draws energy from the op-amp power rails and produces the negative damping effect.



(i) Time domain **(ii)** Energy domain

Figure 5.6: Experimental results for four coupled resonator circuit modules with no damping.

Examining the transient part of the energy plot after the initial condition is released (Figure 5.7(i)), it can be observed that the response of the system is similar in shape to the results obtained from numerical experiments with $N = 4$, $\alpha = 0.246$, and $Q = -1000$ (Figure 5.7(ii)). As the energy in the system builds, the recurrence profile changes, with the energy peaks for mode 2 closing the gap and starting to overlap the energy troughs for mode 1. The number of recurrence cycles for the energy to reach the maximum amplitude in the circuit is similar to that required for the simulation to reach the same amplitude suggesting an effective quality factor of around -1000.

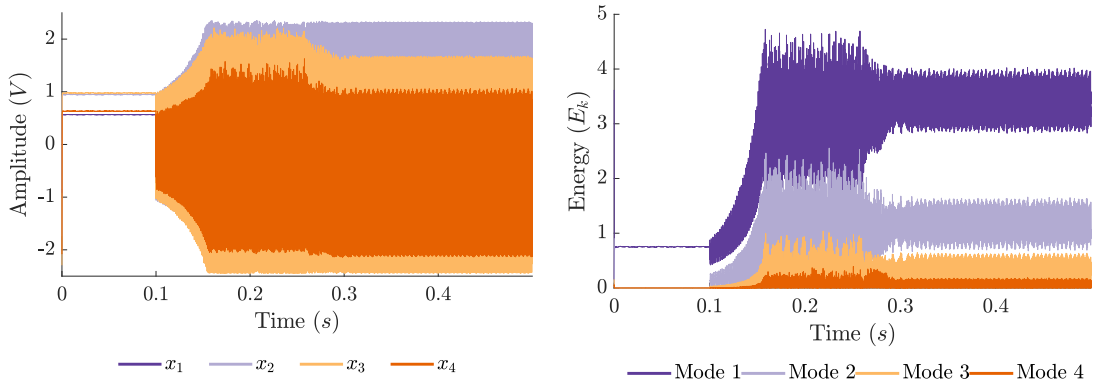


(i) Circuit **(ii)** Simulation ($Q = -1000$, $\alpha = 0.246$)

Figure 5.7: Comparison of experimental circuit results and simulation results for four coupled resonators with no damping.

Lightly damped

To explore the effects of damping on the system, a 16 MΩ resistor was fitted to R_3 on each PCB to provide a DC feedback path. The response of the damped system is shown in Figure 5.8, where a similar response to the undamped system can be observed. One noticeable difference is the time taken for the system to reach a steady state after it has achieved the peak energy value. This does vary in length between individual data captures for the same value of R_3 and should therefore not be considered as related to the level of damping. One possible explanation for this is the influence of other environmental factors, e.g. parasitic noise or temperature, which are not considered here.



(i) Time domain **(ii)** Energy domain

Figure 5.8: Experimental results for four coupled resonator circuit modules with a damping resistance of $R_3 = 16\,\mathrm{M\Omega}$.

Figure 5.9 shows that fitting R_3 has slightly increased the length of time that the system takes to reach its peak energy level. The addition of the damping resistors has therefore decreased the magnitude of the negative damping. However, the effect is not strong enough to positively damp the system and reduce the energy over time. This was anticipated, as with the resistor values being very large at $16\,\mathrm{M\Omega}$, the current available for the damping feedback is very low.

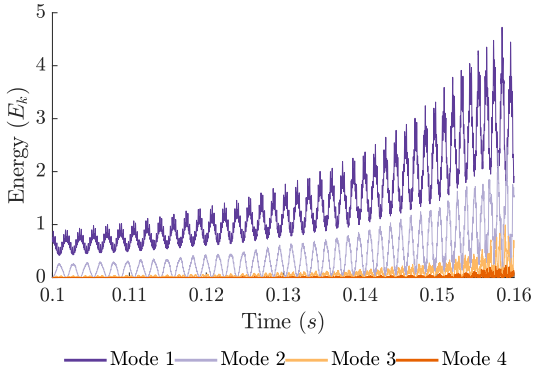
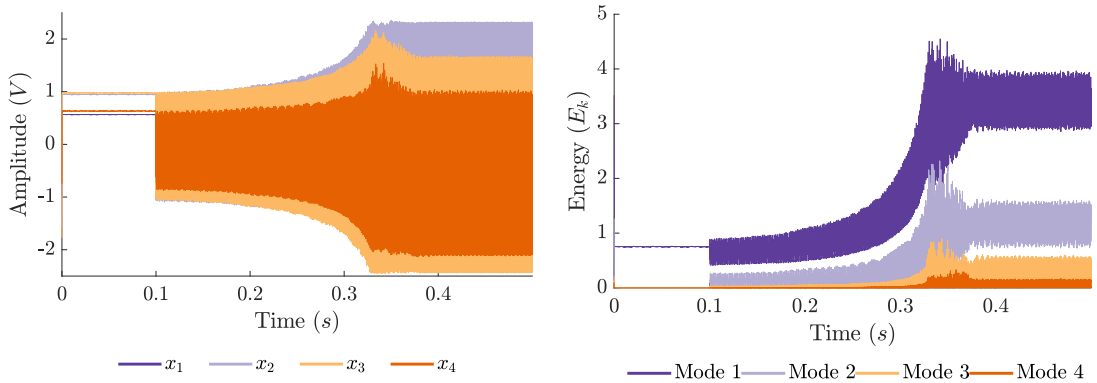


Figure 5.9: Detailed view of the circuit response immediately after the system is released from rest with the energy in the initial condition of the first mode. The system comprises four coupled resonator circuits with a damping resistance of $R_3 = 16\,\mathrm{M\Omega}$.

Moderately damped

In an attempt to compensate for the inherent negative damping, the effective quality factor needs to be reduced further. Since the quality factor is proportional to the damping resistor, the value of R_3 was decreased by a factor of four to 4 MΩ. The results shown in Figure 5.10 show that the energy takes much longer to build in the system and there is a period of very low energy gain before a more rapid increase.



(i) Time domain **(ii)** Energy domain

Figure 5.10: Experimental results for four coupled resonator circuit modules with a damping resistance of $R_3 = 4\,\mathrm{M}\Omega$.

Figure 5.11 examines various sections of the circuit result from Figure 5.10(ii) in more detail. The near steady state FPUT recurrence of the electronic circuit is shown in Figure 5.11(i). Here it can be observed that the shapes of the energy in each mode closely resemble that of the ideal FPUT recurrence observed in the numerical experiments.

The transition between the region of increasing energy to the peak energy region is shown in Figure 5.11(ii), whilst Figure 5.11(iii) shows a continuation of the peak region. These two sections continue to show recurrence, although the peaks of the second mode are overlapping the troughs of the first mode on occasion. The energy modes are also not as cleanly formed.

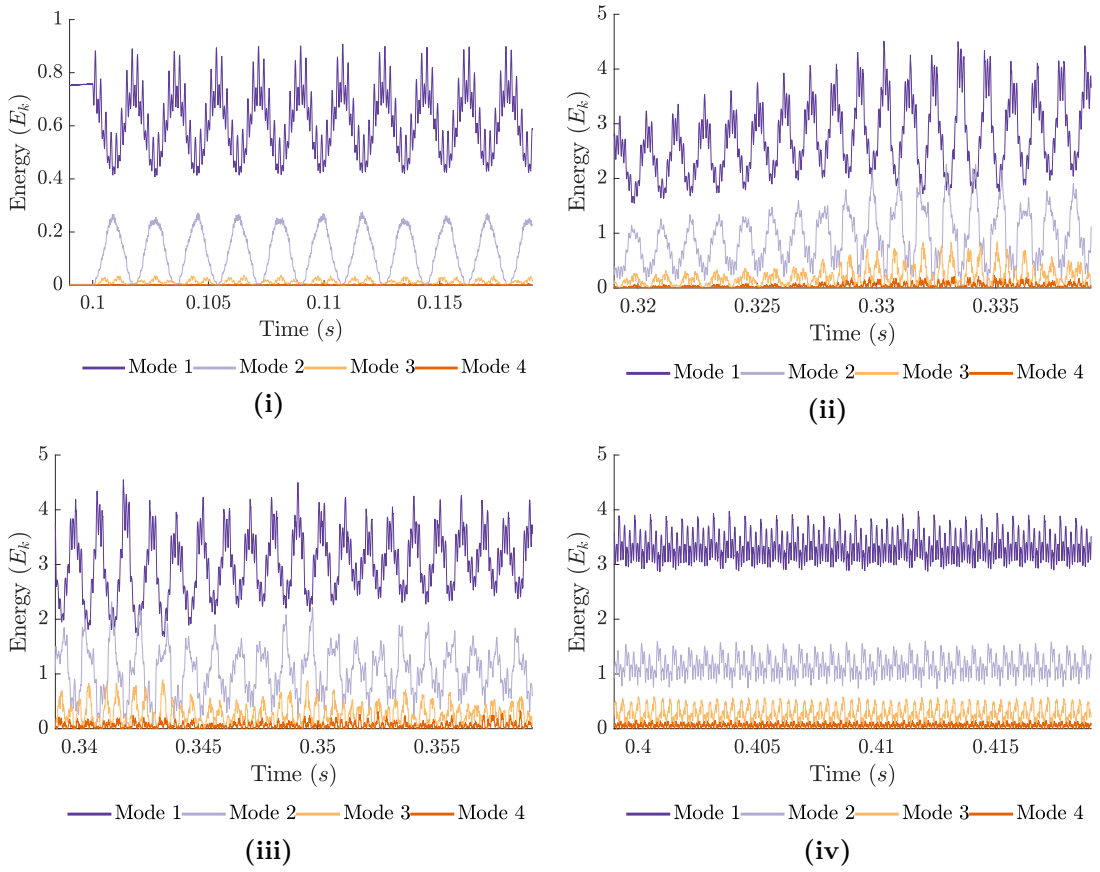


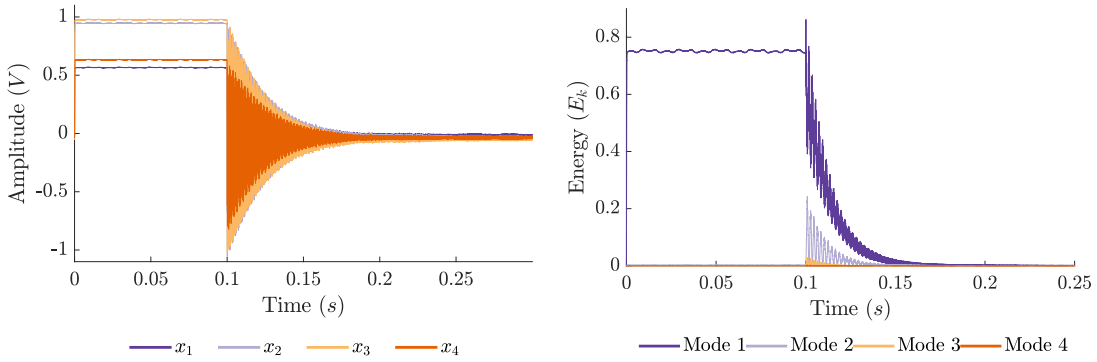
Figure 5.11: Detailed sections of the energy plot in Figure 5.10(ii) showing the circuit response at key points. The system comprises four coupled resonator circuits with a damping resistance of $R_3 = 4\,\mathrm{M\Omega}$.

Finally, Figure 5.11(iv) shows the steady state region. Here it can be seen that although there is some variation of energy in each mode, recurrence is not present. These oscillations of energy appear to be at the fundamental frequency of the circuits, i.e. approximately 10 kHz, suggesting that equilibrium has been reached. It can also be observed that the energy in each mode at equilibrium is a decreasing function of the wave number as noted by Benettin *et al.* [28].

Strongly damped

To test a strongly damped system, the effective quality factor was then reduced by a further factor of four, achieved by decreasing R_3 to $1\,\mathrm{M\Omega}$. Figure 5.12(i) shows that this does result in a system where the energy decays exponentially with time. The energy plot in Figure 5.12(ii) shows that a few cycles of recurrence

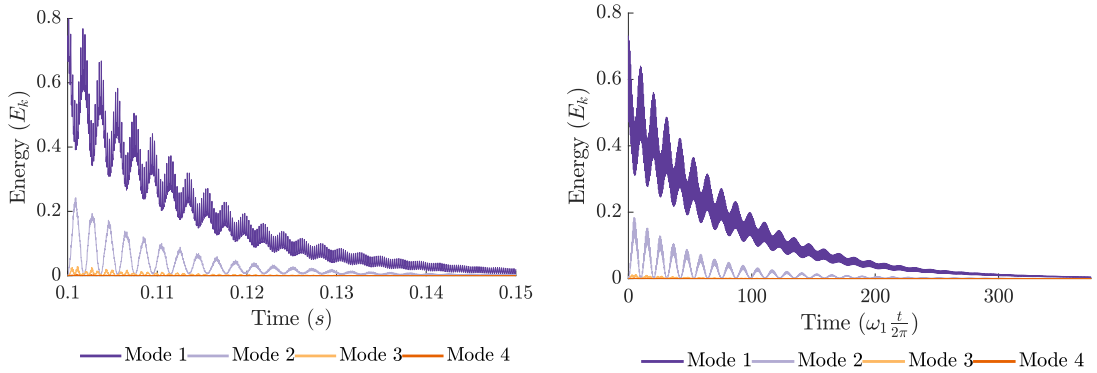
can be observed before the energy is lost from the system. This confirms the predictions made from the results in Chapter 4.



(i) Time domain **(ii)** Energy domain

Figure 5.12: Experimental results for four coupled resonator circuit modules with a damping resistance of $R_3 = 1\,\text{M}\Omega$.

Figure 5.13(i) shows an expanded version of the energy decay for the circuit. Calculating the effective quality factor for the circuit using a value for R_3 of $1\,\text{M}\Omega$ gives $Q = 626$. The results of simulating a system with parameters of $N = 4$, $\alpha = 0.246$, and $Q = 626$ are presented in Figure 5.13(ii). Comparison of these two figures shows a similar decay rate for the system energy.



(i) Circuit **(ii)** Simulation ($Q = 626$, $\alpha = 0.246$)

Figure 5.13: Comparison of experimental circuit results and simulation results for four coupled resonators with a damping resistance of $R_3 = 1\,\text{M}\Omega$.

5.6 Summary

This chapter has presented an electronic resonator circuit designed to emulate the differential equation with quadratic coupling first simulated by Fermi, Pasta, Ulam

and Tsingou. Based on the Tow–Thomas biquad filter, the circuit was constructed in a modular design on printed circuit boards using operational amplifiers and analogue multipliers. The natural frequency of each circuit was measured to obtain a tolerance range for the circuits from the design frequency. The tolerance achieved between circuits was $\pm 0.25\,\%$.

Initially, the circuits were connected together without including the damping term. This was not expected to produce a reliable result due to instability of the circuits. However, with four nodes, the system has been shown to exhibit FPUT recurrence during the period where the energy is building in the system. Once the system reaches the maximum energy constrained by the op-amp rails, recurrence dies away and the system enters a steady state.

Fitting the calculated value of damping resistor ($16\,\mathrm{M\Omega}$) reduced the negative damping in the system, although it did not cause the expected energy decay. This resistance value is very large, resulting in a very small current for the feedback. This is clearly not sufficient to prevent the energy building in the system. Nevertheless, the reduction in negative damping allowed a few more cycles of FPUT recurrence to be observed before the system reached its steady state.

Decreasing the value of resistance by a factor of four to $4\,\mathrm{M\Omega}$ reduced the negative damping in the system further. The initial energy gain of the system was very slow and several cycles of recurrence could be observed before the amplitude of the energy in the first mode started to increase significantly.

A further decrease in the damping resistance to $1\,\mathrm{M\Omega}$ meant that the system was strongly damped. The results obtained here confirmed the simulation results in Chapter 4. Simulations with the design value for the nonlinear coupling strength showed that the equivalent quality factor achieved was in the region of 626. Whilst this is lower than originally considered when designing the circuit, there is scope for this to be increased. By investigating values in the range $1\,\mathrm{M\Omega}$ to $4\,\mathrm{M\Omega}$, it should be possible to find the maximum effective quality factor achievable before the system is subject to negative damping.

6

Conclusions and future work

Contents

6.1 Discussion 148
6.1.1 Variability due to manufacturing tolerance 148
6.1.2 Energy loss due to damping 149
6.1.3 Practical systems 150
6.2 Conclusions 151
6.3 Future Work 152
6.3.1 Further explorations of imperfections 152
6.3.2 Further explorations of practical systems 155

This thesis explored the FPUT-α system from numerical and experimental perspectives. The effects of 'real-world' conditions on an idealised nonlinear system were investigated first. This was followed by building an electronic system to demonstrate the recurrence phenomenon discovered by Fermi, Pasta, Ulam and Tsingou. The motivation behind this research was the increasing nonlinearity in systems as they shrink in size, with a particular thought to applying a rich theoretical literature on nonlinearity to M/NEMS.

This chapter discusses the results obtained during the research, with a brief overview of the problem and then subsections detailing the results found in three main categories: manufacturing tolerance, damping and an electronic circuit

implementation. Areas of future research related to the work contained herein are then suggested.

6.1 Discussion

The numerical experiments conducted by Enrico Fermi, John Pasta, Stanislaw Ulam, and Mary Tsingou [7] have led to an extensive body of computational, theoretical, and experimental work in nonlinear systems. However, it is commonly assumed in studies of FPUT and other lattice systems that the parameters are ideal and often uniform. Physical systems, by contrast, are subject to inherent imperfections, and this can affect recurrence phenomena.

This thesis has examined two major categories of physical imperfection through the use of numerical simulations: variability due to manufacturing tolerance and energy loss due to damping. The results summarised below identify the tolerance boundaries and limits of damping under which one might expect to be able to see recurrence in a physical FPUT-α system. Using these constraints, an electronic circuit was designed and it was demonstrated that observation of recurrence was indeed possible in a physical system.

6.1.1 Variability due to manufacturing tolerance

The inherent tolerances of various manufacturing processes mean that mismatches in physical systems are impossible to avoid. By examining various tolerance structures, it was illustrated that the way in which one constructs an array of nonlinear oscillators, and specifically the way in which one incorporates tolerances into such a system, has a major effect on the qualitative dynamics of such systems. Two types of structures were envisioned for tolerances on coupling: symmetric and asymmetric. Asymmetric tolerance structures were shown to have a more significant impact on recurrences in an FPUT system than symmetric structures.

These results are interesting as any real oscillatory system has mismatches between the components. This means that for extremely tight tolerances of $\pm 0.1\,\%$, the output is close to the ideal, in the sense that the FPUT recurrences resemble

those from the case of homogeneous oscillators. However, noticeable imperfections occur at a tolerance of $\pm 1\,\%$ and for a tolerance of $\pm 5\,\%$, the recurrence phenomenon departs substantially from that in the ideal scenario. To produce a system with a tolerance as low as $\pm 1\,\%$ requires a high degree of precision in manufacturing, which is expensive and often impractical.

Additionally, due to accumulation of tolerances, individual oscillators in electronic and mechanical systems often have stacked tolerances in the order of $\pm 5\,\%$ to $\pm 10\,\%$ even when they are constructed of individual components with very tight tolerances. At these values, recurrence starts to break down. Another key observation is that, for progressively larger arrays, the recurrence stops occurring at ever smaller tolerances; therefore, in practice, one may never be able to see recurrence in any large array.

However, careful consideration of design may help to improve the chance of observing recurrence. For example, arranging the system components in increasing order of tolerance reduces the effect of the tolerances on recurrence. The nonlinear coupling strength is also an important factor to consider. A coupling strength that is very weak (in the order of 0.1) reduces the quality of recurrence. However, with increasing coupling strength the addition of tolerance has a greater impact, reducing recurrence.

6.1.2 Energy loss due to damping

Another key imperfection in many physical systems is energy loss through damping. Whilst damping can be reduced by careful design, it is often difficult to remove completely. However, with a very low level of damping, it is still possible to observe a few cycles of recurrence in a system with a small number of oscillators. This brings its own challenges as recurrence is stronger with a larger number of oscillators. Hence, consideration of other parameters such as increased coupling strength may play a part in enabling recurrence to be observed by reducing the length of the recurrence cycle and therefore enabling more cycles to occur before too much energy is lost from the system.

However, in this scenario, there is a limit to which the coupling strength can be increased as a stronger coupling strength increases the impact of tolerance on the system. If damping and tolerance are combined in the same system, it was observed that the level of tolerance has the most significant effect on the shape of the energy transfer in each mode, whilst the level of damping is the predominant factor for the number of cycles of recurrence that can be observed.

In summary, if the damping and tolerance in a system are low enough, the recurrence phenomenon may be observed in the transient response of the system providing that the number of oscillators is small and the coupling strength is carefully selected.

6.1.3 Practical systems

Technology is shrinking and consequently nonlinearity is becoming hard to avoid. Studying the effects of physical imperfections on nonlinear systems is therefore important as it will provide the conditions under which the theoretical results may be applicable to practical systems.

Although the predominant motivation for the research in this thesis is nonlinear coupling in MEMS, such devices take significant amounts of time and money to manufacture. A quick and cheap alternative is to study the problem electronically. The results of these experiments could then be used as the basis of a design for a MEMS system.

A modular electronic resonator circuit based on the Tow–Thomas biquad filter was constructed on PCBs to emulate the FPUT-α equation. Through careful design, tolerances were kept to $\pm 0.25\,\%$ between modules. Damping was also shown to be within the limits required and controllable through the use of a feedback resistor.

Forming a system from four of the modular PCBs, FPUT recurrence was observed, both with and without damping. Although limited in their scope, the results from the electronic circuit are encouraging. They provide early verification of the predictions made through the numerical experiments on both tolerance and damping.

6.2 Conclusions

The Fermi, Pasta, Ulam and Tsingou phenomenon has been the subject of many simulation based studies since their original paper was published in 1955. However, there is very little evidence of the phenomenon in practical systems. This thesis proposed that this paucity of evidence may be due to imperfections in physical realisations of ideal equations. Through a series of simulations, two main types of imperfection were investigated: tolerance and damping.

The results demonstrated that by tightly controlling manufacturing tolerance between nominally identical components, it may be possible to observe recurrence in an FPUT system with a small number of oscillators. However, tight tolerances are hard to achieve and are often very expensive. Therefore, producing such a system may not be practical.

Similarly, a system must have very low damping for recurrence to be observed. However, this is often easier to achieve through careful design, or changing the environmental conditions, e.g. putting MEMS in a vacuum to reduce viscous damping. It is also worth noting that for seeing better recurrence, a larger number of oscillators is required. However, to handle tolerance and damping, a smaller number of oscillators is better.

Using the limits of tolerance and damping identified by the simulations as key requirements, an electronic system was designed to emulate the FPUT-α equation. With four elements in the system, an initial condition of the first mode and a nonlinear coupling strength of 0.25, recurrence of energy was observed. This is the first time that recurrence phenomena have been extensively simulated under the influence of tolerance and damping, and the results subsequently validated in an electronic system.

In summary, in order to observe good recurrence in a physical FPUT-α system one requires a small number of oscillators, high quality factor and tight tolerances.

6.3 Future Work

Given the extensive scope of the work that has been carried out in the field of nonlinear dynamics since the early experiments of Fermi, Pasta, Ulam and Tsingou, it is not surprising that there is an equally extensive possibility for future investigations that could be conducted in relation to the impact of real-world conditions on ideal scenarios. Further investigation of such phenomena is an important avenue to pursue in light of the ever increasing presence of nonlinearity in systems as technology is shrinking.

For example, incorporating tolerances into parameters for other initial conditions (and other variants of FPUT systems and other types of nonlinear lattices) may lead to behaviours other than those that are discussed in this thesis. Because tolerance has such a major impact on a standard FPUT-α system with sinusoidal input, it would be unreasonable to assume that other scenarios will only be affected minimally. Consequently, it is necessary to revisit investigations of FPUT systems and nonlinear lattices with tolerance in mind.

6.3.1 Further explorations of imperfections

This thesis has focused on the FPUT-α model, however there are many other nonlinear systems that can be explored. Other salient areas include FPUT-β lattices, multi-dimensional FPUT lattices, and fully integrable nonlinear systems such as the Toda lattice [116] which exhibit no chaotic behaviour.

Initial conditions

The scope of the research was limited to a typical sinusoidal initial condition in a 1D FPUT array; other initial conditions have not yet been explored. There are numerous studies that investigate FPUT systems with other initial conditions [10], [18], including those using only the high frequency modes, i.e. the anti-FPU problem [16].

Given the importance of the stochasticity threshold in determining whether the system undergoes relaxation to equilibrium, expanding beyond a fixed initial condition of amplitude 1 is of interest. By altering the amplitude, which for a given

value of α fixes the total energy entering the system, one can investigate how the results presented herein depend on changing the amplitude/energy.

Boundary conditions

Other options to consider would include alternative boundary conditions, such as the periodic boundary conditions used by Zabusky and Kruskal [117] or a circular chain. One can also examine similar considerations in other lattice systems, such as granular crystals, which have Hertzian interactions between components [118], [119].

Energy distribution

In several of the simulations presented in this thesis, increasing the tolerance decreases the energy in modes 2–4. However, not all the energy remains in mode 1 and transfer to higher modes must therefore be occurring. Observation of additional modes in these simulations would aid understanding of how the tolerance changes the coupling between modes. As tolerance effects the period of recurrence, it would also be interesting to see how increasing tolerance affects the time to equipartition.

Other tolerances

The tolerance structures in this thesis have mainly focussed on incorporating tolerance in the x terms of the equation. The asymmetric structure does, within a certain limit, incorporate tolerance on the α term. The work by Jackson [70] concludes that variation on just the α term is of importance by itself when considering recurrence. This would suggest that investigating tolerances on other terms would also be of interest, e.g. the damping term and the quadratic term (i.e. varying the power from an exact value of 2).

Nonlinear damping

The focus of the work on resonant systems was a linear damping term. However, nonlinear damping is also possible [108], [120]. Investigating the effects of additional nonlinearity through the addition of a nonlinear damping term would expand the

study to consider a wider range of physical imperfections. A combination of linear and nonlinear damping would likely also be relevant to a large number of systems.

Driven damped response

Considering that a chain length of 64 or more oscillators is feasible for a real physical system, it is highly unlikely that recurrence will ever be seen in such systems unless damping is so low that the system is effectively undamped. As an alternative, it may be worth considering a driven damped FPUT system, as these have produced interesting results in other types of nonlinear system [17], [22], [72], [118].

Statistical nonlinear dynamics

A significant number of the results presented in this thesis have been carefully chosen from Monte Carlo studies as representative of a subset of the results. A statistical study of the results in order to estimate the probability that a system with a given tolerance distribution will demonstrate the recurrence phenomenon would be of significant interest. This also suggests that there is a wider scope to merge studies in statistics with those of nonlinear dynamics to understand the behaviour of real nonlinear systems.

Matrix evaluation of response

A rich behavioural response is seen in the simulations, so even though recurrence is not seen in the systems with larger tolerance values, the response of the system may still be of use. It may be possible to reverse engineer the plots presented in this thesis, perhaps through the use of eigen vectors. The system would then be applicable to practical problems such as sensing. Eigen based analysis has shown useful results in other applications [65], [121], [122]. Additionally, the concepts introduced by the proportional damping matrix may help with understanding the differences introduced by the asymmetric tolerance structures.

Other areas of nonlinear science

The recurrence phenomenon is only one of the interesting behaviours seen in FPUT lattices [6]. By changing the initial condition, as well as the nonlinearity, a wide range of interesting results have been obtained from these systems, including chaotic behaviour [12], breathers [13], solitons [117], kinks and anti-kinks [73]. These discoveries have led to the development of other areas of nonlinear science from which it is desirable to draw inspiration for additional work. For example, in studies of synchronization on networks, there is a long history of examining the collective properties of coupled phase oscillators (a rather different type of system from the one studied here) with natural frequencies drawn from some distribution [123]. With practical laboratory experiments in mind, it is crucial to conduct systematic investigations of incorporating tolerance into those and other systems.

6.3.2 Further explorations of practical systems

The testing of the op-amp based electronic FPUT-α system has been limited in scope. There are several other investigations that could be carried out with the existing PCB design. These include different coupling strengths, different chain lengths, additional work on the damping strength, and investigations into driven damped systems.

Transition region

Further investigation of the properties of the system in the transition region which occurs when the damping is low enough would help with understanding more about the stochastic threshold in a physical system. As was noted in Chapter 5, the length of this region varies even with seemingly identical starting positions. Clearly, there are other factors affecting the system besides the damping and tolerance already mentioned. One possible route to explore would be the effect of the op-amp rail cut-off voltage on the system.

Other nonlinear coupling types

The circuit described in this thesis uses quadratic type nonlinear coupling only. Investigating other types of nonlinearity and corresponding circuit responses would be straightforward to accomplish as one can simply replace the multiplier with other appropriate components.

Other implementations

To achieve a high quality factor, the ideal solution would be to integrate all the resonators and coupling circuitry into a single chip to further reduce parasitic influences. However, when applied to MEMS the system can be created in a vacuum which will ensure a high quality factor. This is because although some of the damping comes from the material itself which can be reduced through careful design, some also comes from viscous damping which will be almost eliminated in a vacuum.

Other imperfections

In addition to tolerances in the manufacturing output, components may also vary due to other factors such as ambient temperatures, operational temperature of the system, degradation of component parameters over time, and parasitic temporal noise.

References

[1] H. Nelson, M. A. Porter, and B. Choubey, "Variability in Fermi-Pasta-Ulam-Tsingou arrays can prevent recurrences", *Physical Review E*, vol. 98, no. 6, p. 062 210, Dec. 2018.

[2] H. Nelson and B. Choubey, "On the Effect of Variability and Chain Length on Fermi, Pasta and Ulam Matrices", in *2nd IMA Conference on Nonlinearity and Coherent Structures*, Norwich, Jun. 2017.

[3] H. Nelson, "Variability in Fermi, Pasta and Ulam Lattices", in *Dynamics Days Europe 2018*, Loughborough, Sep. 2018.

[4] J. Fernández de Cañete, C. Galindo, and I. García Moral, *System Engineering and Automation : An Interactive Educational Approach*, 1st ed. Berlin: Springer-Verlag, 2011.

[5] M. Kumar, B. Choubey, and H. Bhaskaran, "Nanomechanical resonators show higher order nonlinearity at room temperature", Mar. 2017. arXiv: 1703.03094.

[6] M. Porter, N. Zabusky, B. Hu, and D. Campbell, "Fermi, Pasta, Ulam and the Birth of Experimental Mathematics", *American Scientist*, vol. 97, no. 3, p. 214, 2009.

[7] E. Fermi, J. Pasta, and S. Ulam, "Studies of nonlinear problems", Los Alamos Scientific Laboratory (LASL), Los Alamos, NM (United States), Tech. Rep., May 1955, pp. 977–988.

[8] T. Dauxois, "Fermi, Pasta, Ulam, and a mysterious lady", *Physics Today*, vol. 61, no. 1, pp. 55–57, Jan. 2008.

[9] G. P. Berman and F. M. Izrailev, "The Fermi–Pasta–Ulam problem: Fifty years of progress", *Chaos*, vol. 15, no. 1, p. 015 104, Mar. 2005.

[10] N. J. Zabusky, "Fermi–Pasta–Ulam, solitons and the fabric of nonlinear and computational science: history, synergetics, and visiometrics", *Chaos*, vol. 15, no. 1, p. 015 102, Mar. 2005.

[11] M. Onorato, L. Vozella, D. Proment, and Y. V. Lvov, "Route to thermalization in the α-Fermi–Pasta–Ulam system", *Proceedings of the National Academy of Sciences*, vol. 112, no. 14, pp. 4208–4213, Apr. 2015.

[12] M. Pettini, L. Casetti, M. Cerruti-Sola, R. Franzosi, and E. G. D. Cohen, "Weak and strong chaos in Fermi–Pasta–Ulam models and beyond", *Chaos*, vol. 15, p. 015 106, Mar. 2005.

[13] T. Cretegny, R. Livi, and M. Spicci, "Breather dynamics in diatomic FPU chains", *Physica D: Nonlinear Phenomena*, vol. 119, no. 1-2, pp. 88–98, Aug. 1998.

[14] G. Gallavotti, Ed., *The Fermi–Pasta–Ulam Problem: A Status Report*, 1st ed. Berlin: Springer, 2008, vol. 728.

[15] S. Flach and A. V. Gorbach, "Discrete breathers - Advances in theory and applications", *Physics Reports*, vol. 467, no. 1-3, pp. 1–116, Oct. 2008.

[16] T. Dauxois, M. Peyrard, and S. Ruffo, "The Fermi–Pasta–Ulam 'numerical experiment' : history and pedagogical perspectives", *European Journal of Physics*, vol. 26, no. 5, S3–S11, Jul. 2005.

[17] Y. Watanabe, T. Nishida, Y. Doi, and N. Sugimoto, "Experimental demonstration of excitation and propagation of intrinsic localized modes in a mass–spring chain", *Physics Letters A*, vol. 382, no. 30, pp. 1957–1961, Aug. 2018.

[18] G. Benettin, R. Livi, and A. Ponno, "The Fermi–Pasta–Ulam Problem: Scaling Laws vs. Initial Conditions", *Journal of Statistical Physics*, vol. 135, no. 5-6, pp. 873–893, Jun. 2009.

[19] G. Benettin and A. Ponno, "Time-Scales to Equipartition in the Fermi–Pasta–Ulam Problem: Finite-Size Effects and Thermodynamic Limit", *Journal of Statistical Physics*, vol. 144, pp. 793–812, Aug. 2011.

[20] G. Benettin, "Time scale for energy equipartition in a two-dimensional FPU model", *Chaos*, vol. 15, no. 1, p. 015 108, Mar. 2005.

[21] G. Benettin and G. Gradenigo, "A study of the Fermi–Pasta–Ulam problem in dimension two", *Chaos*, vol. 18, no. 1, p. 013 112, Mar. 2008.

[22] T. Dauxois, R. Khomeriki, and S. Ruffo, "Modulational instability in isolated and driven Fermi–Pasta–Ulam lattices", *The European Physical Journal Special Topics*, vol. 147, no. 1, pp. 3–23, Aug. 2007.

[23] L. Casetti, M. Cerruti-Sola, M. Pettini, and E. G. D. Cohen, "The Fermi-Pasta-Ulam problem revisited: Stochasticity thresholds in nonlinear Hamiltonian systems", *Physical Review E*, vol. 55, no. 6, pp. 6566–6574, Jun. 1997.

[24] N. J. Zabusky and G. S. Deem, "Dynamics of nonlinear lattices I. Localized optical excitations, acoustic radiation, and strong nonlinear behavior", *Journal of Computational Physics*, vol. 2, no. 2, pp. 126–153, Nov. 1967.

[25] T. Dauxois, R. Khomeriki, F. Piazza, and S. Ruffo, "The anti-FPU problem", *Chaos: An Interdisciplinary Journal of Nonlinear Science*, vol. 15, no. 1, p. 015 110, Mar. 2005.

[26] F. M. Izrailev and B. V. Chirikov, "Statistical Properties of a Nonlinear String", *Soviet Physics-Doklady*, vol. 11, no. 1, pp. 30–32, 1966.

[27] F. Fucito *et al.*, "Approach to equilibrium in a chain of nonlinear oscillators", *Journal de Physique*, vol. 43, no. 5, pp. 707–713, May 1982.

[28] G. Benettin, A. Carati, L. Galgani, and A. Giorgilli, "The Fermi–Pasta–Ulam Problem and the Metastability Perspective", in *Lecture Notes in Physics*, 2008, vol. 728, Berlin: Springer, 2008, ch. 4, pp. 151–189.

[29] A. Carati, L. Galgani, and A. Giorgilli, "The Fermi–Pasta–Ulam problem as a challenge for the foundations of physics", *Chaos*, vol. 15, no. 1, p. 015 105, Mar. 2005.

[30] R. Livi, M. Pettini, S. Ruffo, M. Sparpaglione, and A. Vulpiani, "Equipartition threshold in nonlinear large Hamiltonian systems: The Fermi-Pasta-Ulam model", *Physical Review A*, vol. 31, no. 2, pp. 1039–1045, Feb. 1985.

[31] J. De Tullio, "The Fermi–Pasta–Ulam model: the birth of numerical simulation", *Lettera Matematica*, vol. 4, no. 1, pp. 41–48, Mar. 2016.

[32] L. Galgani and A. Giorgilli, "Recent Results on the Fermi–Pasta–Ulam Problem", *Journal of Mathematical Sciences*, vol. 128, no. 2, pp. 2761–2766, Jul. 2005.

[33] J. Ford, "The Fermi–Pasta–Ulam problem: Paradox turns discovery", *Physics Reports*, vol. 213, no. 5, pp. 271–310, May 1992.

[34] J. Tuck and M. Menzel, "The superperiod of the nonlinear weighted string (FPU) problem", *Advances in Mathematics*, vol. 9, no. 3, pp. 399–407, Dec. 1972.

[35] G. Drago and S. Ridella, "Some more observations on the superperiod of the non-linear FPU system", *Physics Letters A*, vol. 122, no. 8, pp. 407–412, Jun. 1987.

[36] S. D. Pace and D. K. Campbell, "Behavior and breakdown of higher-order Fermi-Pasta-Ulam-Tsingou recurrences", *Chaos*, vol. 29, no. 2, p. 023 132, Feb. 2019.

[37] G. Van Simaeys, P. Emplit, and M. Haelterman, "Experimental Demonstration of the Fermi-Pasta-Ulam Recurrence in a Modulationally Unstable Optical Wave", *Physical Review Letters*, vol. 87, no. 3, p. 033 902, Jun. 2001.

[38] A. Mussot, A. Kudlinski, M. Droques, P. Szriftgiser, and N. Akhmediev, "Fermi-Pasta-Ulam Recurrence in Nonlinear Fiber Optics: The Role of Reversible and Irreversible Losses", *Physical Review X*, vol. 4, no. 1, p. 011 054, Mar. 2014.

[39] B. Zhao, D. Tang, and H. Tam, "Experimental observation of FPU recurrence in a fiber ring laser", *Optics Express*, vol. 11, no. 24, p. 3304, Dec. 2003.

[40] R. Hirota and K. Suzuki, "Studies on Lattice Solitons by Using Electrical Networks", *Journal of the Physical Society of Japan*, vol. 28, no. 5, pp. 1366–1367, May 1970.

[41] M. Wu and C. E. Patton, "Experimental Observation of Fermi-Pasta-Ulam Recurrence in a Nonlinear Feedback Ring System", *Physical Review Letters*, vol. 98, no. 4, p. 047 202, Jan. 2007.

[42] D. Midtvedt, A. Croy, A. Isacsson, Z. Qi, and H. S. Park, "Fermi-Pasta-Ulam Physics with Nanomechanical Graphene Resonators: Intrinsic Relaxation and Thermalization from Flexural Mode Coupling", *Physical Review Letters*, vol. 112, no. 14, p. 145 503, Apr. 2014.

[43] "Focus issue: The "Fermi–Pasta–Ulam" problem—the first 50 years", *Chaos*, vol. 15, no. 1, D. K. Campbell, P. Rosenau, and G. M. Zaslavsky, Eds., 2005.

[44] "FPU 50 years since FPU", G. Benfatto *et al.*, Eds., Rome: University of Roma La Sapienza, 2004.

[45] "50 Years of the Fermi–Pasta–Ulam Problem: Legacy, Impact, and Beyond", in *CLNS 25th International Conference*, A. Bishop, D. Campbell, R. Ecke, and A. Saxena, Eds., Santa Fe, NM: Center for Nonlinear Studies, 2005.

[46] "FPU+50: Nonlinear Waves 50 Years After Fermi Pasta And Ulam", J. G. Caputo, Ed., Rouen, France: INSA Rouen, 2005.

[47] T. P. Weissert, *The Genesis of Simulation in Dynamics: Pursuing the Fermi–Pasta–Ulam Problem*. New York, NY: Springer, 1997.

[48] J. A. T. Machado, "A fractional approach to the Fermi–Pasta–Ulam problem", *The European Physical Journal Special Topics*, vol. 222, no. 8, pp. 1795–1803, Sep. 2013.

[49] B. Choubey, M. Ward, and S. Collins, "On readouts of multiple micro/nano resonator sensors with mismatch", in *2008 IEEE Sensors*, Lecce: IEEE, Oct. 2008, pp. 478–481.

[50] PRIME Faraday Partnership, *An Introduction to MEMS (Micro-electromechanical Systems)*. Loughborough: PRIME Faraday Partnership, 2002.

[51] P. Maniraman and L. Chitra, "Comparitive analysis of capacitive type MEMS pressure sensor for altitude sensing", in *2014 IEEE National Conference on Emerging Trends In New & Renewable Energy Sources And Energy Management (NCET NRES EM)*, Chennai: IEEE, Dec. 2014, pp. 195–199.

[52] H. Espinosa, Y. Zhu, and N. Moldovan, "Design and Operation of a MEMS-Based Material Testing System for Nanomechanical Characterization", *Journal of Microelectromechanical Systems*, vol. 16, no. 5, pp. 1219–1231, Oct. 2007.

[53] Y.-F. Wang *et al.*, "Ultrasonic transducer array design for medical imaging based on MEMS technologies", in *2010 3rd International Conference on Biomedical Engineering and Informatics*, vol. 2, Yantai: IEEE, Oct. 2010, pp. 666–669.

[54] C. Jenkins, J. G. Brown, L. Li, W. Johnstone, and D. Uttamchandani, "MEMS Retro-Phase-Modulator for Free-Space Coherent Optical Communications", *IEEE Journal of Selected Topics in Quantum Electronics*, vol. 13, no. 2, pp. 330–335, Apr. 2007.

[55] X. Cheng, J. Chen, C. Li, J.-H. Liu, I.-M. Shen, and P.-C. Li, "A Miniature Capacitive Ultrasonic Imager Array", *IEEE Sensors Journal*, vol. 9, no. 5, pp. 569–577, May 2009.

[56] S. Chowdhury, M. Ahmadi, and W. Miller, "Design of a MEMS acoustical beamforming sensor microarray", *IEEE Sensors Journal*, vol. 2, no. 6, pp. 617–627, Dec. 2002.

[57] A. Jain, D. Greve, and I. Oppenheirn, "A MEMS phased array transducer for ultrasonic flaw detection", in *SENSORS, 2002 IEEE*, vol. 1, Orlando, FL: IEEE, Jun. 2002, pp. 515–520.

[58] T. A. Emadi, G. Thomas, D. A. Buchanan, and S. Pistorius, "A MEMS ultrasonic transducer imager array with beam width, acoustic power, and frequency modulations", in *2012 IEEE International Conference on Imaging Systems and Techniques Proceedings*, Manchester: IEEE, Jul. 2012, pp. 431–435.

[59] F. Beil, A. Wixforth, and R. Blick, "Broadband acoustical tuning of nano-electromechanical sensors", in *SENSORS, 2002 IEEE*, vol. 2, Orlando, FL: IEEE, Jun. 2002, pp. 1285–1289.

[60] H. Shekhar, S. Kumar, P. Shekhar, and P. Rajawat, "High-Q factor nano transducer for medical imaging", in *Fifth International Conference on Advances in Recent Technologies in Communication and Computing (ARTCom 2013)*, Institution of Engineering and Technology, Sep. 2013, pp. 431–435.

[61] T. Chernyakova and Y. Eldar, "Fourier-domain beamforming: the path to compressed ultrasound imaging.", *IEEE transactions on ultrasonics, ferroelectrics, and frequency control*, vol. 61, no. 8, pp. 1252–67, Aug. 2014.

[62] J. A. Jensen, S. I. Nikolov, K. L. Gammelmark, and M. H. Pedersen, "Synthetic aperture ultrasound imaging", *Ultrasonics*, vol. 44 Supplem, e5–e15, Dec. 2006.

[63] G. R. Lockwood, J. R. Talman, and S. S. Brunke, "Real-time 3-D ultrasound imaging using sparse synthetic aperture beamforming.", *IEEE transactions on ultrasonics, ferroelectrics, and frequency control*, vol. 45, no. 4, pp. 980–988, Jul. 1998.

[64] M. F. Rasmussen and J. A. Jensen, "Comparison of 3-D synthetic aperture phased-array ultrasound imaging and parallel beamforming.", *IEEE transactions on ultrasonics, ferroelectrics, and frequency control*, vol. 61, no. 10, pp. 1638–50, Oct. 2014.

[65] B. Choubey, M. Ward, C. Anthony, R. Turnbull, and S. Collins, "Validation of inverse eigenvalue technique for characterisation of coupled micro/nano resonators", in *2010 IEEE Sensors*, Kona, HI: IEEE, Nov. 2010, pp. 841–844.

[66] C. Deng, R. Turnbull, C. Anthony, M. Ward, and S. Collins, "A non-linear resonator for sensing applications", *Procedia Engineering*, vol. 5, pp. 1486–1489, 2010.

[67] B. Choubey, S. Collins, and M. Ward, "On Characterizing Microelectromechanical Processes Using Coupled Resonators", *Journal of Microelectromechanical Systems*, vol. 21, no. 4, pp. 791–800, Aug. 2012.

[68] D. A. McAdams and I. Y. Tumer, "Towards Failure Modeling in Complex Dynamic Systems: Impact of Design and Manufacturing Variations", in *International Design Engineering Technical Conferences and Computers and Information in Engineering Conference*, vol. 3, ASME, Montreal, Oct. 2002, pp. 71–81.

[69] L. Galgani, A. Giorgilli, A. Martinoli, and S. Vanzini, "On the problem of energy equipartition for large systems of the Fermi–Pasta–Ulam type: analytical and numerical estimates", *Physica D: Nonlinear Phenomena*, vol. 59, no. 4, pp. 334–348, Nov. 1992.

[70] E. A. Jackson, "Nonlinear Coupled Oscillators. II. Comparison of Theory with Computer Solutions", *Journal of Mathematical Physics*, vol. 4, no. 5, pp. 686–700, May 1963.

[71] A. J. Martínez, P. G. Kevrekidis, and M. A. Porter, "Superdiffusive transport and energy localization in disordered granular crystals", *Physical Review E*, vol. 93, no. 2, p. 022 902, Feb. 2016.

[72] G. Miloshevich, R. Khomeriki, and S. Ruffo, "Stochastic Resonance in the Fermi-Pasta-Ulam Chain", *Physical Review Letters*, vol. 102, no. 2, p. 020 602, Jan. 2009.

[73] T. Jin, H. Zhao, and B. Hu, "Spatial shift of lattice soliton scattering in the Fermi-Pasta-Ulam model", *Physical Review E*, vol. 81, no. 3, p. 037 601, Mar. 2010.

[74] R. Bivins, N. Metropolis, and J. Pasta, "Nonlinear coupled oscillators: Modal equation approach", *Journal of Computational Physics*, vol. 12, no. 1, pp. 65–87, May 1973.

[75] J. Brandner, "Microstructure devices for process intensification: Influence of manufacturing tolerances and design", *Applied Thermal Engineering*, vol. 59, no. 1-2, pp. 745–752, Sep. 2013.

[76] M. H. Bui, F. Villeneuve, and A. Sergent, "Manufacturing tolerance analysis based on the model of manufactured part and experimental data", *Proceedings of the Institution of Mechanical Engineers, Part B: Journal of Engineering Manufacture*, vol. 227, no. 5, pp. 690–701, May 2013.

[77] J. Lee, M. Lee, K. Kim, C. Kang, H. Jang, and G. Jang, "Monte Carlo simulation of the manufacturing tolerance in FDBs to identify the sensitive design variables affecting the performance of a disk-spindle system", *Microsystem Technologies*, vol. 21, no. 12, pp. 2649–2656, Dec. 2015.

[78] M. A. Khan, I. Husain, M. R. Islam, and J. T. Klass, "Design of Experiments to Address Manufacturing Tolerances and Process Variations Influencing Cogging Torque and Back EMF in the Mass Production of the Permanent-Magnet Synchronous Motors", *IEEE Transactions on Industry Applications*, vol. 50, no. 1, pp. 346–355, Jan. 2014.

[79] B. Bellesia *et al.*, "Magnetic Measurements for Magnets Manufacturing Tolerances Assessment", *IEEE Transactions on Applied Superconductivity*, vol. 24, no. 3, pp. 1–5, Jun. 2014.

[80] N. Pramanik, U. Roy, R. Sudarsan, R. Sriram, and K. Lyons, "A Generic Deviation-Based Approach for Synthesis of Tolerances", *IEEE Transactions on Automation Science and Engineering*, vol. 2, no. 4, pp. 358–368, Oct. 2005.

[81] L. Milić and J. Fidler, "Comparison of effects of tolerance and parasitic loss in components of resistively terminated *LC* ladder filters", *IEE Proceedings G (Electronic Circuits and Systems)*, vol. 128, no. 2, pp. 87–90, Apr. 1981.

[82] A. Serban, M. Karlsson, and S. Gong, "Component Tolerance Effect on Ultra-Wideband Low-Noise Amplifier Performance", *IEEE Transactions on Advanced Packaging*, vol. 33, no. 3, pp. 660–668, Aug. 2010.

[83] P. Horowitz and W. Hill, *The Art of Electronics*, 2nd ed. Cambridge: Cambridge University Press, 1989.

[84] J. F. Wakerly, *Digital Design : Principles and Practices*, 3rd ed. Upper Saddle River, NJ: Prentice Hall, 2001.

[85] G. Zhai, Y. Zhou, and X. Ye, "A Tolerance Design Method for Electronic Circuits Based on Performance Degradation", *Quality and Reliability Engineering International*, vol. 31, no. 4, pp. 635–643, Jun. 2015.

[86] D. Thompson, Ed., *The Pocket Oxford Dictionary*, 8th ed. Oxford: Oxford University Press, 1992.

[87] R. Spence and R. S. Soin, *Tolerance design of electronic circuits*. London: Imperial College Press, 1997.

[88] S. G. Shina, *Concurrent Engineering and Design for Manufacture of Electronics Products*. Springer US, 1991.

[89] R. G. Willhelm and S. C.-Y. Lu, "Tolerance Synthesis to Support Concurrent Engineering", *CIRP Annals*, vol. 41, no. 1, pp. 197–200, Jan. 1992.

[90] R. Spence, "Tolerance analysis and design of electronic circuits", *Computer-Aided Engineering Journal*, vol. 1, no. 3, pp. 91–100, Apr. 1984.

[91] K. W. Chase and W. H. Greenwood, "Design Issues in Mechanical Tolerance Analysis", *Manufacturing Review*, vol. 1, no. 1, pp. 50–59, Mar. 1988.

[92] D. Reid, C. Millar, S. Roy, and A. Asenov, "Understanding LER-Induced MOSFET V_T Variability—Part II: Reconstructing the Distribution", *IEEE Transactions on Electron Devices*, vol. 57, no. 11, pp. 2808–2813, Nov. 2010.

[93] I. Hickman and B. Travis, *The EDN designer's companion*. Oxford: Butterworth-Heinemann, 1994.

[94] W. H. Press, S. A. Teukolsky, W. T. Vetterling, and B. P. Flannery, *Numerical Recipes : The Art of Scientific Computing*, 3rd ed. New York, NY: Cambridge University Press, 2007.

[95] J. Ford, "Equipartition of Energy for Nonlinear Systems", *Journal of Mathematical Physics*, vol. 2, no. 3, pp. 387–393, 1961.

[96] J. De Luca, A. J. Lichtenberg, and M. A. Lieberman, "Time scale to ergodicity in the Fermi–Pasta–Ulam system", *Chaos*, vol. 5, no. 1, pp. 283–297, Mar. 1995.

[97] J. M. Steward, *Python for Scientists*. Cambridge: Cambridge University Press, 2014, p. 220.

[98] D. J. Higham and L. N. Trefethen, "Stiffness of ODEs", *BIT*, vol. 33, no. 2, pp. 285–303, Jun. 1993.

[99] L. F. Shampine and M. W. Reichelt, "The MATLAB ODE Suite", *SIAM Journal on Scientific Computing*, vol. 18, no. 1, pp. 1–22, Jan. 1997.

[100] A. C. Hindmarsh, "ODEPACK, A Systematized Collection of ODE Solvers", in *IMACS Transactions on Scientific Computation*, R. Stepleman, M. Carver, R. Peskin, W. Ames, and R. Vichnevetsky, Eds., vol. 1, Amsterdam: North-Holland, 1983, pp. 55–64.

[101] N. Metropolis and S. Ulam, "The Monte Carlo Method", *Journal of the American Statistical Association*, vol. 44, no. 247, pp. 335–341, Sep. 1949.

[102] N. Metropolis, "The Beginning of the Monte Carlo Method", *Los Alamos Science*, vol. 15, pp. 125–130, 1987.

[103] R. Eckhardt, "Stan Ulam, John Von Neumann, and the Monte Carlo Method", *Los Alamos Science, Special Issue*, vol. 15, pp. 131–141, 1987.

[104] H. D. Young and R. A. Freedman, *Sears and Zemansky's University Physics : with modern physics*, 12th ed. San Francisco, CA: Pearson Addison-Wesley, 2008.

[105] L. Rayleigh, "On Progressive Waves", *Proceedings of the London Mathematical Society*, vol. s1-9, no. 1, pp. 21–26, Nov. 1877.

[106] M. Greenstein and U. Kumar, "Multilayer piezoelectric resonators for medical ultrasound transducers", *IEEE Transactions on Ultrasonics, Ferroelectrics and Frequency Control*, vol. 43, no. 4, pp. 620–622, Jul. 1996.

[107] P. S. Cross and R. V. Schmidt, "Coupled Surface-Acoustic-Wave Resonators", *Bell System Technical Journal*, vol. 56, no. 8, pp. 1447–1482, Oct. 1977.

[108] A. Eichler, J. Moser, J. Chaste, M. Zdrojek, I. Wilson-Rae, and A. Bachtold, "Nonlinear damping in mechanical resonators made from carbon nanotubes and graphene", *Nature Nanotechnology*, vol. 6, pp. 339–342, Jun. 2011.

[109] J. C. Maxwell, "On Faraday's Lines of Force", in *The Scientific Papers of James Clerk Maxwell*, W. D. Niven, Ed., Cambridge: Cambridge University Press, 2011, pp. 155–229.

[110] F. A. Firestone, "A new analogy between mechanical and electrical systems", *The Journal of the Acoustical Society of America*, vol. 4, no. 3, pp. 249–267, Jan. 1933.

[111] U. Tietze, C. Schenk, and E. Gamm, *Electronic Circuits*, 2nd ed. New York: Springer-Verlag Berlin Heidelberg, 2008.

[112] A. M. Soliman, "History and Progress of the Tow–Thomas Biquadratic Filter Part I: Generation and Op Amp Realizations", *Journal of Circuits, Systems and Computers*, vol. 17, no. 01, pp. 33–54, 2008.

[113] B. Gilbert, "A precise four-quadrant multiplier with subnanosecond response", *IEEE Journal of Solid-State Circuits*, vol. 3, no. 4, pp. 365–373, Dec. 1968.

[114] W. Jung, Ed., *Op Amp Applications Handbook*. Burlington, MA: Newnes/Elsevier, 2005.

[115] Quintenz Hybridtechnik, *A Relation between Filter Parameters of the Tow-Thomas-Biquad*.

[116] M. Toda, "Studies of a non-linear lattice", *Physics Reports*, vol. 18, no. 1, pp. 1–123, 1975.

[117] N. J. Zabusky and M. D. Kruskal, "Interaction of "Solitons"in a Collisionless Plasma and the Recurrence of Initial States", *Physical Review Letters*, vol. 15, no. 6, pp. 240–243, Aug. 1965.

[118] C. Chong, M. A. Porter, P. G. Kevrekidis, and C. Daraio, "Nonlinear coherent structures in granular crystals", *Journal of Physics: Condensed Matter*, vol. 29, no. 41, p. 413 003, Oct. 2017.

[119] V. F. Nesterenko, *Dynamics of Heterogeneous Materials*, L. Davison and Y. Horie, Eds. Berlin: Springer, 2001.

[120] L. Cveticanin, "On the truly nonlinear oscillator with positive and negative damping", *Applied Mathematics and Computation*, vol. 243, pp. 433–445, Sep. 2014.

[121] G. Tao, H. Zhang, H. Chang, and B. Choubey, "Inverse Eigenvalue Sensing in Coupled Micro/Nano System", *Journal of Microelectromechanical Systems*, vol. 27, no. 5, pp. 886–895, Oct. 2018.

[122] X. Wei, N. H. Saad, and M. C. Ward, "Analysis of manufacturing variation in a coupled microresonators array based on its designed values and measured eigenfrequencies", *Micro and Nano Letters*, vol. 5, no. 5, pp. 300–303, Oct. 2010.

[123] A. Arenas, A. Díaz-Guilera, J. Kurths, Y. Moreno, and C. Zhou, "Synchronization in complex networks", *Physics Reports*, vol. 469, no. 3, pp. 93–153, Dec. 2008.

Appendices

A

Matlab Code

This is a reprint of the relevant sections of the MATLAB code written by Dauxois *et al.* [16] which is available online at http://perso.ens-lyon.fr/thierry.dauxois/fpu.html

```
N=64;
alpha=0.25;
TMAX=64000;
DT=1;
tspan=[0:DT:TMAX];
options=odeset('Reltol',1e-4);

for I=1:N
    a=1; b(I)=a*sin(pi*I/(N+1)); b(I+N)=0;
    omegak2(I)=4*(sin(pi*I/2/N))^2;
end

[T,Y]=ode45('fpu1',tspan,b',options,N,alpha);

for IT=1:(TMAX/DT)
    TIME(IT)=IT*DT*sqrt(omegak2(1))/2/pi;
    YX(IT,1:N+1)=[0 Y(IT,1:N)];
    YV(IT,1:N+1)=[0 Y(IT,N+1:2*N )];
    sXF(IT,:)=imag(fft([YX(IT,1:N+1) 0  -YX(IT,N+1:-1:2)]))/sqrt
       (2*(N+1));
    sVF(IT,:)=imag(fft([YV(IT,1:N+1) 0  -YV(IT,N+1:-1:2)]))/sqrt
       (2*(N+1));
    Energ(IT,1:N)=(omegak2(1:N).*(sXF(IT,2:N+1).^2)+sVF(IT,2:N+1)
       .^2)/2;
    for J=2:N-1
      DifY(IT,J)=Y(IT,J+1)-Y(IT,J);
    end
end

%fpu1 function
function dy=fpu1(t,y, options, N, alpha)

D(N+1) = y(2) + (-2*y(1)) + alpha*((y(2)-y(1))^2 - y(1)^2);
D(1)   = y(N+1);

D(2*N) = y(N-1) + (-2*y(N)) + alpha*(y(N)^2 - (y(N)-y(N-1))^2);
D(N)   = y(2*N);

for I=2:N-1
 D(N+I) = y(I+1) + y(I-1) + (-2*y(I))
             + alpha*((y(I+1)-y(I))^2 - (y(I)-y(I-1))^2);
 D(I)=y(N+I);
end

dy=D';
```

B

Python Code

```
import numpy as np
import scipy as sp

def d_fpu(y,t,alpha,damper,M_tol,N):
    D[N] = M_tol[0,0+1]*y[1] + 0 + M_tol[0,0]*(-2*y[0]) + alpha
       *(((M_tol[0,0+1]*y[1])-(M_tol[0,0]*y[0]))**2 - (M_tol[0,0]*
       y[0])**2) - damper*y[N]
    D[0] = y[N]

    D[-1]  = 0 + M_tol[0,N-2]*y[N-2] + M_tol[0,N-1]*(-2*y[N-1]) +
       alpha*((M_tol[0,N-1]*y[N-1])**2 - ((M_tol[0,N-1]*y[N-1])-(
       M_tol[0,N-2]*y[N-2]))**2) - damper*y[-1]
    D[N-1] = y[-1]

    for I in range(1,N-1):
        D[N+I]  = M_tol[0,I+1]*y[I+1] + M_tol[0,I-1]*y[I-1] +
           M_tol[0,I]*(-2*y[I]) + alpha*(((M_tol[0,I+1]*y[I+1])-(
           M_tol[0,I]*y[I]))**2 - ((M_tol[0,I]*y[I])-(M_tol[0,I
           -1]*y[I-1]))**2) - damper*y[N+I]
        D[I]    = y[N+I]

    return D

damper = 0.0001
alpha = 0.25
N = 64
no_MC=101 # number of Monte Carlo runs (+1 for Python indexing)
tol=0.001 # tolerance variation in the system (0.01 = +/-1%)

# How many time steps do we want, and over what time period?
TMAX = 64000
DT = 1
TSTEPS = int(TMAX/DT)
# create array of all the times at which equation will be
    estimated
t_array = np.linspace(0, TMAX, TSTEPS+1)

b = np.zeros(2*(N))
omegak2 = np.zeros(N)
D = np.zeros(2*N)
TIME=np.zeros(int(TMAX/DT))
YX=np.zeros((int(TMAX/DT),N+1))
YV=np.zeros((int(TMAX/DT),N+1))
sXF=np.zeros((int(TMAX/DT),2*(N+1)))
sVF=np.zeros((int(TMAX/DT),2*(N+1)))
Energ=np.zeros((int(TMAX/DT),N))
DifY=np.zeros((int(TMAX/DT),N-1))

for K in range(0,N):

    #FPU initial condition
    a=1
    b[K]=a*np.sin(np.pi*((K+1)/(N+1)))
    b[K+N]=0
```

```
    # Mode Frequencies
    omegak2[K]=4*(np.sin(np.pi*(K+1)/2/N))**2


for MC in range(1,no_MC):

    # Generate the tolerance values
    M_tol = 1 + (tol*(1/3)*np.random.randn(1,N))

    # Truncate the matrix to within tolerance range
    M_tol[M_tol>(1+tol)]=1+tol
    M_tol[M_tol<(1-tol)]=1-tol

    # Time integration
    Y_out=sp.integrate.odeint(d_fpu,b,t_array,args=(alpha,damper,
        M_tol,N))

    for IT in range(0,int(TMAX/DT)):     # Time iteration loop
        TIME[IT] = IT*DT*np.sqrt(omegak2[0])/2/np.pi
        YX[IT] = np.append([0],Y_out[IT,0:N])
        YV[IT] = np.append([0],Y_out[IT,N:2*N])
        sXF[IT] = np.imag(np.fft.fft(np.concatenate((YX[IT,0:N
            +1],[0], -1*YX[IT,N:0:-1]))))/np.sqrt(2*(N+1))
        sVF[IT] = np.imag(np.fft.fft(np.concatenate((YV[IT][0:N
            +1],[0],[jk * (-1) for jk in YV[IT][N:0:-1]]))))/np.
            sqrt(2*(N+1))
        Energ[IT]=(omegak2[0:N]*(sXF[IT,1:N+1]**2)+sVF[IT,1:N
            +1]**2)/2
        for J in range(1,N-1):           # Space loop
            DifY[IT,J]=Y_out[IT,J+1]-Y_out[IT,J];
```

C

Full Monte Carlo results for the symmetric system

C.1 Tolerance of $\pm 0.1\,\%$



Figure C.1: Full set of 100 Monte Carlo simulations of 1D FPUT-α arrays with 64 oscillators and a coupling strength of $\alpha = 0.25$ at a tolerance of ± 0.1 %.



Figure C.1: (continued) Full set of 100 Monte Carlo simulations of 1D FPUT-α arrays with 64 oscillators and a coupling strength of $\alpha = 0.25$ at a tolerance of $\pm 0.1\,\%$.



Figure C.1: (continued) Full set of 100 Monte Carlo simulations of 1D FPUT-α arrays with 64 oscillators and a coupling strength of $\alpha = 0.25$ at a tolerance of $\pm 0.1\,\%$.



Figure C.1: (continued) Full set of 100 Monte Carlo simulations of 1D FPUT-α arrays with 64 oscillators and a coupling strength of $\alpha = 0.25$ at a tolerance of $\pm 0.1\,\%$.

C.2 Tolerance of $\pm 1\,\%$

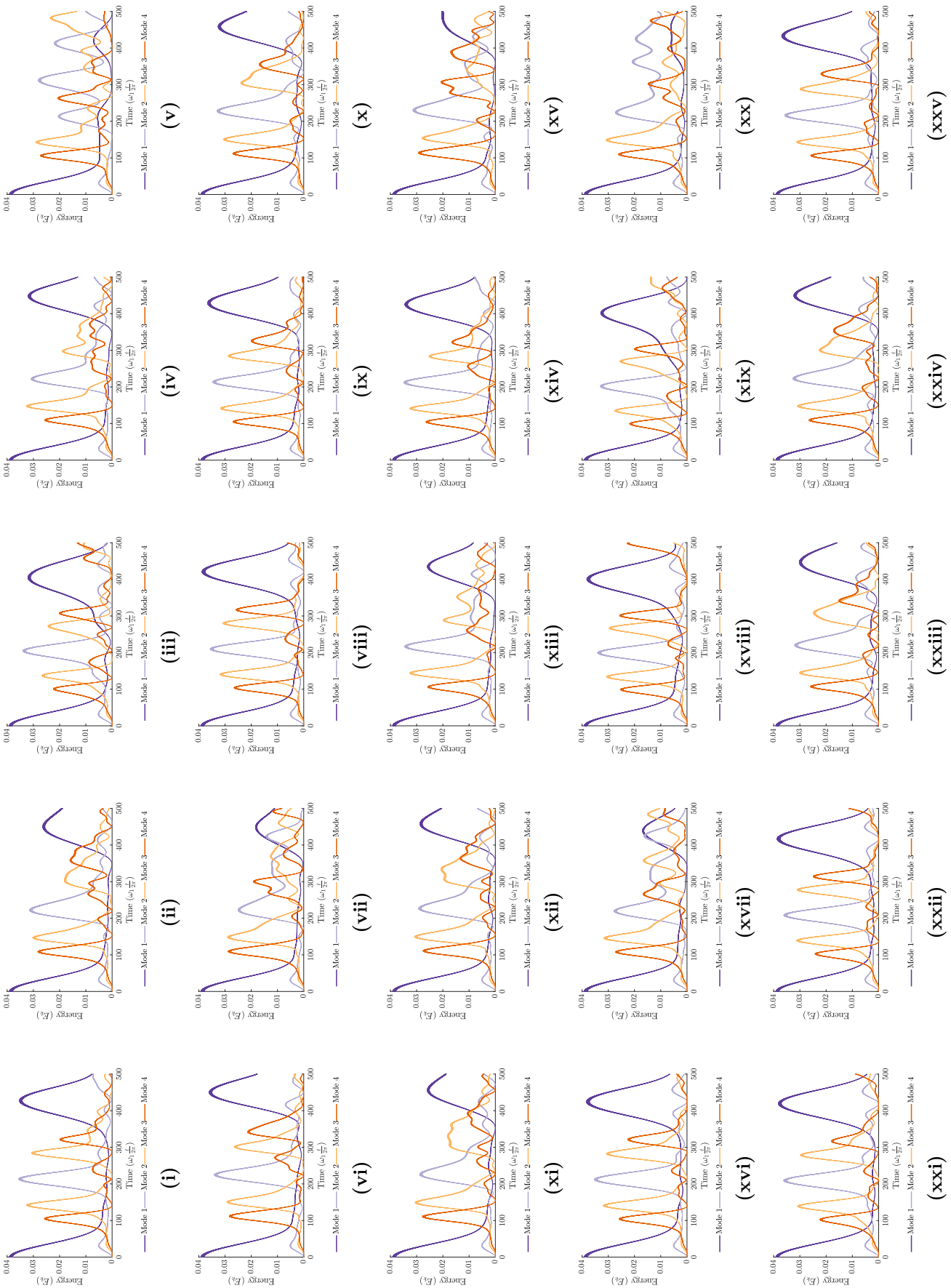


Figure C.2: Full set of 100 Monte Carlo simulations of 1D FPUT-α arrays with 64 oscillators and a coupling strength of $\alpha = 0.25$ at a tolerance of $\pm 1\%$.

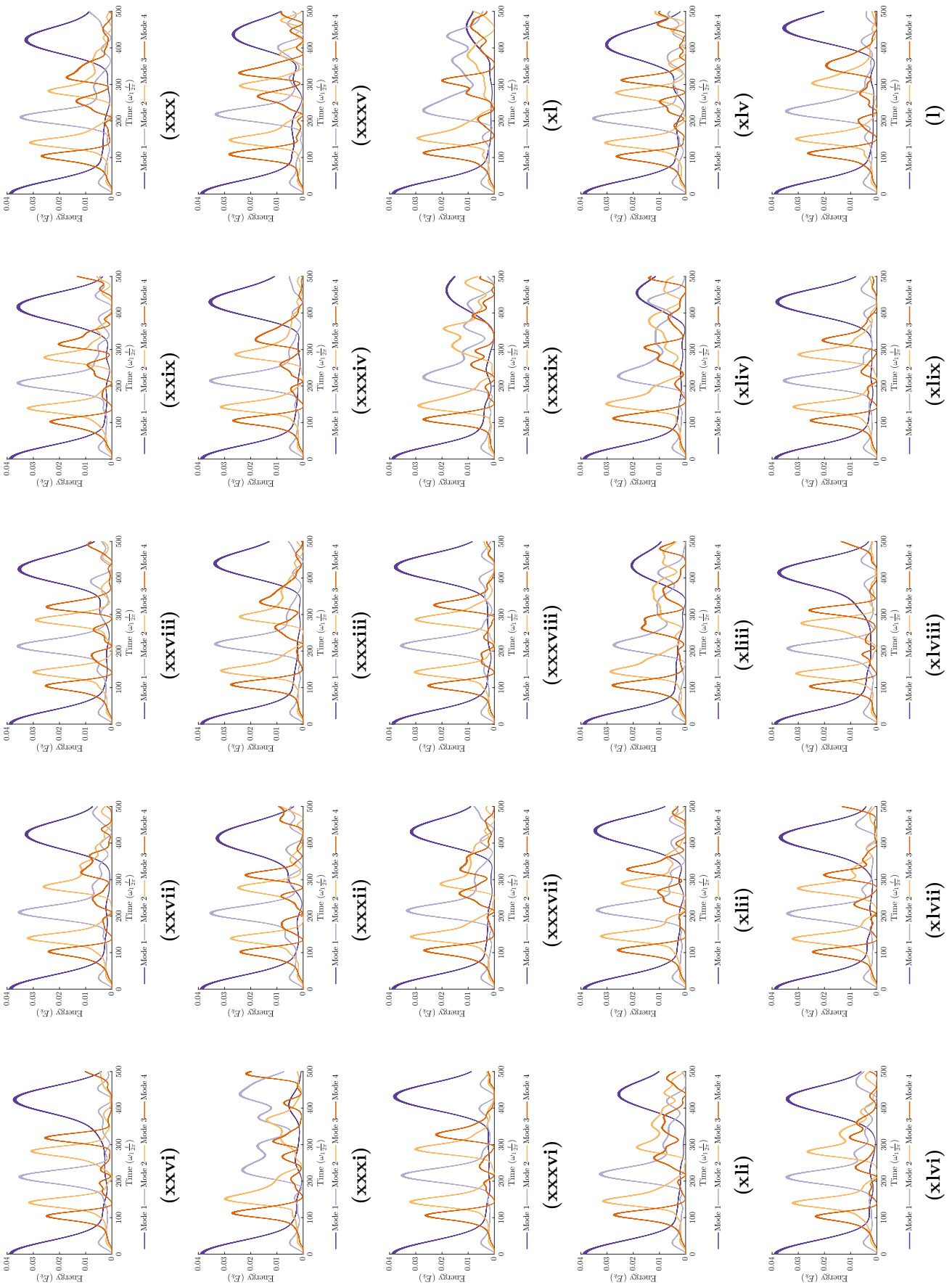


Figure C.2: (continued) Full set of 100 Monte Carlo simulations of 1D FPUT-α arrays with 64 oscillators and a coupling strength of $\alpha = 0.25$ at a tolerance of $\pm 1\,\%$.

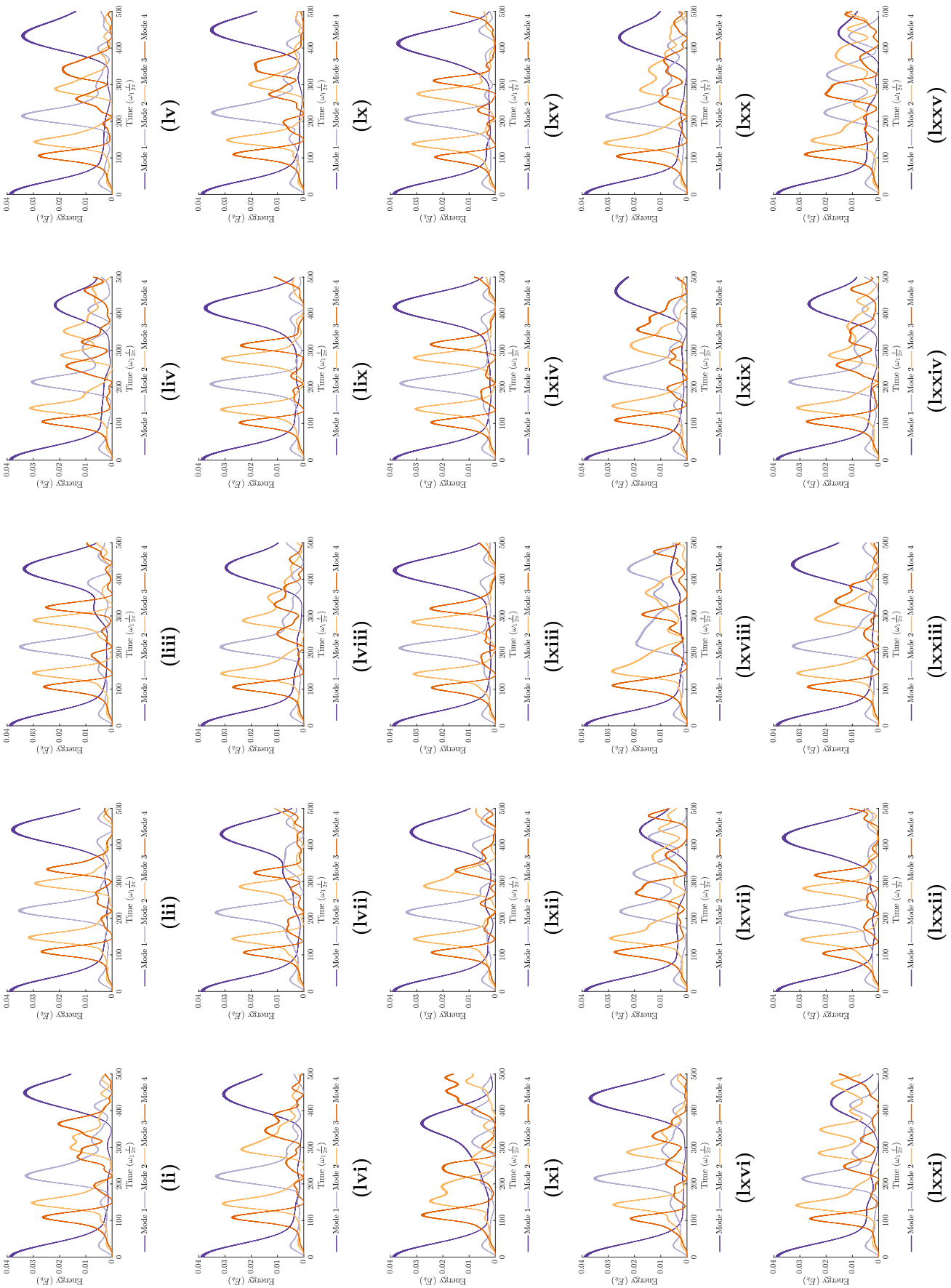


Figure C.2: (continued) Full set of 100 Monte Carlo simulations of 1D FPUT-α arrays with 64 oscillators and a coupling strength of $\alpha = 0.25$ at a tolerance of $\pm 1\,\%$.

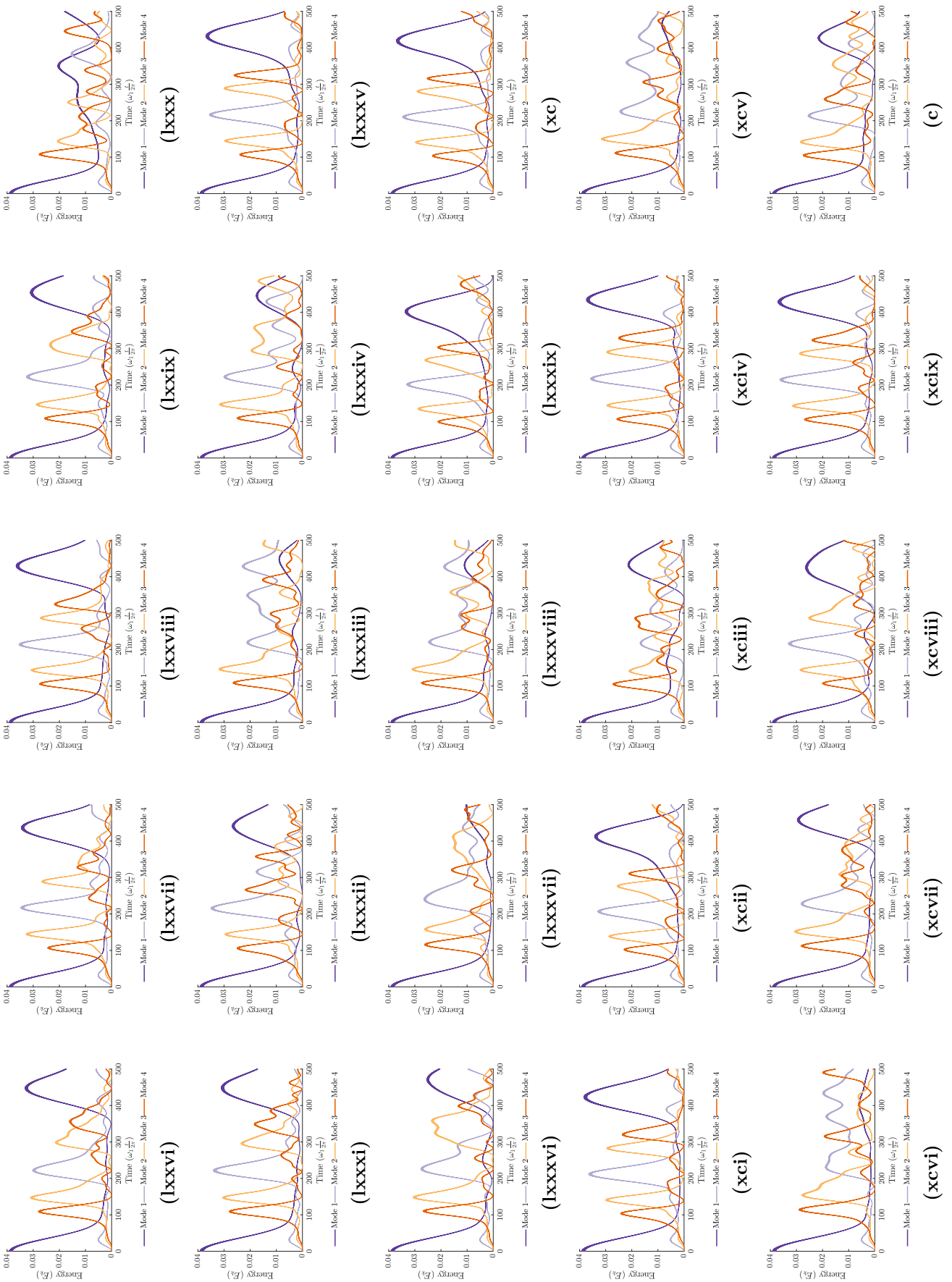


Figure C.2: (continued) Full set of 100 Monte Carlo simulations of 1D FPUT-α arrays with 64 oscillators and a coupling strength of $\alpha = 0.25$ at a tolerance of $\pm 1\,\%$.

C.3 Tolerance of $\pm 5\,\%$

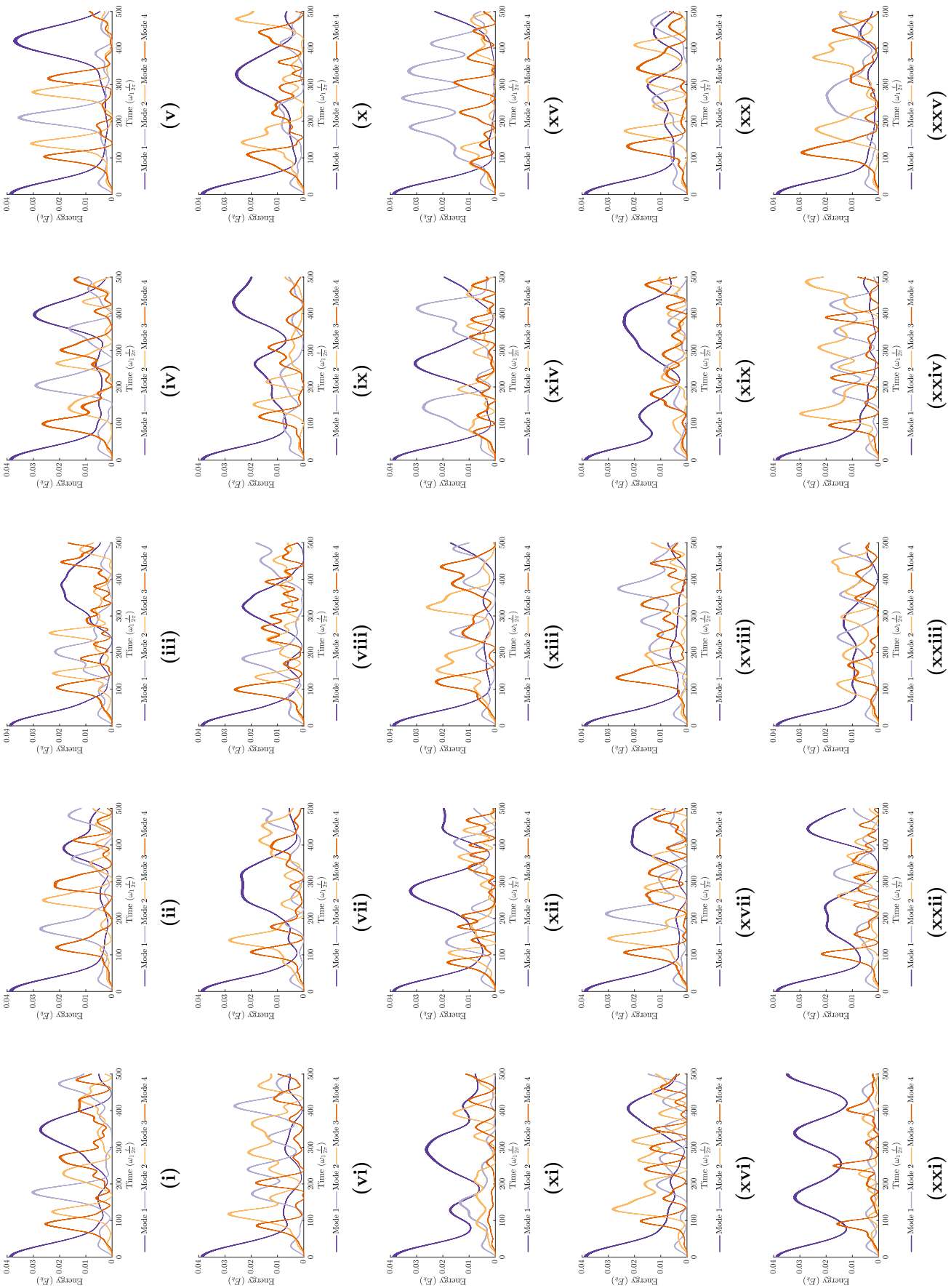


Figure C.3: Full set of 100 Monte Carlo simulations of 1D FPUT-α arrays with 64 oscillators and a coupling strength of $\alpha = 0.25$ at a tolerance of $\pm 5\,\%$.

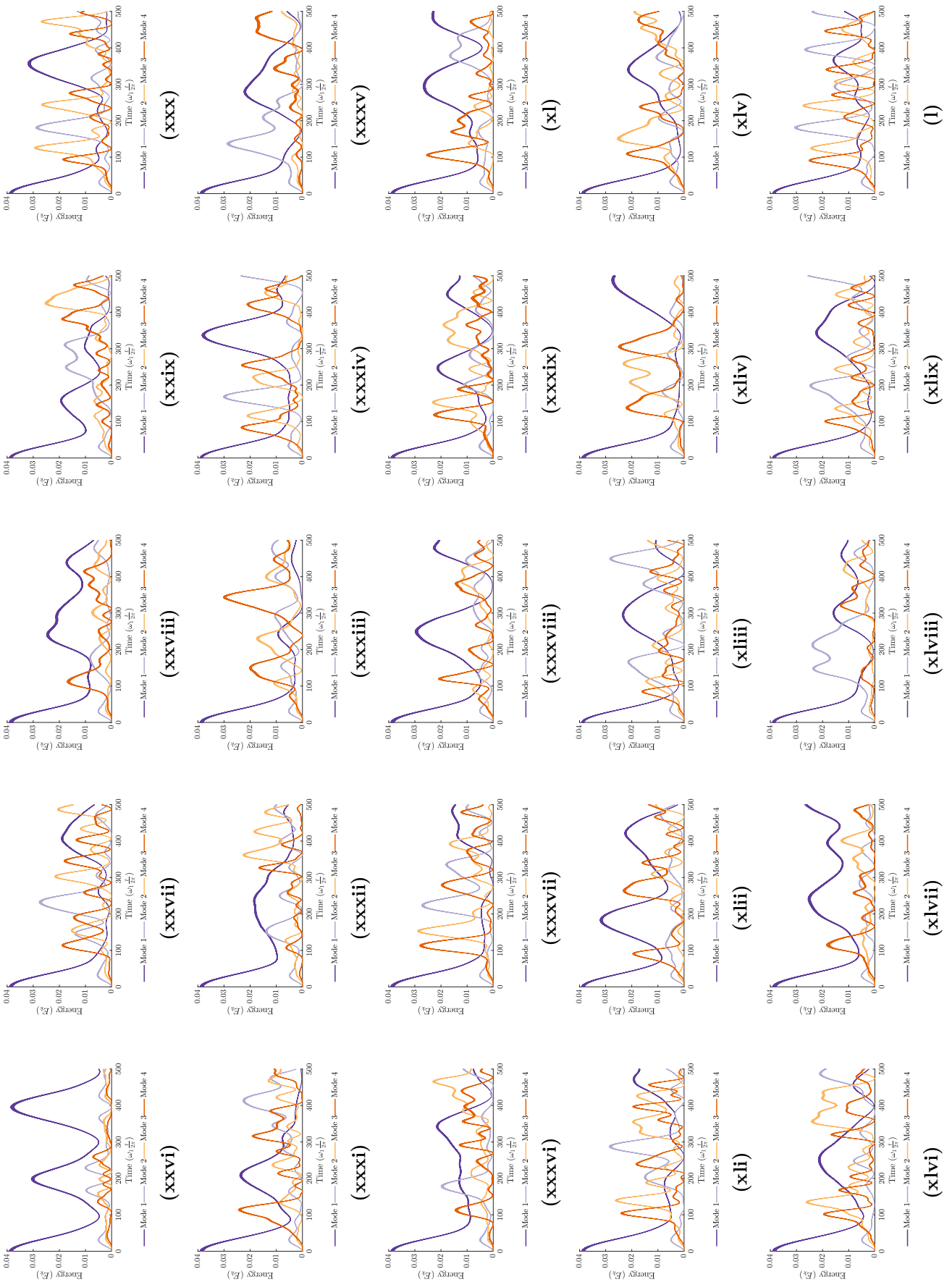


Figure C.3: (continued) Full set of 100 Monte Carlo simulations of 1D FPUT-α arrays with 64 oscillators and a coupling strength of $\alpha = 0.25$ at a tolerance of $\pm 5\,\%$.

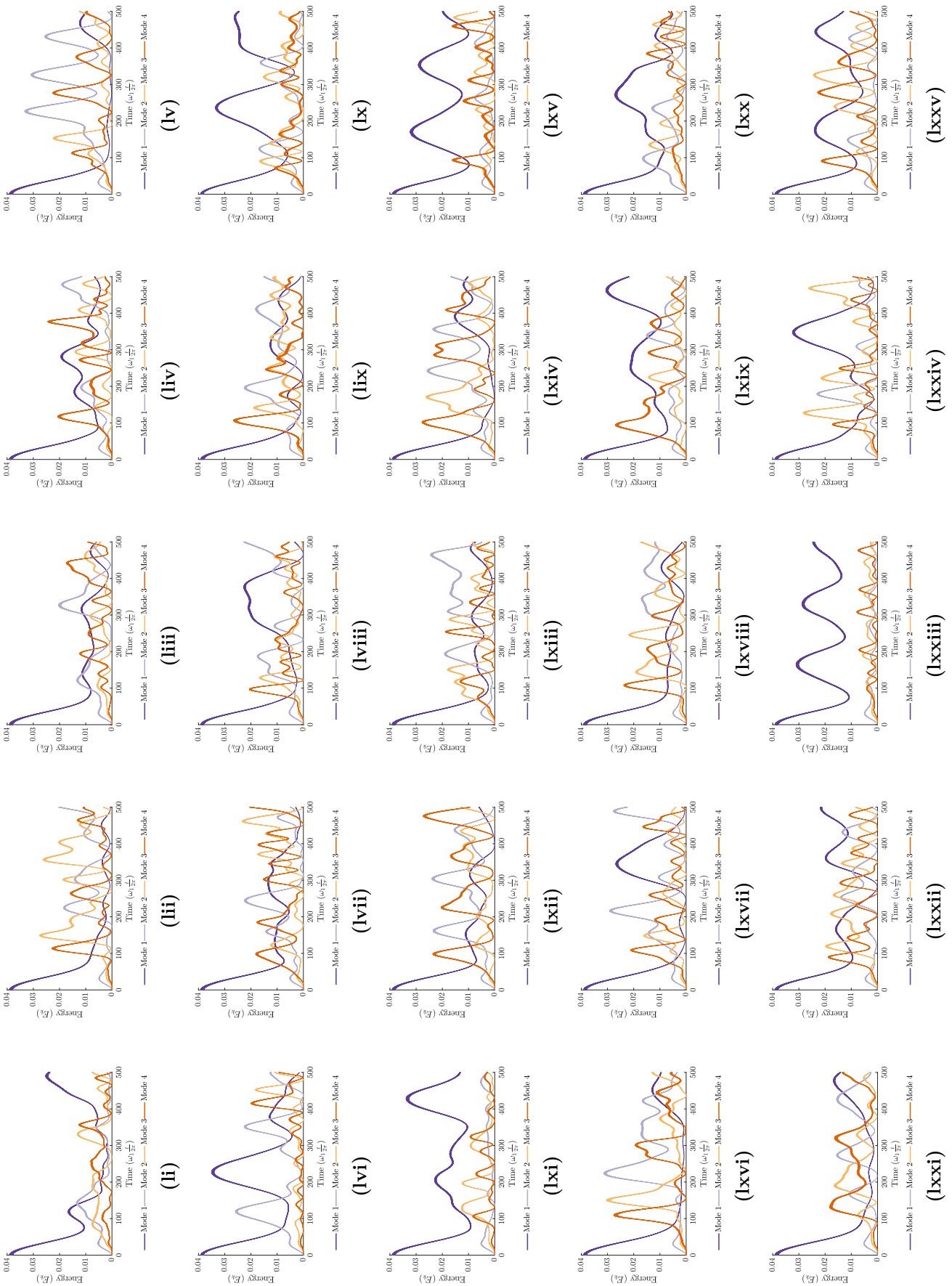


Figure C.3: (continued) Full set of 100 Monte Carlo simulations of 1D FPUT-α arrays with 64 oscillators and a coupling strength of $\alpha = 0.25$ at a tolerance of $\pm 5\,\%$.

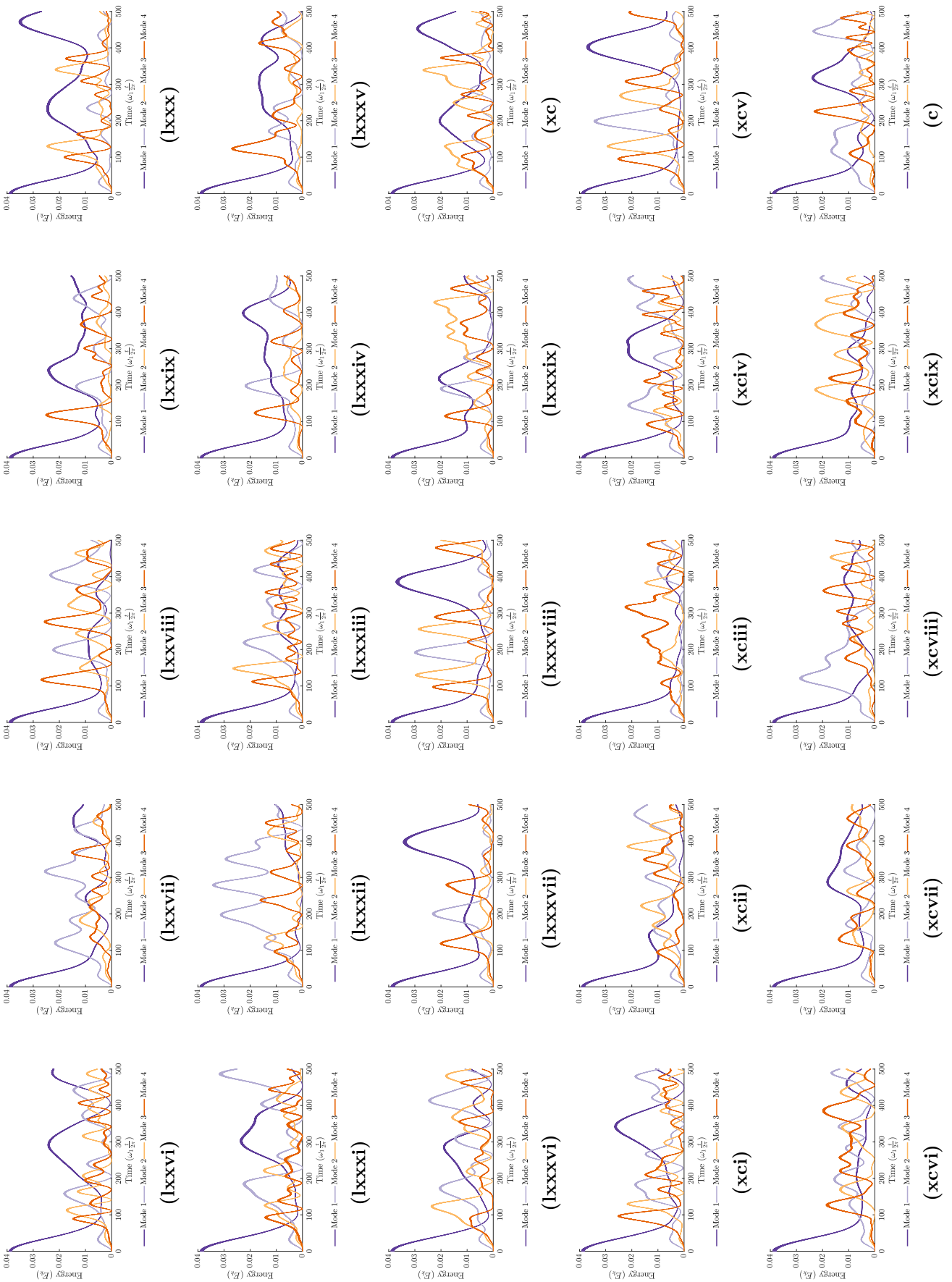


Figure C.3: (continued) Full set of 100 Monte Carlo simulations of 1D FPUT-α arrays with 64 oscillators and a coupling strength of $\alpha = 0.25$ at a tolerance of $\pm 5\,\%$.

C.4 Tolerance of $\pm 10\,\%$

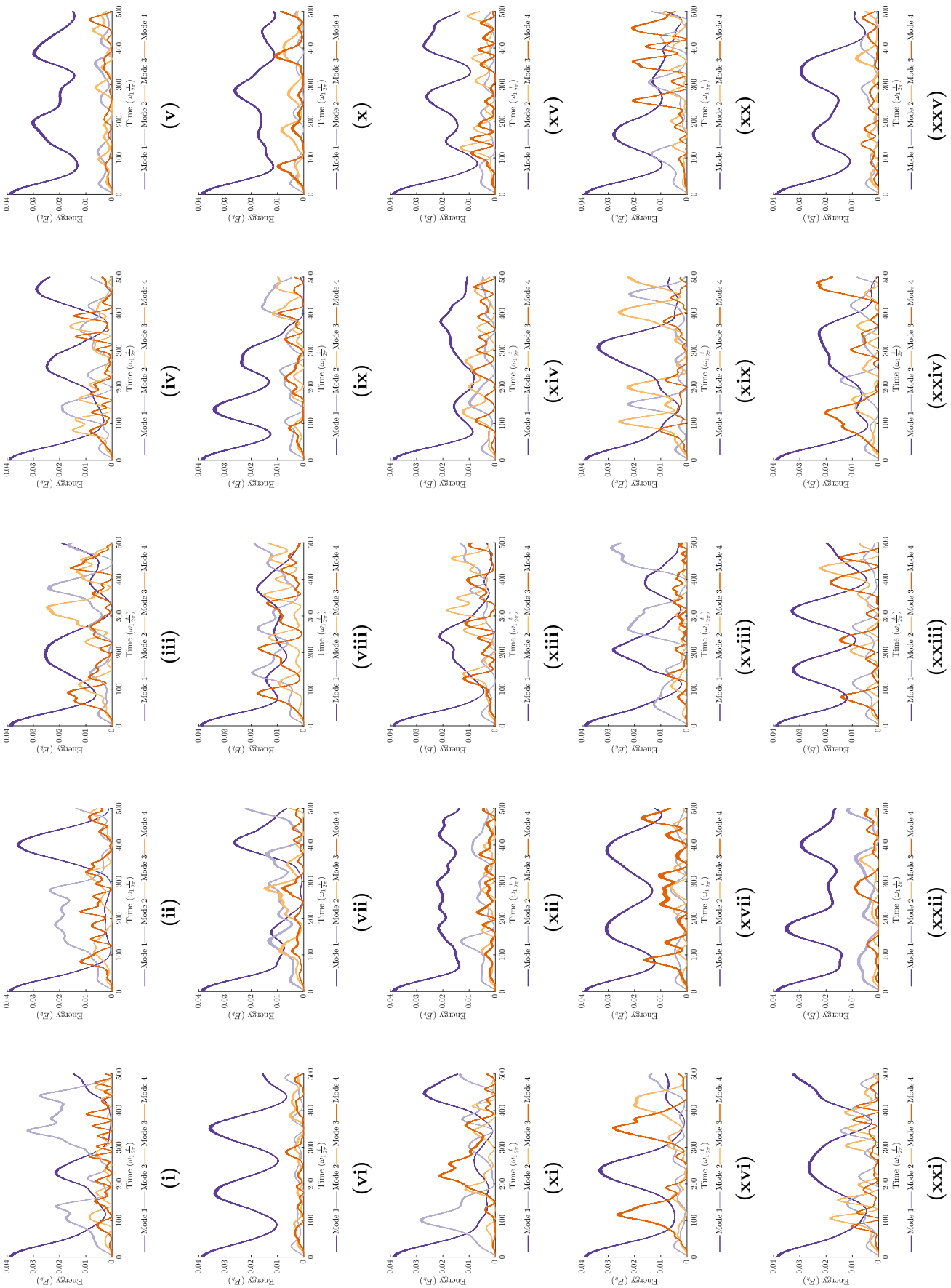


Figure C.4: Full set of 100 Monte Carlo simulations of 1D FPUT-α arrays with 64 oscillators and a coupling strength of $\alpha = 0.25$ at a tolerance of $\pm 10\,\%$.

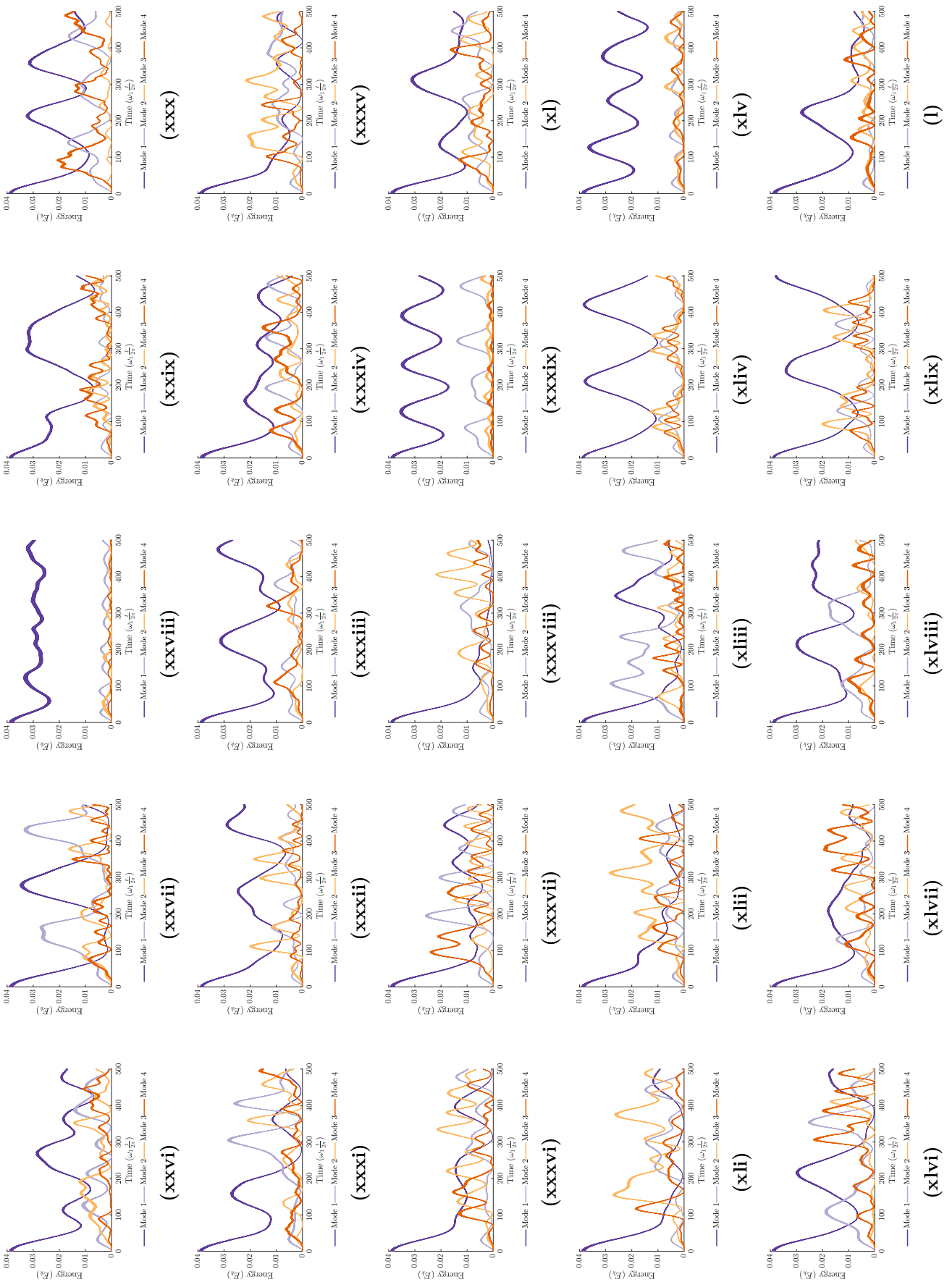


Figure C.4: (continued) Full set of 100 Monte Carlo simulations of 1D FPUT-α arrays with 64 oscillators and a coupling strength of $\alpha = 0.25$ at a tolerance of $\pm 10\,\%$.

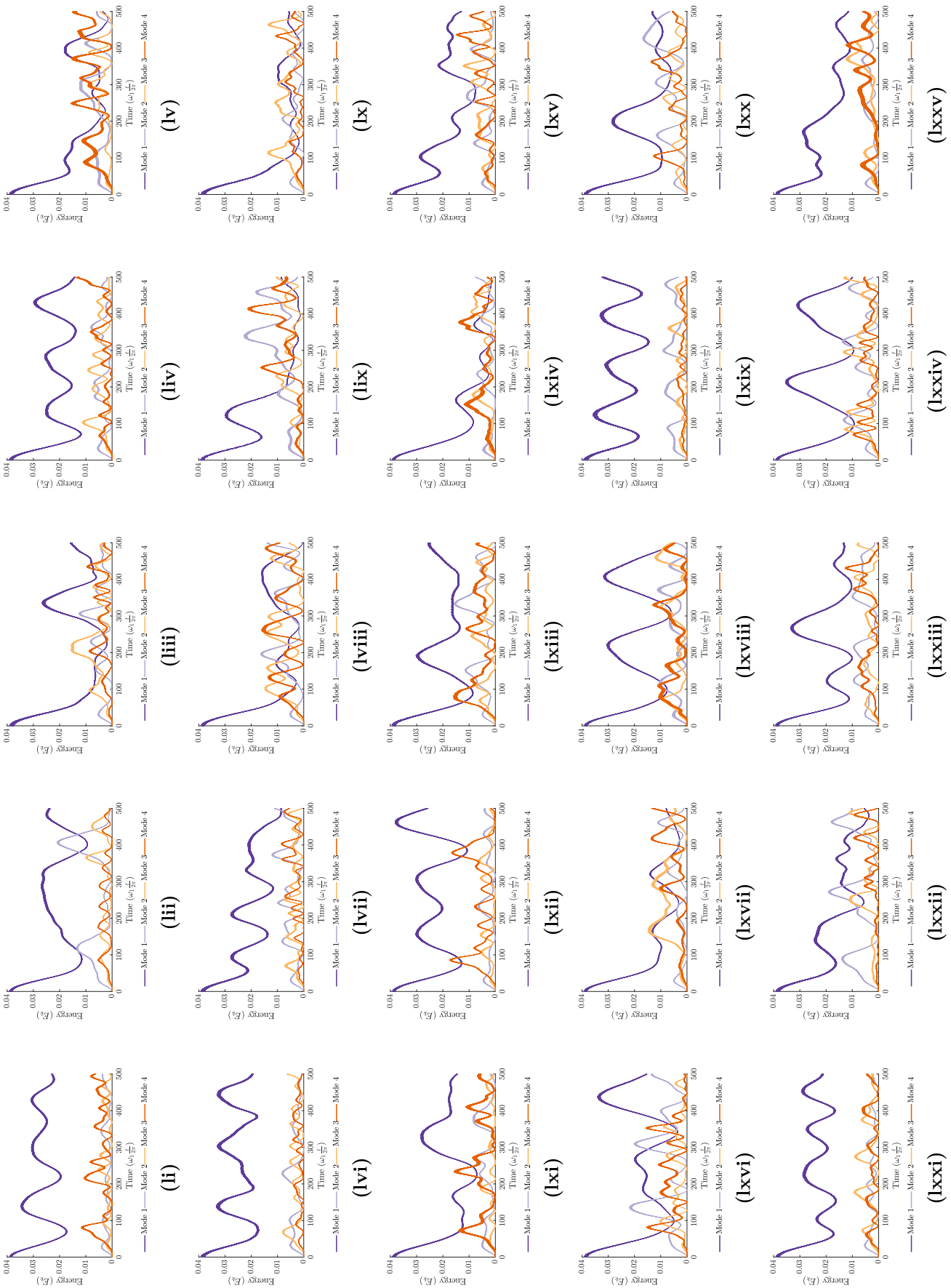


Figure C.4: (continued) Full set of 100 Monte Carlo simulations of 1D FPUT-α arrays with 64 oscillators and a coupling strength of $\alpha = 0.25$ at a tolerance of $\pm 10\,\%$.

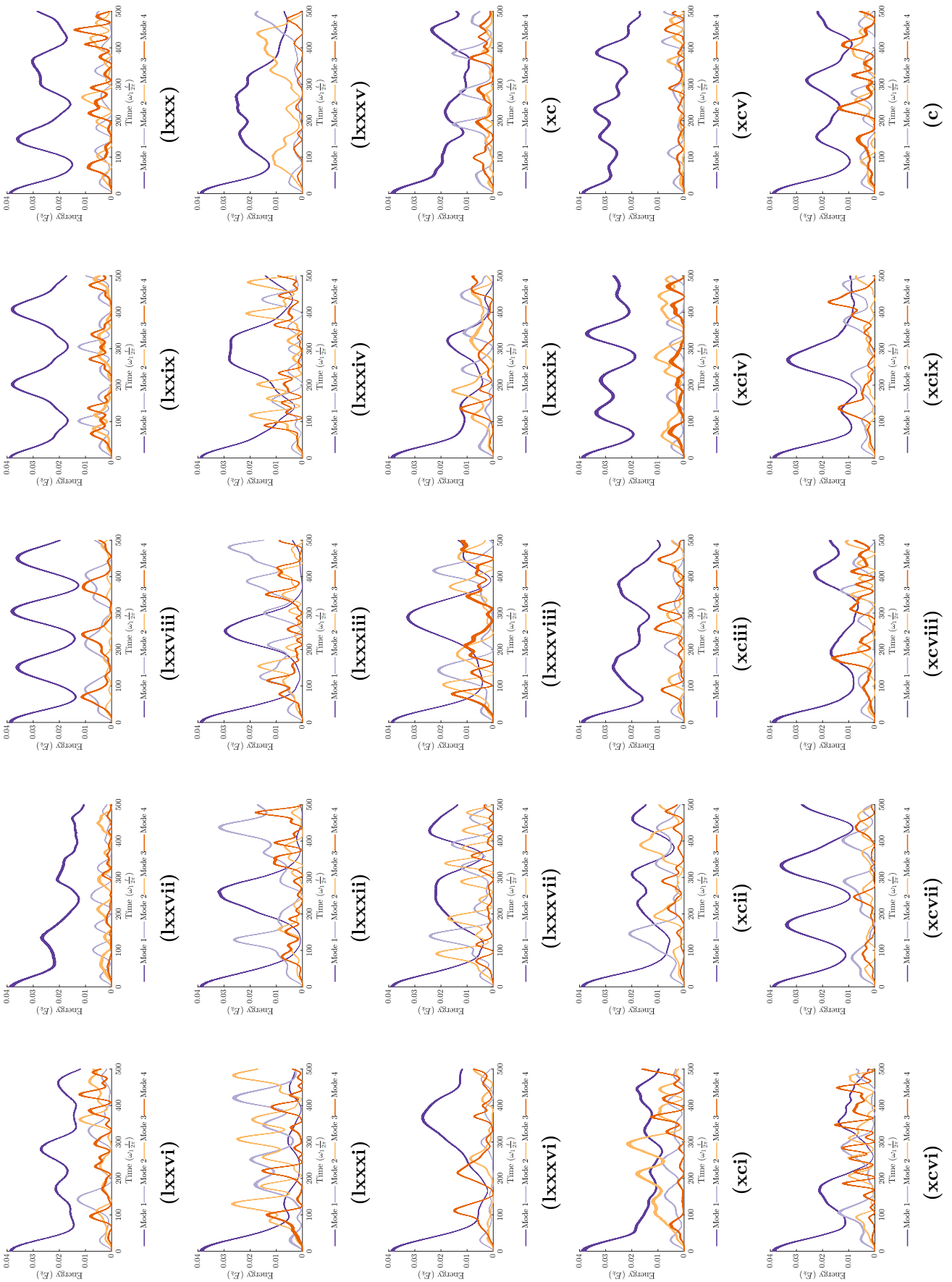


Figure C.4: (continued) Full set of 100 Monte Carlo simulations of 1D FPUT-α arrays with 64 oscillators and a coupling strength of $\alpha = 0.25$ at a tolerance of $\pm 10\,\%$.

D

Full Monte Carlo results for the asymmetric system

D.1 Tolerance of $\pm 0.1\,\%$



Figure D.1: Full set of 100 Monte Carlo simulations of asymmetric 1D FPUT-α arrays with 64 oscillators and a coupling strength of $\alpha = 0.25$ at a tolerance of $\pm 0.1\,\%$.

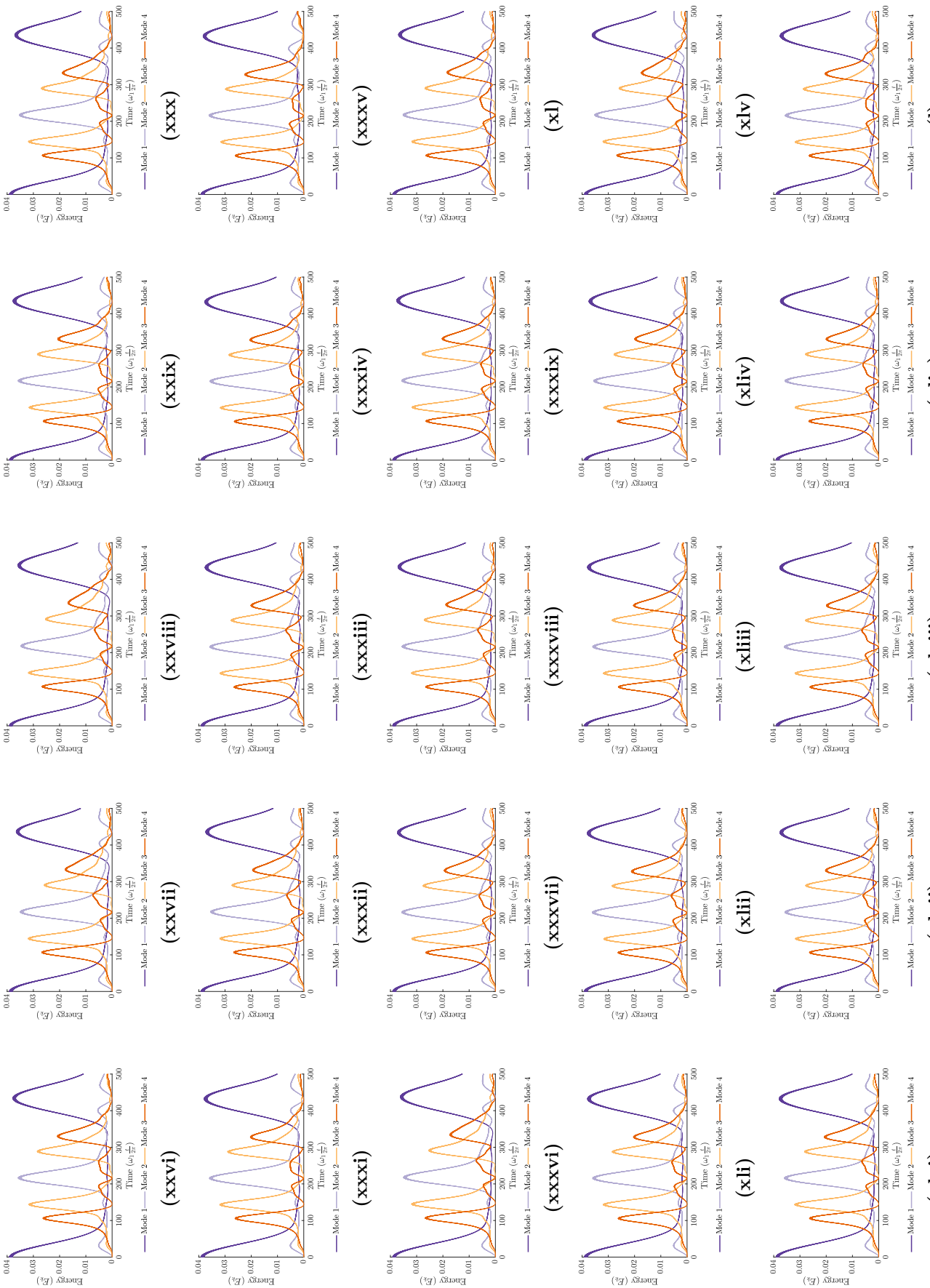


Figure D.1: (continued) Full set of 100 Monte Carlo simulations of asymmetric 1D FPUT-α arrays with 64 oscillators and a coupling strength of $\alpha = 0.25$ at a tolerance of $\pm 0.1\,\%$.



Figure D.1: (continued) Full set of 100 Monte Carlo simulations of asymmetric 1D FPUT-α arrays with 64 oscillators and a coupling strength of $\alpha = 0.25$ at a tolerance of $\pm 0.1\,\%$.



Figure D.1: (continued) Full set of 100 Monte Carlo simulations of asymmetric 1D FPUT-α arrays with 64 oscillators and a coupling strength of $\alpha = 0.25$ at a tolerance of $\pm 0.1\,\%$.

D.2 Tolerance of $\pm 1\,\%$

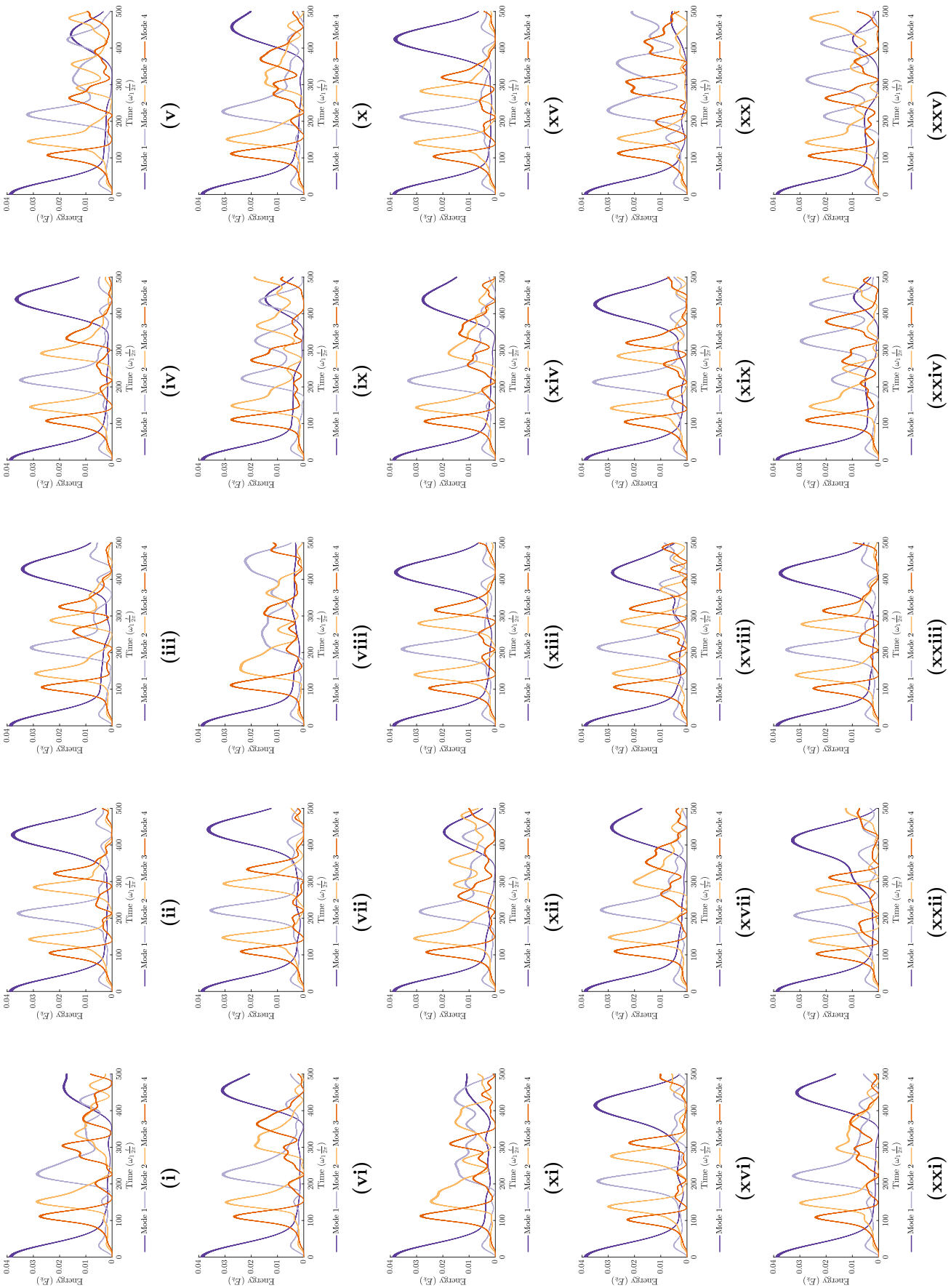


Figure D.2: Full set of 100 Monte Carlo simulations of asymmetric 1D FPUT-α arrays with 64 oscillators and a coupling strength of $\alpha = 0.25$ at a tolerance of $\pm 1\,\%$.



Figure D.2: (continued) Full set of 100 Monte Carlo simulations of asymmetric 1D FPUT-α arrays with 64 oscillators and a coupling strength of $\alpha = 0.25$ at a tolerance of $\pm 1\,\%$.

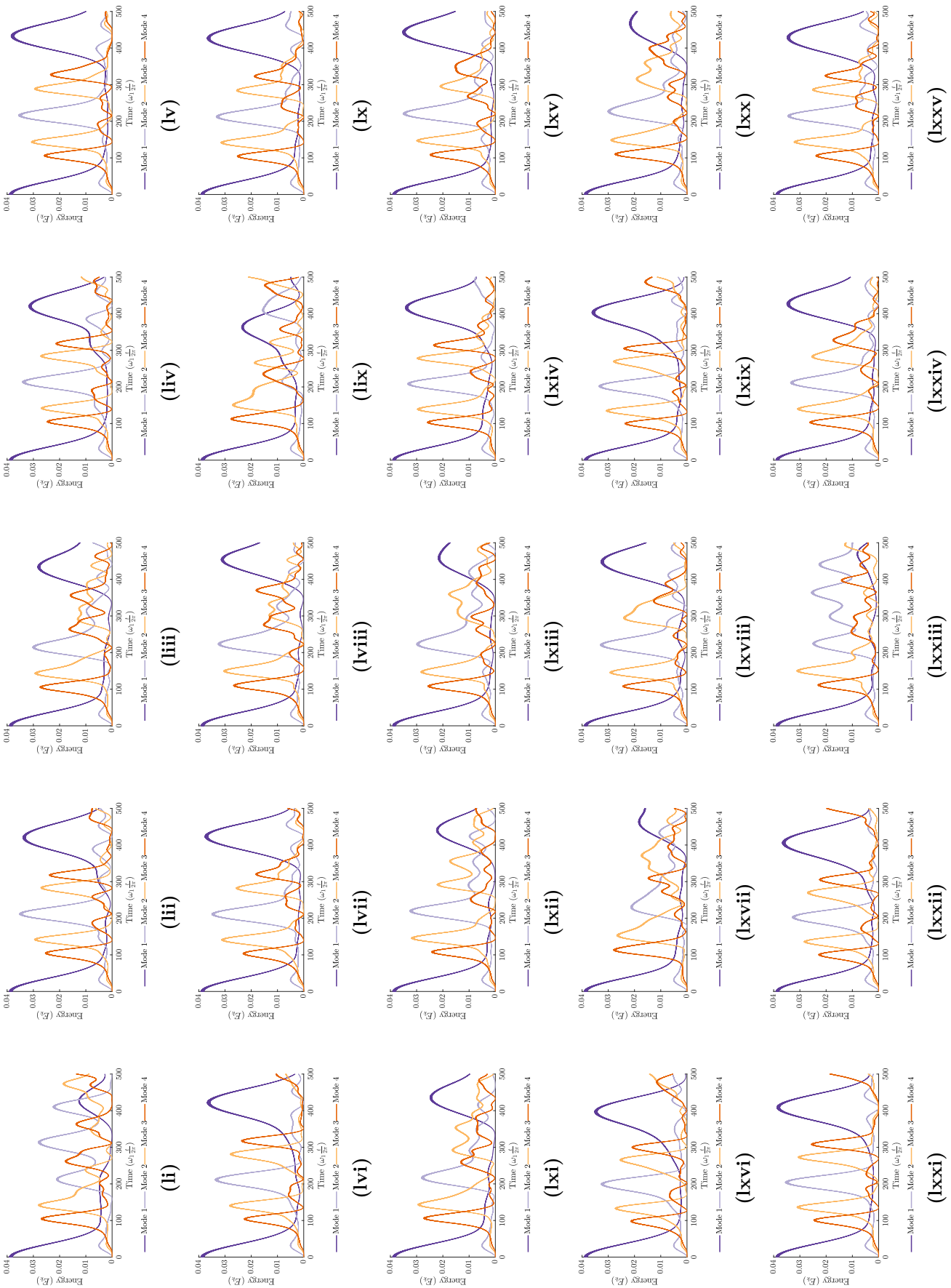


Figure D.2: (continued) Full set of 100 Monte Carlo simulations of asymmetric 1D FPUT-α arrays with 64 oscillators and a coupling strength of $\alpha = 0.25$ at a tolerance of $\pm 1\,\%$.



Figure D.2: (continued) Full set of 100 Monte Carlo simulations of asymmetric 1D FPUT-α arrays with 64 oscillators and a coupling strength of $\alpha = 0.25$ at a tolerance of $\pm 1\,\%$.

D.3 Tolerance of $\pm 5\,\%$

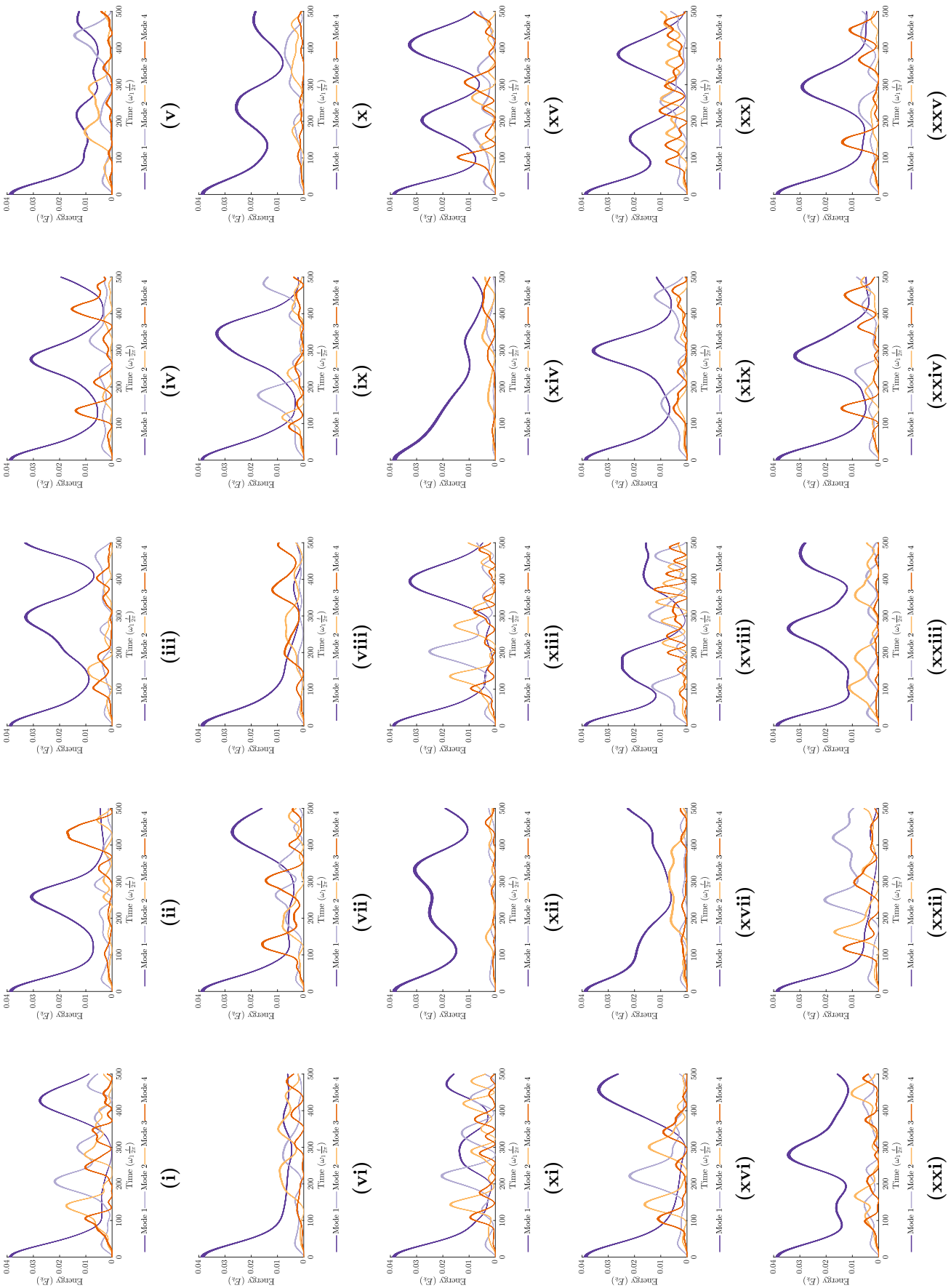


Figure D.3: Full set of 100 Monte Carlo simulations of asymmetric 1D FPUT-α arrays with 64 oscillators and a coupling strength of $\alpha = 0.25$ at a tolerance of $\pm 5\,\%$.

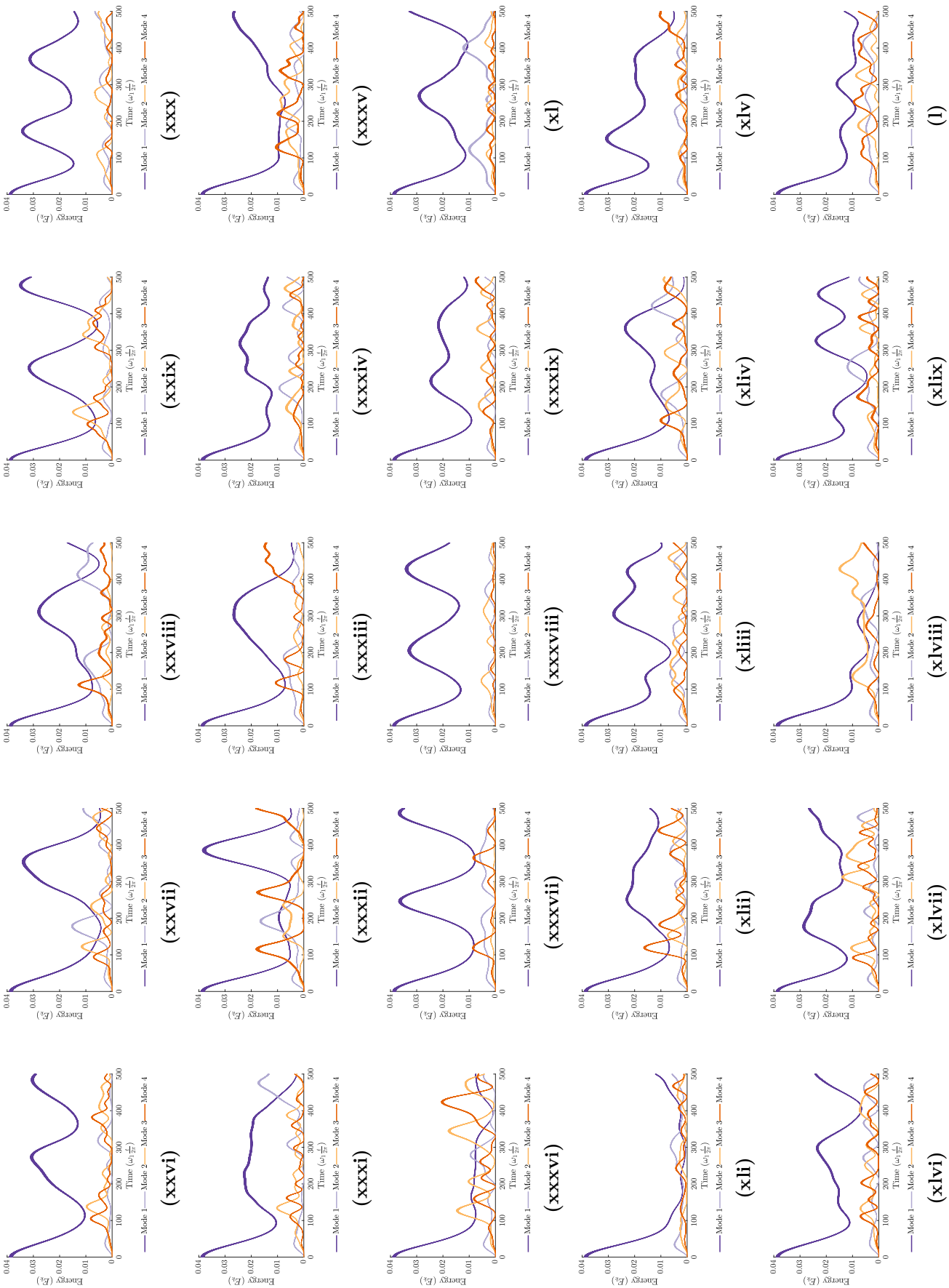


Figure D.3: (continued) Full set of 100 Monte Carlo simulations of asymmetric 1D FPUT-α arrays with 64 oscillators and a coupling strength of $\alpha = 0.25$ at a tolerance of $\pm 5\,\%$.

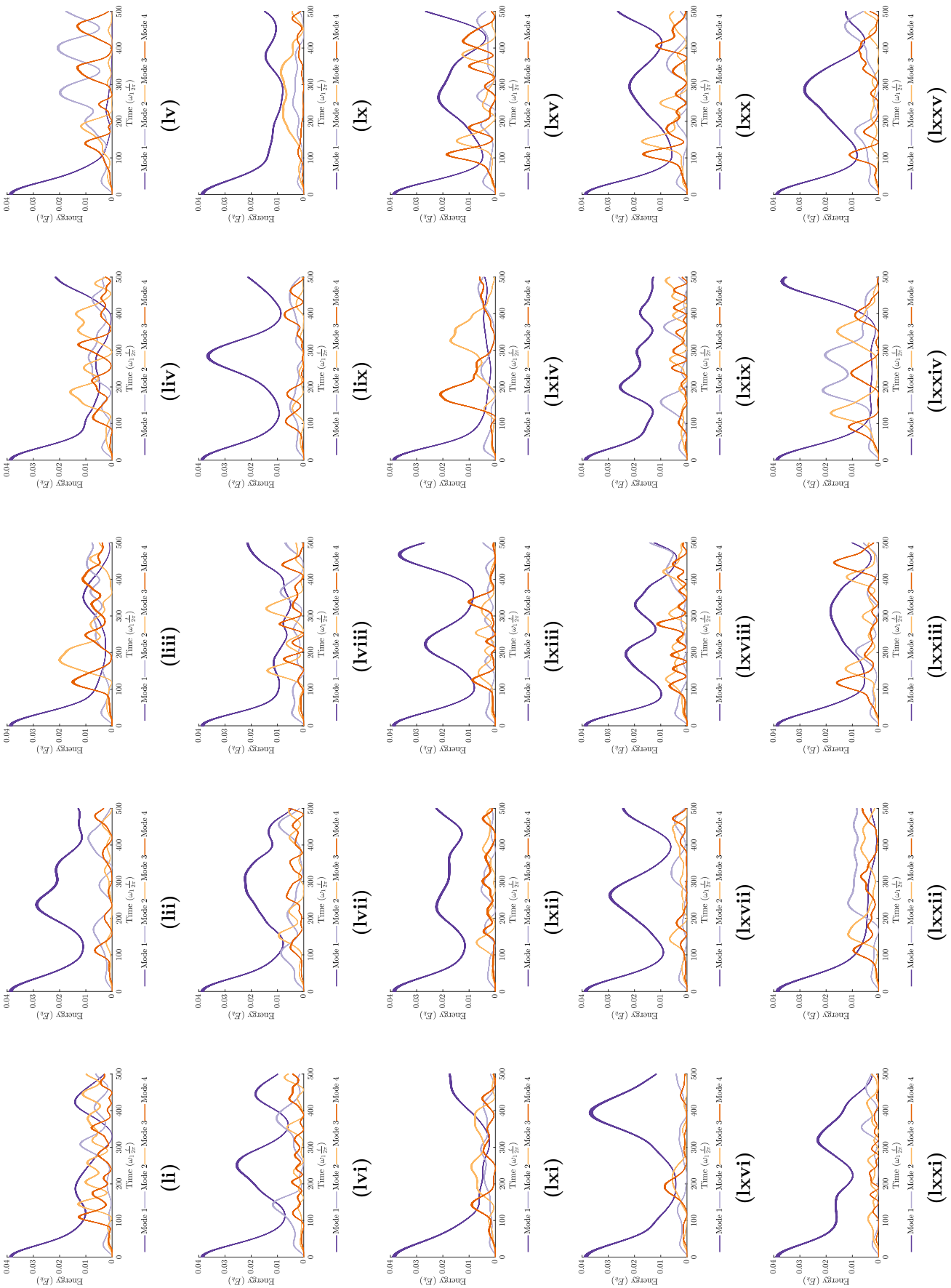


Figure D.3: (continued) Full set of 100 Monte Carlo simulations of asymmetric 1D FPUT-α arrays with 64 oscillators and a coupling strength of $\alpha = 0.25$ at a tolerance of $\pm 5\,\%$.

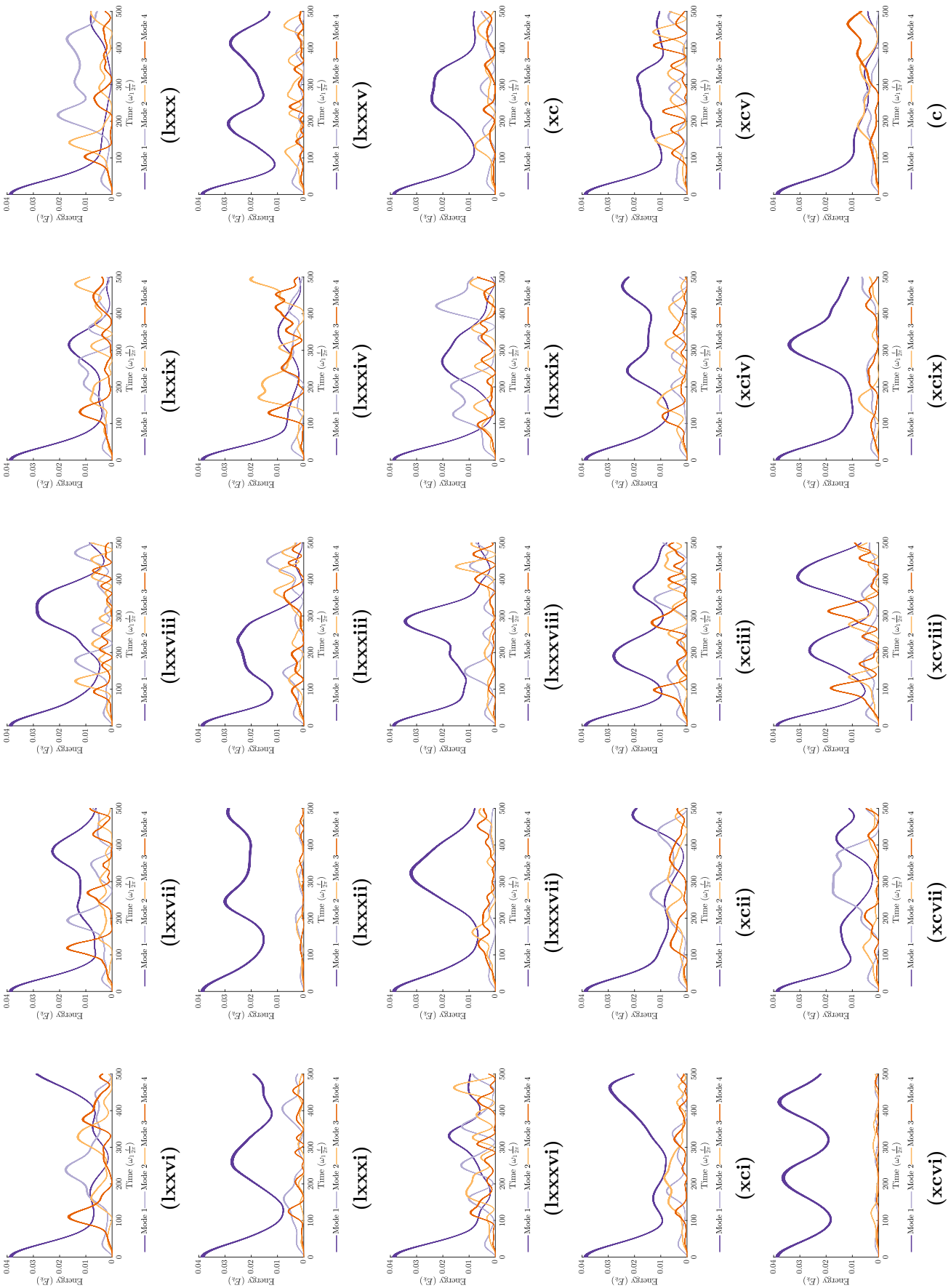


Figure D.3: (continued) Full set of 100 Monte Carlo simulations of asymmetric 1D FPUT-α arrays with 64 oscillators and a coupling strength of $\alpha = 0.25$ at a tolerance of $\pm 5\,\%$.

D.4 Tolerance of $\pm 10\,\%$

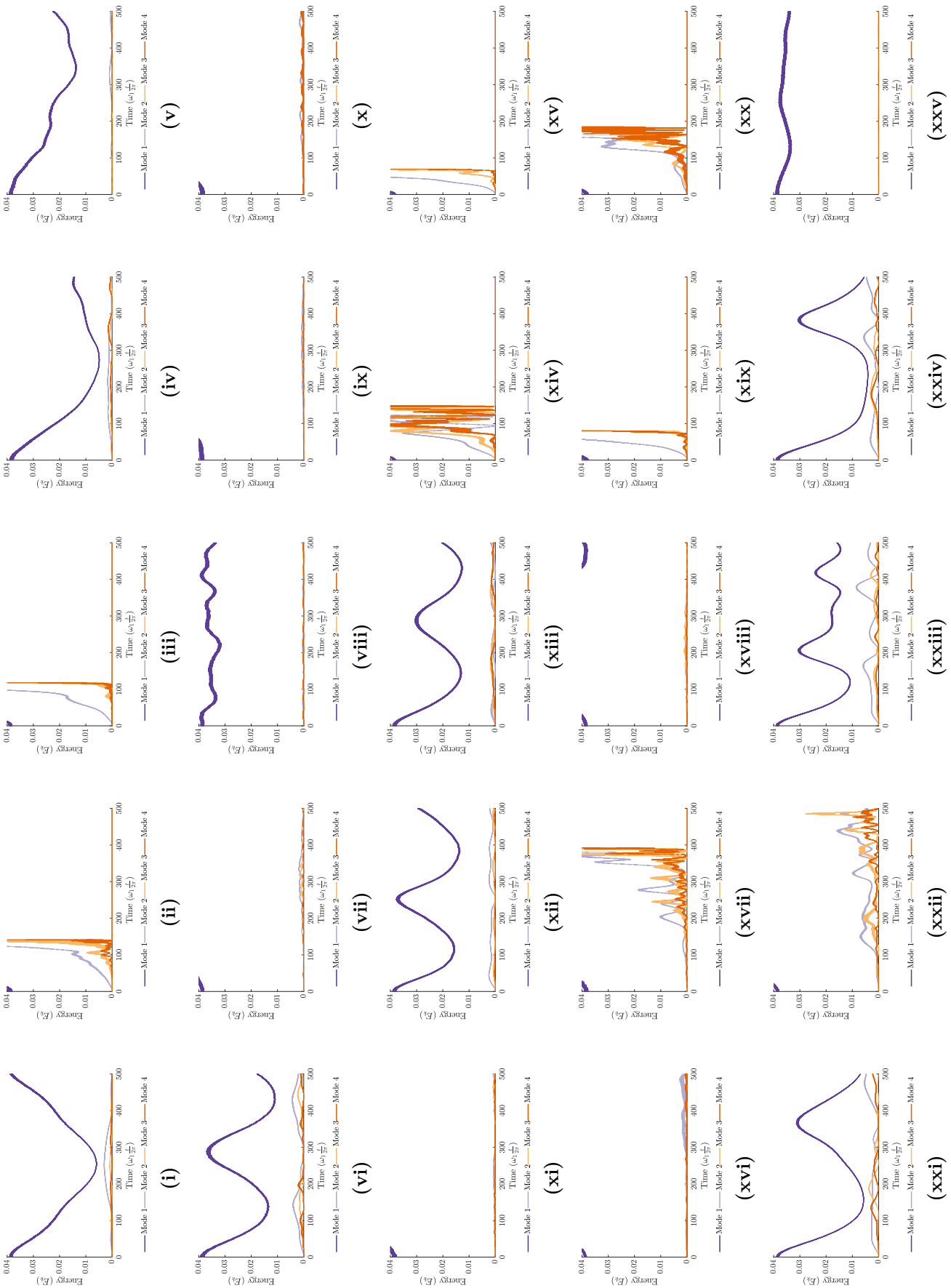


Figure D.4: Full set of 100 Monte Carlo simulations of asymmetric 1D FPUT-α arrays with 64 oscillators and a coupling strength of $\alpha = 0.25$ at a tolerance of $\pm 10\,\%$.

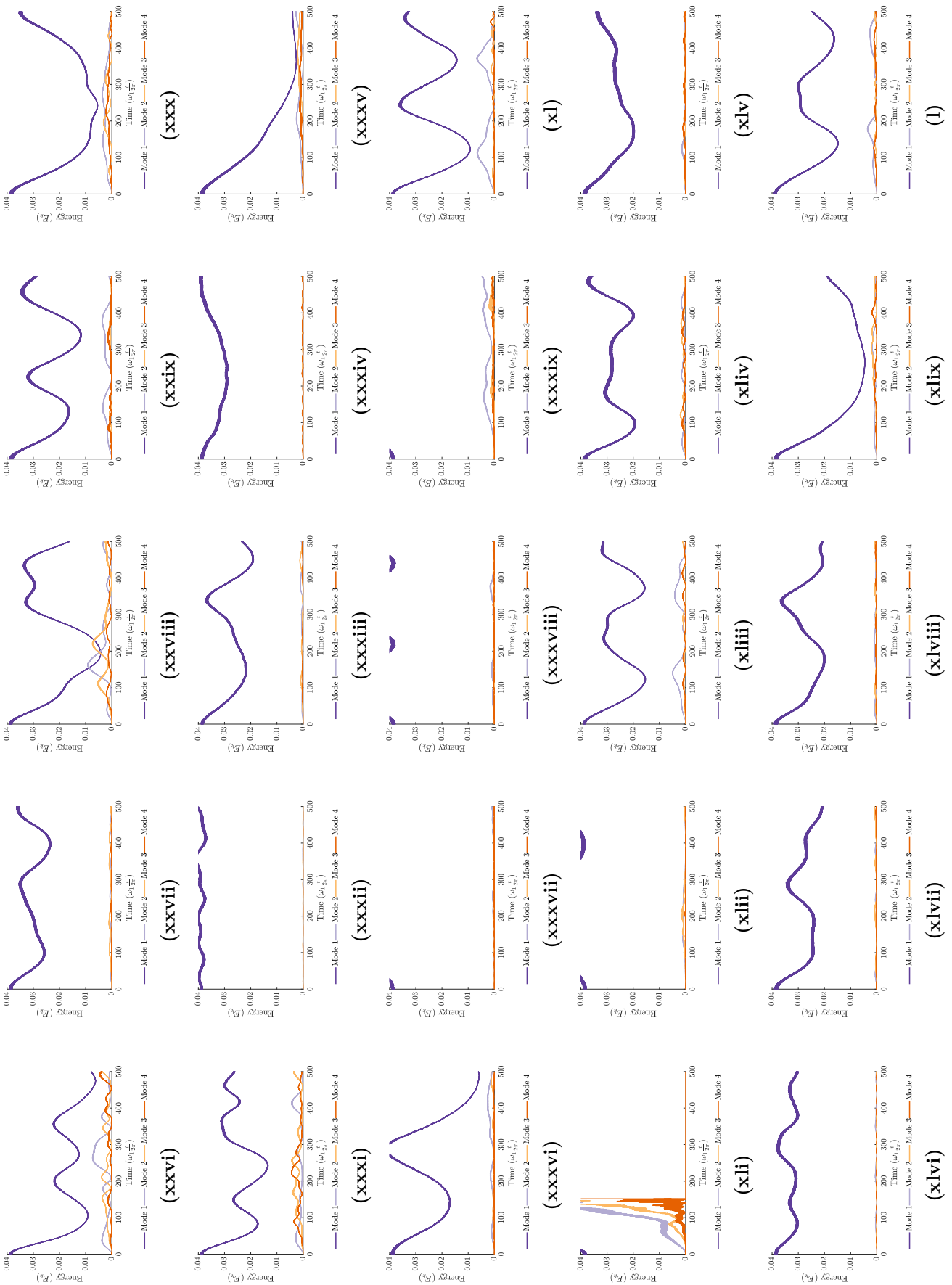


Figure D.4: (continued) Full set of 100 Monte Carlo simulations of asymmetric 1D FPUT-α arrays with 64 oscillators and a coupling strength of $\alpha = 0.25$ at a tolerance of $\pm 10\,\%$.

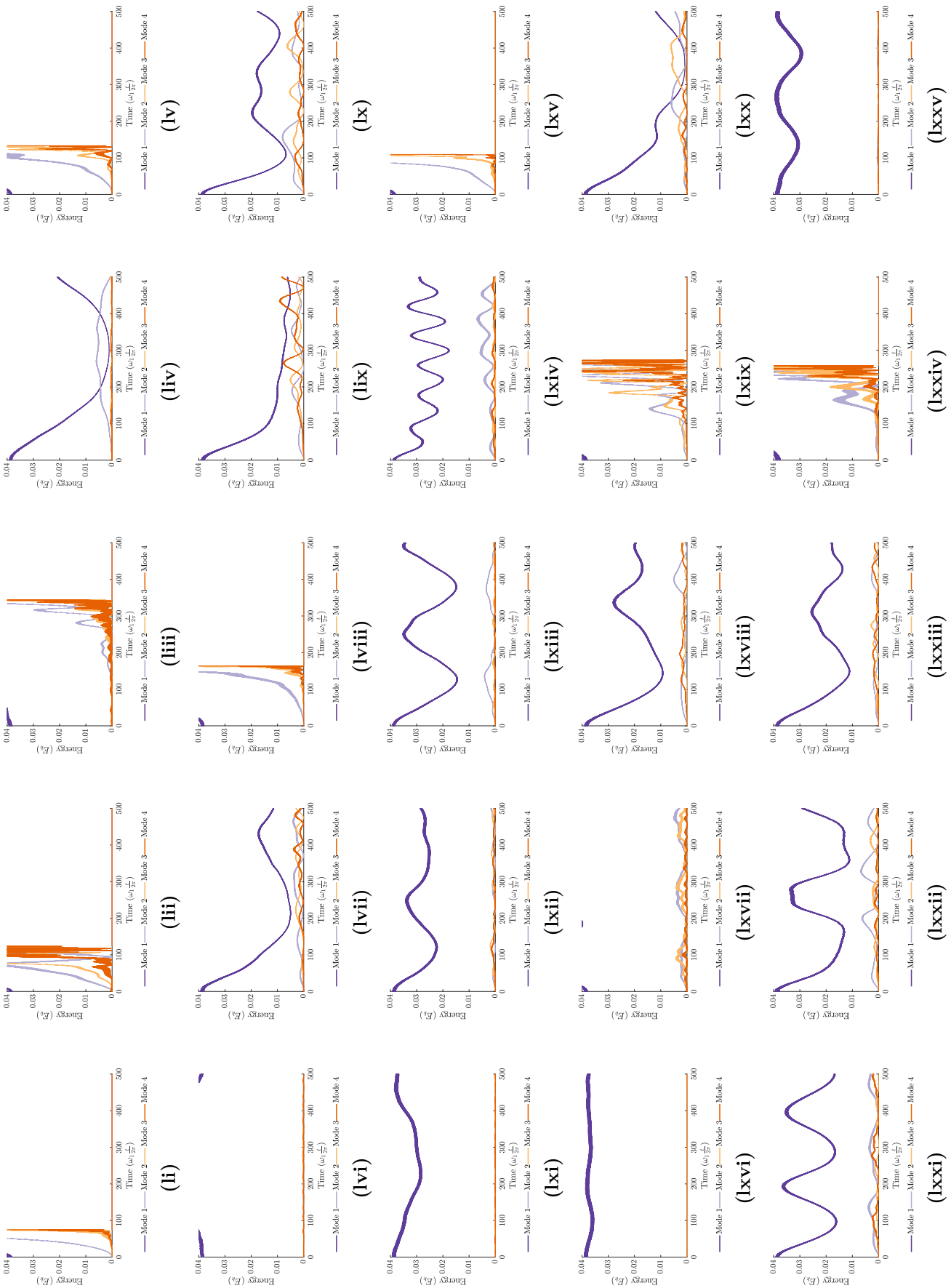


Figure D.4: (continued) Full set of 100 Monte Carlo simulations of asymmetric 1D FPUT-α arrays with 64 oscillators and a coupling strength of $\alpha = 0.25$ at a tolerance of $\pm 10\,\%$.

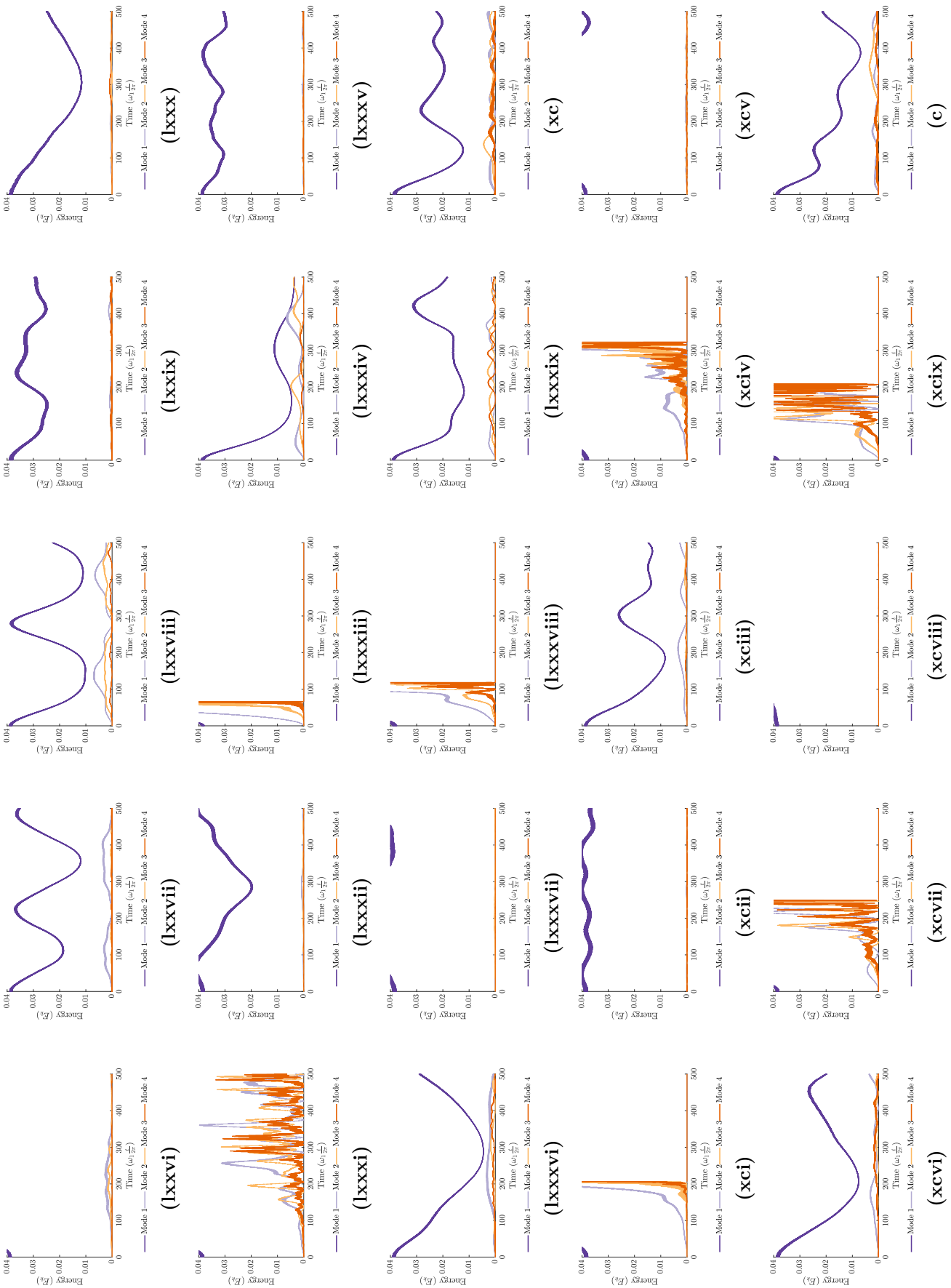


Figure D.4: (continued) Full set of 100 Monte Carlo simulations of asymmetric 1D FPUT-α arrays with 64 oscillators and a coupling strength of $\alpha = 0.25$ at a tolerance of $\pm 10\,\%$.